

Dissertation zur Erlangung des Doktorgrades  
der Fakultät für Chemie und Pharmazie  
der Ludwig-Maximilians-Universität München

**The role of Kindlin-2 for early  
events in integrin activation and  
signaling.**

Sven Moritz Widmaier  
aus München, Deutschland

2014

**Erklärung**

Diese Dissertation wurde im Sinne von § 7 der Promotionsordnung vom 28. November 2011 von Herrn Prof. Dr. Reinhard Fässler betreut.

**Eidesstattliche Versicherung**

Diese Dissertation wurde selbstständig, ohne unerlaubte Hilfe erarbeitet.

München, .....

---

(Moritz Widmaier)

Dissertation eingereicht am 09.10.2014

1. Gutachter                      Prof. Dr. Reinhard Fässler

2. Gutachter                      Prof. Dr. Bernhard Wehrle-Haller

Mündliche Prüfung am 30.10.2014

## Widmung

Für alle, die mich lieben und unterstützt haben.

## Table of Contents

Widmung.....	3
Table of Contents.....	4
Summary.....	6
Abbreviations.....	10
List of Publications.....	12
1. Introduction.....	13
1.1. Integrin receptor family and adhesion.....	13
1.1.1. Receptor subtypes.....	13
1.1.2. Biological significance.....	14
1.2. Molecular mechanisms of integrin mediated adhesion.....	17
1.2.1. Structure of integrins.....	17
1.2.2. Structural mechanisms of ligand binding and affinity regulation.....	19
1.2.3. Integrin activation requires large conformational changes.....	22
1.2.4. Integrin activation can be mediated from “inside” to the “outside” ..	24
1.2.5. Force generation.....	25
1.2.6. Models for off-rate regulation.....	26
1.2.7. Further modes of regulation.....	34
1.3. Methods for the measurement of integrin “activation”.....	36
1.3.1. Adhesion/Migration assays.....	36
1.3.2. Cellular ligand binding assays.....	37
1.3.3. Activity reporting antibodies.....	39
1.3.4. Further Methods.....	41
1.4. Integrin “activation” is mediated through kindlin and talin.....	43
1.4.1. Talin can regulate integrin-mediated adhesion.....	43
1.4.2. Structural organization of talin.....	45
1.4.3. Mechanistic insights into talin mediated integrin activation.....	46
1.4.4. Kindlins contribute to integrin activation via unknown mechanisms ..	49
1.5. Integrin mediated signaling.....	53
1.5.1. Overview of integrin mediated/influenced pathways.....	53
1.5.2. Integrin signaling in anoikis and cancer.....	60
2. Aim of the thesis.....	62

---

3.	Short summary of manuscripts.....	64
3.1.	Kindlin-2 initiates fibroblast adhesion and spreading by recruitment of paxillin and FAK to nascent adhesion sites.....	64
3.2.	Integrin linked kinase at a glance.....	65
3.3.	Loss of Kindlin-1 causes skin atrophy and lethal neonatal intestinal epithelial dysfunction.....	66
3.4.	Kindlin-1 controls Wnt and TGF- $\beta$ availability to regulate cutaneous stem cell proliferation.....	66
3.5.	Sorting nexin 17 prevents lysosomal degradation of $\beta$ 1 integrins by binding to the $\beta$ 1 integrin tail.....	68
4.	References.....	69
5.	Acknowledgements.....	80
6.	Curriculum vitae.....	82
7.	Appendix.....	83
7.1.	Paper I.....	83
7.2.	Paper II.....	83
7.3.	Paper III.....	83
7.4.	Paper IV.....	83
1.1.	Paper IV.....	84

## Summary

Integrins constitute a large family of obligate  $\alpha\beta$  heterodimeric transmembrane receptors that bind extracellular matrix proteins and counter receptors. Since integrins lack enzymatic activities, ligand induced signaling is induced by intracellular adaptor molecules. Furthermore, the intracellular adaptor molecules of the kindlin and talin protein family can regulate the affinity of integrins towards ligand and recruitment of signaling adaptors, such as integrin linked kinase (ILK) and focal adhesion kinase (FAK), and thus control ligand binding and downstream signaling. Integrin activation is a multistep process comprising large conformational changes in the entire integrin molecule and mechanical tensioning of the integrin ligand bond leading to stepwise increases of the binding strength. It has been shown that kindlin and talin proteins can simultaneously interact with the cytoplasmic tail of  $\beta$  integrin tails and that both proteins contribute to integrin activation. However, it remained unclear so far, if one of both proteins alone can mediate the entire activation processes.

In order to analyze the influence of kindlin and talin on integrin activation and integrin signaling, I generated a mouse line, which allowed *Cre*-mediated deletion of the kindlin-2 gene. I also performed the phenotype analysis of conditional kindlin-2 deletion in the skin, which is currently continued by the PhD student Marina Theodosiou under the supervision of Reinhard Fässler and myself. Furthermore, I generated two fibroblast cell lines, which allowed complete deletion of either the talin or kindlin proteins (**Paper I**). Both cell lines almost completely lost their ability to adhere on extracellular ligands and showed defects in integrin mediated signaling leading to reduced proliferation and cell survival, the latter defect was more severely affected in the kindlin deleted cell line. Precise analysis of integrin activation revealed that in contrast to talin, kindlin can initiate integrin activation in cooperation with ligand binding in the earliest steps of adhesion formation. Mechanistically, we could identify the signaling adaptor and FAK activator paxillin as a novel interaction partner of kindlin. Upon integrin activation, kindlin recruits paxillin as well as the previously known interaction partner ILK to the early adhesion complexes leading to initial integrin signaling, which facilitates cell spreading, proliferation and survival on

extracellular matrix (ECM) ligands. As a further consequence, recruitment of talin might be enhanced, leading to a strengthening and maturation of the adhesion and further spreading upon cell contraction.

During my studies I acquired broad insights into integrin mediated signaling pathways and the associated adaptor proteins. I was invited to write a review about the current knowledge of the adaptor protein ILK (**Paper II**). Early research indicated that ILK controls formation of initial integrin mediated contacts to the ECM, cell spreading and actin dynamics, as well as cell signaling important for cell proliferation, survival and tumor development through the interaction with other proteins, most importantly PINCH and parvin, and through its kinase activity. However recent results showed that the kinase domain of ILK is non-functional, which hampers the understanding of ILK-mediated functions.

During my work, I was also able to contribute to other related projects, which will be summarized next.

In mammals, three highly conserved kindlin paralogues are expressed in a tissue specific manner. Kindlin-2 expression can be found in almost all tissues with the exception of the hematopoietic system, kindlin-3 is expressed in all blood cells and kindlin-1 expression is restricted to epithelial cells. Genetic mutations, which disrupt the function of kindlin-1, have been described in human patients and lead to a rare skin disease, termed Kindler Syndrome. This disease is characterized by skin blistering after birth, pigmentation defects, atrophy and an increased risk for tumor development. The increased risk for tumor development remained mysterious, as loss of integrin activation is usually associated with a decreased risk for tumor formation. In **paper III**, we analyzed the consequences of constitutive kindlin-1 deletion in mice. We could identify the defects in kindlin mediated integrin activation as primary cause for the skin blistering phenotype and show that the mutant mice also display adhesion defects in the intestinal epithelium leading to an ulcerative colitis-like disease, which was also confirmed for the human patient by an independent group. Next, we investigated the cancer-promoting mechanisms induced by kindlin-1 deletion (**Paper IV**). Since constitutive deletion of kindlin-1 caused early postnatal lethality due to the intestinal phenotype, we generated a conditional mouse line for conditional deletion

of kindlin-1. Indeed, mice with skin-specific deletion of kindlin-1 survived and developed all typical phenotypes of Kindler Syndrome including an increased risk to form chemically induced tumors. In addition, these mice developed a severe hair follicle phenotype due to a loss of epithelial stem cell homeostasis. In order to separate the effects of kindlin-1 deletion from the consequences resulting from reduced integrin activation, we compared this mouse strain with mice expressing a mutant integrin, which cannot interact with kindlin. In this mouse strain the integrins remain inactive but kindlin-1 is still present. This analysis revealed two novel mechanisms of kindlin-1 function for skin stem cell homeostasis, hair follicle lineage commitment, as well as tumor development; on the one hand, kindlin-1, but not kindlin-2, can bind to the cytoplasmic tail of  $\beta 6$  integrin and thus mediate  $\alpha \beta 6$  integrin-mediated release of TGF $\beta$  from the ECM, which controls stem cell proliferation. On the other hand, cytoplasmic kindlin-1 can regulate the expression levels of several Wnt-ligands and receptors, which is essential for hair follicle development. Consequently, loss of kindlin-1 leads to a decreased TGF $\beta$  release and loss of stem cell quiescence, and an increase of Wnt-mediated  $\beta$ -catenin signaling, which induces stem cells to form aberrant hair follicles. Because both pathways are known for their high oncogenic potential, it is conceivable that they cooperate to promote tumor formation in the absence of kindlin-1 despite impaired integrin activation.

With the cell lines I generated for my PhD thesis (see **Paper I**) I was able to contribute to the progress of several other projects in the lab, which I want to summarize next.

Previous publications have shown that mutations in the kindlin interaction site of  $\beta$  integrins or depletion of kindlin can cause defects in integrin surface expression and in the maturation process of integrins. Since the cause for these observations remained unclear, we attempted to investigate the underlying mechanisms (**Paper V**). To our surprise, we could show that defects in recycling of internalized  $\beta 1$  integrin to the cell surface were not caused by loss of kindlin or mutation of the talin binding site in  $\beta 1$  integrin. Instead, mutation of the kindlin interaction site of  $\beta 1$  integrin caused this defect. A screening for novel interaction partners of this motif revealed that this mutation also strongly affected binding of the endosomal protein sorting nexin 17 (Snx17) and that this interaction was required for targeting of internalized integrins to

exocytotic vesicles instead of targeting to lysosomal vesicles, where the integrins are rapidly degraded.

## Abbreviations

ABD	Actin Binding and Dimerization Domain	GPCR	G-Protein Coupled Receptor
AFM	Atomic Force Microscopy	GSK	Glycogen Synthase Kinase 3
Amino acids	All amino acids are denominated according to the three letter code.	Hic5	Hydrogen peroxide-inducible clone-5
Arf6	ADP-ribosylation factor 6	Hyp	Hydroxyproline
Arp 2/3	Actin related protein 2/3	ICAP1	Integrin Cytoplasmic domain-Associated Protein-1
AXS	Small Angle X-ray scattering	IGFR	Insulin-like Growth Factor Receptor
Bad	Bcl-2-associated death promoter	IP <sub>3</sub>	Inositoltriphosphate
Bax	Bcl2-associated X	Jnk	c-Jun N-terminal Kinase
Bcl-2	B-cell lymphoma-2	LDV	Leu-Asp-Val
Bcl-XL	B-cell lymphoma-XL	LIM	Lin11, Isl-1 & Mec-3
Cdc42	Cell division control protein 42 homolog	LN	Laminin
CRK	Chicken tumor 10 Regulator of Kinase	MAPK	Mitogen Activated Protein Kinase
DAG	Diacylglycerol	MEK	Mitogen-activated protein kinase/ERK Kinase
DOCK1	Dedicator of Cytokinesis 180	MMP-2	Matrix Metallo-Proteinase-2
EGF	Epidermal growth factor	p130CAS	CRK-Associated Substrate
EGF	Epidermal Growth Factor	PAK	P21 Activating Kinase
EGFR	Epidermal Growth Factor Receptor	PALM	Photo-activated Localization Microscopy
EM	Electron microscopy	PAR	Protease-Activated Receptor
ER	Endoplasmic Reticulum	PBS	Phosphate Buffered Saline
ERK	Extracellular-signal Regulated Kinase	PDGFR	Platelet Derived Growth Factor Receptor
FAK	Focal Adhesion Kinase	PI3K	Phosphoinositidol-3-Kinase
FERM	4.1-protein/Ezrin/Radixin/Moesin	PINCH	particularly interesting new Cys-His
FGFR	Fibroblast Growth Factor Receptor	PIX	PAK-Interactive exchange factor
FLIM	Fluorescence Lifetime Imaging	PKB	Protein Kinase B
FN	Fibronectin	PKC	Protein Kinase C
GAP	GTPase-Activating Protein	PMA	Phorbol-12-myristat-13-acetat
GEF	Guanosine Triphosphate Exchange Factors	PTP-PEST	Protein Tyr-Phosphatase with Pro(P)-Glu(E)-Ser(S)-Thr(T) sequence
GFOGER	Gly-Pro-Hyp-Gly-Glu-Arg	Rac	or Ras-related C3 botulinum toxin substrate
GIT	Protein-coupled receptor-kinase-interacting protein	RAP1	Ras-related protein 1

---

Ras	Rat sarcoma protein	STED	Stimulated Emission Depletion
RGD, RGE	Arg-Gly-Asp, Arg-Gly-Glu	STORM	Stochastic Optical Reconstruction Microscopy
Rgnef	RhoA-specific guanine nucleotide exchange factor	TGF $\beta$	Transforming Growth Factor $\beta$
Rho	Rat Sarcoma homologue	TIAM	T lymphoma invasion and metastasis
RIAM	Rap1-GTP-Interacting Adapter Molecule	Wnt	Wingless-related integration site
SH	Src-Homology	$\alpha\beta 2$ ; $\alpha\beta x$	Integrin heterodimer consisting of undefined (x) $\alpha$ or $\beta$ subunit
SMAD	Small body size and Mothers Against Decapentaplegic		
SNX17	Sorting Nexin 17		
SNX31	Sorting Nexin 31		
SOS1	Son Of Sevenless homolog 1		
Src	Cellular Sarcoma (kinase)		

## List of Publications

This thesis is based on the following publications, which are referred in the text by **roman numeral letters (I-V)**:

**Paper I: Widmaier M**, Theodosiou E, Rognoni E, Austen K, Veelders M, Müller D, Strohmeyer N, Bharadwaj M, Zent R, Fässler R. Kindlin-2 initiates fibroblast adhesion and spreading by recruitment of paxillin and FAK to nascent adhesion sites. *In preparation*.

**Paper II: Widmaier M**, Rognoni E, Radovanac K, Azimifar B, Fässler R. Integrin linked kinase at a glance. *J C Sci*. 2012, 125(Pt8), 1839-1843.

**Paper III: Ussar S, Moser M, Widmaier M**, Rognoni E, Harrer C, Genzel-Boroviczeny O, Fässler R. Loss of Kindlin-1 causes skin atrophy and lethal neonatal intestinal epithelial dysfunction. *PLoS Genet*. 2008, 4(12), e1000289.

**Paper IV: Rognoni E, Widmaier M**, Jakobson M, Ruppert R, Ussar S, Katsougkri D, Böttcher RT, Lai-Cheong JE, Rifkin DB, McGrath JA, Fässler R. Kindlin-1 controls Wnt and TGF- $\beta$  availability to regulate cutaneous stem cell proliferation. *Nat Med*. 2014, 20(4), 350-9.

**Paper V: Böttcher RT, Stremmel C, Meves A, Mayer H, Widmaier M**, Tseng HY, Fässler R. Sorting nexin 17 prevents lysosomal degradation of  $\beta$ 1 integrins by binding to the  $\beta$ 1 integrin tail. *Nat Cell Biol*. 2012, 14(6):584-92.

## 1. Introduction

### 1.1. Integrin receptor family and adhesion

The appearance of multicellular organisms during evolution introduces the necessity to coordinate cell-cell and cell-substratum interactions in a highly defined manner. These interactions need to be efficiently and specifically established as well as broken in order to allow dynamic reorganization of multicellular structures into organs during development, the formation of large scale cellular and acellular structures (e.g. vessels and connective tissue respectively) or the invasion of immune cells into an infected organ from the blood stream. This need is partially resolved by the evolution of a specific group of transmembrane receptors (reviewed in <sup>14</sup>). These molecules are termed integrins, as they integrate (i.e. connect) extracellular ligands and the intracellular cytoskeleton. At the same time they allow a biochemical regulation of their ligand affinity, termed inside-out signaling or integrin activation (discussed in 1.2)<sup>13, 14</sup>.

#### 1.1.1. Receptor subtypes

Up to date, integrins have been identified in all multicellular organisms, where they form obligate heterodimeric transmembrane glycoprotein receptors composed of a non-covalently linked  $\alpha$  and  $\beta$  subunit. The specificity of integrin function and ligand binding necessary for mammalian development and homeostasis is mediated through 24 different integrin heterodimers generated by 18  $\alpha$  and 8  $\beta$  subunits (see Fig. 1) <sup>13</sup>.

Integrin heterodimers can be classified into different subgroups according to their ligand specificity (reviewed in <sup>13</sup>) and the evolutionary relationship of their  $\alpha$  subunits (see Fig. 1)(reviewed in <sup>14</sup>):  $\alpha 5$ -,  $\alpha 8$ -,  $\alpha v$ - and  $\alpha IIb$ -subunits constitute the oldest group of integrins, which recognize a short Arg-Gly-Asp (RGD) peptide motif in ligands such as fibronectin (FN), fibrinogen or vitronectin with differing affinities and specificities.  $\beta 5$ ,  $\beta 6$  and  $\beta 8$  integrins can only dimerize with  $\alpha v$ -integrin, while  $\beta 3$  integrin can dimerize with  $\alpha IIb$  and  $\alpha v$  subunits. The promiscuous  $\beta 1$  integrin not only dimerizes with the RGD binding  $\alpha 5$ -,  $\alpha v$ - and  $\alpha 8$  integrin subunits, but also with the groups of Leu-Asp-Val (LDV)-peptide binding  $\alpha 4$ - and  $\alpha 9$ -subunits, which appeared later during evolution. These receptors recognize both FN and Ig-superfamily proteins such as

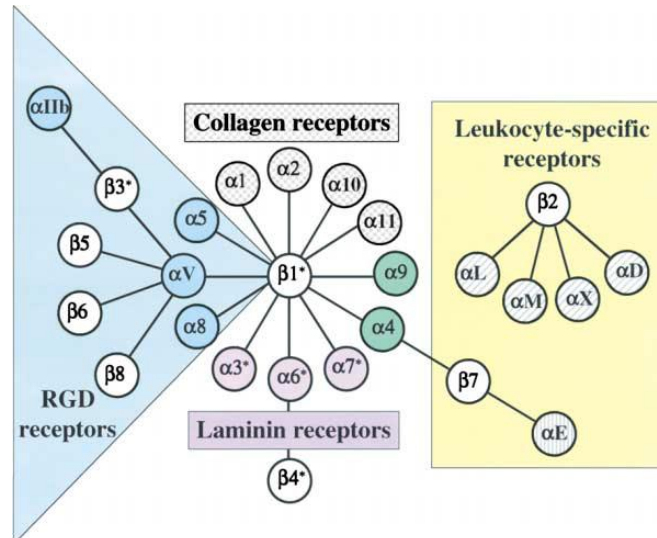


Figure 1: The integrin receptor family <sup>13</sup>. Among all possible dimeric combinations of the shown  $\alpha$ - and  $\beta$  subunits, only 24 combinations are known. These combinations are indicated here by lines. These receptor dimers are further grouped by their ligand specificity or the cell types, in which they are preferentially expressed, as indicated.

VCAM-1. Furthermore  $\beta 1$  integrin dimerizes with a group of  $\alpha$  subunits ( $\alpha 3$ ,  $\alpha 6$ ,  $\alpha 7$ ) which appeared second in evolution and recognize Laminin (LN) through a unknown motif and the evolutionary youngest group of collagen receptors ( $\alpha 1$ ,  $\alpha 2$ ,  $\alpha 10$ ,  $\alpha 11$ ), which recognize Gly-Phe-Hyp-Gly-Glu-Arg (GFOGER; Hyp or O represent Hydroxyproline) peptides. The latter group is

closely related to the leucocyte-specific  $\alpha$  subunits  $\alpha D$ ,  $\alpha M$ ,  $\alpha L$ ,  $\alpha X$  (specific for Intercellular Adhesion Molecule (ICAM), Vascular Cell Adhesion Molecule (VCAM), FN), which dimerize with  $\beta 2$ -subunits, and  $\alpha E$ , which dimerizes with  $\beta 7$  (specific for E-Cadherin). The collagen receptors and the leucocyte specific receptors have evolved by the insertion of an additional domain in their  $\alpha$  subunits ( $\alpha I$ -domain, see 1.2.1).

In line with the evolutionary development of the different integrin classes, the expression pattern of integrins differs strongly. For example  $\beta 1$  integrin heterodimers can be found in almost all tissues, although expression of  $\alpha 5\beta 1$  heterodimers appears to be more restricted to the mesenchymal lineage and the expression of laminin-interacting  $\beta 1$ -heterodimers more to epithelial lineages. Similarly, the heterodimers of  $\beta 2$  and  $\beta 7$  integrins are restricted to the hematopoietic lineage.

### 1.1.2. Biological significance

The hierarchy in the evolutionary development of the different integrin heterodimer subgroups as well as the expression patterns is reflected in the severity of the null phenotypes in transgenic mouse models (see Fig. 2 and reviewed in <sup>13, 15</sup>).

	Integrin	Viability	Unchallenged mutant phenotype
Collagen	$\alpha 1$	+	No phenotype. Cell adhesion defect to collagen IV.
	$\alpha 2$	+	Mild mammary gland branching morphogenesis phenotype. Platelet, fibroblast, and keratinocyte adhesion defect to collagen I.
	$\alpha 10$	+	Mild cartilage defect.
Laminins	$\alpha 11$	+	Incisor eruption defect.
	$\alpha 3$	+/-	Defects of kidney and submandibular gland, decreased bronchial branching of the lungs, skin blisters, abnormal layering of the cerebral cortex.
	$\alpha 6$	+/-	Severe blistering of the skin and other epithelia, absence of hemidesmosomes, altered laminin deposition in the brain, and ectopic neuroblastic outgrowths on the brain and in the eye. Mutants die at birth.
Leucocyte specific RGD	$\alpha 5$	-	Severe defects in posterior trunk and yolk sac mesodermal structures, lack of epithelialization of somites, reduced numbers of Schwann cells and embryonic lethality at E10-E11.
	$\alpha v$	- or +/-	Placental defects and intracerebral, intestinal hemorrhages and cleft palate. Death varies from midgestation to perinatal.
	$\alpha IIB$	+	Bleeding disorder, lack of platelet binding to fibrinogen, absence of fibrinogen in platelet alpha granules, and increased numbers of hematopoietic progenitors in yolk sac, fetal liver, and bone marrow.
	$\alpha L$	+	Reduced immune response, defects in neutrophil adhesion to endothelium, and in osteoclast adhesion.
	$\alpha M$	+	Reduced immune response, reduced neutrophil adhesion to fibrinogen and reduced degranulation of neutrophils.
	$\alpha E$	+	Reduced number of intestinal and vaginal interepithelial lymphocytes, skin inflammation.
	$\beta 1$	-	Null mutants die soon after implantation due to inner cell mass defects in blastocysts.

Figure 2: Integrin deletion phenotypes; modified from <sup>8</sup>.

It has been hypothesized that the presence of two distinct germ layers in diploblastic organisms was facilitated by the development of the two groups of integrins recognizing the germ layer specific ECM ligands laminin and fibronectin, as this allowed germ layer specific, asymmetric interactions with the different types of surrounding ECM <sup>13</sup>. Embryonic development of the germ layers in bilateria is initiated with a single layered blastula structure, which forms three germ layers (ektoderm, endoderm

and mesoderm) during a process called gastrulation. In line with the important role of the mesoderm for embryonic development, deletion of the mesoderm specific  $\alpha$  subunit  $\alpha 5$  gives rise to the earliest (embryonic day 10-11) and most severe phenotype observed for the deletion of a single integrin-heterodimer. The defects affect the posterior somitogenesis and vascular development. Because many integrin heterodimers expose overlapping substrate specificity and expression pattern, compensation can be observed. For example, the role of multiple fibronectin binding integrins for mesoderm development is underlined by the observation that deletion of both,  $\alpha 5$  and  $\alpha v$  integrin subunits leads to an almost complete loss of the mesoderm germ layer <sup>16</sup>. In contrast, deletion of all  $\alpha v$ -containing heterodimers allows normal mesodermal development, but can cause embryonic lethality due to defective placenta formation or perinatal lethality due to intracerebral bleeding, suggesting a

more specialized role of  $\alpha$ v integrins during the development of mesoderm derived tissues. Deletions of single LN-specific heterodimers manifest at later stages of development corresponding to the formation of LN-dependent epithelial tissues. Deletion of  $\alpha$ 3- and  $\alpha$ 6 integrin give rise to perinatal lethality caused by branching defects of the lung and kidney or severe delamination defects of the skin and other epithelia, respectively. When integrin subunits of the hematopoietic system ( $\beta$ 2,  $\alpha$ L,  $\alpha$ M,  $\alpha$ IIb,  $\alpha$ E) are deleted, the resulting defects are limited to blood cells (platelet aggregation defects and leukocyte adhesion deficiencies). However, affected animals are generally viable and fertile. Finally, deletion the evolutionary youngest group of collagen receptors ( $\alpha$ 1,  $\alpha$ 2,  $\alpha$ 10 and  $\alpha$ 11) leads to minor phenotypical alterations without affecting viability or fertility, indicating a higher degree of redundancy and compensation. While the deletion phenotypes of single integrin heterodimers is restricted to the affected germ layer or organ, deletion of the central  $\beta$ 1 integrin subunit, which pairs with multiple classes of integrin receptors (see Fig. 1) leads to combined defects and embryonic lethality at embryonic day 6.5 due to general adhesive defects inhibiting gastrulation.

Generally, integrins do not only mediate cell adhesion on specific substrates, but also induce cell-type and tissue specific signaling (discussed in 1.5), which control differentiation, proliferation and survival important for homeostasis, immune defense

<b>Integrin</b>	<b>Associated disease</b>
$\beta$ 2	Psoriasis
$\alpha$ 4	Multiple sclerosis, Crohn's disease
$\alpha$ 4 $\beta$ 1 & $\alpha$ 4 $\beta$ 7	Asthma
$\alpha$ 4 $\beta$ 7	Ulcerative Colitis
$\alpha$ 5 $\beta$ 1	Renal cell carcinoma, metastatic melanoma, pancreatic cancer
$\alpha$ v $\beta$ 3	Angiogenesis & cancer, rheumatoid arthritis, osteoporosis
$\alpha$ IIb $\beta$ 3	Unstable angina, restenosis, stroke, acute coronary artery disease

Table 1: Integrins and associated diseases; modified from <sup>17</sup>.

against pathogens, organ plasticity or wound healing processes and thus, integrin function is implicated in many human diseases (for an overview, see table 1) <sup>13</sup>. For

example, integrins have been identified as key regulators of inflammatory diseases, like multiple sclerosis, asthma, Crohns Disease and rheumatoid arthritis (reviewed in <sup>17</sup>). Furthermore, increased activity of  $\alpha$ 5 $\beta$ 1 and  $\alpha$ v $\beta$ 3 have been connected to the

development of different cancer types and  $\alpha\text{IIb}\beta\text{3}$  function is clearly essential for thrombus formation and blood clotting<sup>17-19</sup>.

## 1.2. Molecular mechanisms of integrin mediated adhesion

### 1.2.1. Structure of integrins

Major insights into the mechanisms of integrin mediated ligand binding and ligand binding affinity regulation were achieved by the study of crystal structures of complete  $\alpha\text{v}\beta\text{3}$ ,  $\alpha\text{IIb}\beta\text{3}$  and  $\alpha\text{x}\beta\text{2}$  ectodomains and of different integrin fragments. Furthermore, small angle X-ray scattering and electron microscopy (EM)-image averaging techniques of truncated or complete ectodomains and complete  $\alpha\text{IIb}\beta\text{3}$  receptors embedded in membrane nanodiscs have contributed to the understanding of the functional relationship between integrin conformation and ligand binding (discussed in 1.2.2)(reviewed in<sup>13, 20</sup>).

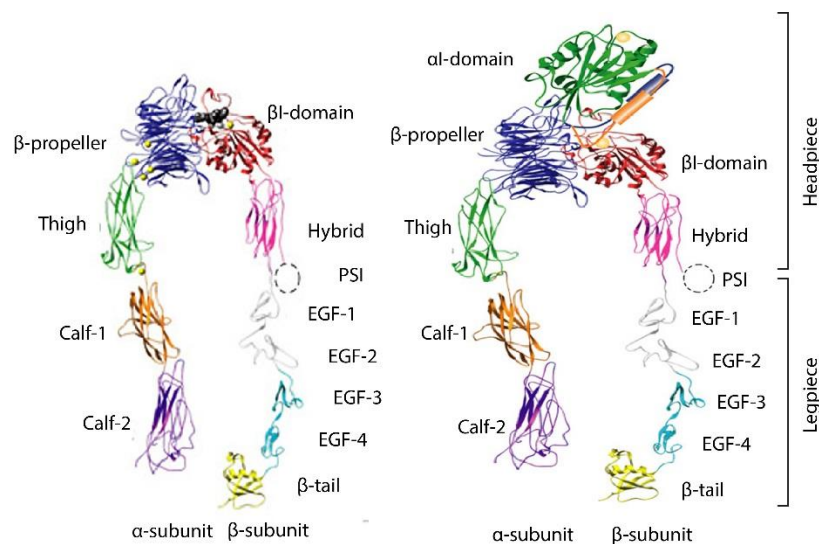


Figure 3: Integrin structure and domain organization. Modified from<sup>21</sup>. The picture represents the structural components of  $\alpha\text{v}\beta\text{3}$  (left) and  $\alpha\text{L}\beta\text{2}$  integrin ectodomains.  $\alpha\text{L}\beta\text{2}$  integrin contains an inserted  $\alpha\text{I}$ -domain; the structure of PSI-domain is not resolved and is therefore indicated as dashed circle.

Each  $\beta$  subunit has a typical size of approximately 700 amino acids and consists of an unstructured, short cytoplasmic tail, an  $\alpha$ -helical transmembrane domain, which crosses the cell membrane in a skewed angle and several protein modules in the extracellular domains, comprising the largest proportion of the protein (compare Fig. 3). The membrane proximal extracellular  $\beta$ -tail domain appears rather flexible, is linked to the transmembrane domain with an unstructured linker and is consequently unlikely to transmit structural constraints of the transmembrane domain to the

extracellular space. The  $\beta$ -tail domain forms together with the adjacent four cysteine-rich, Epidermal Growth Factor (EGF)-like domains the  $\beta$  integrin “legpiece”. All EGF domains are interconnected by cysteine bridges, except the most membrane distal EGF-1 domain to allow a high degree of conformational flexibility. The flexibility is highest between EGF-1- and EGF-2 (“ $\beta$ -knee”) and between the interface of EGF-1 and the adjacent plexin-semaphorin-integrin (PSI) domain. The “ $\beta$ -headpiece” is composed of the PSI-domain harboring an insertion of the hybrid domain, which in turn contains an inserted ligand binding  $\beta$ -I domain that shares similarities with the von Willebrand factor type A found in blood plasma.

Similar to the  $\beta$  subunit, the  $\alpha$  subunit also consists of a largely unstructured, short cytoplasmic domain, a transmembrane domain, which crosses the membrane in a perpendicular manner and several domains forming the leg-piece and head-piece region (Fig. 3). The linker connecting the transmembrane domain with the leg domain is flexible and can be cleaved in several  $\alpha$  subunits ( $\alpha 3$ ,  $\alpha 4$ ,  $\alpha 5$ ,  $\alpha 6$ ,  $\alpha 7$ ,  $\alpha 8$ ,  $\alpha 9$ ,  $\alpha v$ ,  $\alpha E$ ,  $\alpha IIb$ ) in such a way that the extracellular domains remain covalently connected via a disulfide bridge<sup>22</sup>. The legpiece extends from the membrane and is composed of two Calf and one Thigh domain, which share structural similarities to immunoglobulin  $\beta$ -sandwich folds. In contrast to the  $\beta$  integrin legpiece, these domains bear less conformational flexibility. One important mobile interface is located adjacent to the  $\beta$  knee between the Calf-1 and Thigh domain. The other mobile interface can be found between the Thigh and the seven bladed  $\beta$ -propeller of the  $\alpha$ -headpiece domain and is important for ligand binding. Ligand binding in  $\alpha I$ -containing  $\alpha$  integrin subunits (see Fig. 3, right side) is exclusively mediated via an  $\alpha I$  subdomain, which is inserted between blade two and three of the  $\beta$ -propeller. The  $\alpha I$  subdomain shares a high degree of structural similarity with the  $\beta I$  domain of the  $\beta$  integrin subunit.

Multiple interactions between  $\alpha$  and  $\beta$  subunit domains as well as the resulting specific conformation of each single domain contribute differently to the conformational transition from an inactive integrin with low ligand affinity to a fully activated integrin with up to 10.000 times higher affinity ( $\alpha L\beta 2$ ) to its ligand.

### 1.2.2. Structural mechanisms of ligand binding and affinity regulation

The stability of protein interaction between two ligands can be controlled by regulating the on-rate or off-rate of ligand-receptor binding (see 1.2.6). The same methods, which provided insights into the structural composition of integrins, were also used to determine the molecular details of integrin-mediated ligand binding (reviewed in <sup>13,20</sup>). Crystal structures of integrins in complex with their ligands highlight the importance of specific cation coordination sites in the  $\alpha$ I and  $\beta$ I domains together with further interaction sites with the head domains of each  $\alpha\beta$ x integrin.

For example, the long side chain of Arg from RGD locates into a cleft formed by the  $\beta$ -propeller of the  $\alpha$  subunit <sup>23-25</sup>, and another region of the  $\alpha$ 5 integrin  $\beta$  propeller can interact with a “synergy” region located in FN <sup>25,26</sup>. It is very likely that such additional interactions govern the different affinities observed between integrin classes with overlapping substrate specificity <sup>27, 28</sup>, as  $\alpha$ 5 integrin with mutations which perturb interaction with the FN synergy site exposes a 50 fold lower affinity for FN and thus might lose its preference in FN binding over binding to other RGD-containing ligands <sup>25</sup>.

High affinity ligand interaction is mediated via the coordination of a negatively charged Asp residue in RGD-containing ligands with a  $Mg^{2+}$  ion which forms the Metal Ion Dependent Adhesion Site (MIDAS). Interestingly, the conservative mutation of Asp to Glu (RGD to RGE) leads to a dramatic reduction in ligand binding, as the longer side chain of Glu interferes with the formation of further molecular interactions between ligand and integrin <sup>29</sup>. Ligand binding of  $\alpha$ 4/ $\alpha$ 9 integrins,  $\beta$ 2 and  $\alpha$ E $\beta$ 7 integrins and collagen binding integrins is mediated in a similar manner through coordination of an acidic ligand side chain to the MIDAS metal ion. In contrast, the molecular details of laminin binding remain currently unclear. The ligand binding  $Mg^{2+}$  cation of the integrin headpiece is flanked in close proximity by two further affinity regulating  $Ca^{2+}$  ions. While the Adjacent to MIDAS (ADMIDAS)  $Ca^{2+}$  coordination site has an inhibitory influence, the second  $Ca^{2+}$  binding site is referred to as Synergistic Metal ion Binding Site (SyMBS). The synergistic effect of this metal ion binding site can be explained for  $\alpha$ IIb $\beta$ 3 integrin by a Glu residue which coordinates simultaneously the MIDAS and SyMBS cation and thereby stabilizes the ligand binding competent coordination of the

MIDAS cation<sup>30</sup>. Furthermore, multiple other sites in both integrin subunits can coordinate  $\text{Ca}^{2+}$  ions, which partly depends on the ligand binding status that influences the overall integrin conformation. Of note, incubation of isolated integrins or integrins on cell surfaces with high  $\text{Ca}^{2+}$  concentrations (>1mM) induce lower ligand binding affinities, while presence of  $\text{Mn}^{2+}$  ions promote high affinity ligand binding. The underlying mechanisms remain unclear. It can be speculated that the different sizes of the individual metal ions stabilize different conformations of the coordinated protein residues. In contrast, incubation with metal ion chelators, such as EDTA or EGTA, has a concentration dependent influence, which leads to inactivation at intermediate concentrations (most likely through removal of the MIDAS  $\text{Mg}^{2+}$ ) but can also cause activation at higher concentrations, potentially through the removal of  $\text{Ca}^{2+}$  ions.

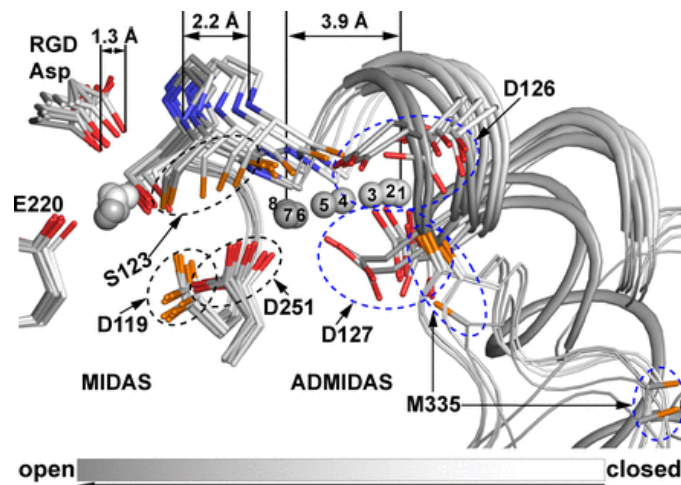


Figure 4: Conformational transition from closed to open  $\alpha\text{IIb}\beta 3$  integrin. Eight individual conformational states of the ligand binding site are superimposed and key residues are shown as stick models. State 1 (light grey) relates to the closed conformation and state 8 to the open conformation (dark grey); distances indicate overall movements between state 1 and 8. The metal ions of MIDAS and ADMIDAS are shown as grey spheres<sup>30</sup>.

Integrins have the unique property to communicate conformational changes of the ligand binding site over long ranges to the region of the legpiece domains through chemical allostery and thus regulate extracellular ligand binding from the intracellular space as well as report ligand binding into the intracellular space. Consequently, the order of conformational changes necessary to induce integrin activation can be described starting from the ligand binding site or reversely from the short cytoplasmic tails. A recent publication has revealed a plausible series of intermediate conformations connecting the low affinity state with closed head piece to the high

affinity state with extended hybrid domain<sup>30</sup>. Of note, in this case the conformational changes required the presence of RGD ligand (see also Fig. 5): First, Asp of the RGD ligand can be bound to the low affinity resting state integrin leading to subsequent movements of the MIDAS and ADMIDAS coordinating residues. Most importantly, Ser-123 residue of the  $\alpha 1$  chain of the  $\beta I$  domain changes its coordination partner from the ADMIDAS metal ion to the MIDAS metal ion. This leads to a chain reaction of rearrangements in the MIDAS and ADMIDAS coordinating residues (mostly from the  $\beta I$ - $\alpha 1$  chain), which induces a sliding movement of the whole RGD binding site and the Asp residue of the RGD ligand towards the  $\alpha$  integrin propeller and major rearrangements in the  $\beta I$ - $\alpha 1$  chain, which in turn promote a pistoning movement of the  $\beta I$ - $\alpha 7$  side chain leading to an outwards movement of the connected hybrid domain (see Fig. 4 for the localization of the hybrid domain and Fig. 5 for the conformational changes of the  $\beta I$ - $\alpha$ -helices)<sup>30</sup>. This hybrid domain “swing-out” is an essential step for integrin activation and is required to stabilize the ligand interaction by decreasing the unbinding rate (off-rate)<sup>31</sup>.

A recent crystallographic study of  $\alpha IIb\beta 3$  integrin further explained several factors important for the increased affinity of the open conformation of  $\alpha IIb\beta 3$  towards the RGD ligand<sup>1,30</sup>: (1) the approach of the MIDAS  $Mg^{2+}$  to the coordinated RGD-Asp; (2) an increase of the positive charge potential of MIDAS  $Mg^{2+}$  towards the RGD Asp, caused by the increased distance of a MIDAS coordinating integrin Asp side chain and the direct linkage of the ADMIDAS and MIDAS metal cations which reduces the negative charge influence of another integrin Asp side chain towards the MIDAS cation; (3) the establishment of additional interactions of the RGD Asp-side chain to the  $\alpha 1$ -loop backbone; and (4) the formation of a binding pocket for RGD Arg in the  $\alpha$  subunit ligand binding surface. In those integrin heterodimers carrying an inserted  $\alpha I$ -domain, the  $\beta I$  domain of the  $\beta$  subunit is thought to bind an invariant Glu ligand within the  $\alpha I$  domain in a similar manner as described above, which propagates according shifts of the  $\alpha 1$  and  $\alpha 7$  helix of the  $\alpha I$  domain, allowing ligand binding. However, the structural details of the conformational changes are slightly different, leading to bigger movements of the MIDAS site<sup>32</sup>.

### 1.2.3. Integrin activation requires large conformational changes

Previous research underlines the essential role of the hybrid domain swing out for integrin activation, but also suggests that different degrees of swing out might correspond to different degrees of affinity and overall conformations of the integrin heterodimer (reviewed in <sup>13, 20, 33</sup>).

In all published crystal structures of the complete integrin ectodomain, the proteins adapt a very compact shape, which is described as “bent” conformation and is suggested to represent the resting or inactive state of the integrin. However, it has to be kept in mind that those heterodimers, which were not analyzed may adopt different conformations in the resting state. Biophysical studies using Förster Resonance Energy Transfer (FRET), FRET Lifetime imaging (FLIM) (see 1.3.4) or analytical ultracentrifugation as well as biochemical cross linking and antibody binding studies (see below) are in agreement with the existence of this bent state *in vitro* and *in vivo* for certain integrins (for example  $\alpha v\beta x$  or  $\alpha IIb\beta 3$ ) <sup>31, 34</sup>, while for other integrins direct structural evidence is sparse ( $\alpha 5\beta 1$  or  $\alpha 4\beta 7$ ). Therefore, the situation remains controversial <sup>2, 25, 35, 36</sup>.

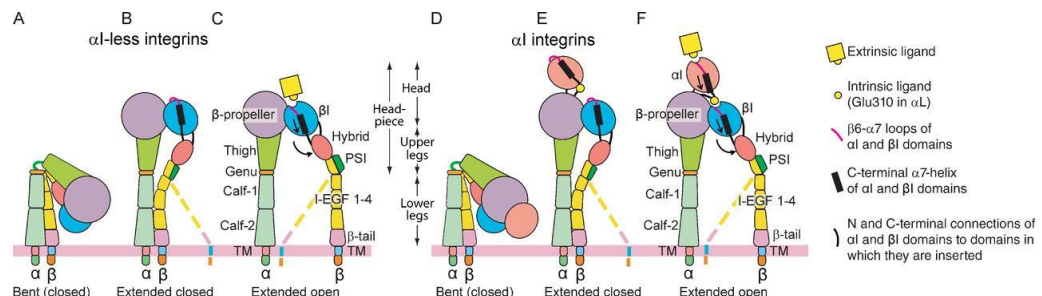


Figure 5: Schematic depiction of gross conformational changes in  $\alpha I$ -less (A-C) and  $\alpha I$ -containing integrins (D-E), leading to integrin activation <sup>30</sup>. In the bent/inactive state (A,D), no ligand binding can occur due to the orientation and closed conformation of the headpiece, stabilized by tight interactions of the hybrid domain and the integrin legpiece regions. Upon integrin “priming” through intracellular cues, the integrin adopts an extended, ligand binding competent conformation (B,E). Ligand binding induces conformational changes in the headpiece, resulting in an “open” conformation and this change is coupled to the hybrid domain via pistoning of the  $\beta I$ - $\alpha 7$ -helix (black cylinder), leading to hybrid domain swing out and stabilization of the “open” high affinity conformation (C,F). The contribution of integrin leg-domain unclasp remains unclear (streaked lines) and similar conformational changes occur in  $\alpha I$ -domain containing integrin heterodimers.

For those integrin heterodimers, which are bent in their inactive state, hybrid domain swing out is thought to be directly coupled to integrin extension, as the movement of the hybrid domain would interfere with interactions formed to the  $\alpha$  integrin leg region

(see Fig. 5A,D). In the bent  $\beta$  integrin several interactions are formed between the  $\alpha$  and the  $\beta$  subunits: the  $\beta$  integrin EGF-2/3 domains interact with the  $\alpha$  integrin Calf-1 domain, the  $\beta$  integrin tail domain interacts with the  $\alpha$  integrin Calf-2 domain and the  $\beta$  integrin transmembrane domain interacts with the  $\alpha$  integrin transmembrane domain. Altogether, this results in an unusual orientation of the integrin head domains towards the cell membrane, interfering with ligand interaction and constituting one mechanism for integrin ligand “on-rate” regulation. Indeed, it has been shown that integrins trapped in this conformation cannot mediate ligand binding when expressed on cell surfaces<sup>31,33</sup>. The affinities of closed, primed and fully activated  $\alpha\text{L}\beta\text{2}$  integrin increase from 2mM over 3 $\mu\text{M}$  to 200nM<sup>6</sup>. This three step-model of on-rate regulation appears very attractive for integrin heterodimers of the hematopoietic system, which need to be tightly regulated in their ligand binding, as “unwanted” or uncontrolled ligand interaction could lead to harmful blood clotting. In contrast, such a tight control would not be necessary for constitutive adherent cells (as fibroblasts or epithelial cells), which are characterized by high expression of  $\beta\text{1}$  integrin heterodimers. In line, EM experiments have indicated that “clasped”  $\alpha\text{5}\beta\text{1}$  integrin under non-stimulatory cation concentrations does not adopt a bent conformation and shows high affinity to FN (35nM), which only slightly increases upon transition into the unclasped, active form (6.3nM)<sup>36</sup>.

The current model of integrin activation suggest that the shallow angle of the hybrid domain towards the  $\beta\text{I}$  domain in the bent state does not allow ligand binding and thus, unbending of the integrin is essentially required to allow high affinity ligand binding (switchblade-activation model; see also Fig. 5B,E)<sup>33</sup>. However, this concept remains controversial, as two publications have observed ligand binding of integrins in a bent conformation, which lead to the suggestion of an alternative “deadbolt” activation model. Further experiments have disproven the suggested underlying molecular mechanism of this model<sup>33</sup> and suggested instead conformational intermediates between the bent and extended form (referred as “breathing”), which might allow ligand binding in a partially unbent integrin connected to a partial release of the conformational constraints of the hybrid domain.

#### 1.2.4. Integrin activation can be mediated from “inside” to the “outside”

The more physiological mechanism of integrin activation is thought to be induced by intracellular ligands of the  $\beta$  integrin subunit (inside-out signaling), suggesting a specific sequence of events during integrin activation. In order to allow such an activation mechanism to work, initial conformational changes are thought to be induced through interaction of talin and kindlin proteins with the cytoplasmic  $\beta$  integrin tails. Most likely, these interaction can lead to the disruption of several interactions of both integrin subunits on the intracellular side, in the transmembrane region and in the extracellular transmembrane region leading to the separation of both subunits (“unclasp”) and subsequent integrin unbending representing a “primed” state of intermediate affinity. Furthermore, unclasp has been shown to allow steeper angles for the hybrid domain swing-out leading to a decrease of the off rate<sup>31, 36</sup>, stabilizing ligand binding and allowing cell spreading and integrin mediated signaling<sup>34, 37</sup>. On the other hand, this picture is most likely not complete, since it has been shown that integrin unclasp is not required for high affinity (“on-rate”) ligand interaction<sup>31, 36</sup> or cell adhesion<sup>2, 37</sup>. This suggests that interaction of talin or kindlin might contribute to integrin extension and affinity regulation also by other means than unclasp. Indeed, talin- or kindlin-mediated integrin interaction and force transduction through activated, ligand bound integrins has been suggested to further decrease the off-rate in unclasp independent ways by unclear molecular mechanisms, which will be discussed next.

### 1.2.5. Force generation

As indicated above, integrin function is tightly coupled to the anchorage to the actin cytoskeleton and transmission of intracellular generated forces through the integrin

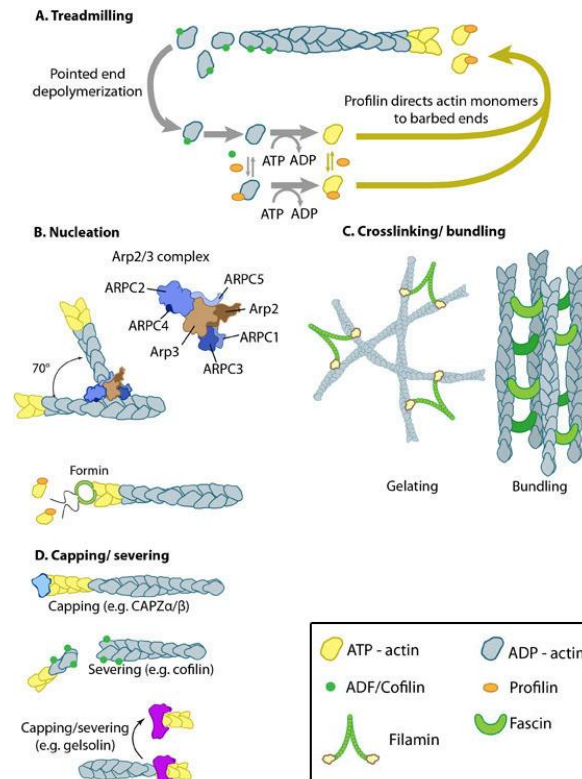


Figure 6: Mechanisms of actin polymerization (modified from MBInfo Wiki). (A) Actin is assembled at higher rate at the barbed end as it disassembles at the pointed end, leading to "treadmilling" actin polymerization. (B) Arp2/3 complex leads to nucleation of actin filaments and actin branching, while formins promote actin filament growth. (C) Actin cross linking proteins organize different actin structures. (D) Actin capping proteins inhibit actin filament growth by blocking the barbed end and severing proteins can promote actin polymerization by cleaving preexisting actin filaments.

onto the ECM, enabling cells to migrate on the ECM or to remodel it through firm interaction. Actin can principally generate force through two distinct mechanisms; via polymerization and molecular motors<sup>38 9</sup>.

Actin polymerizes at the leading edge of the cell membrane, which leads to force generation. On the one hand, the cell membrane is pushed forward, leading to membrane protrusion.

On the other hand, the rate of actin polymerization exceeds the rate of membrane protrusion, which results in a retrograde flow of the actin towards the cell center, which generates force on proteins, which interact with the

actin filaments. The polymerization of actin cables is initiated through an actin nucleating complex of Actin Related Proteins 2/3 (Arp2/3) and further binding of an actin monomers to the barbed end of a preexisting actin cable is favored through ATP hydrolysis and can be enhanced through formins leading to polymer formation (Fig. 6A,B). As long as the polymerization rate exceeds the disassembly rate at the pointed ends (actin treadmilling) the actin cable grows in a directional manner (Fig 6A). The polymerization is tightly controlled by a complex network of proteins providing ATP-bound actin monomers, initiating nucleation and branching, promoting elongating,

cross-linking between actin cables, or severing of cables by proteins such as profilin, Arp2/2, formins, fascin or cofilin, respectively (Fig. 6B,D). These processes are regulated through Rat sarcoma homologue (Rho)-GTPases like RhoA, Cell division control protein 42 homolog (Cdc42) or Ras-related C3 botulinum toxin substrate 1 (Rac1) and their specific Guanosine Triphosphate Exchange Factors (GEFs) and GTPase-Activating Proteins (GAPs), which link actin dynamics to transmembrane receptor signaling. The localized expression and activation of these proteins drives lamellipodial cell protrusion and formation of filopodia, invadopodia or membrane blebbing by generating force upon the cell membrane and attached cell membrane receptors<sup>38,39</sup>. Indeed, it has been shown that lamellipodial actin polymerization leads to the formation of a protrusive dendritic actin network, controls lateral movement of integrins and accumulation of active integrins at the cell periphery as well as nascent adhesion assembly. Conversely, integrin interaction with the dendritic actin network can promote the actin polymerization driven cell membrane protrusion<sup>9,40</sup>.

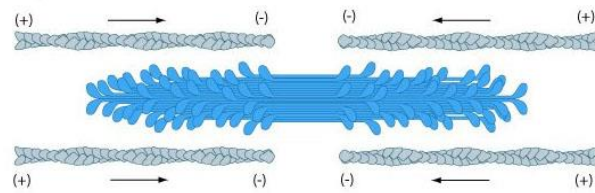


Figure 7: Myosin filaments (blue) promote anti-parallel actin cable movements (modified from MBInfo Wiki).

Myosin motors constitute another mechanism for force generation through the actin cytoskeleton. In fibroblasts, myosin II forms filaments which undergo ATP driven

conformational changes leading to the movement of two anti-parallel actin cables in opposing directions (see Fig 7). The force generated through these myosin II filaments in the region of the central cell body is transmitted through long bundled actin cables, which require  $\alpha$ -actinin for their formation. The linkage of these cables to integrin adhesion sites in turn is mediated through multiple further proteins, most prominently  $\alpha$ -actinin, migfillin, parvin, talin and vinculin. Force transmission through myosin motors to the integrins is associated with adhesion strengthening and formation of larger integrin clusters (see 1.2.6 for details).

#### 1.2.6. Models for off-rate regulation

The abovementioned conformational changes of integrins significantly contribute to the overall adhesive phenotype of cells on integrin ligands. However, also other

mechanisms of integrin mediated cell adhesiveness regulation have been proposed. The factors contributing to this can be classified according to a recent review article <sup>6</sup>: Affinity regulation, valency regulation and adhesion strengthening (see Fig. 8).

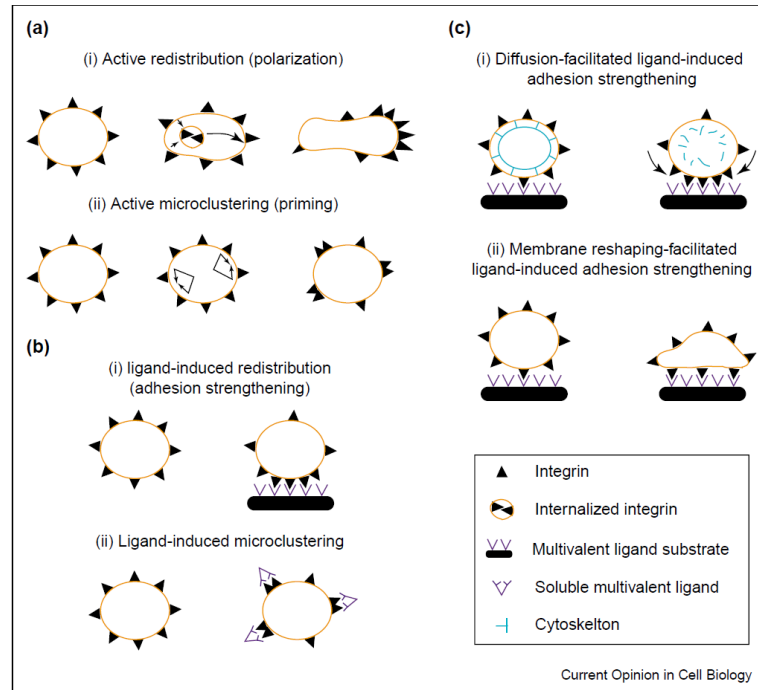


Figure 8: Valency regulation and adhesion strengthening modes <sup>6</sup>. (A) Integrins cluster on the cell surface prior to ligand binding. (B) High densities of surface immobilized ligands or solvent multivalent ligands induce integrin clustering. (C) Detachment of integrins from a cortical actin network facilitates ligand induced integrin clustering (upper side); relaxation of the membrane tension supports integrin-ligand interaction through a higher contact area to surface immobilized ligands.

Affinity regulation comprises conformational changes within single integrin heterodimers as discussed above (1.2). Valency regulation describes changes in the diffusion freedom of single integrins, leading to changes in local density and geometry of integrin containing membrane sections. In contrast, adhesion strengthening describes ligand binding-dependent changes either in the local density of integrin receptors or the adhesive strength of single molecules through receptor interaction with the cytoskeleton. In the following paragraphs the contribution of these factors will be discussed.

#### 1.2.6.1. Valency regulation

Although structural data suggests a clear mechanism for the conformation-dependent regulation of integrin affinity, the measurement of affinity changes on cells is difficult (see also 1.3.2). Multiple reports describe differences in cell adhesiveness despite an apparent lack of differences in the ligand binding capability<sup>41, 42</sup>. For example, increased  $\alpha\text{L}\beta\text{2}$  mediated leukocyte adhesion has been observed upon several intracellular activatory stimuli (e.g. PKC activation or talin overexpression) in the absence of increased soluble ligand binding<sup>42</sup>. This has led to the suggestion that at least in some cases integrin mediated cell adhesiveness might be regulated through changes in the valency rather than through changes in affinity<sup>42</sup>. This hypothesis requires an active redistribution of integrin heterodimers into micro- or even macro-clusters (compare Fig. 8A) in order to increase the general adhesiveness of the affected cell membrane region. However, the mechanisms for such an active redistribution are unclear and experimental evidence remains elusive<sup>6</sup>. For example, lipid rafts have been discussed to promote integrin micro clustering, but the experimental results were controversial. Also, no experimental evidence has been found that homotypic interactions of isolated integrin transmembrane domains, which have been observed in artificial membranes, may also occur in intact cells. Integrin clustering on multivalent ligands could be negatively regulated through mechanisms, which restrict the diffusion of single integrin receptors in the cell membrane. It has been shown that the actin cytoskeleton in close proximity to the cell membrane can define nano-scale membrane domains which limit the long range diffusion of included membrane proteins directly and indirectly<sup>43, 44</sup>. Furthermore phorbol ester (Phorbol-12-myristat-13-acetat; PMA) induced interaction of talin with  $\alpha\text{L}\beta\text{2}$  integrin (see 1.4.3 for details) has been shown to increase diffusion of this leukocyte specific integrin<sup>45</sup>. However, the release of integrins from cytoskeletal constraints through actin depolymerizing drugs or stimulation with PMA does not promote integrin clustering in the absence of a multivalent ligand for  $\alpha\text{L}\beta\text{2}$  or  $\alpha\text{IIb}\beta\text{3}$ , as measured by FRET analysis (see 1.3.4 for details on the method)<sup>46, 47</sup>. Interestingly, it has been shown that soluble ligand-induced integrin clustering cannot induce integrin signaling in comparison to immobilized ligand induced clustering, raising the question which function might be

associated to soluble ligand induced clusters <sup>48</sup>. In summary, integrin clustering on soluble ligands appears as a regulated process with critically depends on the presence of multivalent ligands, however the biological significance of this process for cell adhesion and integrin mediated signaling remains unclear.

#### 1.2.6.2. Adhesion strengthening through integrin off-rate modulation

While the role of integrin clustering in the presence of monovalent, soluble ligands remains unclear, integrin clustering on surface immobilized ligands or soluble multivalent ligands can be readily detected <sup>49</sup>. The driving forces of these processes seem to be due to the affinity regulation of single integrins, while the actin cytoskeleton seems to influence clustering in a rather indirect manner (see above) <sup>6</sup>. A functional hierarchy has been suggested, in which the activation of integrin heterodimers allows their adhesion to their ligand, and the actin cytoskeleton can influence the extent, localization and shape of integrin clusters <sup>6, 9</sup>. For example, integrin clustering can be limited to small clusters or even inhibited, if actin tethering to integrins or myosin dependent force transmission are inhibited <sup>50</sup>.

A model, which was derived from the structural data discussed above, describes the influence of actin cytoskeleton to adhesion strengthening as follows (see Fig. 9)<sup>1</sup>: The connection of a bent integrin heterodimer to the lateral movement of the actin cytoskeleton via kindlin or talin adaptors might induce integrin unbending through frictional effects.

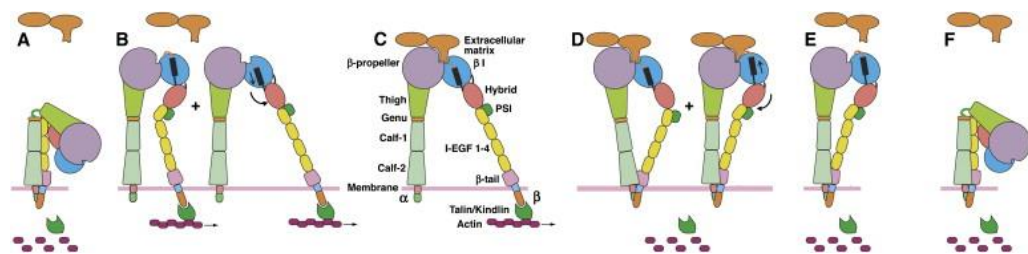


Figure 9: The integrin cycle <sup>1</sup>. (A) In the bent conformation, integrins have low affinity for ligand and adopt a bulky conformation. (B) Connection of the  $\beta$  integrin tail to laterally moving actin cables cause integrin unbending (left molecule) and eventually integrin unclashing (right molecule), which promotes a high affinity conformation of the integrin headpiece. (C) Binding to an immobile ligand leads to force transduction through the integrin molecule, which stabilizes the active conformation. (D) Upon disassembly of the actin cytoskeleton, clamping of the integrin heterodimer is favored (left side), which in turn promotes hybrid domain “swing in” (right side). (E,F) The resulting conformation promotes dissociation of the ligand (E) and bending of the integrin (F).

In the bent conformation the integrin heterodimer is relatively bulky and lateral movement through a crowded environment will induce leg separation, if the integrin heterodimer is pulled only via the  $\beta$  integrin cytoplasmic tail (Fig. 9A,B). Once the integrin adopts an extended conformation the friction is reduced and ligand binding can occur <sup>1</sup>. Next, ligand binding induces hybrid domain swing out, which further stabilizes ligand interaction through a decrease in the off-rate (Fig. 9B,C).

In addition to this off-rate regulation model, two further modes of actin dependent adhesion strengthening are described which do not require hybrid domain swing out: catch-bonds and cyclic mechanical reinforcement. These mechanisms seem to be integrin subunit specific, as they occur for  $\alpha 5\beta 1$  and  $\alpha L\beta 2$  integrins but cannot be confirmed for  $\alpha v\beta 3$  or  $\alpha IIb\beta 3$  integrins <sup>51-56</sup>. Usually the half-life time of the binding between two interaction partners linearly decreases with increasing pulling force between the partners (slip-bond). In contrast, catch-bonds describe a rather unusual binding mode between two interaction partners, in which an increasing pulling force first also decreases the interaction half-life time, but then leads to a strong increase in the interaction stability, which only decreases again at much higher forces. For the catch-bonds formed in  $\alpha L\beta 1$ , molecular modeling suggest a mechanism where a pulling force transmitted through the ligand stiffens the connection of the  $\alpha I$  domain MIDAS to the  $\beta 1$  MIDAS through the  $\alpha I$ - $\alpha 7$  helix leading to a more efficient high affinity conformation induction <sup>57</sup>. For the  $\alpha 5\beta 1$  integrins, experimental and molecular modelling data suggest that enhanced engagement of the FN synergy site under force might explain the observed catch bond behavior <sup>54</sup>. In a follow-up study a further actin-pulling force mediated mechanism is described which enhances  $\alpha 5$  integrin affinity to its ligand and was termed cyclic mechanical reinforcement <sup>55</sup>. In this case, a short interval of high pulling force followed by the release of this force on  $\alpha 5\beta 1$  integrin heterodimers lead to a remarkable increase of the half-life time of the ligand receptor bonds. Unfortunately, the underlying mechanism remains unclear.

Taken together, actin pulling force induced hybrid domain swing out, catch-bonds and cyclic mechanical reinforcement reveal interesting modes to mediate out-side in signaling and to regulate integrin-ECM interactions. Integrin tail separation upon actin mediated pulling forces could be the final step in the transmission of ligand binding

signal into the cell. This would explain why cells usually show no, or only weak signaling responses upon binding of monovalent or multivalent, soluble ligands but robust signaling and spreading on immobile ligands only upon integrin tail separation and force transduction<sup>2, 48, 58</sup>. Furthermore, all these mechanisms could contribute to the detachment of integrins from their ligands during cell migration, as reduced force transduction through integrins would lead to faster disassembly rates (see Fig. 9D-F). The importance of such mechanisms is underlined by experiments with cells expressing hyper activated integrins. Their expression leads to elongated cell morphologies and arrest of cell migration<sup>9</sup>, while inhibition of acto-myosin driven force transmission induces weakened adhesion and integrin mediated signaling<sup>48, 54</sup>.

Interestingly, the mechanical tensioning of integrins through the actin cytoskeleton also seems to be required for the formation of large scale integrin clusters<sup>9</sup> and conversely, a spacing of extracellular ligands larger than 70nm or cell adhesion on soft substrates inhibits the formation of large integrin clusters and formation of catch bonds<sup>54, 59</sup>. The relevance of clustering for adhesion strengthening has been described previously, showing that adhesive strength is determined by the amount and density of adhesive contacts<sup>48, 52</sup>. Furthermore, study of single molecule dynamics in focal adhesions could directly show the underlying principle of adhesion strengthening in clusters, where integrins can undergo several cycles of ligand binding and unbinding within short time<sup>60</sup>.

#### *1.2.6.3. Adhesion strengthening and integrin clustering*

Recently, a compelling hypothesis has been suggested, which can explain the interrelationship between integrin catch bond formation, clustering and signaling<sup>5, 61, 62</sup>: The theory is based on the observation that integrins in the cell membrane are surrounded by a dense environment of glycosylated proteins (glycocalyx), which extends from the cell membrane typically between 30-50nm (see also Fig. 10). Since this distance is usually larger than the length of extended integrins protruding from

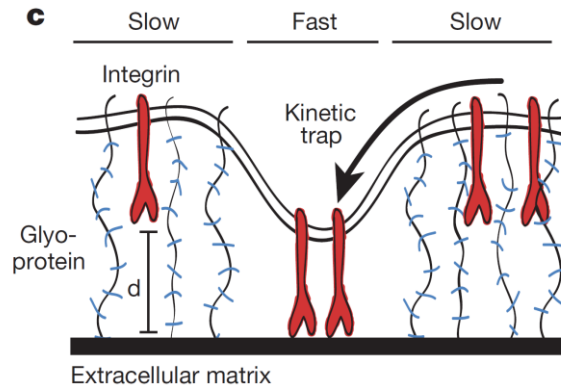


**Figure 10:** The role of glycocalyx for integrin clustering<sup>5</sup>. The glycocalyx is formed by extracellular, membrane bound glycoproteins (blue/black sinuous lines). Integrins (red) cannot reach to the ECM, when the glycocalyx is too high, thus local exclusion or compression of glycocalyx proteins and a membrane deformation are required for initial contact formation (slow process). Once such a structure has formed, other integrin molecules can quickly form further ECM contacts in close vicinity to the initial contact.

the cell membrane (~20nm), initial contact formation with the ECM requires local removal and compression of the glycocalyx and deformation of the cell membrane<sup>5, 63</sup>. Both factors effectively reduce the initial ligand-integrin interaction and thus the on-rate, however further contacts can much easier be formed in close proximity to the first contact. Consequently, integrins cluster around the initial

contact as soon as the contact is stabilized through actin anchorage (see 291.2.6.2). However, it remains unclear, which glycocalyx thickness is required to support this clustering mechanism and if other mechanisms exist in parallel. The force generated through the compression of the surrounding glycocalyx might further contribute to integrin catch-bond formation. Force-mediated integrin unclasp would serve as a positive feed-forward signal (mechano-sensing), through the initiation of integrin signaling which promotes local actin assembly, stress fiber formation and recruitment of integrin activatory adaptor proteins such as talin. Such small clusters can be observed in the leading edge of protruding cells and are termed nascent adhesions.

Interestingly, the exact mechanisms for the formation of such nascent adhesion sites remains unclear, as they can form independent from talin recruitment<sup>64</sup> but require the presence of ILK<sup>65</sup> and the polymerization of a dendritic actin network<sup>66</sup>. The linear actin cable, which is connected to nascent adhesions during the clustering process might serve as lattice for the recruitment of talin<sup>60</sup>, which in turn directs the insertion of further integrin molecules leading to the formation of slightly bigger focal complexes that reside at the border between lamellipodium (the zone of dendritic actin polymerization) and lamellum (see also Fig. 11) and require myosin II-activity<sup>67</sup>. If these complexes can be stabilized long enough, they will further mature into elongated

integrin clusters at a higher distance away from the protruding edge of the cell, termed focal adhesions (FA) (see Fig. 11).

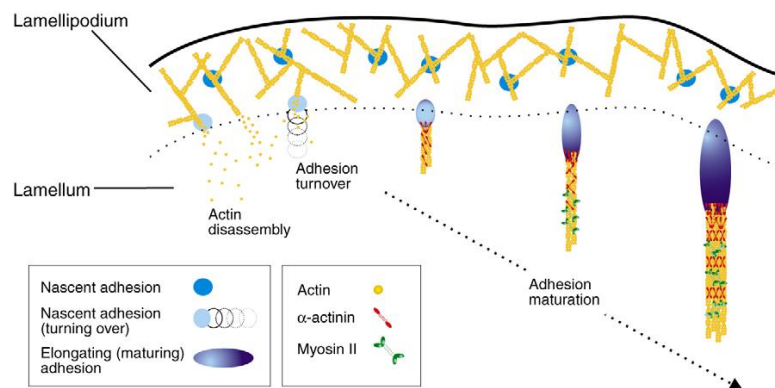


*Figure 11: Adhesion maturation<sup>9</sup>. Initial integrin contacts to the ECM are established in the lamellipodium, leading to the formation of nascent adhesions. Nascent adhesions are relatively short lived structures and disassemble when they enter the border between lamellipodium and lamellum. However, few nascent adhesions persist and mature into focal complexes and focal adhesions.*

The continuous actin mediated pulling force on the integrins in focal complexes and FAs leads to a centripetal translocation of  $\alpha 5\beta 1$  integrins, which are transported to the cell center, while  $\alpha \nu\beta 3$  integrins remain more static at the place of their initial insertion<sup>60, 68</sup>. Consequently, this leads to the formation of adhesion structures termed fibrillar adhesions, which are characterized by their elongated shape, localization in the cell center and enrichment of  $\alpha 5\beta 1$  integrin, ILK and tensin, while paxillin is absent<sup>69</sup>. These structures have been shown to be essential for the reassembly of the underlying fibronectin matrix into dense, fibrillar networks, dependent on actin contractility and presence of ILK<sup>65, 70, 71</sup>.

Finally, tight actin bundling coordinated with polymerization mediated by fascin, Arp2/3, Mammalian Diaphanous (mDia) and Neural Wiskott–Aldrich Syndrome Protein (N-WASP) can lead in a cell type-specific manner to the formation of invadopodia and podosomes characterized by a central actin core, which is usually smaller in podosomes. The actin rich core of invadopodia contains integrins and associated adaptor proteins with the exception of vinculin, while all of these proteins are excluded from the central actin structure of podosomes, leading to a characteristic ring shaped distribution. However, both structures share the feature of delivering vesicles containing enzymes with degrading properties, such as matrix membrane type 1 matrix

metalloprotease (MT1-MMP) or lysosomal proteins and protons. The release of the enzymes can lead to a localized degradation of ECM or calcified bone material, important for bone remodeling or cell invasion into dense ECM<sup>38,72,73</sup>.

#### 1.2.7. Further modes of regulation

In addition to integrin activation and adhesion strengthening, other mechanisms have been discovered modifying adhesion strength and integrin mediated cell migration: proteolytic cleavage, integrin co-receptors and integrin trafficking.

Degradation of the surrounding ECM is a phenomenon often observed in tumor and immune system cells during invasion events. Integrins have been shown to localize degradation to sites of adhesion (see 1.2.6.3 and<sup>74</sup>) and the resulting loss of adhesive stiffness promotes disassembly of integrin adhesion complexes (as discussed in 1.2.6.2 and<sup>75</sup>) allowing the cells to reorganize their cytoskeleton and invade the newly formed gap in the ECM. Furthermore, proteolytic Matrix Metalloproteinase-2 (MMP-2)-mediated degradation of  $\beta 1$  integrin or proteolytic activation of  $\alpha \beta 3$  integrin itself can contribute to increased motility of tumor cells<sup>74,76</sup>.

Cellular adhesion to the ECM and signaling in response to ECM interaction can be transmitted through various cell membrane receptors<sup>77</sup>, and is best understood for integrins and the family of syndecan receptors (reviewed in<sup>78</sup>). Syndecans consist of a membrane spanning core protein and a large network of glycosaminoglycans, which mediate the interaction to distantly located ECM proteins and growth factors. Intriguingly, many ECM ligands contain interaction sites for integrins and syndecans which are bound in a cooperative manner. Focal adhesion formation and cell spreading on FN depend on engagement of  $\alpha 5 \beta 1$  integrin and syndecan-4, while similar observations have been made for  $\alpha \beta 3$ -/ $\alpha \beta 5$  integrin with syndecan-1 on vitronectin and  $\alpha 2 \beta 1$ -/ $\alpha 6 \beta 4$  integrin with syndecans on laminin. In contrast, other integrin heterodimers, such as  $\alpha 4 \beta 1$  or  $\alpha 7 \beta 1$ , have been reported to function syndecan-independent. Mechanistically, it has been suggested that Protein Kinase C (PKC)-recruitment through the cytoplasmic tail of syndecan-4 can promote integrin mediated adhesion and signaling through direct effects of the PKC kinase, downstream formation of phosphatidylinositol (PtdIns)-4,5-bisphosphate (PtdIns-P<sub>2</sub>) and PKC-controlled integrin internalization (for details, see 1.4.3 and 1.5.1). Furthermore,

syndecans have been described to assist integrin-mediated activation of cellular Sarcoma kinase (Src) and Focal Adhesion Kinase (FAK).

Besides the aforementioned mechanisms, which control integrin clustering and affinity modulation, the localized internalization and exocytosis as well as trafficking of integrin containing vesicles are important mechanisms to control integrin function, which just currently evolves to be understood (reviewed in <sup>79</sup>). Recent studies indicate that integrin trafficking controls integrin stability, integrin distribution on the cell surface, and the signaling crosstalk with growth factor receptors and Rho GTPases, thereby affecting cell migration and tumor cell invasion directly and indirectly. Interestingly, inactive integrins and ligand-bound, active integrins use distinct trafficking routes, but the molecular mechanisms underlying their different trafficking are unknown. A recent publication shows that high  $\text{Ca}^{2+}$  concentrations in the ER and Golgi are required for correct folding and maintenance of integrins in an inactive conformation, which supposedly facilitates integrin maturation and export, while at the same time preventing ligand binding <sup>80</sup>. Therefore, it appears surprising that the integrin activation promoting adaptors talin and kindlin are suggested to influence integrin recycling as well as integrin maturation in the Golgi network <sup>81-84</sup>. In an early study talin deficiency correlates with retention of  $\alpha 5\beta 1$  integrin in the ER or Golgi accompanied by decreased glycosylation, indicative for a role of talin in the transport of this integrin through the ER and Golgi and its glycosylation. However, in a later study mutation of the talin interaction motif of  $\beta 1$  integrin as well as talin depletion leads to increased surface presentation and decreased internalization while no effect on integrin maturation can be observed <sup>83</sup>. In the same study, the influence of the kindlin-interacting motif and kindlin depletion is analyzed as well, leading to the suggestion that kindlin promotes maturation of  $\alpha 5\beta 1$  integrin and prevents its degradation after internalization and thus stabilizes surface expression. The role of kindlin on integrin maturation is confirmed in a further publication <sup>84</sup>, however a study similar to the first one cannot confirm any direct influence of kindlin on the integrin surface expression or recycling <sup>81</sup>. Instead, this work and a following publication suggest that the endosomal proteins Sorting Nexin 17 and 31 (SNX17 and SNX31), which bind to the same cytoplasmic  $\beta$  integrin tail motif as kindlins, favor the recycling of endocytosed

integrins over lysosomal degradation<sup>81,85</sup>. The conflicting observations might indicate that kindlin and talin influence integrin maturation in a cell type-specific manner.

### 1.3. Methods for the measurement of integrin “activation”

The aforementioned processes of integrin trafficking, valency regulation and integrin clustering as well as integrin conformational changes affect the adhesive and migratory behavior of cells. However, the assessment of these factors in living cells remains challenging and the interpretation of the resulting data can be complicated. Some of the most important methods to measure these processes will be discussed in the next paragraphs.

#### 1.3.1. Adhesion/Migration assays

The probably most intuitive way to study integrin function is the measurement of cell adhesion, spreading and migration on integrin specific ligands (reviewed in<sup>86,87</sup>). While adhesion assays measure the ability and kinetics of cells to adhere to a specific ligand, spreading and migration assays can help to understand the cellular response towards ligand binding. It is important to note that most cell lines can generate their own matrix upon plating. Also, typical supplements of cell culture media, such as fetal bovine serum, contain soluble integrin ligands like vitronectin or FN and differing concentrations of integrin affinity modulating divalent cations and growth factors. Therefore, caution has to be used in the choice of assay conditions and the length of the experiment. Ideally, assays have to be performed in defined media and for timescales shorter than one to two hours. Also the washing conditions used to remove unbound cells can critically influence the outcome of the experiment and reproducibility and have to be considered.

Ideally, adhesion assays are performed with variable timescales and densities of the integrin ligands in order to assess differences in adhesion kinetics, which can indicate differences in the induction and strengthening of adhesions. Adhesion strengthening and cell rolling caused by intermediate integrin activation can further be analyzed with the use of flow chambers, where a defined hydrodynamic shear stress is induced by pumping medium through a small channel<sup>88</sup>. Similar assays in substrate coated adhesion chambers, small glass capillaries or even in cremaster muscle arterioles of living mice are successfully used to study adhesion strengthening and integrin-

mediated cell rolling<sup>89-92</sup>. However, all these assays are mostly limited to the study of weak, initial adhesion, as detachment of strongly adherent cells cannot be achieved under such conditions. Furthermore, all these assays reveal only limited insight into the exact mechanisms of adhesion, as the molecular mechanisms of the observed cellular affinity remain unclear and need to be complemented with further analysis methods as discussed below. Also the study of the kinetics of cell spreading and cell migration has similar limitations and requires complementation with further methods (see below).

In order to improve the insights gained from adhesion and cell detachment assays, improved methods have been developed such as the spinning disc assay and probing of cells with ligand coated Atomic Force Microscopy (AFM) probes, coated beads in combination with magnetic tweezers or fluid chambers. For the spinning disc assay, cells are seeded on circular, ligand coated glass plates and rotated in Phosphate Buffered Saline (PBS) with defined speeds. By assessing the amount of detached cells in respect to the applied force, approximate measurement of ligated integrins and testing of different adhesion times and ligand densities, approximate estimations of the on- and off-rates of single integrins can be made. The usage of ligand-coated AFM probes or beads allows similar measurements in a more direct manner. By varying the contact time between the ligand and the cell and application and measurement of defined forces, rates for the interaction formation and dissociation can be estimated. However, also in these cases the underlying mechanisms of ligand interaction remain unresolved.

### 1.3.2. Cellular ligand binding assays

A more direct approach to the study of integrin activation is the analysis of the ligand binding ability of isolated cells. Full length ECM proteins, protein fragments or small molecule ligand mimetics can be used as ligands, as well as ligand mimetic antibodies (reviewed in<sup>88, 93</sup>). Cells are studied after detachment from their substratum by incubation with their ligand in solution, and ligand binding is measured after washing of unligated ligands in flow cytometry using either directly fluorescence labeled ligands or fluorescent antibodies. Under normal conditions, however, these assays are relatively insensitive and mostly report the on-rate of the measured integrins<sup>6</sup>. The

bent, low affinity conformation (2mM for  $\alpha\text{L}\beta\text{2}$ ) should usually not allow ligand binding, while the extended conformation with intermediate binding affinity (3 $\mu\text{M}$  for  $\alpha\text{L}\beta\text{2}$ <sup>6</sup>), which may represent the predominant conformation on non-hematopoietic cell lineages, binds ligand at intermediate affinity<sup>34</sup>. The difference between intermediate and high affinity is integrin heterodimer-specific; it is low for  $\alpha\text{5}\beta\text{1}$  (~5.5-fold; <sup>36</sup>) and a bit higher for  $\alpha\text{L}\beta\text{2}$  (~15-fold; <sup>6</sup>). Ligand binding is sufficient to induce the conformational transition from intermediate to high conformation. Thus, ligand binding assays will usually not distinguish or underemphasize the difference between intermediate and low affinity conformation. Also the contribution of hybrid domain swing out, which is supposed to stabilize ligand binding mostly through a decrease in the off-rate<sup>31, 36</sup> cannot be measured with standard ligand binding assays<sup>88</sup>. In order to circumvent these problems, recent progress has been made with flow cytometers, which allow the exact timed addition of ligands to the cells<sup>88</sup>. Through variation of incubation times and further addition of agonists or competitors, on- and off-rates can be determined. However, these measurements require highly advanced machines and trained operating scientists.

Similar to the binding of monovalent ligands, multivalent ligands are often used to measure the influence of micro-clustering on ligand binding affinity. The measurement of multivalent ligands typically results in higher signal intensities in comparison to monovalent fragments, which is interpreted as more stable binding through integrin clustering on these ligands<sup>94, 95</sup>. However, the interpretation of these results is often further complicated by the possibility that binding of a multivalent ligand through a single integrin also leads to an increase in signal intensity, since the multivalent ligand usually harbors more fluorescence tags. In addition, the same problems as reported for monovalent binding assays are even more pronounced here, because the micro-clustering of integrins should exclusively control the off-rate of ligand binding. Furthermore the mechanisms controlling integrin clustering in suspended cells remain unclear (see 1.2.6.1) and will most likely differ from the mechanisms required for integrin clustering on immobilized ligands (see 1.2.6.2 and 1.2.6.3). Altogether, the information received from ligand binding experiments is mostly limited to the on-rate of integrin-ligand interaction, as under the usual washing conditions ligand dissociation rarely occurs<sup>88</sup>.

### 1.3.3. Activity reporting antibodies

As an additional tool for the study of integrin activation, conformation dependent antibodies were generated in mice and rat, which prevalently recognize human integrins<sup>93,96</sup>. These antibodies are easy to use and can be of tremendous importance for the study of integrin activation, as they specifically recognize integrins in distinct conformations, induced by ligand binding or divalent cations (reviewed in<sup>93,97</sup>).

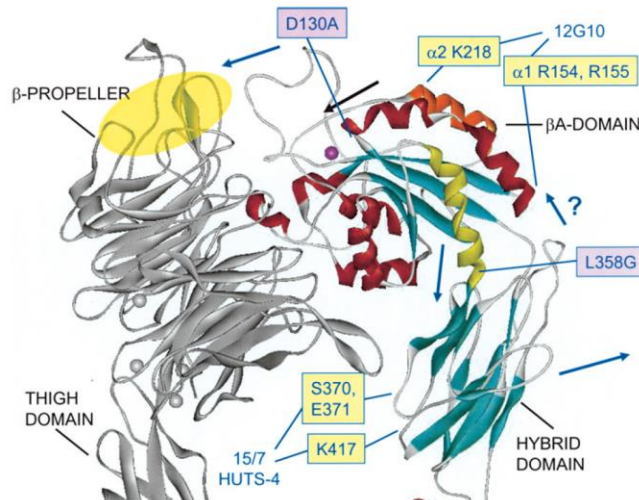
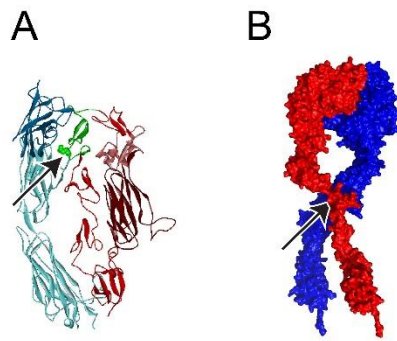


Figure 12: Epitopes of 12G10 and HUTS-4 antibodies<sup>4</sup>.

However, care must be taken, as many of these antibodies not only report but also induce the exposure of activation dependent epitopes and thereby influence the activation status of the analyzed integrin. The majority of activation reporting antibodies bind to the headpiece domain of the integrin heterodimer. For example, 12G10 antibody, which binds to the  $\alpha 1$ - and  $\alpha 2$ -helices of the  $\beta 1$ -domain of the  $\beta 1$  subunit only in the active conformation (see Fig. 12)<sup>98</sup>, can be used to detect the conformational changes important for on-rate regulation<sup>99</sup>. However, 12G10 has been shown to be a strong inducer of integrin ligand binding and therefore, is only of limited use for the study of integrin activation<sup>99,100</sup>. Accordingly, HUTS antibody can only bind to the hybrid domain after swing out and thus reports an important step for off-rate regulation (see Fig. 12), but also stabilizes this conformation leading to an equilibrium change<sup>2,98</sup>. In contrast to the described examples, the exact binding site and associated integrin conformation of many other integrin reporting antibodies is unknown or map to the leg regions of the integrin heterodimer, which further complicates the interpretation of results. For example, SNAKA51 antibody detects an active, extended conformation of the  $\alpha 5$  legpiece domain important for FN assembly into fibrils. However, in cell stainings it preferentially labels fibrillar adhesions and much less FA<sup>35</sup>, raising the question which conformation this antibody reports and

how its binding to floating cells can be interpreted. Also, since this antibody labels a region of the integrin heterodimer, which is quite distantly localized from the ligand binding site, the question remains, how exposure of the referring epitope correlates to ligand binding. Similarly, binding of 9EG7 and KIM127 antibody to the EGF-2 domain of the  $\beta$ 1- or  $\beta$ 2-legpiece domain, respectively, have been associated to integrin activation, although the understanding of the associated conformations remains unclear<sup>2,101</sup>.



*Figure 13: 9EG7 epitope exposure in bent and extended conformations (modified from<sup>1,2</sup>). (A) Legpiece domains of a molecular model of bent  $\alpha$ 5 $\beta$ 1 integrin. The headpiece is not shown,  $\alpha$ -subunits are drawn in blue shades and  $\beta$  subunits in red shades. The EGF-2 domain is highlighted in green and an arrow indicates the position of 9EG7 epitope, which is concealed in this conformation. (B) Molecular model of "primed"  $\alpha$ 5 $\beta$ 1 integrin;  $\alpha$ -subunits are blue and  $\beta$  subunits are red. The arrow indicates the position of the 9EG7 epitope, which is also not accessible.*

Both antibodies can only be weakly induced by factors which modulate integrin headpiece activation (ligand binding,  $Mn^{2+}$ ,  $Ca^{2+}$ , EDTA) but show excellent correlation with the ability of a cell to adhere<sup>102</sup>. For 9EG7 binding it has therefore been suggested that this reports integrin-"priming", dependent on the separation of the integrin heterodimer leg domains, which render the  $\alpha$ 5 $\beta$ 1 integrin into a ligand binding competent state with intermediate affinity of the integrin headpiece domain<sup>2</sup>. In the referred publication, the authors further suggest that integrin bending would conceal the 9EG7 epitope (see Fig. 13A) and integrin extension could reveal it. However

the question, if  $\alpha$ 5 $\beta$ 1 integrin actually exists in the assumed bent state is unclear (see 1.2.3). The same authors report that the 9EG7 epitope remains concealed in integrins after induction of hybrid domain swing out and in integrins which mediate cell adhesion and spreading. These results suggest that 9EG7 epitope also remains concealed in an extended conformation until the integrin leg domains are separated. In line, molecular modelling supports this alternative interpretation of the results and suggests that the 9EG7 epitope is concealed between the EGF-2 domain of the  $\beta$ 1

subunit and the Calf-2 domain of the  $\alpha 5$  subunit (see Fig. 13B) and only unmasked upon integrin unclasping (see 1.2).

In summary, although activation reporting antibodies still constitute the most powerful tool to reveal changes in integrin conformations induced by intracellular and extracellular stimuli, care must be taken in the interpretation of the results, as structural data clarifying the exact nature of the bound conformation is mostly missing.

#### 1.3.4. Further Methods

Since integrin activation is coupled to large conformational changes such as unbending and separation of the two leg domains, further methods have been developed to directly study these changes. Many of these methods take advantage of non-radiative energy transfer from an excited to a non-excited fluorophor leading to fluorescence of the initially non-excited fluorophor, referred to as FRET (reviewed in <sup>10</sup>). This energy transfer requires that the excitation spectra of the used fluorophores do not overlap, while the emission spectrum of the donor fluorophor should overlap with the excitation spectrum of the acceptor fluorophor. Furthermore, the efficiency of this transfer strongly decreases with the distance between the two fluorophores allowing approximate distance measurements in the range of up to 10nm. While FRET measurements can be done with standard microscopes, differences in fluorophor densities and weak overlap of the excitation spectra from both fluorophores often lead to artifacts. In order to achieve more exact measurements, bleaching of the fluorescence acceptor can be used allowing end-point measurements. Alternatively, the decrease of fluorescence lifetime of the fluorescence donor caused by the FRET can be measured (Fluorescence Lifetime Imaging; FLIM), allowing multiple measurements at one location <sup>10</sup>.

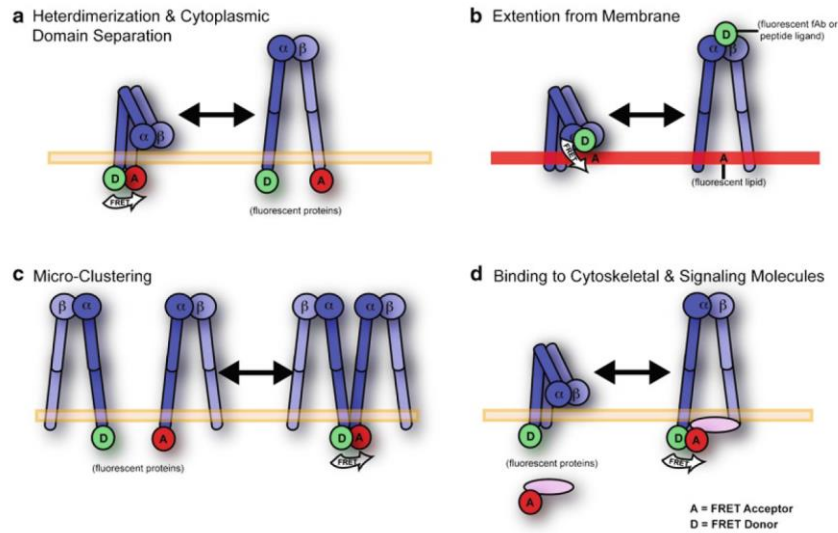


Figure 14: Usage of FRET sensors for measurement of different modes of integrin activation<sup>10</sup>. FRET/FLIM sensors allow the measurement of integrin unclashing (A), unbending (B), clustering (C) or binding of intracellular proteins (D).

For example, fluorescence labeling of the integrin head domain and the plasma membrane allows direct observation of integrin bending in response to different stimuli using the FRET and FLIM imaging (see Fig 14B)<sup>2, 10, 88</sup>. Similarly, the separation of the integrin leg domains has been studied by expressing integrin heterodimers with covalently tagged fluorescence markers (Fig. 14A) and integrin micro-clustering (Fig. 14C) has been measured by analysis of FRET between individual integrin heterodimers<sup>10, 46, 47</sup>. In a related approach, the angle in which the  $\beta 1$  integrin transmembrane domain transverses the cell membrane, influenced by talin could be studied<sup>103</sup>. The disadvantage of all these methods is that they require expression of integrins covalently conjugated to fluorescence tags or labeling with antibodies, which often compromise the function of the integrin heterodimer or cannot be used for the analysis of the endogenously expressed integrin.

The distribution of integrins into adhesive structures (also discussed in 1.2.6.3) and the dynamics of the formation and disassembly of these structures has extensively been studied with fluorescence microscopy. However, due to the limitation of the resolution to  $\sim 200\text{-}600\text{nm}$  governed by the wavelength of the used light, integrin localization and dynamics could only be studied for ensembles of molecules. Recent advances in microscopy have allowed to study integrin distribution and diffusion dynamics in a sub-

diffraction resolution of about  $\sim 50\text{nm}$  using Photo-activated Localization Microscopy (PALM)/Stochastic Optical Reconstruction Microscopy (STORM) or Stimulated Emission Depletion (STED) microscopy<sup>10</sup>. Briefly, the resolution limit of normal light field microscopy can be circumvented, if only single fluorescent molecules are studied at a time, which can be achieved through the usage of photo-switchable fluorophores. Although the fluorescence of these molecules still appears as a circular spot with a diameter of  $\sim 200\text{-}600\text{nm}$  (Airy-disc), the center of this airy disc, where the fluorophore is located, can be determined at much higher precision. Complete pictures of highly resolved structures can be achieved by frequent repetitions of single molecule imaging processes. Alternatively, the diffusional behavior of these single molecules can be tracked<sup>10</sup>. Such studies allow to track the diffusion of single integrin heterodimers in FA sites and the reconstruction of the spatial distribution of integrin molecules inside and outside of FAs<sup>5, 60, 104</sup>. Although these methods provide a clear improvement in the optical resolution, clustering of molecules at distances below  $50\text{nm}$  can only be indirectly assessed. Another arising approach is the study of fluorescence correlation between lowly concentrated fluorescent molecules. This method is based on the principle that two interacting, fluorescently tagged proteins diffuse as a pair in and out of a small optical field of view, leading to the correlation of the observed fluorescence intensity changes. With this methods, it was recently confirmed that certain proteins (like ILK, Pinch or parvin) enter and leave FA sites as a complex<sup>105</sup> and that initiation of  $\alpha 5\beta 1$  integrin adhesion to the ECM is accompanied by the formation of a stable complex with first kindlin and then talin<sup>104</sup>. However, it has to be noted that this method is not sensitive enough to track very short interactions and thus cannot be used to unconditionally exclude the possibility that such interactions occur.

#### 1.4. Integrin “activation” is mediated through kindlin and talin

As already indicated above, integrin activation is usually considered as a process, which is initiated upon binding of intracellular adaptor proteins such as kindlins and talins to the  $\beta$  integrin cytoplasmic tail. The details of this process will be discussed next.

##### 1.4.1. Talin can regulate integrin-mediated adhesion

Over ten years ago, it has been shown that the interaction of talin with integrin  $\beta$ -tail is important for integrin activation<sup>106</sup>. In mammalian cells two talin paralogues, talin-1 and -2 are expressed with differing tissue specificity. Interestingly, splice variants of

talin-2 are expressed in almost every tissue. However, full-length talin-2 is found at highest abundance in muscle tissues. Here, talin-2 is often co-expressed with the ubiquitously expressed talin-1, which is exclusively expressed as full length protein<sup>107</sup>. While a big range of experiments demonstrates an important influence of talin to cell adhesion *in vivo*, only few publications directly measure integrin activation. For example talin-1 is essential for integrin activation in platelets<sup>108, 109</sup>, but in muscle tissues which express talin-1 and talin-2 the situation is rather unclear<sup>110</sup>: Constitutive deletion of talin-2 leads to a mild muscle dystrophy<sup>110</sup> and deletion of both talin paralogues in skeletal mouse muscles impairs muscle development with a similar severity, as compared to  $\beta 1$  integrin deletion. However, neither  $\beta 1$  integrin activation measured with 9EG7 binding nor adhesion of isolated cells to ECM substrates are affected<sup>110</sup> suggesting that in this tissue talin might be more important for the connection of integrins to the intracellular actin cytoskeleton than for integrin activation. This hypothesis is supported by the observation of similar effects in the muscles of *D. Melanogaster*<sup>111-113</sup> and *C. Elegans*<sup>114</sup>. Furthermore, mutations, which affect talin binding to integrins do not recapitulate the developmental defects seen after depletion of kindlin-integrin interaction or  $\beta$  integrin depletion in developing zebra fish embryos<sup>115</sup>. Also *in vitro* experiments indicate that talin function is not sufficient to fully activate integrins. While most experiments demonstrate that talin controls integrin-mediated ligand binding<sup>108, 109</sup>, some reports indicate that talin depletion does not influence monovalent ligand binding of  $\alpha 11\beta 3$  or  $\alpha 4\beta 1$  integrins in suspended cells<sup>94, 116</sup>. Further experiments with talin depleted cells demonstrate a requirement for talin to stabilize initial adhesions against intracellular contraction, while cell adhesion and spreading are talin independent<sup>117</sup>. Finally, experiments with purified full length, lipid bilayer embedded  $\alpha 11\beta 3$  integrins showed that talin can induce integrin unbending and ligand binding only in a small fraction of the observed molecules<sup>118</sup>.

### 1.4.2. Structural organization of talin

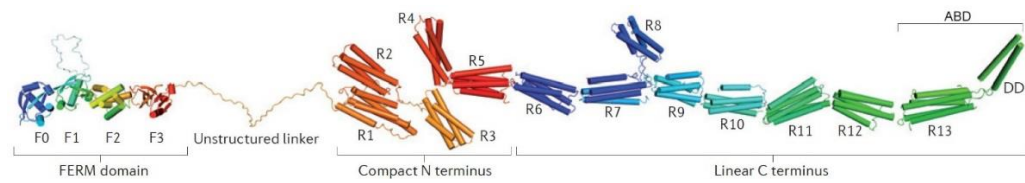


Figure 15: Domain organization and structural model of full-length talin (modified from <sup>119</sup>). The scheme shows a hypothetical structure of talin, composed of single structurally resolved sub-domains. Domains are indicated; F0-4 represents FERM sub-domains 0-4, R1-13 represents rod domains 1-13, DD stands for dimerization domain and ABD for actin binding and dimerization domain.

The highly conserved domain structure of talin-1 and -2 (see Fig. 15) gives mechanistic clues for the understanding of integrin activation, clustering and actin coupling activities of talin (reviewed in: <sup>119, 120</sup>). Talin is composed of a N-terminal 4.1-protein/Ezrin/Radixin/Moesin (FERM) homology domain and long rod formed by a series of thirteen 4- or 5- $\alpha$ -helix bundles and an C-terminally located actin binding and dimerization domain (ABD). The rod and FERM domain are connected by a large, most likely unstructured flexible linker region, allowing the whole molecule to adopt a fully extended conformation of approximately 60nm length as well as a globular dimeric conformation which is considered inactive. It is well established that talin directly interacts with the actin cytoskeleton via actin binding sites in the FERM domain, in the rod domain and in the ABD and indirectly through interaction with actin binding adaptor proteins as vinculin. The majority of vinculin interaction sites are buried in the  $\alpha$ -helix bundles and become exposed upon mechanical extension of the talin rod domain. Furthermore, several interaction sites for the Ras-related protein 1 (Rap1) GTPase effector Rap1-GTP-Interacting Adapter Molecule (RIAM) can be found in the rod domains. Talin binds to integrins via two integrin binding sites (IBS): the N-terminal FERM domain (IBS1) and the more c-terminally located IBS2, formed by two  $\alpha$ -helix bundles. The FERM domain consists of four subdomains (F0,F1,F2,F3), which adopt in contrast to other FERM domains an extended structure. Furthermore, the F1-3 domains harbour a series of basic amino acids which mediate binding to negatively charged PtdIns(4,5)P<sub>2</sub> rich cell membranes. For the F3 phospho-tyrosine-binding like domain, crystal structures have been resolved in complex with the hyaluronan receptor laylin, PtdInsP kinase  $\iota$  and several  $\beta$  integrin tails, which altogether showed similar but not identical binding modes resulting in different binding affinities <sup>121</sup>. Furthermore, FAK and the Rac1-GEF T Lymphoma Invasion and Metastasis (TIAM1)

have been shown to bind the F3 domain of talin. Interestingly, the interaction surface of FAK and  $\beta$  integrin tails in F3-domain mostly overlap, suggesting that F3 subdomain can either bind to  $\beta$  integrin tails or to FAK<sup>122</sup>. Importantly, the F3 and F2 domains have also been shown to interact with several negatively charged  $\alpha$ -helix bundles of the talin rod domain, masking the positively charged membrane binding domains and the integrin interaction site<sup>123</sup>.

### 1.4.3. Mechanistic insights into talin mediated integrin activation

Altogether, these structural features allow to understand how talin can become activated, bind to integrins and assist in integrin activation and clustering and finally

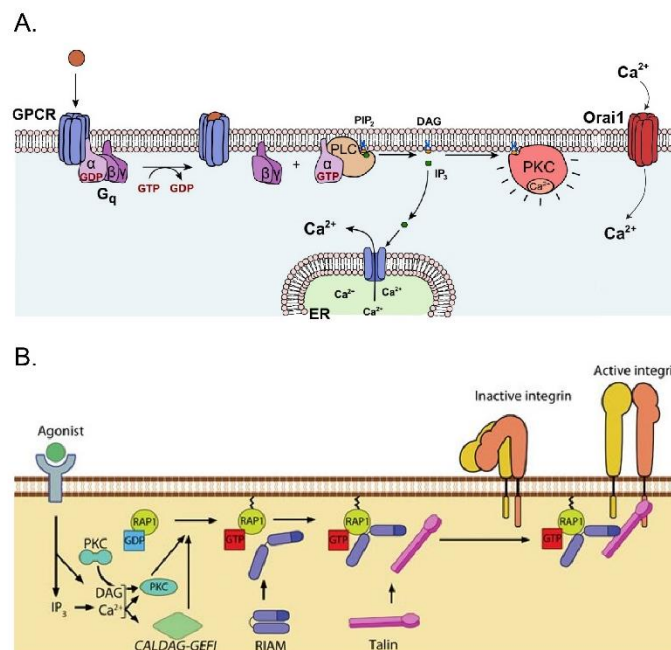


Figure 16: PKC mediated activation of talin. (A) Activation of PKC through Ca<sup>2+</sup> and Diacylglycerol (DAG). (modified from 7). Extracellular ligand binding by G-Protein Coupled Receptors (GPCR) leads to activation of G-proteins and Phospholipase C (PLC). PLC cleaves PtdIns(4,5)P<sub>2</sub> into DAG and Inositoltrisphosphate (IP<sub>3</sub>), which activates Ca<sup>2+</sup>-channels of the Endoplasmic Reticulum (ER). DAG serves as membrane anchor for PKC. Ca<sup>2+</sup>-influx is also stimulated through Orai1 channel involving Kindlin-3. High intracellular Ca<sup>2+</sup> levels activate PKC. (B) Receptor induced signaling leads to the activation and membrane recruitment of Rap1, which in turn recruits and activates RIAM (MBInfo Wiki). The Rap1-RIAM complex recruits active talin to the cell membrane, leading to integrin activation.

contribute to mechanosensitive adhesion strengthening and signaling (reviewed in<sup>119</sup>). In the cytosol talin is supposed to adopt a globular closed conformation, which inhibits membrane binding and interaction with integrins. The auto inhibitory rod domains not only masks the integrin binding site of the FERM domain but also prevents interaction with the cell membrane through its negatively charged surface<sup>123</sup>.

Several factors seem to cooperate in releasing talin from this auto-inhibited conformation: First, presence of PtdIns(4,5)P<sub>2</sub> in the cell membrane<sup>123,124</sup>. Second, binding of vinculin to the rod  $\alpha$ -helix

bundles that interact with the FERM domain can release auto-inhibition and promote membrane targeting of talin. Third, membrane targeting can be mediated through Rap1-GTPase, which becomes activated upon protease-activated receptor (PAR) stimulation or through Protein Kinase C (PKC), which also explains the stimulatory potential of PKC activating phorbol esters mentioned above (see Fig. 16A,B). Activated Rap1 localizes to the cell membrane, where it forms a complex with RIAM which in turn can recruit talin to the cell membrane in a PtdIns (4,5)P<sub>2</sub> dependent manner. Interestingly, presence of kindlin has been shown to be required for the Rap1-Riam mediated talin activation. However, the mechanism remains unclear<sup>125</sup>. Both talin activatory pathways share dependency on the presence of PtdIns (4,5)P<sub>2</sub> in the cell membrane. Fourth, talin can enhance its own activation and recruitment during early adhesion formation in a positive feed forward regulatory loop, as it recruits PtdInsP kinase Iy, leading to the formation of more activatory PtdIns (4,5)P<sub>2</sub>. In line, depletion of PtdInsP kinase Iy leads to slower recruitment of talin and vinculin to FAs<sup>126</sup>. Furthermore, talin recruitment of TIAM1 could lead to increased actin polymerization through a localized Rac1 stimulation, which further stimulates adhesion formation and cell spreading. Adhesion contacts increase PtdIns(4,5)P<sub>2</sub> levels, which raises the question how talin is localized to early adhesion sites or during initial cell adhesion. Finally, a recent publication has shown that the interaction of talin with FAK is required to localize talin to nascent adhesion sites. However the question how FAK was localized to these sites remains unclear<sup>122</sup>.

Once active talin has reached the cell membrane, it interacts with  $\beta$  integrin tails and promotes the dissociation of the membrane proximal interactions between the integrin  $\alpha$  and  $\beta$  subunits (see Fig 17A-D). Talin interacts with three regions of the  $\beta$  integrin tail and the interaction with a conserved Trp...Asn-Pro-x-Tyr (W...NPxY) motif (see Fig. 17A) appears to be important for the interaction strength. Interestingly, talin-1 and -2 show differences in their affinities towards  $\beta$ 3 and  $\beta$ 1A/ $\beta$ 1D cytoplasmic tails due to differences in the interaction interfaces. This explains, why talin-1, which has a much lower affinity than talin-2 to the  $\beta$ 1D isoform, cannot completely compensate loss of talin-2 in muscle<sup>127</sup>. In line, phosphorylation or mutation of the Tyr in the talin interaction site, as well as presence of proteins which compete with talin for integrin

binding, such as Dedicator Of Cytokinesis 180 (Dock1) or filamin, interfere with talin mediated integrin activation.

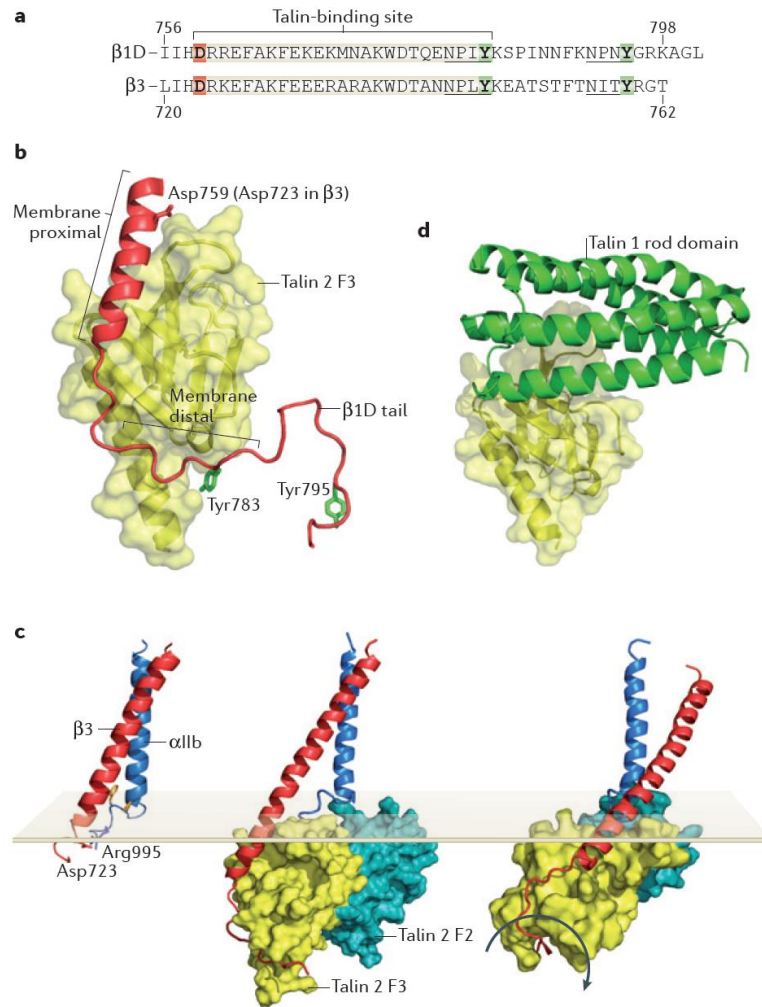


Figure 17: Mechanism of talin mediated integrin activation <sup>119</sup>. (A) Talin interaction site in  $\beta 1A$  and  $\beta 3$  integrin cytoplasmic tails. (B) Crystal structure of talin in complex with the 1D tail; Asp-759 and Tyr-783 are highlighted as key residues, important for talin mediated integrin activation and talin-integrin interaction respectively. (C) Model of talin mediated integrin activation: Tight interaction of the  $\alpha$ - and  $\beta$ -integrin transmembrane domains and a salt bridge between Asp-723 of the  $\beta$ -tail and Arg-995 of the  $\alpha$ -tail keeps the integrin in inactive conformation (left). Interaction of talin with the  $\beta$  integrin tail disrupts the salt bridge (middle). Next, interaction of talin with the cell membrane induces tilting of the bound  $\beta$ -tail, which promotes integrin tail separation (right). (D) Crystal structure of talin-FERM domain in complex with auto inhibitory rod domain.

The interaction with a membrane proximal Asp of the  $\beta$  tail seems to contribute to integrin activation (Fig. 17B,C), as this residue otherwise forms a salt bridge to the  $\alpha$  subunit that stabilizes integrin hetero dimerization. Furthermore, the interaction of the multiple basic residues of talin FERM domain with the cell membrane assist in tilting the whole transmembrane domain of the  $\beta$  integrin, which leads to the release

of the interactions between the  $\alpha$  and the  $\beta$  subunit in this region (Fig. 17C). The second IBS of talin is also essential for integrin mediated processes *in vivo*<sup>128</sup>, but the underlying mechanisms are less clear.

The potential to bind two integrins through IBS1, IBS2 in concert with the talin dimerization through ABD domain<sup>129</sup> suggest a role of talin as a scaffold for integrin clustering. In this respect it appears surprising that expression of the FERM domain alone can promote integrin clustering on soluble and immobilized ligands<sup>49, 94, 124</sup>.

Further, talin can also function as a mechanosensor as it responds to forces transduced through the actin cytoskeleton: a pulling force on talin leads to the exposure of cryptic vinculin binding sites, which in turn promotes further recruitment of vinculin. Consequently, talin can link several actin strands to one active  $\beta$  integrin tail, underlining the essential role of talin for the establishment of stable integrin-actin linkage and potential catch bond formation. Interestingly, the affinity of talin to a specific  $\beta$  integrin cytoplasmic tail can modulate the extent of this mechanosensing in such a way that higher affinities support better spreading, stress fiber formation and signaling on soft substrates<sup>121</sup>. This could also explain, why expression of talin head fragments was sufficient to stimulate integrin mediated ligand binding<sup>106</sup> but could not rescue signaling defects observed in talin depleted cells<sup>117</sup>.

In summary, current knowledge suggests a convincing mechanism, which explains how talin can promote integrin activation upon intracellular signaling and eventually contribute to actin linkage and adhesion strengthening through integrin clustering and catch bond formation. However, the observations in muscle tissue and other conflicting data suggest that talin alone is not sufficient for integrin activation or clustering. Furthermore it remains unclear, how talin gets initially recruited to nascent integrin adhesions.

#### 1.4.4. Kindlins contribute to integrin activation via unknown mechanisms

More recently, a second group of proteins essential for integrin activation has been identified, the kindlins. The kindlin family consists of three proteins in mammals with tissue specific expression pattern<sup>130</sup> and orthologues can be found in *D. Melanogaster*

(Fermitin1 and -2) and *C. Elegans* (UNC112)<sup>131</sup>. Depletion studies in the latter two model organisms demonstrate integrin-mediated attachment defects in the affected organs<sup>132, 133</sup> and integrin activation defects can be observed in mice for all three paralogues<sup>134-136</sup>. While the *in vivo* significance of kindlins for integrin mediated adhesion is evident, the mechanism(s) underlying kindlin-mediated integrin activation remain elusive. In *in vitro* studies, kindlin overexpression can only potentiate talin-mediated  $\alpha$ IIb $\beta$ 3 activation but not  $\alpha$ 5 $\beta$ 1 activation and overexpression of kindlin alone has no effects or even causes reduced integrin activation<sup>137, 138</sup>. Also, interaction of purified kindlin with integrin tails is not sufficient to unclasp the integrin heterodimer interaction at the level of the cell membrane<sup>139</sup>. One potential explanation for these observations might be that the high affinity of kindlin towards the integrin tail<sup>115, 139</sup> in combination with high endogenous expression levels might render most cell lines systems in a saturated situation in which further expression does not lead to further increase in integrin activation. This concept is underlined by the observation that minimal expression levels of kindlin-3 (~5%) are sufficient to maintain most integrin mediated functions, while complete deletion leads to a loss of integrin activation (personal communication by M Moser and<sup>135</sup>). The situation might be further complicated by the observation that the influence of kindlin or talin to integrin activation can only be observed after agonist stimulation (e.g. PMA stimulation) in several cell systems<sup>116, 140</sup>. Taken together, *in vivo* and *in vitro* studies draw a picture which appears paradoxically inverse to the situation observed for talin proteins: while all *in vivo* data clearly agree that kindlins are required for integrin activation, *in vitro* studies remain controversial.

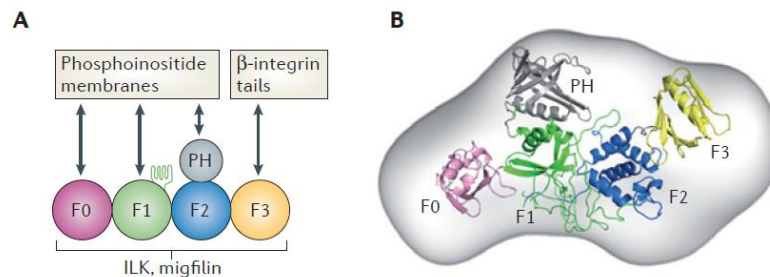


Figure 18: Kindlin domain structure<sup>119</sup>. (A) Schematic representation of kindlin domains and associated interaction partners. (B) Model of a hypothetical kindlin structure, obtained by SAX experiments (grey hull) and modelling of kindlin amino acids onto structures of talin and single resolved domain structures of kindlin.

Up to date, no complete structure of kindlin has been resolved. However, fragments could be analysed by NMR and crystallography. Kindlins consist of a FERM domain with high similarities to the talin FERM, which may also adopt an elongated structure (see Fig. 18A,B)<sup>141,142</sup>. Kindlins lack the long N-terminal rod domain of talins (reviewed in <sup>119,131</sup>). The second major difference to talin FERM domains is the insertion of a Pleckstrin Homology (PH) domain into the F2-subdomain, which mediates interaction with phospholipids in the cell membrane and assists in integrin interaction, but it remains unclear if the kindlin PH domain prefers PtdIns(4,5)P<sub>2</sub> over PtdIns(3,4,5)P<sub>3</sub><sup>143-145</sup>.

Similar to talin, the interaction of the F3 subdomain of kindlin with a membrane distal Thr-Thr...Asn-x-x-Tyr (TT...NxxY) motif in the  $\beta$  integrin tail (see also Fig. 17A)<sup>137</sup> is essential for integrin activation in isolated cells and *in vivo*<sup>81,135,136</sup>. Studies with mutated talin and kindlin interaction sites suggest that integrin activation requires binding of kindlin and talin to the same  $\beta$  integrin molecule. However, it remains unclear if this interaction needs to occur simultaneously or in a sequential manner (see Fig. 19)<sup>146,147</sup>.

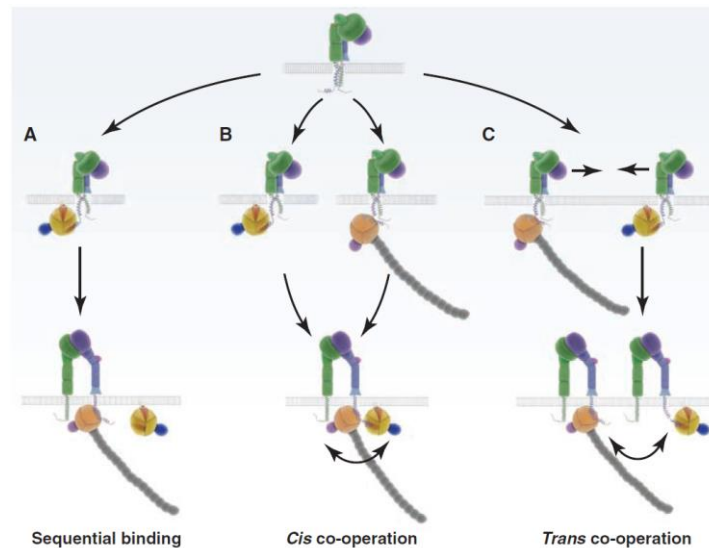


Figure 19: Different modes of co-operative integrin activation by kindlin and talin<sup>11</sup>. (A) Sequential binding of kindlin or talin. (B,C) Simultaneous binding of kindlin and talin at the same molecule (B) or two distinct molecules (C) leading to Cis-co-operation or Trans-co-operation respectively.

Kindlin isoforms differ in their  $\beta$  integrin tail binding affinities: kindlin-1 strongly binds to  $\beta$ 1 and  $\beta$ 6 integrin tails, kindlin-2 interacts strongly with  $\beta$ 1 and to a lesser degree with  $\beta$ 2 and  $\beta$ 3 tails and kindlin-3 seems to show weak binding to  $\beta$ 1-tails and may prefer  $\beta$ 2 tails<sup>119,136,148-150</sup>.

Mechanisms, which can explain these differences are emerging: A recent study shows that kindlin affinity to  $\beta$  integrin tails is modulated through the charges in the C-terminal proportion of the

$\beta$  tail. Kindlin-2 directly binds to the COOH terminus of  $\beta$ 1 integrin and presence of a positively charged Arg residue in the C-terminal proportion of  $\beta$ 2-tails reduces the affinity of this interaction<sup>115,139</sup>. Furthermore, binding of Integrin Cytoplasmic domain-Associated Protein-1 (ICAP1) competes with kindlin for overlapping interaction sites in the integrin tail and phosphorylation of the Tyr in the NxxY motif of  $\beta$  integrin tails recognized by kindlin interferes with interaction.

In contrast to talin, no clear mechanism is available describing how kindlins activate integrins. Interestingly, however, recent results<sup>149,151</sup> indicate that the region, which links the PH-domain of kindlin to its F2 subdomain mediates interaction with ILK<sup>134,152</sup>, and that this interaction may contribute to kindlin-mediated integrin activation<sup>143</sup>. In *C. Elegans* this interaction is proposed to mediate kindlin activation by regulating the ability of kindlin to interact with  $\beta$  integrin tails<sup>153,154</sup>. However, this function cannot be confirmed for mammalian cells, suggesting that this mechanism might be specific to nematodes<sup>149,151</sup>. Nevertheless, the interaction of ILK with the PH-domain region of kindlin seems to be required for the enhancement of kindlin recruitment to focal adhesions, kindlin mediated integrin activation and integrin signaling, although the mechanisms for these functions remain unclear<sup>149,151</sup>. ILK also interacts with lipid membranes through a PH domain<sup>155</sup>, which leads to the tempting hypothesis that membrane interaction of kindlin fulfils a similar role as for talin. This opens the possibility that kindlin could unclasp integrin heterodimers in a supporting membrane environment in concert with ILK interaction. Furthermore, migfilin binds kindlin and filamin with its Lin11, Isl-1 & Mec-3 (LIM) homology domains and interaction of migfilin to filamin competes with the interaction of filamin to  $\beta$  integrin tails<sup>156,157</sup>. Thus, it is suggested that kindlin mediated recruitment of migfilin to integrins may contribute to integrin activation by sequestering filamin<sup>119,157</sup>. However, mice deleted for migfilin show no integrin activation defects, raising the question how relevant this interaction is for integrin activation<sup>158</sup>. Similar to talin, kindlin controls integrin ligand binding through the induction of integrin clustering. While in one report the underlying mechanism remains unclear<sup>95</sup>, in the other case<sup>159</sup> kindlin regulates increased localization of the calcium channel Orai1 to adhesion sites under shear flow conditions.

Consequently, increased  $\text{Ca}^{2+}$  influx stimulates recruitment of talin via PKC signaling (see also Fig. 16) and growth of the integrin clusters.

In summary, the question if kindlin is essentially required for integrin activation remains controversial and mechanistic insights into the mode of kindlin mediated integrin activation are lacking. However, recent results showing that early adhesion complexes can form in the absence of talin<sup>122</sup> and that kindlin forms stable interactions with integrins in nascent adhesion sites before talin<sup>104</sup> question previously proposed models where kindlin recruitment to talin containing adhesion sites enhances integrin activation<sup>119, 160</sup>. Furthermore, these results raise the question, how the signaling molecules FAK and paxillin become recruited to and activated at nascent adhesion sites in absence of talin<sup>104, 122, 161</sup>.

## 1.5. Integrin mediated signaling

### 1.5.1. Overview of integrin mediated/influenced pathways

While those integrin functions, which relate to cell adhesion, migration and cytoskeletal organization can be explained by the ability of integrins to mechanically link the intracellular actin cytoskeleton to the ECM, conversion of those interactions into biochemical signals requires integrin mediated signaling in response to ligand interaction and tension sensing<sup>162</sup>. Because integrins lack intrinsic kinase activity, all these signaling processes have to be mediated by the recruitment of co-receptors as well as cytoplasmic adaptor and signaling proteins. The signaling outcome further depends on the composition of these signaling complexes, which changes over time and is further influenced by the size, shape and sub-cellular localization of the signaling complex (see also 1.2.6.3).

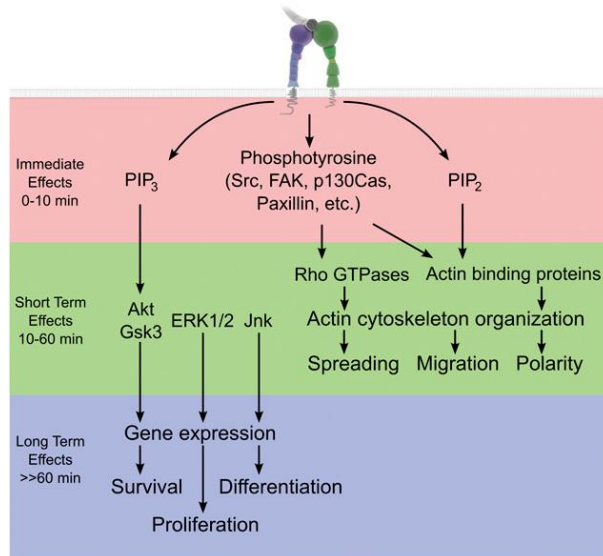


Figure 20: Consequences of integrin activation <sup>12</sup>.

High affinity interaction of integrins with their ligand requires direct interaction of the short cytoplasmic  $\beta$  integrin tail with the adaptor proteins kindlin and talin (discussed above, 1.4) in a process termed integrin activation or inside-out signaling. Upon establishment of the first contact of such an active integrin with the ECM, further integrins

and adaptor proteins are recruited to mediate integrin signaling (termed outside-in signaling) and firm adhesion. In several attempts to identify the participating proteins via mass spectrometric analysis an interaction network consisting of over 250 proteins has been identified, and over half of these interactions appear to be controlled via intracellular signaling pathways <sup>163, 164</sup>. The resulting signals can be grouped according to the time of their initiation during adhesion formation into immediate (0-10 minutes), short term (10-60 minutes) and long term effects (>60 minutes) <sup>12</sup>. The immediate cellular signaling events upon integrin activation comprise a local increase of lipid second messengers such as phosphatidylinositol PtdIns-4,5-P<sub>2</sub> and PtdIns-3,4,5-P<sub>3</sub> and increased Tyr phosphorylation of specific substrates, which assist the further recruitment of proteins and thus serves as signal amplifying mechanism. The increase in lipid secondary messengers is regulated via recruitment of Phosphatidylinositol 4-phosphate 5-kinase  $\gamma$  (PtdInsP kinase I $\gamma$ ) through talin, which in turn promotes further talin activation and recruitment (see also 1.4.3)<sup>126</sup>. The increased Tyr phosphorylation can be attributed to the paxillin dependent recruitment of focal adhesion kinase (FAK). FAK is a Tyr kinase which becomes activated at sites of active integrins and serves as a signaling platform for further kinases and signaling proteins, such as Src-family kinases and CRK-associated substrate (Cas) (see 1.5.1.4 and 1.5.1.5 for details). Furthermore, the second important signaling platform of integrins adhesion sites is ILK, which belongs to the earliest proteins recruited to initial adhesion

sites (see 1.5.1.2 for details). In the short term time range, cells can adopt the actin cytoskeleton to the newly formed adhesion sites, allowing changes in cell morphology and migration (as discussed in 1.2.5). Furthermore, the signals initiated during the immediate phase are transduced through Protein Kinase B (PKB also known as Akt), Glycogen Synthase Kinase (GSK), Extracellular-signal Regulated Kinases 1/2 (ERK1/2) and c-Jun n-terminal kinase (Jnk) activation. Finally, prolonged signal propagation through the latter proteins leads to changes in gene expression allowing the regulation of cell growth, proliferation and survival as well as adaptation to the local environment and differentiation. The exact mechanisms and dynamics underlying these processes, namely the role of kindlin, ILK, FAK, Paxillin and associated proteins will be discussed in detail next.

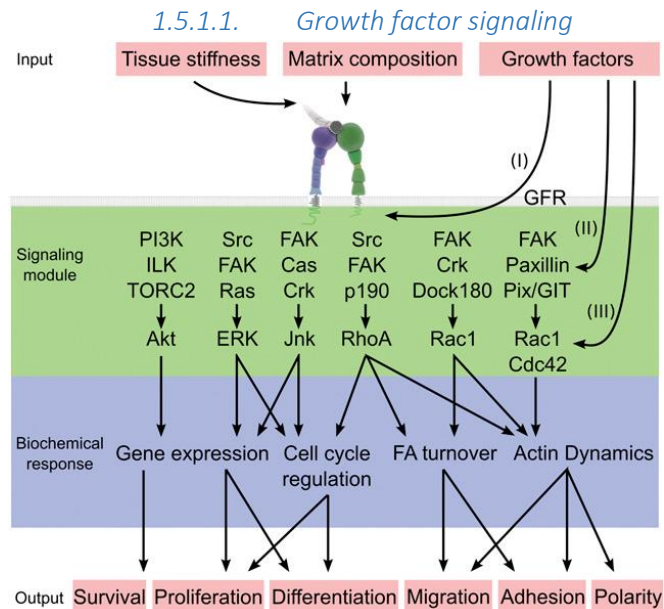


Figure 21: Integrin signaling and influence of growth factor signaling. Several exemplary signaling complexes downstream of integrins and influences of growth factor signaling are shown. Growth factor signaling has direct influence on the integrins (I), associated signaling adaptors (II) or indirectly feeds into downstream pathways (III). The biochemical responses of the affected pathways and the resulting phenotypical outputs are indicated below<sup>12</sup>.

As mentioned above, integrins lack enzymatic activity and thereby depend in their signaling capability on the recruitment of signaling adaptors. In this context, integrins are known to cooperate with growth factor signaling on multiple layers, leading to prolonged and enhanced signaling intensity of growth factor induced signaling (see Fig. 21 for an overview; reviewed in<sup>12, 164</sup>). On the other hand, growth factor signaling can also control

integrin signaling by influencing integrin activation through phosphorylation of the integrin tails, by regulation of integrin-associated signaling proteins such as FAK, Src and Phosphatidylinositol-4,5-bisphosphate 3-Kinase (PI3K) and by regulating the

activity of downstream pathways, such as ERK, Akt, Jnk and the Rho GTPases. Conversely, integrins can induce specific phosphorylations on the Epidermal Growth Factor (EGF)-Receptor (EGFR) required for downstream signaling events and mediate growth-factor independent clustering of growth factor receptors, such as EGFR, Platelet Derived Growth Factor Receptor (PDGFR) or Fibroblast Growth Factor Receptor (FGFR), which leads to their activation. In addition, cooperation between integrin and Insulin-like Growth Factor Receptor (IGFR) signaling has been described in muscle homeostasis. Although the interconnection of these signaling pathways is complex, a few integrin associated signaling adaptors stand out as central signaling nodes, which will be discussed in more detail next.

#### 1.5.1.2. *ILK*

Despite of its name (integrin linked kinase), an increasing amount of evidence shows that ILK does not function as a kinase (reviewed in <sup>12, 155</sup>): Instead, the multiple interactions with its binding partners are supposed to regulate integrin signaling in a kinase-independent manner. Furthermore, the interaction with kindlin is required for recruitment of ILK to integrin adhesion sites. ILK consists of five tandemly arranged N-terminal ankyrin repeats, followed by a PH-domain and a pseudo-kinase domain at the C-terminus. ILK exists as an obligate complex with the interaction partners of the PINCH family (PINCH-1/-2), which interact with the ankyrin repeats, and the parvin family ( $\alpha,\beta,\gamma$ -parvin), which interact with the pseudo-kinase domain, and thereby forms several ILK-PINCH-parvin (IPP) complexes with different downstream signaling properties.

Multiple, isotype-specific interactions of PINCH and parvin with actin modulatory proteins and other signaling factors are thought to orchestrate the specific downstream effects of the IPP complex. The IPP complex can interact with the actin cytoskeleton through paxillin and parvin and is directly connected to growth factors through a connection of PINCH to Nck2. Consequently, cells depleted of ILK show reduced spreading, focal adhesion site formation and maturation in concert with decreased responsiveness to growth factor signaling and Akt activation, however the mechanisms for the later processes remain obscure.

#### 1.5.1.3. Kindlin

In addition to its ability to recruit the IPP complex to integrin adhesion sites, kindlin-2 has recently been shown to regulate Rat sarcoma (Ras) protein signaling via complex formation with Son Of Sevenless homolog 1 (SOS1)<sup>165</sup>, Transforming Growth Factor  $\beta$  (TGF $\beta$ )-signaling through interaction with TGF $\beta$  Receptor type I (T $\beta$ RI) and Small body size and Mothers Against Decapentaplegic (SMAD) 3<sup>166</sup> and Wingless-related integration site (Wnt)/ $\beta$ -catenin signaling through a direct interaction with  $\beta$ -catenin<sup>167</sup>. However these data remain strongly controversial, as in a later publication for example, the interaction with  $\beta$ -catenin could not be confirmed. Instead it was shown that kindlin-1 influences  $\beta$ -catenin signaling indirectly by regulating Wnt-expression levels<sup>150</sup>. Also the influence on TGF $\beta$  signaling seems to be more complex, as the latter publication also shows that kindlin-1 mediated activation of  $\alpha\beta$ 6 integrin leads to an increased liberation of TGF $\beta$  and enhanced SMAD signaling<sup>150</sup>.

#### 1.5.1.4. FAK

In contrast to ILK, FAK mediates Tyr kinase activity, especially important for auto-phosphorylation of the activation determining epitope Tyr-397 in FAK itself (an overview of FAK signaling functions can be found in<sup>12</sup>). FAK consists of an N-terminal FERM domain, followed by a kinases domain, a proline rich linker domain and a focal adhesion targeting domain. In the inactive state, the FERM domain interacts with the substrate binding region of the kinase domain and thus blocks the kinase activity (Fig. 22, left side). The processes necessary to initially recruit FAK to adhesion sites and its localized activation just emerge. There is evidence indicating that FAK signaling requires integrin clustering, unclasping and actin tethering, however the underlying mechanisms remained unclear<sup>37, 48, 168</sup>. Now a series of publications sheds new light on the mechanisms required for FAK recruitment to nascent adhesion sites and its activation. First, the interaction between FAK and talin is required to recruit talin to nascent adhesion sites and not the other way around<sup>122</sup>, excluding talin as the

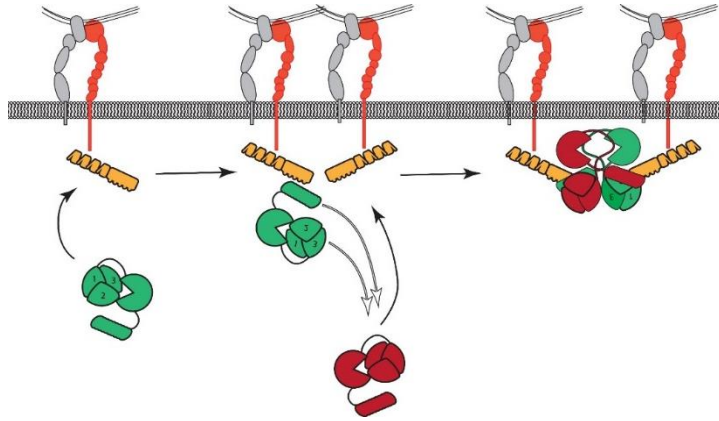


Figure 22: Paxillin and integrin clustering mediated FAK activation. Paxillin residing at integrin adhesion sites (left panel) recruits FAK through interaction with FAK-FAT-domain. FAK kinase domain is blocked by the interaction with FAK-FERM domain. In the presence of integrin clusters two paxillin-FAK complexes can interact in trans (middle), leading to a conformational change which allows the FAK-kinase domain to trans-activate the other FAK molecule at Tyr-397 through phosphorylation.

essential adaptor for early FAK activation and recruitment. Second, FAK essentially depends on the interaction with RhoA-specific guanine nucleotide exchange factor (Rgnef) in order to mediate membrane recruitment, which occurs independent of paxillin<sup>169,170</sup>. Finally, a

study using crystal structures and Small Angle X-ray scattering (SAX) structure determination could show how paxillin contributes to FAK activation at sites of clustered integrins<sup>171</sup> (see Fig. 22 for the following mechanism): The first important step of this mechanism is the enhanced recruitment of FAK to integrins through interaction of Paxillin with the focal adhesion targeting (FAT) domain of FAK. Upon integrin clustering two such recruited FAK molecules can dimerize. Importantly, the FAK molecules interact in *trans* through their FAT and FERM domains and this interaction is further stabilized through simultaneous paxillin interaction. This mode of dimerization stabilizes a conformation, where the FERM domain moves away from the kinase domain, allowing the trans-phosphorylation of the two FAK molecules at the activating Tyr-397 residue.

Upon phosphorylation on Tyr-397 FAK can interact with Src-family kinases, leading to further phosphorylations in the protein, which in turn allow complex formation with and phosphorylation of multiple Src-Homology 2 (SH2) domain containing proteins (for an overview, see Fig. 21), most prominently Arp2/3, N-Wasp, P130Cas- Chicken tumor 10 Regulator of Kinase (CRK)-DOCK complex, paxillin-protein-coupled receptor-kinase-interacting protein (GIT)-PAK-Interactive exchange factor (PIX) complex. Actin dynamics are controlled by the FAK-p130Cas-Crk-DOCK and paxillin-GIT-PIX complexes, which lead to the activation of Rac. Also, the concerted recruitment of N-

Wasp and Arp-2/3 complex contribute to localized actin polymerization. Furthermore, p130Cas and Src can induce ligand-independent phosphorylation of EGFR, and importantly, the activated FAK-Src complex controls downstream signaling through a Ras-Mitogen-activated protein kinase/ERK Kinase (MEK)-Mitogen Activated Protein Kinase (MAPK) pathway. Furthermore, FAK is involved in Phosphoinositidol-3-Kinase (PI3K)-Akt signaling by recruiting PI3K to focal adhesion sites. Consequently, cells depleted of FAK show defects in the initiation of nascent adhesion sites and a decrease in the turnover of enlarged FA sites leading to slower migration. Altogether, FAK activation at adhesion sites controls actin and FA dynamics as well as signaling pathways important for cell proliferation, survival and differentiation. Although current publications show a complete picture of FAK activation, the question how paxillin becomes recruited to nascent adhesion sites remains unclear.

#### 1.5.1.5. Paxillin

Paxillin has early been described as an essential component of integrin adhesion sites (reviewed in <sup>3, 172</sup>). Paxillin and its two paralogues Hydrogen peroxide-inducible clone-5 (Hic5) and leupaxin, which differ in their tissue expression pattern, share a similar protein domain architecture (Fig. 24) <sup>3</sup>.

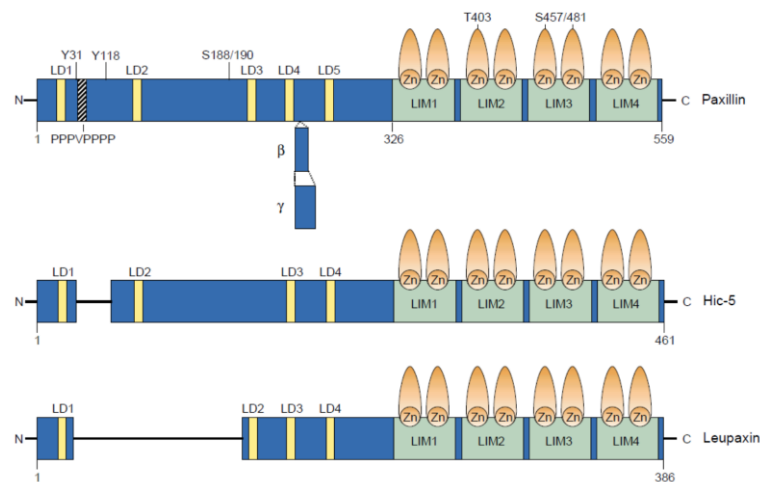


Figure 23: Paxillin domain structure (modified from <sup>3</sup>).

All three proteins are highly similar in the occurrence of four LIM domains, which consist each of two zinc finger domains. It has been shown that the LIM-2/3 domains are important for the localization of paxillin to FAs. However, the underlying

mechanisms remain obscure <sup>172</sup>. Furthermore, interactions with the Protein Tyrosine Phosphatase with Pro(P)-Glu(E)-Ser(S)-Thr(T) sequence (PTP-PEST) as well as microtubules have been located to the paxillin LIM domains. Both interaction sites are thought to facilitate FA turnover <sup>172</sup>. The three paralogues show a higher degree of dissimilarity in the organization of their N-terminal Leu- and Asp (LD)- rich domains, which are heavily phosphorylated upon integrin signaling and serve as a major platform for integrin associated signaling adaptors (Fig. 23)<sup>3</sup>. Prominent interaction partners of the LD domains include vinculin, ILK, FAK, parvin, PKL/GIT and CRK leading to an important influence of paxillin to the function of these interacting proteins <sup>172</sup>. In detail, the paxillin N-terminus contains five highly conserved LD domains, which provide - despite their high degree of conservation - defined, non-overlapping interaction sites for interacting proteins <sup>172</sup>. Although Hic5 and leupaxin contain only four of these sites many interaction partners are shared by the paxillin family <sup>3</sup>. Besides the influence on FAK activation, paxillin regulates actin dynamics through Rac and Rho signaling <sup>9, 12</sup>. For example, phosphorylation of paxillin on Tyr-31 and Tyr-118 by activated FAK-Src complex leads to the recruitment of Crk-p130Cas-Dock180 complex important for Rac activation and Rac-mediated actin dynamics (see also 1.2.5). Phosphorylation of paxillin on Ser-273 through P21-Activating Kinase 1 (PAK1) leads to the formation of a GIT-PIX-PAK1 complex. PAK1 can directly regulate Rac activity and GIT can activate the small GTPase ADP-ribosylation factor 6 (Arf6) through its Arf-GAP domain, which in turn can also modulate Rac activation. Altogether, paxillin constitutes a central signaling platform which integrates prominent integrin signaling pathways and leads to the activation of several Rac-stimulatory pathways, important role for cell spreading; however the mechanism which mediates paxillin recruitment to integrin adhesion sites remains unknown.

### 1.5.2. Integrin signaling in anoikis and cancer

The relevance of integrin-mediated signaling is further underlined by the influence of integrins on cancer progression and apoptotic cell death upon detachment from the ECM substrate (anoikis) (reviewed in <sup>19</sup>): The contact of cells to their surrounding matrix allows proliferation and survival. Consequently, the expression of an organ and cell type-specific integrin profile prevents proliferation of cells in “foreign” organs. Therefore, it is an essential step during cancer cell development to achieve partial

resistance to anoikis, which facilitates migration out of the primary tumor and extravasation, and to achieve expression of the corresponding integrin heterodimers necessary to invade and allow persistent survival in novel ECM environments.

Cell detachment initiates anoikis by reducing the anti-apoptotic integrin signaling and the release of cytoskeletal-associated pro-apoptotic factors that can induce the intrinsic apoptosis pathway and the extrinsic apoptosis pathway via the cell rounding-dependent activation of tumor necrosis factor receptor family members. Both apoptosis pathways depend on the release of mitochondrial cytochrome-c through membrane channels induced by oligomerization of Bcl2-associated X (Bax)/ Bcl-2-associated death promoter (Bad) proteins. Integrin signaling strongly affects the apoptosis inducing activity of Bax/Bad proteins by regulating their inhibitors B-cell lymphoma-2 (Bcl-2) and B-cell lymphoma-XL (Bcl-XL). Akt signaling induced through FAK or ILK can lead to a release of Bcl-2 and inhibition of Bad proteins. Furthermore, MAPK signaling controlled by ILK, FAK and integrin dependent growth factor signaling can inhibit apoptosis through their influence on apoptosis-stimulatory and -inhibitory pathways. These observations suggest that the upstream regulatory proteins have profound influence on anoikis. Indeed, the presence of specific integrin heterodimers can influence anoikis, e.g.  $\alpha\beta 5$  integrin sensitizes while  $\alpha\beta 6$  integrin can protect cells from anoikis. Also overexpression of kindlin and talin have been identified as anti-apoptotic influence, which promotes cancer development. However, the exact mechanisms how kindlin and talin contribute to integrin signaling are still under investigation<sup>173-176</sup>. It will be interesting for future research to identify, in which situations the anti-apoptotic functions of talin and kindlin are interdependent and in which independent of each other.

## 2. Aim of the thesis

Integrin activation and signaling are complex multi-step processes, regulated by the cytoplasmic adaptor proteins kindlin and talin. The current opinion in the field points to an important influence of both proteins to these processes. Structural and biochemical data have described and explained single steps of integrin activation for various integrin heterodimers. The influence of kindlin and talin to  $\beta 2$  integrin activation in hematopoietic cell lines, which are mainly non-adherent, has been relatively well characterized. However, the influence of kindlin and talin on the activation of  $\beta 1$  integrin, the main integrin in adherent cells such as fibroblasts or epithelial cells, remains poorly characterized and understood. In these cells, which constitute the majority of all body cells, mechanistic insights are mostly available for the function of talins but not for kindlins. There is an ongoing controversy concerning the importance of kindlin function for integrin activation. It was suggested that kindlins rather enhance than promote integrin activation. Furthermore, recent data and own observations suggest that very low levels of kindlin and talin are sufficient to support most of their functions in vitro and in vivo questioning the interpretation of knock-down or overexpression studies. Up to date only few publications are available, which could address these issues in cells lacking one of both protein families. For adherent cells no data with gene deletion of both activators is available. In order to resolve some of these gaps in our understanding, I focused my PhD project on the role of kindlin and talin for integrin activation and signaling in fibroblast cell lines, as a model for adherent cell lines.

To allow comparative analysis of kindlin and talin functions my **first aim** was to generate two fibroblast cell lines, which allow conditional deletion of all expressed kindlin or talin isoforms. In order to achieve this aim, I generated a transgenic mouse line for conditional deletion of kindlin-2, which is currently analyzed by a further PhD student. The generated cell lines were used for my analyses and proved as an essential model system for further related projects.

My **second aim** was to compare the influence of kindlin and talin to integrin activation and signaling in these cell lines, leading to a thorough analysis of these processes and

improved understanding of the individual protein functions especially in the initial spreading phase.

In addition, my **third aim** was to improve our understanding of kindlin-mediated signaling functions by screening for novel interaction partners of kindlin. For this purpose, mass spectrometry assisted analysis of immuno-precipitations, adhesomes and yeast two hybrid screenings were performed. They lead to the identification of paxillin as a novel kindlin interaction partner.

In parallel I was also interested in broadening my understanding of kindlin functions in mouse development, tumor development and the molecular mechanisms underlying the signaling through the most prominent kindlin interaction partner. For this purpose my **fourth aim** was to study the impact of kindlin-1 deletion on early mouse development and tumor development.

Finally, together with a student fellow I wrote a review article, in which I summarized and discussed the current knowledge gathered by numerous laboratories on ILK.

### 3. Short summary of manuscripts

#### 3.1. Kindlin-2 initiates fibroblast adhesion and spreading by recruitment of paxillin and FAK to nascent adhesion sites.

Moritz Widmaier, Marina Theodosiou\*, Emanuel Rognoni\*, Katharina Austen, Maik Veelders, Daniel Müller, Mitasha Bharadwaj, Zdenek Petrasek, Roy Zent, Reinhard Fässler. (\*contributed equally)

Integrins are  $\alpha\beta$  heterodimeric transmembrane receptors which mediate cell adhesion and signaling by binding to ligands of the ECM or other cells. Prior to ligand binding and signaling, integrins need to be activated through interaction of talin and kindlin proteins with the cytoplasmic tails of  $\beta$  integrins. This activation comprises allosterically linked conformational changes in the ligand binding site and separation of the tight interaction of the  $\alpha\beta$  heterodimer in the proximity of the transmembrane domains. Upon initial adhesion formation, integrins form clusters, which leads to adhesion strengthening and integrin signaling through the recruitment of adaptor proteins. Previous reports show an important influence of kindlin and talin to integrin-mediated cell adhesion. However it remains controversial how kindlins contribute to integrin activation or signaling.

In this study, we generated two fibroblast cell lines, which lack the expression of talin or kindlin isoforms, respectively. Our studies revealed that both proteins are required to mediate cell adhesion on fibronectin (FN) and robust integrin signaling. In line, both cell lines showed proliferation defects and furthermore, kindlin-deleted cells displayed survival defects. Interestingly, integrin tail separation measured with the 9EG7-antibody revealed that both cell lines were severely affected. However, ligand binding was only perturbed in kindlin-deleted cells. Furthermore, stimulation with  $Mn^{2+}$  and FN ligand, which stimulates integrin leg separation, partially rescued adhesion of both cell lines on FN ligand. However, only talin-deleted cells were able to spread. Further analysis excluded differences in integrin clustering between the two cell lines suggesting that kindlin can promote isotropic cell spreading. When we searched for the responsible protein that mediated this kindlin effect we identified paxillin as novel interaction partner of kindlin by using yeast two hybrid analysis. We show that during isotropic cell

spreading, kindlin recruits ILK and paxillin to nascent adhesion sites; ILK regulates actin dynamics and paxillin activates FAK, which in turn promotes cell spreading, proliferation and survival.

Altogether, these results suggest that in fibroblasts kindlin might initiate integrin activation and signaling and that talin is required to enhance these processes, stabilize nascent adhesions and promote their maturations into FAs.

### 3.2. Integrin linked kinase at a glance.

Moritz Widmaier, Emanuel Rognoni, Korana Radovanac, Babak Azimifar, Reinhard Fässler.

Integrins constitute a large family of heterodimeric transmembrane receptors, important for cytoskeletal dynamics and signaling in response to cell adhesion. As integrins lack enzymatic activity, their signaling properties rely on the recruitment of intracellular signaling proteins and adaptor proteins. Integrin-linked kinase (ILK) is one of the best described examples of these signaling adaptors, influencing actin rearrangement, cell polarization and survival. Furthermore, ILK has been shown to function in subcellular compartments which do not directly depend on integrins, such as cell-cell-adhesion sites, centrosomes and the nucleus. While recent evidence clearly showed that the proposed kinase activity of ILK is missing, many of the ILK-mediated functions can be explained through the ability to assemble many important signaling proteins into a large signaling platform. Most importantly, ILK requires interaction with PINCH and parvin proteins to maintain a stable conformation and to be protected against degradation. Furthermore, PINCH and parvin influence actin cytoskeleton dynamics through binding to ILK. Direct interaction of ILK with a complex of mDia1 and IQGAP1 directs microtubule tips to integrin adhesion sites, which enhances adhesion turnover. Furthermore, ILK interacts with many other central signaling proteins, such as paxillin, PKB/Akt, Src or ILKAP and might assist in integrating information into complex signaling activities at integrin adhesion sites. ILK is also found in other sites than adhesion. They include cell-cell contacts, the nucleus and centrosomes. It will be important to shed light on ILK's function at these sites and to delineate how Akt and GSK3 $\beta$  are activated by ILK.

### 3.3. Loss of Kindlin-1 causes skin atrophy and lethal neonatal intestinal epithelial dysfunction.

Siegfried Ussar, Markus Moser, Moritz Widmaier, Emanuel Rognoni, Christian Harrer, Orsolya Genzel-Boroviczeny, Reinhard Fässler.

Integrins are obligate heterodimeric transmembrane receptors formed by  $\alpha$  and  $\beta$  subunits which mediate cell attachment to extracellular ligands and downstream signaling important for cell migration, proliferation and survival. Integrin mediated ligand binding and associated signaling is controlled by interaction of the cytoplasmic  $\beta$ -tail with adaptor proteins, such as kindlins. In humans and mice, three kindlin isoforms are expressed (kindlin-1/-2/-3) and mutations of the human *KINDLIN-1* gene, which is co-expressed in various epithelial tissues with kindlin-2, has been shown to give rise to the Kindler syndrome, characterized by defects of the skin, like skin detachment from the underlying basement membrane (blistering), skin atrophy, pigmentation defects and an increased risk to develop skin cancer.

In order to gain better understanding of the underlying pathogenic mechanisms of Kindler syndrome, we generated a mouse line, in which the kindlin-1 gene was constitutively deleted. This mouse line recapitulated major phenotypes observed in Kindler syndrome patients, such as skin blistering and skin atrophy. However, in contrast to the human patients, the mice died early after birth, as they suffered from an ulcerative colitis-like phenotype of the intestine. Our results showed that reduced integrin activation due to kindlin-1 deletion renders the skin and especially the intestinal epithelium more sensitive to mechanical stress leading to local detachment of the affected epithelia and a severe inflammation. Interestingly, ulcerative-colitis like symptoms were also observed in Kindler Syndrome patients, which are, however, less severe.

### 3.4. Kindlin-1 controls Wnt and TGF- $\beta$ availability to regulate cutaneous stem cell proliferation.

Emanuel Rognoni, Moritz Widmaier, Madis Jakobson, Raphael Ruppert, Siegfried Ussar, Despoina Katsougri, Ralph T. Böttcher, Joey E. Lai-Cheong, Daniel B. Rifkin, John McGrath, Reinhard Fässler.

The rare human disease Kindler syndrome is caused by mutations in the human *KINDLIN-1* gene and characterized by regional skin blistering, hyperkeratosis, atrophy and pigmentation defects accompanied by an increased risk for skin cancer development. In a previous publication we could show that constitutive loss of kindlin-1 expression in mice leads to cell attachment defects and early lethality caused by reduced integrin function in the skin and intestinal epithelium. Integrins are heterodimeric transmembrane receptors which can mediate adhesion and migration as well as signaling on ECM ligands. Their ligand binding affinity can be controlled by intracellular adaptor proteins such as kindlin-1 and increased integrin activation is associated with increased risk for cancer development. The contradiction of the increased cancer prevalence in Kindler syndrome patients despite decreased integrin function suggested that kindlin-1 controls potent, integrin-independent tumor promoting signaling pathways, which were unknown when we started the project.

In this study, we developed a conditional deletion of kindlin-1 in keratinocytes to circumvent lethality. This allowed to study the role of kindlin-1 in tumor development. In order to distinguish between direct effects of kindlin-1 deletion and defects caused by loss of  $\beta 1$  integrin function, we compared this mouse line to a recently described mouse expressing a kindlin-binding deficient  $\beta 1$  integrin in keratinocytes. Our analysis revealed that kindlin-1 controls  $\alpha v\beta 6$  integrin mediated release of TGF $\beta$  in the skin stem cell compartment as well as expression levels of Wnt ligands and receptors independent of  $\beta 1$  integrin function. Changes in TGF $\beta$ - and Wnt/ $\beta$ -catenin signaling could be confirmed in Kindler patients as well. In mice, misregulation of both pathways caused overshooting skin stem cell activity, aberrant induction of hair follicle development and early onset of chemically induced tumor development. Altogether our analysis revealed that kindlin-1 contributes to activation of  $\beta 1$  integrins and controls skin stem cell fate, proliferation and tumor development through regulation of TGF $\beta$ -release and Wnt/ $\beta$ -catenin signaling.

### 3.5. Sorting nexin 17 prevents lysosomal degradation of $\beta$ 1 integrins by binding to the $\beta$ 1 integrin tail.

Ralph Thomas Böttcher, Christopher Stremmel, Alexander Meves, Hannelore Mayer, Moritz Widmaier, Hui-Yuang Tseng, Reinhard Fässler.

Integrins mediate cell adhesion to ECM ligands, cell migration and signaling important for survival and proliferation. These integrin functions are regulated by intracellular proteins, which bind directly or indirectly to the intracellular integrin tail domains, which control the affinity of integrins to their ligand, their internalization and efficient recycling to adhesion sites. Here we show that two FERM domain containing proteins, kindlin-2 and the SNX17 directly interact with the same motif in  $\beta$  integrin tails. However, binding occurs in different subcellular compartments. Interaction of kindlin-2 takes place at the plasma membrane and controls the affinity of integrins towards their ligand, and interaction of SNX17 occurs in endosomes and is required to ensure recycling of internalized integrins back to the cell surface. In absence of SNX17 or when the interaction of SNX17 with  $\beta$  integrin is perturbed, internalized integrins become quickly degraded via the lysosomal degradation pathway.

## 4. References

1. Zhu, J. *et al.* Structure of a complete integrin ectodomain in a physiologic resting state and activation and deactivation by applied forces. *Molecular cell* **32**, 849-861 (2008).
2. Askari, J.A. *et al.* Focal adhesions are sites of integrin extension. *The Journal of cell biology* **188**, 891-903 (2010).
3. Turner, C.E. Paxillin and focal adhesion signalling. *Nature cell biology* **2**, E231-236 (2000).
4. Humphries, M.J., Travis, M.A., Clark, K. & Mould, A.P. Mechanisms of integration of cells and extracellular matrices by integrins. *Biochemical Society transactions* **32**, 822-825 (2004).
5. Paszek, M.J. *et al.* The cancer glycoalyx mechanically primes integrin-mediated growth and survival. *Nature* **511**, 319-325 (2014).
6. Carman, C.V. & Springer, T.A. Integrin avidity regulation: are changes in affinity and conformation underemphasized? *Current opinion in cell biology* **15**, 547-556 (2003).
7. Horton, H.R. *Principles of biochemistry*, Edn. 4th. (Pearson Prentice Hall, Upper Saddle River, NJ; 2006).
8. Barczyk, M., Carracedo, S. & Gullberg, D. Integrins. *Cell and tissue research* **339**, 269-280 (2010).
9. Vicente-Manzanares, M., Choi, C.K. & Horwitz, A.R. Integrins in cell migration-the actin connection. *Journal of cell science* **122**, 199-206 (2009).
10. Carman, C.V. Overview: imaging in the study of integrins. *Methods in molecular biology* **757**, 159-189 (2012).
11. Moser, M., Legate, K.R., Zent, R. & Fassler, R. The tail of integrins, talin, and kindlins. *Science* **324**, 895-899 (2009).
12. Legate, K.R., Wickstrom, S.A. & Fassler, R. Genetic and cell biological analysis of integrin outside-in signaling. *Genes & development* **23**, 397-418 (2009).
13. Hynes, R.O. Integrins: bidirectional, allosteric signaling machines. *Cell* **110**, 673-687 (2002).
14. Johnson, M.S., Lu, N., Denessiouk, K., Heino, J. & Gullberg, D. Integrins during evolution: evolutionary trees and model organisms. *Biochimica et biophysica acta* **1788**, 779-789 (2009).
15. Srichai, M.B. & Zent, R. Integrin Structure and Function. *Cell-Extracellular Matrix Interactions in Cancer*, 19-41 (2010).
16. Yang, J.T. *et al.* Overlapping and independent functions of fibronectin receptor integrins in early mesodermal development. *Dev Biol* **215**, 264-277 (1999).
17. Huvoneers, S., Truong, H. & Danen, H.J. Integrins: signaling, disease, and therapy. *International journal of radiation biology* **83**, 743-751 (2007).
18. Shattil, S.J., Kim, C. & Ginsberg, M.H. The final steps of integrin activation: the end game. *Nature reviews. Molecular cell biology* **11**, 288-300 (2010).
19. Paoli, P., Giannoni, E. & Chiarugi, P. Anoikis molecular pathways and its role in cancer progression. *Biochimica et biophysica acta* **1833**, 3481-3498 (2013).

20. Campbell, I.D. & Humphries, M.J. Integrin structure, activation, and interactions. *Cold Spring Harbor perspectives in biology* **3** (2011).
21. Shimaoka, M. & Springer, T.A. Therapeutic antagonists and conformational regulation of integrin function. *Nature reviews. Drug discovery* **2**, 703-716 (2003).
22. Lissitzky, J.C. *et al.* Endoproteolytic processing of integrin pro-alpha subunits involves the redundant function of furin and proprotein convertase (PC) 5A, but not paired basic amino acid converting enzyme (PACE) 4, PC5B or PC7. *The Biochemical journal* **346 Pt 1**, 133-138 (2000).
23. Springer, T.A., Zhu, J. & Xiao, T. Structural basis for distinctive recognition of fibrinogen gammaC peptide by the platelet integrin alphabeta3. *The Journal of cell biology* **182**, 791-800 (2008).
24. Xiong, J.P. *et al.* Crystal structure of the extracellular segment of integrin alpha Vbeta3 in complex with an Arg-Gly-Asp ligand. *Science* **296**, 151-155 (2002).
25. Nagae, M. *et al.* Crystal structure of alpha5beta1 integrin ectodomain: atomic details of the fibronectin receptor. *The Journal of cell biology* **197**, 131-140 (2012).
26. Mould, A.P. *et al.* Structure of an integrin-ligand complex deduced from solution x-ray scattering and site-directed mutagenesis. *The Journal of biological chemistry* **278**, 39993-39999 (2003).
27. Huvenerers, S., Truong, H., Fassler, R., Sonnenberg, A. & Danen, E.H. Binding of soluble fibronectin to integrin alpha5 beta1 - link to focal adhesion redistribution and contractile shape. *Journal of cell science* **121**, 2452-2462 (2008).
28. Takahashi, S. *et al.* The RGD motif in fibronectin is essential for development but dispensable for fibril assembly. *The Journal of cell biology* **178**, 167-178 (2007).
29. Chen, C.Y. *et al.* Effect of D to E mutation of the RGD motif in rhodostomin on its activity, structure, and dynamics: importance of the interactions between the D residue and integrin. *Proteins* **76**, 808-821 (2009).
30. Zhu, J., Zhu, J. & Springer, T.A. Complete integrin headpiece opening in eight steps. *The Journal of cell biology* **201**, 1053-1068 (2013).
31. Takagi, J., Petre, B.M., Walz, T. & Springer, T.A. Global conformational rearrangements in integrin extracellular domains in outside-in and inside-out signaling. *Cell* **110**, 599-511 (2002).
32. Luo, B.H., Carman, C.V. & Springer, T.A. Structural basis of integrin regulation and signaling. *Annual review of immunology* **25**, 619-647 (2007).
33. Zhu, J., Boylan, B., Luo, B.H., Newman, P.J. & Springer, T.A. Tests of the extension and deadbolt models of integrin activation. *The Journal of biological chemistry* **282**, 11914-11920 (2007).
34. Askari, J.A., Buckley, P.A., Mould, A.P. & Humphries, M.J. Linking integrin conformation to function. *Journal of cell science* **122**, 165-170 (2009).
35. Clark, K. *et al.* A specific alpha5beta1-integrin conformation promotes directional integrin translocation and fibronectin matrix formation. *Journal of cell science* **118**, 291-300 (2005).

36. Takagi, J., Erickson, H.P. & Springer, T.A. C-terminal opening mimics 'inside-out' activation of integrin alpha5beta1. *Nature structural biology* **8**, 412-416 (2001).
37. Zhu, J. *et al.* Requirement of alpha and beta subunit transmembrane helix separation for integrin outside-in signaling. *Blood* **110**, 2475-2483 (2007).
38. Ridley, A.J. Life at the leading edge. *Cell* **145**, 1012-1022 (2011).
39. Wu, Y.I. *et al.* A genetically encoded photoactivatable Rac controls the motility of living cells. *Nature* **461**, 104-108 (2009).
40. Galbraith, C.G., Yamada, K.M. & Galbraith, J.A. Polymerizing actin fibers position integrins primed to probe for adhesion sites. *Science* **315**, 992-995 (2007).
41. Bazzoni, G. & Hemler, M.E. Are changes in integrin affinity and conformation overemphasized? *Trends in biochemical sciences* **23**, 30-34 (1998).
42. van Kooyk, Y. & Figdor, C.G. Avidity regulation of integrins: the driving force in leukocyte adhesion. *Current opinion in cell biology* **12**, 542-547 (2000).
43. Kusumi, A. *et al.* Paradigm shift of the plasma membrane concept from the two-dimensional continuum fluid to the partitioned fluid: high-speed single-molecule tracking of membrane molecules. *Annual review of biophysics and biomolecular structure* **34**, 351-378 (2005).
44. Gowrishankar, K. *et al.* Active remodeling of cortical actin regulates spatiotemporal organization of cell surface molecules. *Cell* **149**, 1353-1367 (2012).
45. Kucik, D.F., Dustin, M.L., Miller, J.M. & Brown, E.J. Adhesion-activating phorbol ester increases the mobility of leukocyte integrin LFA-1 in cultured lymphocytes. *J Clin Invest* **97**, 2139-2144 (1996).
46. Kim, M., Carman, C.V., Yang, W., Salas, A. & Springer, T.A. The primacy of affinity over clustering in regulation of adhesiveness of the integrin {alpha}L{beta}2. *The Journal of cell biology* **167**, 1241-1253 (2004).
47. Buensuceso, C., de Virgilio, M. & Shattil, S.J. Detection of integrin alpha IIbbeta 3 clustering in living cells. *The Journal of biological chemistry* **278**, 15217-15224 (2003).
48. Shi, Q. & Boettiger, D. A novel mode for integrin-mediated signaling: tethering is required for phosphorylation of FAK Y397. *Mol Biol Cell* **14**, 4306-4315 (2003).
49. Cluzel, C. *et al.* The mechanisms and dynamics of (alpha)v(beta)3 integrin clustering in living cells. *The Journal of cell biology* **171**, 383-392 (2005).
50. Schiller, H.B. & Fassler, R. Mechanosensitivity and compositional dynamics of cell-matrix adhesions. *EMBO reports* **14**, 509-519 (2013).
51. Kong, F., Garcia, A.J., Mould, A.P., Humphries, M.J. & Zhu, C. Demonstration of catch bonds between an integrin and its ligand. *The Journal of cell biology* **185**, 1275-1284 (2009).
52. Roca-Cusachs, P., Gauthier, N.C., Del Rio, A. & Sheetz, M.P. Clustering of alpha(5)beta(1) integrins determines adhesion strength whereas alpha(v)beta(3) and talin enable mechanotransduction. *Proceedings of the National Academy of Sciences of the United States of America* **106**, 16245-16250 (2009).

53. Litvinov, R.I. *et al.* Dissociation of bimolecular  $\alpha$ IIb $\beta$ 3-fibrinogen complex under a constant tensile force. *Biophysical journal* **100**, 165-173 (2011).
54. Friedland, J.C., Lee, M.H. & Boettiger, D. Mechanically activated integrin switch controls  $\alpha$ 5 $\beta$ 1 function. *Science* **323**, 642-644 (2009).
55. Kong, F. *et al.* Cyclic mechanical reinforcement of integrin-ligand interactions. *Molecular cell* **49**, 1060-1068 (2013).
56. Chen, W., Lou, J. & Zhu, C. Forcing switch from short- to intermediate- and long-lived states of the  $\alpha$ A domain generates LFA-1/ICAM-1 catch bonds. *The Journal of biological chemistry* **285**, 35967-35978 (2010).
57. Xiang, X. *et al.* Structural basis and kinetics of force-induced conformational changes of an  $\alpha$ A domain-containing integrin. *PLoS one* **6**, e27946 (2011).
58. Kim, M., Carman, C.V. & Springer, T.A. Bidirectional transmembrane signaling by cytoplasmic domain separation in integrins. *Science* **301**, 1720-1725 (2003).
59. Cavalcanti-Adam, E.A. *et al.* Lateral spacing of integrin ligands influences cell spreading and focal adhesion assembly. *Eur J Cell Biol* **85**, 219-224 (2006).
60. Rossier, O. *et al.* Integrins  $\beta$ 1 and  $\beta$ 3 exhibit distinct dynamic nanoscale organizations inside focal adhesions. *Nature cell biology* **14**, 1057-1067 (2012).
61. Paszek, M.J., Boettiger, D., Weaver, V.M. & Hammer, D.A. Integrin clustering is driven by mechanical resistance from the glycocalyx and the substrate. *PLoS computational biology* **5**, e1000604 (2009).
62. Boettiger, D. Mechanical control of integrin-mediated adhesion and signaling. *Current opinion in cell biology* **24**, 592-599 (2012).
63. Boettiger, D. & Wehrle-Haller, B. Integrin and glycocalyx mediated contributions to cell adhesion identified by single cell force spectroscopy. *Journal of physics. Condensed matter : an Institute of Physics journal* **22**, 194101 (2010).
64. Lawson, C. & Schlaepfer, D.D. Integrin adhesions: who's on first? What's on second? Connections between FAK and talin. *Cell adhesion & migration* **6**, 302-306 (2012).
65. Elad, N. *et al.* The role of integrin-linked kinase in the molecular architecture of focal adhesions. *Journal of cell science* **126**, 4099-4107 (2013).
66. Alexandrova, A.Y. *et al.* Comparative dynamics of retrograde actin flow and focal adhesions: formation of nascent adhesions triggers transition from fast to slow flow. *PLoS one* **3**, e3234 (2008).
67. Giannone, G. *et al.* Lamellipodial actin mechanically links myosin activity with adhesion-site formation. *Cell* **128**, 561-575 (2007).
68. Pankov, R. *et al.* Integrin dynamics and matrix assembly: tensin-dependent translocation of  $\alpha$ (5) $\beta$ (1) integrins promotes early fibronectin fibrillogenesis. *The Journal of cell biology* **148**, 1075-1090 (2000).
69. Zamir, E. *et al.* Dynamics and segregation of cell-matrix adhesions in cultured fibroblasts. *Nature cell biology* **2**, 191-196 (2000).
70. Wu, C., Keivens, V.M., O'Toole, T.E., McDonald, J.A. & Ginsberg, M.H. Integrin activation and cytoskeletal interaction are essential for the assembly of a fibronectin matrix. *Cell* **83**, 715-724 (1995).

71. Ohashi, T., Kiehart, D.P. & Erickson, H.P. Dual labeling of the fibronectin matrix and actin cytoskeleton with green fluorescent protein variants. *Journal of cell science* **115**, 1221-1229 (2002).
72. Linder, S. Invadosomes at a glance. *Journal of cell science* **122**, 3009-3013 (2009).
73. Schmidt, S. *et al.* Kindlin-3-mediated signaling from multiple integrin classes is required for osteoclast-mediated bone resorption. *The Journal of cell biology* **192**, 883-897 (2011).
74. Stefanidakis, M. & Koivunen, E. Cell-surface association between matrix metalloproteinases and integrins: role of the complexes in leukocyte migration and cancer progression. *Blood* **108**, 1441-1450 (2006).
75. Stehbens, S.J. *et al.* CLASPs link focal-adhesion-associated microtubule capture to localized exocytosis and adhesion site turnover. *Nature cell biology* **16**, 561-573 (2014).
76. Kryczka, J. *et al.* Matrix metalloproteinase-2 cleavage of the beta1 integrin ectodomain facilitates colon cancer cell motility. *The Journal of biological chemistry* **287**, 36556-36566 (2012).
77. Geiger, B., Bershadsky, A., Pankov, R. & Yamada, K.M. Transmembrane crosstalk between the extracellular matrix--cytoskeleton crosstalk. *Nature reviews. Molecular cell biology* **2**, 793-805 (2001).
78. Morgan, M.R., Humphries, M.J. & Bass, M.D. Synergistic control of cell adhesion by integrins and syndecans. *Nature reviews. Molecular cell biology* **8**, 957-969 (2007).
79. Bridgewater, R.E., Norman, J.C. & Caswell, P.T. Integrin trafficking at a glance. *Journal of cell science* **125**, 3695-3701 (2012).
80. Tiwari, S., Askari, J.A., Humphries, M.J. & Bulleid, N.J. Divalent cations regulate the folding and activation status of integrins during their intracellular trafficking. *Journal of cell science* **124**, 1672-1680 (2011).
81. Bottcher, R.T. *et al.* Sorting nexin 17 prevents lysosomal degradation of beta1 integrins by binding to the beta1-integrin tail. *Nature cell biology* **14**, 584-592 (2012).
82. Martel, V. *et al.* Talin controls the exit of the integrin alpha 5 beta 1 from an early compartment of the secretory pathway. *Journal of cell science* **113 ( Pt 11)**, 1951-1961 (2000).
83. Margadant, C., Kreft, M., de Groot, D.J., Norman, J.C. & Sonnenberg, A. Distinct roles of talin and kindlin in regulating integrin alpha5beta1 function and trafficking. *Current biology : CB* **22**, 1554-1563 (2012).
84. Margadant, C., Kreft, M., Zambruno, G. & Sonnenberg, A. Kindlin-1 regulates integrin dynamics and adhesion turnover. *PLoS one* **8**, e65341 (2013).
85. Tseng, H.Y. *et al.* Sorting Nexin 31 Binds Multiple beta Integrin Cytoplasmic Domains and Regulates beta1 Integrin Surface Levels and Stability. *Journal of molecular biology* (2014).
86. Humphries, M.J. Cell-substrate adhesion assays. *Current protocols in cell biology / editorial board, Juan S. Bonifacino ... [et al.] Chapter 9*, Unit 9 1 (2001).
87. Mould, A.P. Analyzing integrin-dependent adhesion. *Current protocols in cell biology / editorial board, Juan S. Bonifacino ... [et al.] Chapter 9*, Unit 9 4 (2011).

88. Chigaev, A. & Sklar, L.A. Overview: assays for studying integrin-dependent cell adhesion. *Methods in molecular biology* **757**, 3-14 (2012).
89. Sperandio, M. *et al.* P-selectin glycoprotein ligand-1 mediates L-selectin-dependent leukocyte rolling in venules. *The Journal of experimental medicine* **197**, 1355-1363 (2003).
90. Sperandio, M. Selectins and glycosyltransferases in leukocyte rolling in vivo. *The FEBS journal* **273**, 4377-4389 (2006).
91. Moser, M. *et al.* Kindlin-3 is required for beta2 integrin-mediated leukocyte adhesion to endothelial cells. *Nature medicine* **15**, 300-305 (2009).
92. Bagher, P. & Segal, S.S. The mouse cremaster muscle preparation for intravital imaging of the microcirculation. *Journal of visualized experiments : JoVE* (2011).
93. Byron, A. *et al.* Anti-integrin monoclonal antibodies. *Journal of cell science* **122**, 4009-4011 (2009).
94. Bunch, T.A. Integrin alphallbbeta3 activation in Chinese hamster ovary cells and platelets increases clustering rather than affinity. *The Journal of biological chemistry* **285**, 1841-1849 (2010).
95. Ye, F. *et al.* The mechanism of kindlin-mediated activation of integrin alphallbbeta3. *Current biology : CB* **23**, 2288-2295 (2013).
96. Humphries, M.J., Symonds, E.J. & Mould, A.P. Mapping functional residues onto integrin crystal structures. *Current opinion in structural biology* **13**, 236-243 (2003).
97. Mould, A.P., Garratt, A.N., Puzon-McLaughlin, W., Takada, Y. & Humphries, M.J. Regulation of integrin function: evidence that bivalent-cation-induced conformational changes lead to the unmasking of ligand-binding sites within integrin alpha5 beta1. *The Biochemical journal* **331 ( Pt 3)**, 821-828 (1998).
98. Humphries, M.J. Monoclonal antibodies as probes of integrin priming and activation. *Biochemical Society transactions* **32**, 407-411 (2004).
99. Mould, A.P., Garratt, A.N., Askari, J.A., Akiyama, S.K. & Humphries, M.J. Identification of a novel anti-integrin monoclonal antibody that recognises a ligand-induced binding site epitope on the beta 1 subunit. *FEBS letters* **363**, 118-122 (1995).
100. Mould, A.P., Garratt, A.N., Askari, J.A., Akiyama, S.K. & Humphries, M.J. Regulation of integrin alpha 5 beta 1 function by anti-integrin antibodies and divalent cations. *Biochemical Society transactions* **23**, 395S (1995).
101. Lu, C., Ferzly, M., Takagi, J. & Springer, T.A. Epitope mapping of antibodies to the C-terminal region of the integrin beta 2 subunit reveals regions that become exposed upon receptor activation. *Journal of immunology* **166**, 5629-5637 (2001).
102. Bazzoni, G., Ma, L., Blue, M.L. & Hemler, M.E. Divalent cations and ligands induce conformational changes that are highly divergent among beta1 integrins. *The Journal of biological chemistry* **273**, 6670-6678 (1998).
103. Kim, C., Ye, F., Hu, X. & Ginsberg, M.H. Talin activates integrins by altering the topology of the beta transmembrane domain. *The Journal of cell biology* **197**, 605-611 (2012).
104. Bachir, A.I. *et al.* Integrin-Associated Complexes Form Hierarchically with Variable Stoichiometry in Nascent Adhesions. *Current biology : CB* (2014).

105. Hoffmann, J.E., Fermin, Y., Stricker, R.L., Ickstadt, K. & Zamir, E. Symmetric exchange of multi-protein building blocks between stationary focal adhesions and the cytosol. *eLife* **3**, e02257 (2014).
106. Calderwood, D.A. *et al.* The Talin head domain binds to integrin beta subunit cytoplasmic tails and regulates integrin activation. *The Journal of biological chemistry* **274**, 28071-28074 (1999).
107. Debrand, E. *et al.* Talin 2 is a large and complex gene encoding multiple transcripts and protein isoforms. *The FEBS journal* **276**, 1610-1628 (2009).
108. Petrich, B.G. *et al.* Talin is required for integrin-mediated platelet function in hemostasis and thrombosis. *The Journal of experimental medicine* **204**, 3103-3111 (2007).
109. Nieswandt, B. *et al.* Loss of talin1 in platelets abrogates integrin activation, platelet aggregation, and thrombus formation in vitro and in vivo. *The Journal of experimental medicine* **204**, 3113-3118 (2007).
110. Conti, F.J., Monkley, S.J., Wood, M.R., Critchley, D.R. & Muller, U. Talin 1 and 2 are required for myoblast fusion, sarcomere assembly and the maintenance of myotendinous junctions. *Development* **136**, 3597-3606 (2009).
111. Brown, N.H. *et al.* Talin is essential for integrin function in Drosophila. *Developmental cell* **3**, 569-579 (2002).
112. Tanentzapf, G. & Brown, N.H. An interaction between integrin and the talin FERM domain mediates integrin activation but not linkage to the cytoskeleton. *Nature cell biology* **8**, 601-606 (2006).
113. Helsten, T.L. *et al.* Differences in regulation of Drosophila and vertebrate integrin affinity by talin. *Mol Biol Cell* **19**, 3589-3598 (2008).
114. Cram, E.J., Clark, S.G. & Schwarzbauer, J.E. Talin loss-of-function uncovers roles in cell contractility and migration in *C. elegans*. *Journal of cell science* **116**, 3871-3878 (2003).
115. Fitzpatrick, P., Shattil, S.J. & Ablooglu, A.J. C-terminal COOH of integrin beta1 is necessary for beta1 association with the kindlin-2 adapter protein. *The Journal of biological chemistry* **289**, 11183-11193 (2014).
116. Hyduk, S.J. *et al.* Talin-1 and kindlin-3 regulate alpha4beta1 integrin-mediated adhesion stabilization, but not G protein-coupled receptor-induced affinity upregulation. *Journal of immunology* **187**, 4360-4368 (2011).
117. Zhang, X. *et al.* Talin depletion reveals independence of initial cell spreading from integrin activation and traction. *Nature cell biology* **10**, 1062-1068 (2008).
118. Ye, F. *et al.* Recreation of the terminal events in physiological integrin activation. *The Journal of cell biology* **188**, 157-173 (2010).
119. Calderwood, D.A., Campbell, I.D. & Critchley, D.R. Talins and kindlins: partners in integrin-mediated adhesion. *Nature reviews. Molecular cell biology* **14**, 503-517 (2013).
120. Critchley, D.R. Biochemical and structural properties of the integrin-associated cytoskeletal protein talin. *Annual review of biophysics* **38**, 235-254 (2009).
121. Pinon, P. *et al.* Talin-bound NPLY motif recruits integrin-signaling adapters to regulate cell spreading and mechanosensing. *The Journal of cell biology* **205**, 265-281 (2014).

122. Lawson, C. *et al.* FAK promotes recruitment of talin to nascent adhesions to control cell motility. *The Journal of cell biology* **196**, 223-232 (2012).
123. Song, X. *et al.* A novel membrane-dependent on/off switch mechanism of talin FERM domain at sites of cell adhesion. *Cell research* **22**, 1533-1545 (2012).
124. Saltel, F. *et al.* New PI(4,5)P<sub>2</sub>- and membrane proximal integrin-binding motifs in the talin head control beta3-integrin clustering. *The Journal of cell biology* **187**, 715-731 (2009).
125. Kahner, B.N. *et al.* Kindlins, integrin activation and the regulation of talin recruitment to alpha11beta3. *PLoS one* **7**, e34056 (2012).
126. Legate, K.R. *et al.* Integrin adhesion and force coupling are independently regulated by localized PtdIns(4,5)P<sub>2</sub> synthesis. *The EMBO journal* **30**, 4539-4553 (2011).
127. Anthis, N.J., Wegener, K.L., Critchley, D.R. & Campbell, I.D. Structural diversity in integrin/talin interactions. *Structure* **18**, 1654-1666 (2010).
128. Ellis, S.J., Pines, M., Fairchild, M.J. & Tanentzapf, G. In vivo functional analysis reveals specific roles for the integrin-binding sites of talin. *Journal of cell science* **124**, 1844-1856 (2011).
129. Gingras, A.R. *et al.* The structure of the C-terminal actin-binding domain of talin. *The EMBO journal* **27**, 458-469 (2008).
130. Ussar, S., Wang, H.V., Linder, S., Fassler, R. & Moser, M. The Kindlins: subcellular localization and expression during murine development. *Experimental cell research* **312**, 3142-3151 (2006).
131. Karakose, E., Schiller, H.B. & Fassler, R. The kindlins at a glance. *Journal of cell science* **123**, 2353-2356 (2010).
132. Bai, J. *et al.* RNA interference screening in Drosophila primary cells for genes involved in muscle assembly and maintenance. *Development* **135**, 1439-1449 (2008).
133. Rogalski, T.M., Mullen, G.P., Gilbert, M.M., Williams, B.D. & Moerman, D.G. The UNC-112 gene in *Caenorhabditis elegans* encodes a novel component of cell-matrix adhesion structures required for integrin localization in the muscle cell membrane. *The Journal of cell biology* **150**, 253-264 (2000).
134. Montanez, E. *et al.* Kindlin-2 controls bidirectional signaling of integrins. *Genes & development* **22**, 1325-1330 (2008).
135. Moser, M., Nieswandt, B., Ussar, S., Pozgajova, M. & Fassler, R. Kindlin-3 is essential for integrin activation and platelet aggregation. *Nature medicine* **14**, 325-330 (2008).
136. Ussar, S. *et al.* Loss of Kindlin-1 causes skin atrophy and lethal neonatal intestinal epithelial dysfunction. *PLoS genetics* **4**, e1000289 (2008).
137. Ma, Y.Q., Qin, J., Wu, C. & Plow, E.F. Kindlin-2 (Mig-2): a co-activator of beta3 integrins. *The Journal of cell biology* **181**, 439-446 (2008).
138. Harburger, D.S., Bouaouina, M. & Calderwood, D.A. Kindlin-1 and -2 directly bind the C-terminal region of beta integrin cytoplasmic tails and exert integrin-specific activation effects. *The Journal of biological chemistry* **284**, 11485-11497 (2009).
139. Bledzka, K. *et al.* Spatial coordination of kindlin-2 with talin head domain in interaction with integrin beta cytoplasmic tails. *The Journal of biological chemistry* **287**, 24585-24594 (2012).

140. Nakazawa, T. *et al.* Agonist stimulation, talin-1, and kindlin-3 are crucial for alpha(IIb)beta(3) activation in a human megakaryoblastic cell line, CMK. *Experimental hematology* **41**, 79-90 e71 (2013).
141. Shi, X. *et al.* The MIG-2/integrin interaction strengthens cell-matrix adhesion and modulates cell motility. *The Journal of biological chemistry* **282**, 20455-20466 (2007).
142. Yates, L.A., Fuzery, A.K., Bonet, R., Campbell, I.D. & Gilbert, R.J. Biophysical analysis of Kindlin-3 reveals an elongated conformation and maps integrin binding to the membrane-distal beta-subunit NPXY motif. *The Journal of biological chemistry* **287**, 37715-37731 (2012).
143. Yates, L.A. *et al.* Structural and functional characterization of the kindlin-1 pleckstrin homology domain. *The Journal of biological chemistry* **287**, 43246-43261 (2012).
144. Hart, R., Stanley, P., Chakravarty, P. & Hogg, N. The kindlin 3 pleckstrin homology domain has an essential role in lymphocyte function-associated antigen 1 (LFA-1) integrin-mediated B cell adhesion and migration. *The Journal of biological chemistry* **288**, 14852-14862 (2013).
145. Xu, Z., Gao, J., Hong, J. & Ma, Y.Q. Integrity of kindlin-2 FERM subdomains is required for supporting integrin activation. *Biochemical and biophysical research communications* **434**, 382-387 (2013).
146. Moser, M., Legate, K.R., Zent, R. & Fassler, R. The Tail of Integrins, Talin, and Kindlins. *Science* **324**, 895-899 (2009).
147. Meves, A., Stremmel, C., Bottcher, R.T. & Fassler, R. beta1 integrins with individually disrupted cytoplasmic NPXY motifs are embryonic lethal but partially active in the epidermis. *The Journal of investigative dermatology* **133**, 2722-2731 (2013).
148. Schiller, H.B. *et al.* beta1- and alphav-class integrins cooperate to regulate myosin II during rigidity sensing of fibronectin-based microenvironments. *Nature cell biology* **15**, 625-636 (2013).
149. Huet-Calderwood, C. *et al.* Differential binding to the ILK complex determines kindlin isoform adhesion localization and integrin activation. *Journal of cell science* (2014).
150. Rognoni, E. *et al.* Kindlin-1 controls Wnt and TGF-beta availability to regulate cutaneous stem cell proliferation. *Nature medicine* (2014).
151. Fukuda, K. *et al.* Molecular basis of kindlin-2 binding to integrin-linked kinase (ILK) pseudokinase for regulating cell adhesion. *The Journal of biological chemistry* (2014).
152. Mackinnon, A.C., Qadota, H., Norman, K.R., Moerman, D.G. & Williams, B.D. C. elegans PAT-4/ILK functions as an adaptor protein within integrin adhesion complexes. *Current biology : CB* **12**, 787-797 (2002).
153. Qadota, H. *et al.* Suppressor Mutations Suggest a Surface on PAT-4 (Integrin Linked Kinase) that Interacts with UNC-112 (Kindlin). *The Journal of biological chemistry* (2014).
154. Qadota, H., Moerman, D.G. & Benian, G.M. A molecular mechanism for the requirement of PAT-4 (integrin-linked kinase (ILK)) for the localization of UNC-112 (Kindlin) to integrin adhesion sites. *The Journal of biological chemistry* **287**, 28537-28551 (2012).

155. Widmaier, M., Rognoni, E., Radovanac, K., Azimifar, S.B. & Fassler, R. Integrin-linked kinase at a glance. *Journal of cell science* **125**, 1839-1843 (2012).
156. Brahme, N.N. *et al.* Kindlin binds migfilin tandem LIM domains and regulates migfilin focal adhesion localization and recruitment dynamics. *The Journal of biological chemistry* **288**, 35604-35616 (2013).
157. Lad, Y. *et al.* Structural basis of the migfilin-filamin interaction and competition with integrin beta tails. *The Journal of biological chemistry* **283**, 35154-35163 (2008).
158. Moik, D.V., Janbandhu, V.C. & Fassler, R. Loss of migfilin expression has no overt consequences on murine development and homeostasis. *Journal of cell science* **124**, 414-421 (2011).
159. Dixit, N. *et al.* Leukocyte function antigen-1, kindlin-3, and calcium flux orchestrate neutrophil recruitment during inflammation. *Journal of immunology* **189**, 5954-5964 (2012).
160. Ye, F., Kim, C. & Ginsberg, M.H. Reconstruction of integrin activation. *Blood* **119**, 26-33 (2012).
161. Zhang, X., Moore, S.W., Iskratsch, T. & Sheetz, M.P. N-WASP-directed actin polymerization activates Cas phosphorylation and lamellipodium spreading. *Journal of cell science* **127**, 1394-1405 (2014).
162. Roca-Cusachs, P., Iskratsch, T. & Sheetz, M.P. Finding the weakest link: exploring integrin-mediated mechanical molecular pathways. *Journal of cell science* **125**, 3025-3038 (2012).
163. Zaidel-Bar, R. & Geiger, B. The switchable integrin adhesome. *Journal of cell science* **123**, 1385-1388 (2010).
164. Winograd-Katz, S.E., Fassler, R., Geiger, B. & Legate, K.R. The integrin adhesome: from genes and proteins to human disease. *Nature reviews. Molecular cell biology* **15**, 273-288 (2014).
165. Wei, X. *et al.* Kindlin-2 regulates renal tubular cell plasticity by activation of Ras and its downstream signaling. *American journal of physiology. Renal physiology* (2013).
166. Wei, X. *et al.* Kindlin-2 mediates activation of TGF-beta/Smad signaling and renal fibrosis. *Journal of the American Society of Nephrology : JASN* **24**, 1387-1398 (2013).
167. Yu, Y. *et al.* Kindlin 2 forms a transcriptional complex with beta-catenin and TCF4 to enhance Wnt signalling. *EMBO reports* **13**, 750-758 (2012).
168. Miyamoto, S. *et al.* Integrin function: molecular hierarchies of cytoskeletal and signaling molecules. *The Journal of cell biology* **131**, 791-805 (1995).
169. Miller, N.L. *et al.* A non-canonical role for Rgnef in promoting integrin-stimulated focal adhesion kinase activation. *Journal of cell science* **126**, 5074-5085 (2013).
170. Hu, Y.L. *et al.* FAK and paxillin dynamics at focal adhesions in the protrusions of migrating cells. *Scientific reports* **4**, 6024 (2014).
171. Brami-Cherrier, K. *et al.* FAK dimerization controls its kinase-dependent functions at focal adhesions. *The EMBO journal* **33**, 356-370 (2014).
172. Deakin, N.O. & Turner, C.E. Paxillin comes of age. *Journal of cell science* **121**, 2435-2444 (2008).

173. An, Z. *et al.* Kindlin-2 is expressed in malignant mesothelioma and is required for tumor cell adhesion and migration. *International journal of cancer. Journal international du cancer* **127**, 1999-2008 (2010).
174. Gong, X. *et al.* Kindlin-2 controls sensitivity of prostate cancer cells to cisplatin-induced cell death. *Cancer letters* **299**, 54-62 (2010).
175. Sakamoto, S., McCann, R.O., Dhir, R. & Kyprianou, N. Talin1 promotes tumor invasion and metastasis via focal adhesion signaling and anoikis resistance. *Cancer research* **70**, 1885-1895 (2010).
176. Zhan, J. *et al.* Opposite role of Kindlin-1 and Kindlin-2 in lung cancers. *PLoS one* **7**, e50313 (2012).

## 5. Acknowledgements

With the completion of my PhD project, I have become a different person, than when I started this work. I have grown with the challenges imposed on me, and this would not have been possible without the support of many people, to whom I want to express my deep gratefulness at this point.

First, I want to thank my supervisor and mentor, Prof. Reinhard Fässler, who made all of this possible. He supported me through his trust and always believed that I can succeed as a scientist. In many hours of discussions he taught me to be critical and not be satisfied with hasty, superficial explanations. Besides of the time he invested, he provided without hesitation all the materials and support I needed to complete my work.

Second, I want to thank the members of my thesis-comitee. My special thanks go to Prof. Bernhard Wehrle-Haller, who supported my work with inspiring discussions and who unhesitatingly agreed to travel from Switzerland to join my defense. I further want to thank Prof. Markus Sperandio, Prof. Christian Wahl-Schott, Prof. Stefan Zahler and Prof. Angelika Vollmar for their willingness to examine my work.

Third, I want to thank my colleagues, many of which have become good friends over time. My special thanks go to Dr. Emanuel Rognoni, with whom I started my work. During uncounted hours of scientific and non-scientific discussions he inspired and encouraged me for my work and my private life. He let me partake in his research and never hesitated to help me with complicated experiments or problems. Also, I want to thank my predecessor Dr. Siegfried Ussar, who introduced me into the lab, raised my enthusiasm for kindlins and integrins and taught me the basics to deal with my project. I further want to thank Marina Theodosiou, who joined our lab in a late phase of my project. She proved to be a fast learning, highly skilled scientist and supported my work with important results. Furthermore, I want to thank Prof. Roy Zent, Prof. Ambra Pozzi, Dr. Michaela Hermann, Dr. Maik Veelders, Dr. Julien Polleux, Dr. Ralph Böttcher, Dr. Sarah Wickstroem, Dr. Ina Rohwetter, Dr. Johannes Altstätter, Dr. Kyle Legate, Dr. Eloi Montanez, Dr. Ezra Karaköse, Dr. Annika Böttcher, Dr. Alex Meves, Dr. Raphael

Ruppert, Hui-Yuang Tseng, Dr. Carsten Grashoff, Katharina Austen, Dr. Armin Lambacher, Dr. Sussanne Seidl and many more people, who supported my work by various means.

Fourth, I want to thank the people, who supported my work with technical assistance, directly and indirectly. My special thanks go to Ursula Kuhn, who supported my work during uncounted hours with her fabulous abilities in gene cloning and Southern blotting; I had a great time with her. Furthermore, I want to thank Simone Bach, Klaus Weber and Ines Lach-Kusevic for their help. I further want to express my thankfulness towards the whole staff of the animal facility, directed by Dr. Heinz Brandstetter and Corinna Mörth as well as the staff of the biochemistry core facility, directed by Dr. Stephan Uebel. The services offered by these facilities were of invaluable importance for my work.

Last, I want to thank my family for their continuous support and especially my loving wife, Verena. She has, after all, made everything possible by giving me strength to persevere and by letting me participate in her unique perspective of the world.

## 6. Curriculum vitae

### **Personal Data**

Full name: Sven Moritz Widmaier  
 Born: in Munich, Germany, on September 19<sup>th</sup>, 1981  
 Nationality: German  
 Email: [widmaier@biochem.mpg.de](mailto:widmaier@biochem.mpg.de)

### **Education:**

March 2008-current: PhD thesis at the Max-Planck-Institute of Biochemistry  
 July 2007: Degree Master of Science in Biochemistry  
 August 2005: Degree Bachelor of Science in Biochemistry  
 October 2002: Onset of study course Biochemistry at the TU-Munich  
 2001: Abitur (High school-degree) at Luitpold Gymnasium in Munich  
 1987-1991: Elementary school at Gebele-Schule in Munich

### **Publications in order of appearance:**

Rognoni E, **Widmaier M**, Haczek C, Mantwill K, Holzmüller R, Gansbacher B, Kolk A, Schuster T, Schmid RM, Saur D, Kaszubiak A, Lage H, Holm PS. Adenovirus-based virotherapy enabled by cellular YB-1 expression in vitro and in vivo. *Cancer Gene Ther.* 2009; 16(10), 753-763.

Ussar S, Moser M, **Widmaier M**, Rognoni E, Harrer C, Genzel-Boroviczeny O, Fässler R. Loss of Kindlin-1 causes skin atrophy and lethal neonatal intestinal epithelial dysfunction. *PLoS Genet.* 2008, 4(12), e1000289.

Böttcher RT, Stremmel C, Meves A, Mayer H, **Widmaier M**, Tseng HY, Fässler R. Sorting nexin 17 prevents lysosomal degradation of  $\beta$ 1 integrins by binding to the  $\beta$ 1 integrin tail. *Nat Cell Biol.* 2012, 14(6):584-92.

**Widmaier M**, Rognoni E, Radovanac K, Azimifar B, Fässler R. Integrin linked kinase at a glance. *J C Sci.* 2012, 125(Pt8), 1839-1843.

Rognoni E, **Widmaier M**, Jakobson M, Ruppert R, Ussar S, Katsougkri D, Böttcher RT, Lai-Cheong JE, Rifkin DB, McGrath JA, Fässler R. Kindlin-1 controls Wnt and TGF- $\beta$  availability to regulate cutaneous stem cell proliferation. *Nat Med.* 2014, 20(4), 350-9.

**Widmaier M**, Theodosiou E, Rognoni E, Austen K, Veelders M, Müller D, Strohmeyer N, Bharadwaj, Petrasek Z, Zent R, Fässler R. Kindlin-2 initiates fibroblast adhesion and spreading by recruitment of paxillin and FAK to nascent adhesion sites. *In preparation.*

## 7. Appendix

The appendix includes reprints of the paper I to V. The supplementary materials (figures, tables and movies) for each paper, which are not printed, can be found on the enclosed CD.

### 7.1. Paper I

Kindlin-2 initiates fibroblast adhesion and spreading by recruitment of paxillin and FAK to nascent adhesion sites.

**Moritz Widmaier**, Marina Theodosiou\*, Emanuel Rognoni\*, Katharina Austen, Maik Veelders, Daniel Müller, Mitasha Bharadwaj, Zdenek Petrsek, Roy Zent, Reinhard Fässler. (\*contributed equally)

#### Supplemental material

PDF file

Supplementary figures 1-5

### 7.2. Paper II

Integrin linked kinase at a glance.

**Moritz Widmaier**, Emanuel Rognoni, Korana Radovanac, Babak Azimifar, Reinhard Fässler.

### 7.3. Paper III

Loss of Kindlin-1 causes skin atrophy and lethal neonatal intestinal epithelial dysfunction.

Siegfried Ussar, Markus Moser, **Moritz Widmaier**, Emanuel Rognoni, Christian Harrer, Orsolya Genzel-Boroviczeny, Reinhard Fässler.

#### Supplemental material

Supplementary Figures 1-11

### 7.4. Paper IV

Kindlin-1 controls Wnt and TGF- $\beta$  availability to regulate cutaneous stem cell proliferation.

Emanuel Rognoni, **Moritz Widmaier**, Madis Jakobson, Raphael Ruppert, Siegfried Ussar, Despoina Katsougkri, Ralph T. Böttcher, Joey E. Lai-Cheong, Daniel B. Rifkin, John McGrath, Reinhard Fässler

#### Supplementary material

PDF file

Supplementary Figures 1-8

Supplementary Table 1, *P*-values for relative amount of SC subpopulations over time analyzed by FACS

Supplementary Table 3, Wnt ligand and receptor transcript analysis

Supplementary Table 4, List of qPCR oligonucleotides

Extended Experimental Procedure

Supplemental References

Excel file

Supplementary Table 2, Microarray data with significant gene expression changes of  $\geq 2$  fold

#### 1.1. Paper IV

Sorting nexin 17 prevents lysosomal degradation of  $\beta 1$  integrins by binding to the  $\beta 1$  integrin tail.

Ralph Thomas Böttcher, Christopher Stremmel, Alexander Meves, Hannelore Mayer, Moritz Widmaier, Hui-Yuang Tseng, Reinhard Fässler.

#### Supplemental material:

PDF file

Supplemental table 1, detailed results of  $\beta$  integrin tail pull down experiments

Supplemental movie 1, comparison of cell spreading kinetics

Supplemental movie 2, comparison of cell migration kinetics

# **Kindlin-2 initiates fibroblast adhesion and spreading by recruitment of paxillin and FAK to nascent adhesion sites**

Moritz Widmaier<sup>1</sup>, Marina Theodosiou<sup>1\*</sup>, Emanuel Rognoni<sup>1\*</sup>, Katharina Austen<sup>2</sup>, Maik Veelders<sup>1</sup>, Daniel Müller<sup>3</sup>, Mitasha Bharadwaj<sup>3</sup>, Zdenek Petrsek<sup>4</sup>, Roy Zent<sup>4</sup>, Reinhard Fässler<sup>1</sup>

<sup>1</sup>Department of Molecular Medicine, Max Planck Institute of Biochemistry, Martinsried, Germany; <sup>2</sup>Molecular Mechanotransduction Group, Max Planck Institute of Biochemistry, Martinsried, Germany; <sup>3</sup>ETH Zürich, Department Biosystems Science and Engineering, 4058 Basel, Switzerland; <sup>4</sup>Department Cellular and Molecular Physics, Max Planck Institute of Biochemistry, Martinsried, Germany; <sup>5</sup>Division of Nephrology, Department of Medicine, Vanderbilt University, and the Department of Medicine, Veterans Affairs Medical Center, Nashville, 37232 Tennessee.

\* contributed equally

## **Abstract**

Integrins are  $\alpha/\beta$  heterodimers that mediate cell-matrix and cell-cell adhesion. Integrins require an activation step prior to ligand binding, clustering and the recruitment of signalling and adaptor proteins to their cytoplasmic domains. Integrin activation and signalling are induced upon binding of talin and kindlin proteins to the  $\beta$  tails of integrins. Although kindlins are essential for integrin function their contributions to integrin activation and signalling are unclear. Here we report that fibroblast cell lines lacking either talin or kindlin expression bind normal amounts of soluble fibronectin (FN) ligand but fail to bind the anti- $\beta$ 1 integrin 9EG7 antibody and to adhere to a FN-coated substrate indicating that both talin and kindlin are required to shift the  $\alpha$ 5 $\beta$ 1 integrin into the high affinity state. When the high affinity state is induced with  $Mn^{2+}$  talin-deficient but not kindlin-deficient cells show increased binding to soluble FN and 9EG7 and initiate adhesion to FN and isotropic spreading indicating that kindling can maintain a  $Mn^{2+}$ -induced active integrin and initiate signalling. Mechanistically, kindlin executes these tasks by directly binding to paxillin in small integrin adhesion sites, which is followed by recruiting focal adhesion kinase (FAK), lamellipodia induction and growth and pro-survival signalling. Our findings identify two steps during FN-induced adhesion and cell spreading that are controlled by talin and kindlin; in the first step talin and kindlin cooperatively activate integrins leading to FN-integrin binding and adhesion, and in a second step kindlin recruits paxillin and FAK to initiate spreading and signalling, while talin links integrins to F-actin to stabilize and mature the adhesion sites.

## Introduction

Integrins are heterodimeric transmembrane receptors that mediate cell adhesion to the extracellular matrix (ECM) and to other cells <sup>1</sup>. The consequence of integrin-mediated adhesion is the assembly of a large molecular network that induces various signalling pathways resulting in cell migration, proliferation, survival and differentiation <sup>2</sup>. The quality and the strength of integrin signalling are controlled by the interaction between integrins and substrate-attached ligands, which in turn is controlled by the on- and off-rates of the integrin ligand binding process <sup>3</sup>. The on-rate of the integrin-ligand binding reaction (also called integrin activation) is characterized by switching the unbound form of integrins from the inactive (low affinity) to the active (high affinity) state. The affinity switch is allosteric and proceeds in at least two major steps; the bent and clasped integrin dimer extends into an intermediate ligand binding affinity. This step is followed by the unclasp of the proximal leg domains, transmembrane domains and cytoplasmic tails of the  $\alpha$  and  $\beta$  subunits, and a “swing-out” of the hybrid domain that connects  $\beta$  leg and head domains leading to full ligand binding affinity <sup>1, 4</sup>. The allostery is of chemical nature and induced with the binding of the two adaptor proteins talin and kindlin to the  $\beta$  integrin cytoplasmic domain <sup>5, 6</sup> and requires the presence of divalent cations in the ligand-binding pocket <sup>1</sup>.

The off-rate of an integrin-ligand complex is controlled by two mechanisms, integrin clustering and catch bond formation between integrin and bound ligand, and is believed to be of equal importance as the on-rate regulation. Both off-rate mechanisms stabilize integrin-ligand complexes and are therefore, important regulators of the duration and strength of adhesion and signalling <sup>7-11</sup>. The stabilizing effect of clustered integrins is due to the increased probability for dissociated integrin-ligand complexes to rebind before they leave the adhesion site <sup>8, 10</sup>, while catch bonds are receptor-ligand bonds whose lifetime increases with force <sup>12-14</sup>. In contrast to the integrin activation model, integrin clustering as well as catch bond formation depend on the association of integrins with the actin cytoskeleton <sup>10, 15</sup>, which is mediated, at least in part, by talins and kindlins <sup>10, 16</sup>.

The talin family consists of two (talin-1 and -2) and the kindlin family of three isoforms (kindlin-1-3), which show tissue-specific expression patterns <sup>17, 18</sup>. They activate integrins and associate active integrins either directly and/or indirectly with the actin cytoskeleton <sup>19, 20</sup>. Since the binding sites of talin and kindlin in  $\beta$  integrin cytoplasmic tails are in close proximity it has been proposed that talin and kindlin may bind sequentially to  $\beta$  tails and function consecutively rather than conjointly to control the on- and off-rates of the integrin ligand binding process <sup>5, 21, 22</sup>. Indeed, there is experimental evidence that talin and kindlin

fulfil non-overlapping role(s) during integrin-ligand binding. The role that the two proteins play is hotly debated. For example, it was shown that talin-1 activates  $\alpha$ IIB $\beta$ 3, while kindlin-3 stabilizes the integrin-ligand complex by stimulating  $\alpha$ IIB $\beta$ 3 clustering<sup>16</sup>. On the other hand, there is also experimental evidence for a primary role of talin in integrin clustering rather than activation<sup>23</sup>. Further evidence demonstrates that talin is not associated with integrin tails during the nucleation of nascent adhesions (NAs;<sup>24</sup>), that talin recruitment is not required for NAs development<sup>25</sup>, that talin loss allows fibroblasts adhesion and isotropic spreading<sup>26</sup>, and that the recombinant talin-FERM domain inefficiently induces the separation of  $\alpha$ IIB $\beta$ 3 and  $\beta$ 3 subunits inserted into lipid discs<sup>21</sup>.

In the present paper we report the generation and characterisation of a cell model system that allowed a direct functional comparison of talin and kindlin for fibronectin (FN) binding integrins on fibroblasts. The implications of the results are discussed.

## Results

### Kindlins and talins control cell morphology, adhesion and integrin expression

Fibroblasts express talin-1 and kindlin-2, whose deficiencies were compensated by the de novo expression of talin-2 and kindlin-1, respectively (Suppl. 1A). The low talin-2 and kindlin-1 levels were sufficient to allow adhesion and cell spreading, although to a lesser extent than control cells (Suppl. 1B). To prevent the compensatory upregulation of talin-2 and kindlin-1, we generated mice with loxP flanked (floxed; fl) talin-1 and nullizygous talin-2 alleles or with floxed kindlin-1 and -2 alleles ( $Tln^{Ctr}$ ;  $Kind^{Ctr}$ ; Fig.1A), isolated, immortalized and cloned kidney fibroblasts with comparable integrin surface levels (Suppl. 1C), and deleted the floxed alleles by adenovirally transducing *Cre* recombinase resulting in talin-1, -2 ( $Tln^{Ko}$ ) and kindlin-1, -2 ( $Kind^{Ko}$ ) deficient cells, respectively (Fig. 1A-C). The  $Tln^{Ctr}$  and  $Kind^{Ctr}$  control cells showed the same morphologies and behaved the same in all experiments tested. Therefore, we display only one control cell line in the majority of the result panels. *Cre*-mediated deletion of talin-1 or kindlin-1/2 was efficient (Fig. 1B) and resulted in cell rounding, poor adhesion in a few cells (Fig. 1C) and significantly reduced proliferation rates (Suppl. 1D). To exclude cell passage-induced abnormalities, we used cells up to 12 passages after *Cre*-mediated gene deletions.

To define the adhesion defects we performed plate and wash assays on different substrates and observed that  $Tln^{Ko}$  and  $Kind^{Ko}$  cells almost completely lost adhesion on fibronectin (FN), laminin-111 (LN), type I collagen (COL) and vitronectin (VN). Treatment with  $Mn^{2+}$  induced a comparable increase of  $Tln^{Ko}$  and  $Kind^{Ko}$  cell adhesion to FN, while adhesion to LN was induced in  $Tln^{Ko}$  cells only and adhesion to VN and COL in neither cell line (Fig. 1D).

Next we used flow cytometry to determine whether changes in integrin surface levels accounted for the differential adhesion properties of  $Tln^{Ko}$  and  $Kind^{Ko}$  cells. The experiments revealed that the levels of  $\beta 1$  and  $\beta 3$  were significantly reduced in  $Kind^{Ko}$  and unaffected in  $Tln^{Ko}$  cells. The levels of  $\alpha 2$ ,  $\alpha 3$  were reduced in both cell lines,  $\alpha 6$  was elevated in  $Tln^{Ko}$  and decreased in  $Kind^{Ko}$  cells and the  $\alpha 3$  levels were significantly more decreased in  $Kind^{Ko}$  than in  $Tln^{Ko}$  cells (Fig. 1E) explaining the absent adhesion of both cell lines on COL and their differential adhesion behaviour on LN (Fig. 1D). Although  $\beta 1$  and  $\beta 3$  levels were differentially affected,  $\alpha 5$  and  $\alpha v$  integrins were slightly reduced but not significantly different between  $Tln^{Ko}$  and  $Kind^{Ko}$  cells and  $\beta 5$  was similarly increased in  $Tln^{Ko}$  and  $Kind^{Ko}$  cells (Fig. 1E), which altogether provides an explanation why adhesion to FN was similar between  $Tln^{Ko}$  and  $Kind^{Ko}$  cells (Fig. 1D). Likewise, the pronounced reduction of the COL-binding  $\alpha 2$  in

Tln<sup>Ko</sup> as well as Kind<sup>Ko</sup> cells was in line with the severely reduced adhesion to collagen (Fig. 1D). Since the levels of the FN binding  $\alpha 5\beta 1$  and  $\alpha v$ -class integrins were similar on Tln<sup>Ko</sup> and Kind<sup>Ko</sup> cells and their adhesion on FN identical we decided to perform all further experiments on FN.

### **Integrin binding to FN requires talin and kindlin-2**

Cell adhesion and spreading on substrate bound ligands requires integrin activation, ligand binding, clustering and adhesion re-enforcement<sup>3</sup>. To test whether loss of talin or kindlin affected integrin activation we used flow cytometry to measure binding of soluble, Cy5-labelled wild type FN-III<sub>7-10</sub> (FN-RGD) or an integrin-binding deficient FN-III<sub>7-10</sub> fragment carrying an aspartic acid to glutamate substitution in the RGD binding motif (FN-RGE), to which wild type fibroblasts adhered poorly and failed to spread (Suppl. 2A). We found that Tln<sup>Ctrl</sup> and Kind<sup>Ctrl</sup> as well as Tln<sup>Ko</sup> and Kind<sup>Ko</sup> cells bound similar amounts of FN-RGD (Fig. 2A). As expected, Mn<sup>2+</sup> treatment induced a strong and comparable FN-RGD binding on Tln<sup>Ctrl</sup> and Kind<sup>Ctrl</sup> cells. Interestingly, the strong Mn<sup>2+</sup>-induced increase of FN-RGD binding was slightly but not significantly different between Tln<sup>Ko</sup> and Tln<sup>Ctrl</sup> cells, while the Mn<sup>2+</sup>-induced increase of FN-RGD binding was significantly less pronounced on Kind<sup>Ko</sup> compared to Kind<sup>Ctrl</sup> cells (Fig. 2A) indicating that kindlin-2 increases ligand binding affinity (on-rates) and/or stabilizes ligand binding in concert with Mn<sup>2+</sup> and the FN ligand.

It has been reported that the ligand binding affinities of clasped and unclasped  $\alpha 5\beta 1$  integrin ectodomains differ by around 5.5-fold<sup>27</sup>. This difference in affinity is caused by combined effects of lower on- and higher off-rates and Mn<sup>2+</sup> stimulation can only normalize the on-rate. To test whether the diminished FN-RGD binding of Mn<sup>2+</sup>-treated Kind<sup>Ko</sup> cells is due to an impaired integrin unclasping, we measured the binding of the 9EG7 antibody, which binds only to unclasped  $\beta 1$  integrins<sup>4, 27</sup>. These measurements revealed that Tln<sup>Ctrl</sup> and Kind<sup>Ctrl</sup> cells bound high levels of 9EG7, while Tln<sup>Ko</sup> and Kind<sup>Ko</sup> cells almost entirely lost 9EG7 binding (Fig. 2B). Next we treated our cells with Mn<sup>2+</sup> and FN to test their allosteric influence on 9EG7 binding to the  $\alpha 5\beta 1$  integrin. In line with an increased FN-RGD binding by Tln<sup>Ko</sup> cells (Fig. 2A), Mn<sup>2+</sup> and FN treatment also induced significantly more 9EG7 binding in Tln<sup>Ko</sup> compared to Kind<sup>Ko</sup> cells (Fig. 2B). These findings confirm that in contrast to talin, kindlin-2 is sufficient to elevate Mn<sup>2+</sup>-induced binding of 9EG7 (reporting integrin unclasping) and FN-RGD.

In order to analyse to which extent talin and kindlin-2 impair adhesion strength to FN, we attached the Tln<sup>Ctrl</sup>, Kind<sup>Ctrl</sup>, Tln<sup>Ko</sup> or Kind<sup>Ko</sup> cells to ConA-coated cantilevers of an atomic

force microscope (AFM), allowed them to contact FN-RGD- or FN- $\Delta$ RGD-coated surfaces for increasing time periods and then measured the forces required to disrupt binding to the FN fragments (Fig. 2C,D). As expected, none of the cell lines adhered to FN- $\Delta$ RGD. After a 5 s contact time to FN-RGD neither cell line showed significant adhesion. The force required for disrupting the adhesion of Tln<sup>Ctrl</sup> and Kind<sup>Ctrl</sup> cells to FN-RGD averaged out at 3 nN after contact time of 20 s and increased to 4 and 5 nN after contact times of 20 and 120 s, respectively (Fig. 2C). Tln<sup>Ko</sup> cells also required around 3 nN force to disrupt the adhesion to FN-RGD after a 20 s contact time. Interestingly, after contact times of 50 and 120 s we observed two Tln<sup>Ko</sup> cell populations which greatly differed with respect to their adhesion forces; in one Tln<sup>Ko</sup> population the adhesion force increased concomitantly with the contact times, while the second cell population showed no significant adhesion. In sharp contrast, Kind<sup>Ko</sup> cells were unable to establish a measurable adhesion to FN-RGD irrespective of the contact time (Fig. 2C). Although the treatment with Mn<sup>2+</sup> enabled adhesion of Kind<sup>Ko</sup> cells to FN-RGD, the adhesion strength of Tln<sup>Ko</sup> cells was significantly higher and decreased to background level in the presence of EDTA (Fig. 2D). The weaker adhesion strength in Kind<sup>Ko</sup> cells suggest that kindlin  $\alpha$ 5 $\beta$ 1 integrin remains in the intermediate affinity conformation, which leads to reduced rates of ligand binding, and an increased off-rate, leading to weaker adhesion forces in the presence of Mn<sup>2+</sup>.

Although unstimulated Tln<sup>Ko</sup> and Kind<sup>Ko</sup> cells bound similar amounts of FN after 30 min, (Fig. 2A), assembly of soluble FN into fibrils, which requires the stable association of active  $\alpha$ 5 $\beta$ 1 integrin to the actin cytoskeleton<sup>28</sup>, occurred neither in Tln<sup>Ko</sup> nor in Kind<sup>Ko</sup> cells (Fig. 2E). As expected, re-expression of full-length, Venus-tagged talin (Tln1V) in Tln<sup>Ko</sup> or GFP-tagged kindlin-2 (K2GFP) in Kind<sup>Ko</sup> cells rescued 9EG7 binding, adhesion to FN and FN fibril assembly (Fig. 2E-G and Suppl. 2B). Importantly, however, neither overexpression of the talin-1 head (THD) or K2GFP in Tln<sup>Ko</sup> cells, nor Tln1V or THD in Kind<sup>Ko</sup> cells significantly improved 9EG7 binding or adhesion to FN (Fig. 2F,G and Suppl. 2B).

These results suggest that  $\alpha$ 5 $\beta$ 1 integrins exists in an intermediate affinity (clasped/extended) state in untreated Tln<sup>Ko</sup> and Kind<sup>Ko</sup> cells, that the allosteric transition into the high affinity (unclasped/extended) state triggered by the addition of Mn<sup>2+</sup> and FN and monitored by 9EG7 binding requires talin and kindlin-2, although kindlin-2 can induce a small but significant binding of the 9EG7 antibody as well as weak adhesion to FN measured by AFM. However, firm adhesion to and assembly of FN fibrils requires both talin and kindlin-2, as an elevation of kindlin-2 levels in Tln<sup>Ko</sup> and talin levels in Kind<sup>Ko</sup> cells are unable to reverse the defects.

## Kindlin-2 controls spreading together with EGF

The off-rates of integrin-ligand complexes differ between  $Tln^{Ko}$  and  $Kind^{Ko}$  cells. Off-rates are regulated by integrin clustering, which can be induced by seeding cells on immobilized ligand<sup>29</sup>. To investigate integrin clustering we plated our cell lines on FN-coated culture dishes or kept them in suspension and measured large scale integrin clustering by immunofluorescence (IF) confocal microscopy and small scale clustering by combining stochastic optical reconstruction microscopy (STORM) and total internal reflection fluorescence (TIRF) microscopy. To ensure that only surface  $\beta 1$  integrin was stained and analysed all experiments were performed without permeabilizing membrane. In line with a previous report<sup>30</sup>, IF staining of suspended  $Tln^{Ctr}$  and  $Kind^{Ctr}$  cells revealed aggregates of  $\beta 1$  integrins in actin-containing membrane spikes, which were indistinguishable from  $Tln^{Ko}$  or  $Kind^{Ko}$  cells, remained unaffected by  $Mn^{2+}$  and disappeared upon latrunculin A treatment (Fig. 3A; Suppl. 3A). When  $Tln^{Ctr}$  or  $Kind^{Ctr}$  cells were seeded on FN, the small membrane spikes were lost and  $\beta 1$  integrins clustered together with ILK, paxillin, talin and kindlin-2 (Suppl. 3B) in NAs and focal adhesions (FAs), whose size and frequency increased upon  $Mn^{2+}$  treatment (Fig. 3B). In contrast, the few weakly adhering  $Tln^{Ko}$  and  $Kind^{Ko}$  cells were small and formed finely dispersed, small  $\beta 1$  integrin clusters over the entire cell.  $Mn^{2+}$  treatment improved adhesion of  $Tln^{Ko}$  and  $Kind^{Ko}$  cells (Fig. 1D) and induced isotropic spreading in around 24 %  $Tln^{Ko}$  and anisotropic spreading in around 21 %  $Kind^{Ko}$  cells with small, NA-like  $\beta 1$  integrin clusters enriched at the cell periphery (Fig. 3B,C). Interestingly,  $Mn^{2+}$  induced lamellipodia formation and spreading of  $Tln^{Ko}$  cells were only observed on FN and in the presence of EGF or serum (Fig. 3C,D). Re-expression of  $Tln1V$  in  $Tln^{Ko}$  cells or  $K2GFP$  in  $Kind^{Ko}$  cells normalized the morphology and the FA formation of upon FN seeding (Suppl. 3C). These findings indicate no prominent role of talin and kindlin-2 for the formation of integrin micro-clusters. However, in the presence of EGF and  $Mn^{2+}$  kindlin-2 but not talin induced high affinity integrin-ligand interactions, which facilitated the formation of small, peripheral integrin clusters and large lamellipodia.

STORM microscopy of  $Mn^{2+}$ -treated  $Kind^{Ctr}$  and  $Tln^{Ctr}$  cells showed  $\beta 1$  integrin clusters that were enriched in paxillin-containing FAs (acquired with diffraction limited resolution) and in the cell periphery. Interestingly,  $Mn^{2+}$ -treated  $Tln^{Ko}$  and  $Kind^{Ko}$  cells also displayed  $\beta 1$  integrin clusters in their periphery, which were of similar size as in  $Kind^{Ctr}$  cells (Fig. 3E). Due to the stochastic process of STORM image acquisition and the resolution of ~50 nm we could not resolve individual integrin molecules, and hence the  $\beta 1$  integrin staining-densities represent clusters of several  $\beta 1$  integrin molecules (up to four considering their 12 nm size).

Since each  $\beta 1$  integrin cluster is defined through multiple signal detections and the collected signals per cluster were similar for all cell lines, we conclude that the number of  $\beta 1$  integrins per cluster is similar between Kind<sup>Ctrl</sup>, Tln<sup>Ko</sup> and Kind<sup>Ko</sup> cells (Suppl. 3D,E). To define the spatial organization of the integrin clusters, we determined the nearest neighbour distance (NND) in- and outside of adhesion sites as well as the numbers of separate integrin clusters in close proximity, as they can be found in FAs (Fig. 3F,G). In Tln<sup>Ctrl</sup> and Kind<sup>Ctrl</sup> cells, the NND of  $\beta 1$  clusters within FAs was around ~60-80 nm (Fig. 3F), which was also found by others for normal fibroblasts<sup>31-33</sup>. The NND outside of FAs was 140 nm for  $\beta 1$  (Fig. 3F) and the numbers of  $\beta 1$  integrin clusters per  $\mu\text{m}^2$  was normal in Tln<sup>Ko</sup> and reduced in Kind<sup>Ko</sup> cells (Suppl. 3F), which is in line with their reduced  $\beta 1$  integrin surface levels (Fig.1E). In Tln<sup>Ctrl</sup> and Kind<sup>Ctrl</sup> cells, around 28 % of the  $\beta 1$  clusters formed aggregates with more than six and 18 % with 4-6 clusters in paxillin-positive FAs, while the remaining 54 % of  $\beta 1$  clusters assembled mainly in small aggregates (1-3 clusters) outside of FAs (Fig. 3E,G). Since Tln<sup>Ko</sup> and Kind<sup>Ko</sup> cells lack classical FAs we analysed the spatial distribution of all  $\beta 1$  clusters (Fig. 3F,G) and found no overt differences among the size or the NNDs of the cluster aggregates compared to Tln<sup>Ctrl</sup> and Kind<sup>Ctrl</sup> cells.

Our findings demonstrate that the size distribution of Mn<sup>2+</sup> induced  $\beta 1$  integrin clusters was similar in control, Tln<sup>Ko</sup> and Kind<sup>Ko</sup> cells seeded on immobilized FN, and that kindlin can induce NA-like adhesion sites in the cell periphery and large lamellipodia.

### **Kindlin-2 binds and recruits paxillin to NAs**

Our data indicate that kindlin-2 can mediate adhesion, spreading and formation of small, NA-like integrin clusters in lamellipodia of Tln<sup>Ko</sup> cells. To identify the binding partner(s) of kindlin-2 that mediate this function, we performed yeast two hybrid assays with kindlin-2 as bait against a human cDNA library containing all possible open reading frames (ORFs). We identified 26 cDNAs, all of which coded for leupaxin. Immuno-precipitation of overexpressed GFP-tagged paxillin family members, paxillin, Hic-5 and leupaxillin in HEK-293 cells with an anti-GFP antibody efficiently co-precipitated FLAG-tagged kindlin-2 (K2flag) (Fig. 4A). Since fibroblasts express high levels of paxillin (Suppl. 4A), we performed all further interaction analysis with paxillin. Immuno-precipitations of GFP-tagged paxillin as well as kindlin-2 truncation mutants revealed that the interaction between kindlin-2 and paxillin was dramatically reduced in the absence of the LIM1-4, LIM2-4 or LIM3-4 domains of paxillin (Fig. 5B), or the PH domain (K2 $\Delta$ PHGFP) or the N-terminus including the F0, F1 domains and the N-terminal proportion of the F2 domain excluding the PH domain of kindlin-2

(K2NTGFP; Fig. 4C). The interaction between kindlin-2 and ILK (Montanez et al., 2009) via the C-terminal pseudokinase domain of ILK<sup>34</sup> was not affected by the deletion of the PH domain (Fig. 4C). Pull down experiments with recombinant kindlin-2 and the recombinant LIM3 domain of paxillin demonstrated that the binding is direct and Zn<sup>2+</sup> ion-dependent (Fig. 4D). Furthermore, expression of K2GFP in Kind<sup>Ko</sup> cells rescued spreading, paxillin recruitment to NAs and 9EG7 levels, while expression of K2ΔPHGFP failed to normalize spreading, paxillin recruitment to NAs and 9EG7 levels (Fig. 4E; Suppl. 4B). However, mature FAs of K2ΔPHGFP-rescued cells seeded for 30 or 60 min on FN and connected to a contractile F-actin cytoskeleton contained significant amounts of paxillin (Fig. 4E). These findings indicate that kindlin-2 directly binds the LIM3 domain of paxillin via the PH domain to recruit paxillin to NAs.

### **The kindlin-2/paxillin complex promotes FAK-mediated cell spreading and survival**

Our findings revealed that kindlin-2 recruits paxillin to NAs. Paxillin in turn, was shown to bind, cluster and activate FAK in NAs, which leads to the recruitment of Cas130, Crk and Dock to the activation of Rac1 and the induction of cell spreading, and in concert with growth factor signals to the activation of Akt-1 and Erk-2 and the induction of cell proliferation and survival<sup>35-38</sup>. We therefore hypothesized that the recruitment of paxillin and FAK by kindlin-2 triggers the improved spreading and survival of Tln<sup>Ko</sup> cells. To test this hypothesis, we seeded our cell lines on FN or PLL in the presence or absence of EGF and Mn<sup>2+</sup> (Fig. 5A; Suppl. 5A). We found that EGF induced a similar phosphorylation of tyrosine-992 (Y992) of the epidermal growth factor receptor (pY992-EGFR) in FN seeded Kind<sup>Ctr</sup>, Tln<sup>Ko</sup> and Kind<sup>Ko</sup> cells. The phosphorylation of tyrosine-397 of FAK was strongly induced after adhesion of Kind<sup>Ctr</sup> cells onto FN and further elevated after additional treatment with EGF and Mn<sup>2+</sup> (Fig. 5A). Tln<sup>Ko</sup> cells also increased pY397-FAK levels after adhesion to FN, although significantly less compared to Kind<sup>Ctr</sup> cells (Fig. 5A; Suppl. 5A). Furthermore, Tln<sup>Ko</sup> cells showed a stepwise increase of pY397-FAK levels to EGF and additional Mn<sup>2+</sup> treatments and localized pY397-FAK to their peripheral NA-like adhesions (Fig. 5A, B; Suppl. 5A). In sharp contrast, FN adhesion, EGF and Mn<sup>2+</sup> treatments of Kind<sup>Ko</sup> cells failed to increase pY397-FAK levels (Fig. 5A, Suppl. 5A) and to localize pY397-FAK to peripheral membrane regions (Fig. 5B). Stable expression of K2GFP in Kind<sup>Ko</sup> cells rescued pY397-FAK levels (Fig. 5C), co-precipitated paxillin and FAK with K2GFP (Suppl. 5B) and co-localized K2GFP with paxillin and pY397-FAK in small NAs during isotropic cell spreading (Suppl. Fig. 5C), while stable expression of K2ΔPHGFP failed to induce pY397-FAK (Fig. 5C), to co-precipitate

paxillin and FAK (Suppl. 5B), and to co-localize paxillin and FAK at integrin adhesion sites (Suppl. 5C).

In line with previous reports showing that the paxillin/FAK complex can trigger the activation of p130Cas<sup>37</sup>, and in cooperation with EGFR signalling the activation of Akt and Erk<sup>39, 40</sup>, we observed pY410-p130Cas and after EGF treatment pS473-Akt and pS202/pY204-Erk1/2 in FN seeded Kind<sup>Ctrl</sup> and to a slightly lesser extent in Tln<sup>Ko</sup> cells (Fig. 5D). In contrast, Kind<sup>Ko</sup> cells failed to activate p130Cas and responded with reduced activation of Akt and Erk to EGF (Fig. 5D), which provides an explanation for their reduced spreading (Fig. 3C,D), proliferation (Suppl. 1D) and survival rates (Suppl. 5D).

Finally, we tested whether the impaired activity of FAK contributed to the spreading defect of Kind<sup>Ko</sup> cells by chemically inhibiting FAK activity in Tln<sup>Ko</sup> cells or by overexpressing FAK in Kind<sup>Ko</sup> cells (Fig 5E-G). The experiments revealed that inhibiting FAK reduced lamellipodia formation and spreading of Tln<sup>Ko</sup> cells to an extent that was similar to untreated Kind<sup>Ko</sup> cells (Fig. 5E). Conversely, overexpression of FAKGFP in Kind<sup>Ko</sup> cells resulted in a robust FAK activation (Fig. 5F) and significant improvement of cell spreading (Fig. 5B; Suppl. 5E).

Altogether these findings show that kindlin-2 recruits paxillin to NAs, which is followed by the activation of FAK and cell spreading.

## Discussion

Although talin binding to  $\beta$  integrin tails has been proposed to be essential and sufficient for integrin activation<sup>16, 21, 41, 42</sup> several reports indicate that, at least in non-hematopoietic cells, initial phases of cell adhesion and spreading can occur in the absence of talin<sup>26, 27, 43-45</sup>. The molecular mechanism(s) leading to adhesion, formation of small integrin aggregates, formation of lamellipodia and isotropic spreading is unclear<sup>26, 37</sup>. Candidate proteins for at least some of these talin-independent functions are kindlins; they are co-expressed with talin and their gene deletions in mice and cells severely impair integrin functions<sup>7, 11-15</sup>. In the present paper we tested this hypothesis by establishing and comparing cells lacking either talin or kindlin expression and searching for new kindlin binding partners.

Our experiments revealed that the co-expression of talin and kindlin is essential for fibroblast survival, proliferation, adhesion and cell surface expression of several integrins. Although our fibroblasts expressed similar levels of  $\alpha_v$  and  $\alpha_5$  integrins before and after Cre-mediated deletion of talin-1/-2 (Tln<sup>Ko</sup>) or kindlin-1/-2 (Kind<sup>Ko</sup>) and bound similarly low amounts of soluble FN-RGD, they were basically unable to adhere to a FN-coated substrate. The binding of soluble FN-RGD by our fibroblasts irrespective whether they express or lack talin or kindlin was in line with observations showing that  $\alpha_5\beta_1$  integrins, unlike  $\beta_2$  and  $\beta_3$  integrins<sup>46, 47</sup>, do not adopt a bent but rather an extended, clasped conformation with intermediate ligand binding affinity in their resting state<sup>27, 45</sup>. The inability of Tln<sup>Ko</sup> or Kind<sup>Ko</sup> cells to adhere to a FN-coated substrate indicated that unclasping of  $\alpha_5\beta_1$  and/or adhesion reinforcement are controlled by the two proteins.

Our findings show that the 9EG7 monoclonal antibody, which binds an epitope located on the EGF-2 domain of the  $\beta_1$  subunit and accessible only upon unclasping<sup>4</sup>, neither binds Tln<sup>Ko</sup> nor Kind<sup>Ko</sup> cells indicating that talin and kindlin cooperate to unclasp and induce the high affinity state of  $\alpha_5\beta_1$  integrins. When the talin/kindlin-dependent unclasping is bypassed with Mn<sup>2+</sup><sup>27, 48, 49</sup>, only kindlin expressing (Tln<sup>Ko</sup>) cells are able to stabilize the exposure of the 9EG7 epitope, facilitate adhesion to FN, albeit to a lesser extent than control cells, aggregate integrins into small, NA-like clusters and induce lamellipodia and isotropic cell spreading. However, the lamellipodia have a short lifetime and retract around 45 min after cell seeding, which results in cell rounding. This clearly indicates that kindlin requires talin to stabilize membrane protrusions and to sustain cell spreading, which is in agreement with observations obtained with talin-2-depleted talin-1<sup>-/-</sup> cells<sup>26, 37</sup>. Consistent with this study<sup>26</sup>, we found that the talin head was unable to rescue lamellipodia formation and FA, formation in Tln<sup>Ko</sup> cells indicating that the linkage between integrin and actin mediated by full length talin is essential

to further strengthen the affinity state of  $\alpha 5\beta 1$ . Strengthening of integrin-ligand bonds reduces bond off-rates and is thought to be mediated by integrin clustering and/or catch bond formation<sup>10, 12, 14, 50</sup>. Our experiments revealed similar integrin clusters in  $Tln^{Ko}$  and  $Kind^{Ko}$  cells suggesting that the main mechanism to reinforce integrin ligand binding occurs probably through the formation of catch bonds.

In search for a mechanistic explanation for the isotropic spreading by kindlin in  $Tln^{Ko}$  cells, we identified paxillin as a novel and direct binding partner of kindlin-2 in NAs. The principal task of the kindlin-2/paxillin complex is the recruitment of FAK<sup>51</sup>, which in turn recruits<sup>25</sup>, or more likely maintains talin in NAs<sup>24</sup>, and cooperates with the EGF receptor to induce signaling pathways that activate Erk and Akt to promote proliferation and survival and Arp2/3 and Rac1 to induce actin polymerization and membrane protrusion (Fig. 6D). Interestingly, re-expression of a PH domain-deficient kindlin-2 ( $K2\Delta PHGFP$ ) in  $Kind^{Ko}$  cells blocks the formation of NAs but enables the development of large, stress fiber-linked and paxillin-positive FAs. This finding indicates that that paxillin supports kindlin-2-mediated stabilization of unclasped, activated integrins in NAs. Moreover, it also shows that FAs must contain a second, yet unknown protein that targets paxillin to these sites. This unknown FA protein must bind, like kindlin, the LIM3 domain of paxillin as this site is believed to be the sole FA targeting site of paxillin<sup>52</sup>.

While our results shed light on the role of kindlin and talin for initial  $\alpha 5\beta 1$  integrin activation and integrin signaling in fibroblasts, previous publications indicate differential requirements of specific integrins for kindlin and talin mediated activation<sup>16, 30</sup>. Future research will be required to explain, how kindlin is recruited to NAs and how kindlin contributes to integrin activation, potentially in concert with ILK<sup>34</sup>, in order to explain these differences.

Our findings suggest a model of a stepwise activation of  $\alpha 5\beta 1$  integrin, in which  $\alpha 5\beta 1$  integrins reside in an extended and clasped conformation with intermediate/low affinity for ligand (Fig. 6A). It is possible that this conformation allows fibroblasts and probably also epithelial cells to continuously probe the ECM with short-lived and weak contacts (Fig. 6A,B), which would be deleterious for blood cells, which therefore keep their integrins in a bent conformation. Talin and kindlin must cooperate to induce unclasping and the hybrid domain swing out to shift  $\alpha 5\beta 1$  into the high affinity state (Fig. 6C). In this phase, kindlin recruits paxillin and FAK as well as ILK and induces signaling leading to cell spreading (Fig. 6D), while talin links the adhesion site to F-actin leading to re-enforcement of the integrin-ligand interactions, presumably through the formation of catch bonds (Fig. 6E).

Clearly, kindlin is essential for integrin activation in fibroblasts and for inducing initial spreading.

## Figure Legends

**Figure 1: Kindlin and talin control integrin-mediated cell adhesion.** (A) Scheme showing talin and kindlin gene modifications. Orange diamonds indicate *loxP* sites and rectangles exons; untranslated regions are marked grey. (B) Western blot of Tln<sup>Ko</sup> and Kind<sup>Ko</sup> cells. Keratinocytes (Kerat.) served as control for kindlin-1 expression. (C) Bright field images of Tln<sup>Ctrl</sup>, Kind<sup>Ctrl</sup>, Tln<sup>Ko</sup> and Kind<sup>Ko</sup> cells (scale bar indicates 10  $\mu$ m). (D) Quantification of cell adhesion for 30 min on indicated substrates (n=3 independent experiments, error bars indicate SEM). (E) Quantification of integrin surface expression levels relative to the Tln<sup>Ctrl</sup> and Kind<sup>Ctrl</sup> cell lines (independent experiments: n=10 for  $\beta$ 1; n=4 for  $\beta$ 3,  $\alpha$ 5,  $\alpha$ v; n=3 for remaining integrin subunits; error bars indicate SEM; significances are calculated between the pairs connected by brackets or between indicated cells and corresponding control cell)

**Figure 2: FN binding by Tln<sup>Ko</sup> and Kind<sup>Ko</sup> cells.** (A) Quantification of binding of soluble, fluorescently labelled FN-RGD fragment relative to the FN-RGE fragment. Binding was measured in the presence of 1 mM MgCl<sub>2</sub> (Ctr) or 5 mM MnCl<sub>2</sub> (independent experiments: n=10 for Kind and Tln cell lines, n=3 for pKO; error bars indicate SEM; significances are given for pairs connected with brackets). (B) Quantification of 9EG7 antibody binding in the presence of either 1 mM MgCl<sub>2</sub> (Ctr) or 5 mM MnCl<sub>2</sub> and 0,3  $\mu$ M FN (FN+Mn<sup>2+</sup>) (n=3 independent experiments; error bars indicate SEM; significances are calculated between Ctr and indicated condition). (C,D) Scatterplot analysis of adhesion forces generated through cells interacting with surface immobilized FN. Cells were immobilized on ConA coated AFM cantilevers and pressed onto FN-Fragment (RGD) or mutated fragment ( $\Delta$ RGD) coated surfaces for varying contact times (C) and in presence of Mn<sup>2+</sup> or EDTA (D) (each sphere represents one measurement; the bars indicate median values). (D) FN staining after plating cells on a FN-coated dish for 24 h. FN fibril assembly requires both talin and kindlin. (F) FACS quantification of total  $\beta$ 1-antibody and 9EG7-antibody binding to Tln<sup>Ctrl</sup> and Kind<sup>Ctrl</sup> cells and cells reconstituted with Tln1V, K2GFP or THD (n>3 independent experiments; significances are given for indicated pairs; error bars indicate SEM). (G) Indicated cell lines were plated on FN and after 30 min adherent cells were quantified (values are normalized to Tln<sup>Ctrl</sup> and Kind<sup>Ctrl</sup> and rescued cell lines; n=3 independent repeats; error bars indicate SEM).

**Figure 3: Integrin clustering in Tln<sup>Ko</sup> and Kind<sup>Ko</sup> cells.** (A) Confocal sections from suspended cells stained for  $\beta$ 1 integrin and phalloidin. (B) Confocal images from the ventral

side of adherent cells in the absence or presence of  $Mn^{2+}$  stimulation. (C) Quantifications of cell morphologies of  $Mn^{2+}$ -treated  $Tln^{Ko}$  and  $Kind^{Ko}$  cells seeded on FN or PLL. (D) Quantification of EGF- or PDGF-treated  $Tln^{Ko}$  and  $Kind^{Ko}$  cells. (n=3 independent experiments, >100 cells were counted for each condition and experiment; error bars indicate SEM). (E) TIRF-STORM pictures of  $\beta 1$  integrin clusters (green; arrowhead) obtained from immunostaining of non-permeabilized cells overlaid with paxillin staining following permeabilization (red, normal resolution). Boxed areas show a threefold magnification, dashed lines indicate cell borders. (F) Binning histograms of nearest neighbour distance (NND) measurements (n=3 STORM images per cell line with 1400-11000 identified clusters for  $\beta 1$ ). The NNDs of  $Tln^{Ctr}$  and  $Kind^{Ctr}$  cells were combined and subdivided into NNDs within paxillin-positive FAs (dark grey area) and outside of FAs (light grey area). The NND profiles of the total cell area in  $Tln^{Ko}$  and  $Kind^{Ko}$  cell lines are shown as blue and red lines. (G)  $\beta 1$  integrin clusters with a maximal distance of 140 nm were defined as aggregates. The bar graphs represent the percentage of indicated integrin clusters in aggregate sizes of 1-3 (small aggregate), 4-6 (intermediate sized aggregate), and >6 (large aggregate). Scale bars: (A) and (B): 10  $\mu m$ ; (C): 500 nm;  $Mn^{2+}$  indicates presence of 5 mM  $MnCl_2$ .

**Figure 4: Kindlin binds and recruits paxillin to FA.** (A) GFP-IP of cell lysates from cells overexpressing GFP-tagged paxillin, Hic5 and leupaxin constructs (Pxn, paxillin; Hic5; Lpx, leupaxin) and K2flag reveal interaction of kindlin-2 with all three paxillin family members. (B) GFP-IP of lysates from cells overexpressing GFP-tagged paxillin truncation mutants and K2flag identifies the paxillin LIM3 domain as kindlin-2-binding domain. (C) GFP-IP of lysates from cells overexpressing GFP-tagged kindlin-2 truncation/deletion mutants and Cherry-tagged paxillin (PxnCH) identify the kindlin-2 PH domain as paxillin binding domain. (D) Purified His-tagged paxillin-LIM3 domain pulls down recombinant kindlin-2 in a  $Zn^{2+}$ -dependent manner. (E) Re-expression of K2GFP and K2 $\Delta$ PHGFP in  $Kind^{Ko}$  cells followed by paxillin and phalloidin staining.

**Figure 5: Kindlin-mediated paxillin induces FAK signalling and cell spreading.** (A) FAK and EGFR activation after seeding serum-starved  $Kind^{Ctr}$ ,  $Tln^{Ko}$  and  $Kind^{Ko}$  cells on PLL or FN and treating them with or without EGF and  $Mn^{2+}$ . (B) Immunofluorescence staining of activated (Tyr-397 phosphorylated) FAK and filamentous actin in cells stimulated with  $Mn^{2+}$  and EGF, 30 min after seeding (FAKGFP indicates exogenous expression of FAKGFP fusion protein; scale bar indicates 10  $\mu m$ ). (C) FAK activation and total FAK levels in  $Kind^{Ko}$  cells

stably transduced with K2GFP or K2 $\Delta$ PHGFP either seeded on FN or kept in suspension. GFP indicates similar expression of transduced GFP-tagged constructs. GAPDH levels served to control loading. (D) Levels of phosphorylated signalling mediators downstream of FAK in serum-starved or EGF-treated Kind<sup>Ctrl</sup>, Tln<sup>Ko</sup> and Kind<sup>Ko</sup> cells. GAPDH levels served to control loading. (E) Quantification of lamellipodia formation after treating Tln<sup>Ko</sup> and Kind<sup>Ko</sup> cells with DMSO, the FAK inhibitor PF-228 or Latrunculin A (n=3 independent repeats; >100 cells/condition; error bars indicate SEM; significances are given in comparison to DMSO control). (F) FAK activity in Tln<sup>Ko</sup> and Kind<sup>Ko</sup> cells stably transduced with FAKGFP (n=3 independent experiments; significances are given in comparison to untreated control; error bars indicate SEM). (G) Quantification of lamellipodia formation in Tln<sup>Ko</sup> and Kind<sup>Ko</sup> cells stably transduced with FAKGFP (n=3 independent experiments; significances are given in comparison to untreated control; error bars indicate SEM).

**Fig. 6. Roles of talin and kindlin during inside-out and outside-in signalling of  $\alpha 5\beta 1$  integrin.** Integrin subunits are modelled according to Zhu et al.<sup>53</sup> with the  $\alpha 5$  subunit in green and the  $\beta 1$  subunit in blue; fibronectin ligand as grey cables. (A,B)  $\alpha 5\beta 1$  integrin in an extended and clasped conformation, shows intermediate ligand binding affinity and oscillates between ligand unbound (A) and bound (B) states; the clasped conformation with the EGF-2 domain of the  $\beta$  subunit in close contact with the calf domain of the  $\alpha 5$  subunit prevents exposure of the 9EG7 epitope (highlighted in pink). Kindlin and autoinhibited talin are in the cytoplasm and/or kindlin is anchored with the PH domain at the plasma membrane. (C) Binding of kindlin and talin to the  $\beta 1$  tail is associated with the unclasp of the  $\alpha 5\beta 1$  subunits, hybrid domain swing out, and 9EG7 epitope exposure (highlighted in pink). (D) Independent of talin binding to the  $\beta 1$  tail kindlin recruits paxillin and FAK through the kindlin PH domain and ILK/PINCH/parvin (IPP; not shown) through the ILK pseudokinase domain to induce cell spreading, proliferation and survival. (E) The  $\alpha 5\beta 1$  integrin is in the high affinity state which becomes stabilized by talin binding to the  $\beta 1$  tail by coupling the integrin to the actin cytoskeleton, which is followed by force transmission and catch bond formation.

## Legends to Supplemental Figures

**Suppl. Figure 1:** (A) Western blots showing that floxed talin-1 fibroblasts activate the *talin-2* gene and floxed kindlin-2 fibroblast the *kindlin-1* gene. Keratinocytes expressing high levels of kindlin-1 served as control for the anti-kindlin-1 antibody. GAPDH served to control loading. (B) Talin-1- and kindlin-2-deficient fibroblasts can induce partial spreading (bright field imaging, left panels) and form paxillin-positive adhesion sites (immunostaining, right panels) upon activation of the talin-2 or kindlin-1 gene, respectively. (C) Integrin expression profile of Tln<sup>Ctrl</sup> and Kind<sup>Ctrl</sup> cells measured by flow cytometry and presented as histograms. The antibody isotype control is shown in grey. (D) Cell number increase of Tln<sup>Ctrl</sup>, Kind<sup>Ctrl</sup>, Tln<sup>Ko</sup> and Kind<sup>Ko</sup> cells per day; (n=12 independent experiments; error bars indicate SEM). Scale bars indicate 10  $\mu$ M.

**Suppl. 2:** (A) Cell spreading on FNIII-7-10-fragments. Bright field images of WT fibroblasts plated on FN-RGD or mutant FN-RGE immobilized to the plate surface with Tris-NTA coupled gold beads. (B) Western blot analysis of cell lysates from Tln<sup>Ko</sup> and Kind<sup>Ko</sup> cells reconstituted Tln1V, THD or K2GFP.

**Suppl. 3:** (A) Confocal stacks of untreated and Latrunculin A-treated Kind<sup>Ctrl</sup> cells stained for  $\beta$ 1 and with phalloidin. Although Latrunculin A treatment abrogates F-actin containing membrane spikes,  $\beta$ 1-integrin aggregates prevail. (B) Confocal images of the ventral plasma membrane of adherent, Mn<sup>2+</sup>- and EGF-treated Kind<sup>Ctrl</sup>, Tln<sup>Ko</sup> and Kind<sup>Ko</sup> cells stained for ILK, paxillin, talin, and kindlin-2 (green) together with phalloidin (red). Formation of nascent and focal adhesions can be observed in Kind<sup>Ctrl</sup> cells, while Tln<sup>Ko</sup> and Kind<sup>Ko</sup> cells show small, NA-like aggregates of FA proteins (scale bar indicates 10  $\mu$ m; for Tln<sup>Ko</sup> and Kind<sup>Ko</sup> threefold magnifications of indicated areas are shown). (C) Confocal image of Tln<sup>Ko</sup> and Kind<sup>Ko</sup> cells reconstituted with K2GFP or Tln1V, respectively. (D) TIRF-STORM image of  $\beta$ 1 integrin clusters (green) overlaid with diffraction-limited resolution image of anti-paxillin staining (red) and single detection events of the STORM acquisition (pink); right panel depicts a threefold magnification of the indicated area. Green  $\beta$ 1 integrin clusters are defined by multiple single detection events and likely consist of several  $\beta$ 1 integrin molecules. (E) Binning histogram showing the quantification of STORM detection events per green integrin cluster. The  $\beta$ 1 integrin clusters show an average of ~10 detection events and are similar among Tln<sup>Ctrl</sup> and Kind<sup>Ctrl</sup> (Ctr), Tln<sup>Ko</sup> and Kind<sup>Ko</sup> cells. (F) Average  $\beta$ 1 integrin cluster density

in STORM images expressed as clusters  $\mu\text{m}^{-2}$  (n=3 cells and images per cell line, error bars indicate standard deviation).

**Suppl. 4:** (A) qPCR of paxillin (Pxn), Hic5, and leupaxin (Lpxn) from cDNAs generated from wild type fibroblasts (Fibrobl.), keratinocytes (Kerat.), RAW cells (RAW) and T cells (TC). Results are normalized to the isoform with highest expression in the respective cell types (n=3 independent repeats, error bars show SEM). (B) Quantification of pan- $\beta$ 1 integrin antibody and 9EG7 antibody binding to Kind<sup>Ko</sup> cells reconstituted with K2GFP or K2 $\Delta$ PHGFP (n=3 independent experiments; significances are given in comparison to K2GFP rescue; error bars indicate SEM).

**Suppl. 5:** (A) Densitometric quantification of western blot signals of lysates from untreated, EGF- and Mn<sup>2+</sup>-treated Kind<sup>Ctrl</sup>, Tln<sup>Ko</sup> and Kind<sup>Ko</sup> cells seeded either on FN or PLL and probed with anti-Tyr-397 phosphorylated FAK (pY397-FAK) antibodies (n=3 independent repeats; significances are calculated with respect to PLL adherent cells; error bars indicate SEM). (B) GFP-IP in lysates of K2GFP, K2 $\Delta$ PHGFP or GFP reconstituted Kind<sup>Ko</sup> cells overexpressing Myc-tagged FAK (FAK-Myc) and Cherry-tagged paxillin (PxnCH). K2GFP but not K2 $\Delta$ PHGFP forms a ternary complex with paxillin and FAK. (C) Localization of paxillin, pY397-FAK and K2GFP in Kind<sup>Ko</sup> cells reconstituted with K2GFP and K2 $\Delta$ PHGFP seeded for 30 min on FN-coated circular micropatterns (diameter 30  $\mu\text{m}$ ; scale bar indicates 10  $\mu\text{m}$ ). (D) Cell number counts 30 d after Cre-mediated *kindlin-1* and *kindlin-2* gene deletion. 70.000 Kind<sup>Ctrl</sup> or Tln<sup>Ctrl</sup> cells stably expressing tamoxifen-inducible Cre were treated with tamoxifen for 24 h after seeding, cultured for 4 weeks before trypan blue treatment and counting (n=3 independent experiments; error bars indicate SEM). (E) Cell spreading area of Tln<sup>Ctrl</sup>, Kind<sup>Ctrl</sup>, Tln<sup>Ko</sup> and Kind<sup>Ko</sup> cells measured by image quantification (n=3 independent repeats are pooled; >100 cells/condition and repeat; resulting areas are shown as box-blots: bar indicates median, boxes and whiskers cover 50% and 90% of the results, respectively).

## Material and Methods

### Mouse strains and cell lines and cell culture

The floxed *kindlin-1* (*Fermt-1<sup>lox/lox</sup>*), floxed talin-1 and the constitutive talin-2-null mouse strains have been described<sup>41, 43, 54</sup>. The floxed *kindlin-2* (*Fermt-2<sup>lox/lox</sup>*) mouse strain generated via recombinant recombination in embryonic stem cells<sup>55</sup> carries *loxP* sites flanking exon 15, which contains the stop codon and the polyadenylation signal of the *Fermt-2* gene. Homologous recombination and germ line transmission were verified by Southern

blots, and the *frt*-flanked neo cassette was removed with a transgenic mouse strain carrying a deleter-flipase recombinase gene. Floxed talin-1 and talin-2-null mice, and floxed kindlin-1 and kindlin-2 mice were intercrossed to generate *Tln-1<sup>flox/flox</sup> Tln-2<sup>-/-</sup>* and *Fermt-1<sup>flox/flox</sup> Fermt-2<sup>flox/flox</sup>* mice. Fibroblasts were isolated from the kidneys of 21 d old animals, immortalized by retrovirally transducing the SV40 large T antigen, cloned and finally infected with an adenovirus to transduce the *Cre* recombinase and to generate talin-null ( $Tln^{Ko}$ ) and kindlin-null ( $Kind^{Ko}$ ) cells.

All cell lines were cultured under standard cell culture conditions using DMEM supplemented with 8 % FCS and Penicillin/Streptomycin.

### **Flow cytometry**

Flow cytometry was carried out using standard procedures. Fibroblasts were incubated with primary antibodies diluted in FACS-Tris buffered saline (30 mM Tris, pH 7.4, 180 mM NaCl, 3.5 mM KCl, supplemented with 1 mM  $CaCl_2$ , 1 mM  $MgCl_2$ , 3% BSA, 0,02%  $NaN_3$ ) for 1 h on ice, or in the case of  $Mn^{2+}$  treatment for 1 h at 37 °C, washed twice with cold FACS-TBS and finally incubated with the secondary antibody for 45 min on ice. Flow cytometry was carried out with a FACSCantoTMII cytometer (BD Biosciences) equipped with FACS DiVa software (BD Biosciences). Data analysis was conducted using the FlowJo program (version 9.4.10).

### **Real-time polymerase chain reaction (PCR)**

Total RNA was extracted with the RNeasy Mini extraction kit (Qiagen) from cultured cells, cDNAs were prepared with an iScript cDNA Synthesis Kit (Biorad) and real-time PCR was performed with an iCycler (Biorad). Each sample was measured in triplicate and values were normalized to *Gapdh*. Primer sequences for *Lpxn* and *Pxn* were from PrimerBank<sup>56</sup> (*Lpxn*: 26080416a1; *aPxn*: 114326500c2; *bPxn*: 22902122a1), *GAPDH* primers were described before<sup>54</sup> and *Hic5* primers were newly designed (*Hic5*-fwd: 5'-ttccttgagcagcggtgttcc-3'; *Hic5*-rev: 5'-ggttacagaagccacatcgtggg-3').

### **Antibodies and inhibitors**

The following antibodies or molecular probes were used at indicated concentrations for western blot (W), Immunofluorescence (IF) or flow cytometry (FACS): kindlin-1 (home made,<sup>57</sup>; W: 1:5000, IF: 1:1000; kindlin-2 (MAB2617 from Millipore) W: 1:1000, IF: 1:500; talin (8D4 from Sigma) W: 1:1000; talin (sc-7534 from Santa Cruz) IF: 1:500; talin-1

(ab57758 from Abcam) W: 1:2000; talin-2 (ab105458 from Abcam) W: 1:2000; GAPDH (6C5 from Calbiochem) W: 1:10000; Paxillin (610051 from BD Transduction Laboratories) W: 1:1000, IF: 1:400; integrin  $\beta$ 1-488 (102211 from Biolegend) IF: 1:400, FACS: 1:200; integrin  $\beta$ 1 (MAB1997 from Chemicon) IF: 1:50 for EM; FACS: 1:400; integrin  $\beta$ 1-647 (102213 from Biolegend) IF: 1:200; integrin  $\beta$ 3-biotin (PharMingen; 553345; FACS: 1:200), integrin  $\beta$ 3 (Emfret; M031-0; IF: 1:200), integrin  $\beta$ 5 (a gift from Dean Sheppard, University of California, USA) FACS: 1:200; integrin  $\beta$ 6 (10D5 from Chemicon) FACS: 1:200; integrin  $\alpha$ 2-FITC (554999 from BD Biosciences) FACS: 1:100; integrin  $\alpha$ 3 (AF2787 from R&D) FACS: 1:200; integrin  $\alpha$ 5-biotin (557446 from Pharmingen) FACS: 1:200; integrin  $\alpha$ 6-FITC (555735 from Pharmingen) FACS 1:100; integrin  $\alpha$ v-biotin (551380 from Pharmingen) FACS: 1:200;  $\beta$ 1-integrin 9EG7 (550531 from BD Biosciences) FACS: 1:200; fibronectin (AB2033 from Millipore) IF: 1:500; Tritc-Phalloidin (P1951 from Sigma) IF: 1:400; Flag-tag-HRP (8592 from Sigma) W: 1:10000; GFP (A11122 from Invitrogen) W: 1:2000; Cherry (PM005 from MBL) W:1:1000; Myc (05-724 from Millipore) 1:2000; FAK (06-543 from Upstate) W: 1:1000; FAK phosphorylated Y397 (44624G from Biosource) W: 1:1000, IF: 1:400; ILK (611803 from Transduction Labs) W: 1:5000; IF: 1:500; EGFR phosphorylated Y992 (2235 from Cell Signaling) W: 1:2000; p130 Cas (P27820 Transduction Labs) W: 1:1000; p130 Cas phosphorylated Y410 (4011S from Cell Signaling) W: 1:1000; Akt (9272 from Cell Signaling) W: 1:1000; Akt phosphorylated S473 (4060 from Cell Signaling) W: 1:1000; Erk1/2 (9102 from Cell Signaling) W: 1:1000; Erk1/2 phosphorylated T202 Y204 (4376 Cell Signaling) W: 1:1000.

The following secondary antibodies were used: goat anti-rabbit Alexa 488 (A11008), goat anti-mouse Alexa 488 (A11029), goat anti-mouse Alexa 546 (A11003), goat anti-rabbit Alexa 647 (A21244) (all from Invitrogen) FACS: 1:500, IF: 1:500; streptavidin-Cy5 (016170084) FACS: 1:400; goat anti-rat horseradish peroxidase (HRP) (712035150) (both from Dianova) W: 1:10,000), goat anti-mouse HRP (172-1011) and goat anti-rabbit HRP (172-1019) (both from Biorad) W: 1:10,000.

The FAK inhibitor PF-228 (PZ0117 from Sigma) was dissolved in DMSO at 10 mM and used at 1:2000. The actin polymerization inhibitor Latrunculin A (L5163 from Sigma) was dissolved in DMSO at 125  $\mu$ M and used at 1:500.

### **Constructs and transfections**

K2 $\Delta$ PHGFP was cloned by PCR using the K2GFP cDNA<sup>18</sup> as template and the Kind2fwd (5'-ctcgaggaggtatggctctggacgggataag -3', Kind2PHrev 5'-**tggtcttgcctttaatatagtcagcaagtt** -3'),

Kind2PHfwd (5'-**ctatattaaggca**agaccatggcagacag -3') and Kind2rev (5'-tctagatcacaccaaccactggtga-3') primers. The two fragments containing homologous regions (bold nucleotides in the primer sequences) were fused by another round of amplification using the most 5' and 3' primers (Kind2fwd and Kind2rev).

The resulting PCR product was cloned into the K2GFP vector. The N- and C-terminal truncation constructs of kindlin-2 were cloned by PCR using K2GFP as template and recipient vector for the synthesized PCR fragments. The primer sequences were: Kind2-NT-fwd 5'-ctgtacaagtcggactc-3', Kind2-NT-rev 5'-gcgccgcctattttgctttatcaagaagagc-3', Kind2-CT-fwd 5'-ctcgagctatggataaagcaaaaaccaaccaag-3', Kind2-CT-rev 5'-gttatctagagcggccgc-3'.

The Cre-ERT2 cDNA obtained from Thomas Wunderlich (Max Planck Institute for Metabolism Research, Cologne) was subcloned into the ITR-IRES-Puro-E2A-Thy1.1 vector, allowing puromycin selection for stable integrations. Stable expression of K2ΔPHGFP and FAKGFP- or Myc-FAK (a gift from Dr. Ambra Pozzi; Vanderbilt University, Nashville), and Cre-ERT2 cDNAs was achieved with the sleeping beauty transposase system<sup>58</sup>. For stable expression of murine talin-1 and THD (amino acids1-443) the corresponding cDNAs were N-terminally tagged with venus and cloned into the retroviral pLPCX vector. The constructs for GFP-tagged paxillin-LIM truncation mutants with stop codons 5' of each LIM domain were generated by PCR from GFP- and Cherry-tagged α-paxillin<sup>59</sup> template and cloned into the retroviral pLPCX vector. The primer sequences were: stop codon in bold: ΔLIM1-4fwd 5'-caccgtgccaat**g**agggtctgtggagcc -'3, ΔLIM1-4rev 5'- ggctccacagaccct**c**atttgcaacggtg -'3, ΔLIM2-4fwd 5'- cagcctcttctccccat**g**acgctgctactactg -'3, ΔLIM2-4rev 5'- cagtagtagcagc**g**tcattggggagaagaggctg -'3, ΔLIM3-4fwd 5'- aagattacttcgacatgtttgct**g**accaagtgcggc -'3, ΔLIM3-4rev 5'- gccgcacttgg**g**tcagcaaacatgtcgaagtaattctt -'3, ΔLIM4fwd 5'- ggcgcggtc**g**tgactgtgctccgg -'3, ΔLIM4rev 5'- ccggagcacag**t**cacgagccgcgcc -'3). The cDNA of murine Hic5 was amplified from a cDNA derived from murine vascular smooth muscle cells, cloned into pCR2.1-TOPO (Invitrogen) and subcloned into pEGFP-C1 vector. Murine leupaxin cDNA (cloneID: 5065405 from Thermo Scientific) was PCR-amplified (Lpxn-fwd: 5'-ctcgagcaatggaagagctggatgcctattg -3'; Lpxn-rev 5'- gaattcctactgtgaaaagagcttagtgaagc -3') and subcloned into the pEGFP-C1 vector.

To express recombinant murine kindlin-2 and paxillin-LIM3 (A473-S533) cDNAs they were fused with an N-terminal tandem tags consisting of 10x-Histidine followed by a SUMO3-tag and cloned into pCoofy17. The primer sequences for amplifying the paxillin-LIM3 domain were: LIM3fwd 5'-aaccggtggagctcccaagtgc-3' and LIM3rev 5'-ttctcgagttacgagccgcgcc-3'.

The plasmid carrying FNIII<sub>7-10</sub> cDNA has been described previously<sup>60</sup>. For Y2H analysis, the kindlin-2 cDNA was PCR amplified using the primers K2-Bamfw: 5'-gggatcccactgggctaattggctctggacgggataagg-3' and K2-Salrev: 5'-gtgtcgacgtcacaccaaccactggtgagtttg-3' and cloned into the pGBKT7 plasmid to obtain a kindlin-2 version that was N-terminally fused with Gal4-DNA binding domain. Screening of this construct against a human full ORF library was conducted by the Y2H protein interaction screening service of the German Cancer Research Center in Heidelberg.

### **Expression and purification of recombinant proteins**

The recombinant expression of Kindlin2 and paxillin-LIM3 in *E. coli* Rosetta cells (Merck Millipore) was induced with 1 mM and 0,2 mM IPTG, respectively, at 18 °C for 24 h. After cell lysis and clarification of the supernatant, kindlin-2 was purified by Ni-NTA affinity chromatography (Qiagen). Eluate fractions containing kindlin-2 were pooled, cleaved with SenP2 protease and purified by size-exclusion chromatography (Superdex 200 26/60, GE Healthcare) yielding unmodified murine kindlin-2 and N-terminally His/SUMO3-tagged paxillin-LIM3-domain.

The Alexa 647-labeled FNIII<sub>7-10</sub> fragment was purified and fluorescence labeled as described<sup>61</sup>.

### **Immunostaining**

For immunostaining, cells were cultured on plastic ibidi- $\mu$ -slides (80826 from Ibidi) coated with 20  $\mu\text{g ml}^{-1}$  FN (Calbiochem). Cells were routinely fixed with 4 % PFA in Phosphate buffered saline (PBS; 180 mM NaCl, 3.5 mM KCl, 10 mM Na<sub>2</sub>HPO<sub>4</sub>, 1.8 mM K<sub>2</sub>H<sub>2</sub>PO<sub>4</sub>) for 10 min at room temperature (RT) or with -20 °C cold Acetone-Methanol when indicated. If necessary, cells were solubilized with staining buffer (PBS supplemented with 0,1 % Tx100 and 3 % BSA) or with -20 °C cold Methanol for kindlin-2 staining. Background signals were blocked by incubating cells with staining buffer for 1 h at RT in staining buffer. Subsequently, they were incubated with primary and secondary antibodies diluted in staining buffer in the dark. Fluorescent images were acquired with a LSM 780 confocal microscope (Zeiss) equipped with a x100/1.4 oil objective and with a DMIRE2-SP5 confocal microscope (Leica) equipped with a 40 $\times$ oil objective using Leica Confocal software (version 2.5 build 1227). Brightfield images were acquired with an Axioskop (Carl Zeiss) 40 $\times$  NA 0.75 objective and DC500 camera with IM50 software (Leica). For further image analysis, z-stack projection and contrast adjustments imageJ (v1.47) were used.

The super-resolution imaging was carried out by Direct Stochastic Optical Reconstruction Microscopy (dSTORM)<sup>62</sup>, which is based on precise emitter localization. To induce reversible switching of the Alexa 647 label and to reduce photobleaching, imaging was performed in imaging solution (50 % Vectashield (v/v) (vector laboratories; H-1000), 50 % TBS (v/v; pH=8)) supplemented with 50 mM  $\beta$ -mercaptoethylamine (sigma-aldrich; M9768). dSTORM was implemented on a Zeiss Axio Observer D1 microscope with a Slider TIRF illumination module. The sample was excited with a 642 nm laser in a total internal reflection mode using the Zeiss Plan-Apochromat 100x/NA 1.46 oil TIRF objective. The emitted light was detected in the spectral range 660-740 nm. The images were recorded with an iXon Ultra DU-897U emCCD camera (Andor Technology Ltd., Belfast, UK), with its EM gain set to 300. Additional magnification by a factor of 2.5 resulted in the pixel size of 65 nm. For each final image, in total 6000 frames with the exposure time of 0.1 s were recorded.

A standard TIRF imaging of the same sample in the green channel (paxillin) was achieved by illumination with a 491 nm laser and detection in the spectral range 500-550 nm. Simultaneous dual-colour imaging of both the green and the red channels was realized with the Optosplit II (Cairn Research, Faversham, UK) image splitter mounted between the microscope and the camera. Image analysis was carried out with the imageJ plugins ThunderSTORM<sup>63</sup>, Nnd\_.class (Yuxiong Mao) and standard tools of imageJ.

### **AFM-based single-cell force spectroscopy (SCFS)**

Tipless, 200  $\mu$ m long V-shaped cantilevers (spring constants of 0.06 N m<sup>-1</sup>; NP-O, Bruker) were prepared for cell attachment as described<sup>64</sup>. Briefly, plasma cleaned cantilevers were incubated in 2 mg ml<sup>-1</sup> concanavalin A (ConA from Sigma) in PBS at 4 °C overnight. Polydimethylsiloxan (PDMS) masks were overlaid on glass bottoms of Petri dishes (35 mm FluoroDish, World Precision Instruments, US) to allow different coatings of the glass surface<sup>65</sup>. PDMS framed glass surfaces were incubated overnight with 50  $\mu$ g ml<sup>-1</sup> FN-RGD and 50  $\mu$ g ml<sup>-1</sup> FN- $\Delta$ RGD in PBS at 4 °C. Overnight serum-starved fibroblasts (Tln<sup>Ctr</sup>, Kind<sup>Ctr</sup>, Tln<sup>Ko</sup>, Kind<sup>Ko</sup>) grown on FN-coated (Calbiochem, USA) 24 well plates (Thermo Scientific, Roskilde, Denmark) to confluency of ~ 80 % were washed with PBS and detached with 0.25 % (w/v) trypsin/EDTA (Sigma). Detached cells were suspended in single-cell force spectroscopy (SCFS) medium (DMEM supplemented with 20 mM HEPES) containing 1 % (v/v) FCS, pelleted and further resuspended in serum-free SCFS medium. Detached cells were left suspended in SCFS media to recover from detachment for ~1 h<sup>66</sup>. For the activation or chelation assay, the detached cells were incubated in SCFS media supplemented with 0.5 mM

Mn<sup>2+</sup> or 5 mM EDTA, respectively, for ~1 h and SCFS was performed in the presence of the indicated supplement. SCFS was performed using an AFM (NanoWizard II, JPK Instruments) equipped with a CellHesion module (JPK Instruments) mounted on an inverted optical microscope (Axiovert 200 M, Zeiss, Jena, Germany). Measurements were performed at 37 °C, controlled by a PetriDish Heater (JPK Instruments). Cantilevers were calibrated using the equipartition theorem<sup>67</sup>.

To attach a single cell to the cantilever, cell suspensions were pipetted to the region containing the FN-ΔRGD coating. The ConA functionalized cantilever was lowered onto a single cell with a velocity of 10 μm s<sup>-1</sup> until reaching a contact force of 5 nN. After 5 s contact, the cantilever was retracted from the Petri dish by 50 μm and the cantilever-bound cell was left for incubation for >10 min. For adhesion experiments, the cantilever-bound cell was brought into contact with the FN-ΔRGD coated support at a contact force of ~2 nN for 5, 20, 50 and 120 s and then retracted while measuring the cantilever deflection and the distance travelled. Subsequently, the cell adhesion to the FN-RGD coated support was characterized as described. In case cantilever attached cells showed morphological changes (e.g. spreading) they were discarded. The approach and retract velocity of the cantilever was 5 μm s<sup>-1</sup>. The deflection of the cantilever was recorded as force-distance curves. Adhesion forces were extracted from retraction force-distance curves using the AFM data processing software (JPK Instruments).

### **Peptide pulldowns, recombinant protein pulldown and GFP-IP.**

Pull-downs with β1 integrin peptides were performed as described<sup>58</sup> and GFP-IPs were performed using μ-MACS anti-GFP magnetic beads (130-091-288 from Miltenyi). For recombinant paxillin-LIM3 pulldowns 3 μg purified LIM3 domain was incubated in 100 μl pulldown buffer (150 mM Tris pH 7.4, 0.4 mM MgCl<sub>2</sub>, 3.2 mM NaCl, 1 mM DTT, 0.1 % Tx100) with equilibrated Ni-NTA-Agarose (50 μl slurry; 1018244 from Quiagen) for 4 h at 4 °C. After three washes 100 μl buffer containing 3 μg of purified kindlin-2 and Zn<sup>2+</sup> or EDTA was added for 1 h at 4 °C to allow interaction, before the beads were washed further three times and remaining LIM3-kindlin-2 were eluted by boiling in 2xLaemmli buffer.

### **Generation of FN-coated nanopatterns.**

Disc-shaped adhesive micropatterns on glass surrounded by adhesion repellent PEG were produced as described previously<sup>68</sup> and coated with 20 μg ml<sup>-1</sup> FN (Calbiochem) before usage.

### Spreading and adhesion assays.

Cells were grown to 70 % confluency and then detached using trypsin/EDTA. Suspended cells were serum starved for at least 1 h in adhesion assay buffer (10 mM HEPES pH 7.4; 137 mM NaCl; 1 mM MgCl<sub>2</sub>; 1 mM CaCl<sub>2</sub>; 2.7 mM KCl; 4.5 g L<sup>-1</sup> Glucose; 3% BSA) before 40.000 cells per well were plated out in the same buffer supplemented with 25 ng ml<sup>-1</sup> EGF and 5 mM Mn<sup>2+</sup> if indicated. Plastic ibidi-μ-slides (80826 from Ibidi) were coated with 10 μg ml<sup>-1</sup> FN (Calbiochem) for adhesion or 20 μg ml<sup>-1</sup> FN for spreading assays, 10 μg ml<sup>-1</sup> LN (11243217001 from Roche), 10 μg ml<sup>-1</sup> COL (5005B from Advanced Bio Matrix), 10 μg ml<sup>-1</sup> VN (07180 from StemCell) or 0,01 % Poly-L-Lysine (PLL; P4707 from Sigma) diluted in PBS. Seeded cells were centrifuged at 600 rpm in a Beckman centrifuge for 30 min at 37 °C before they were fixed with 4 % PFA in PBS and stained with Phalloidin-TRITC and DAPI. For cell adhesion assays, nuclear staining of the whole well was imaged using a 2.5x objective and cell numbers were counted using ITCN plugin for imageJ<sup>69</sup>. For cell spreading assays 12 confocal images of different regions of Phalloidin and DAPI stained cells were acquired using a Leica confocal microscope, cell spreading was quantified using imageJ.

### Statistical analyses.

Experiments were routinely repeated at least three times and the repeat number was increased according to the effect size or sample variation. All statistical significances (\*P<0.05; \*\*P<0.01; \*\*\*P<0.001; n.s., not significant) were determined by two-tailed unpaired *t*-test. In the boxplot the middle line represents the median, the box ends represent the 25<sup>th</sup> and 75<sup>th</sup> percentiles and the whisker ends show the 5<sup>th</sup> and 95<sup>th</sup> percentiles. Statistical analysis of the SCFS was performed with Prism (GraphPad, La Jolla, USA).

1. Hynes, R.O. Integrins: bidirectional, allosteric signaling machines. *Cell* **110**, 673-687 (2002).
2. Winograd-Katz, S.E., Fassler, R., Geiger, B. & Legate, K.R. The integrin adhesome: from genes and proteins to human disease. *Nature reviews. Molecular cell biology* **15**, 273-288 (2014).
3. Boettiger, D. Mechanical control of integrin-mediated adhesion and signaling. *Current opinion in cell biology* **24**, 592-599 (2012).
4. Askari, J.A. *et al.* Focal adhesions are sites of integrin extension. *The Journal of cell biology* **188**, 891-903 (2010).

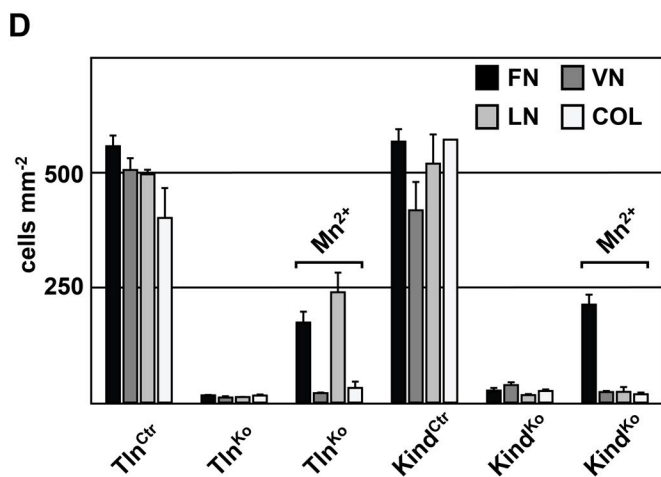
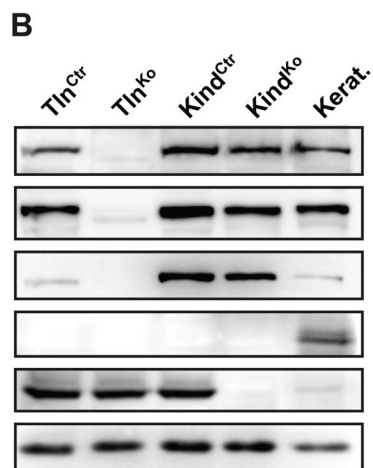
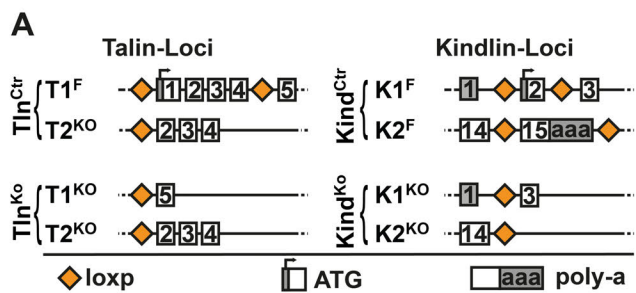
5. Moser, M., Legate, K.R., Zent, R. & Fassler, R. The tail of integrins, talin, and kindlins. *Science* **324**, 895-899 (2009).
6. Ye, F., Kim, C. & Ginsberg, M.H. Reconstruction of integrin activation. *Blood* **119**, 26-33 (2012).
7. Koo, L.Y., Irvine, D.J., Mayes, A.M., Lauffenburger, D.A. & Griffith, L.G. Co-regulation of cell adhesion by nanoscale RGD organization and mechanical stimulus. *Journal of cell science* **115**, 1423-1433 (2002).
8. van Kooyk, Y. & Figdor, C.G. Avidity regulation of integrins: the driving force in leukocyte adhesion. *Current opinion in cell biology* **12**, 542-547 (2000).
9. Maheshwari, G., Brown, G., Lauffenburger, D.A., Wells, A. & Griffith, L.G. Cell adhesion and motility depend on nanoscale RGD clustering. *Journal of cell science* **113 ( Pt 10)**, 1677-1686 (2000).
10. Roca-Cusachs, P., Gauthier, N.C., Del Rio, A. & Sheetz, M.P. Clustering of alpha(5)beta(1) integrins determines adhesion strength whereas alpha(v)beta(3) and talin enable mechanotransduction. *Proceedings of the National Academy of Sciences of the United States of America* **106**, 16245-16250 (2009).
11. Coussen, F., Choquet, D., Sheetz, M.P. & Erickson, H.P. Trimers of the fibronectin cell adhesion domain localize to actin filament bundles and undergo rearward translocation. *Journal of cell science* **115**, 2581-2590 (2002).
12. Kong, F., Garcia, A.J., Mould, A.P., Humphries, M.J. & Zhu, C. Demonstration of catch bonds between an integrin and its ligand. *The Journal of cell biology* **185**, 1275-1284 (2009).
13. Chen, W., Lou, J. & Zhu, C. Forcing switch from short- to intermediate- and long-lived states of the alphaA domain generates LFA-1/ICAM-1 catch bonds. *The Journal of biological chemistry* **285**, 35967-35978 (2010).
14. Kong, F. *et al.* Cyclic mechanical reinforcement of integrin-ligand interactions. *Molecular cell* **49**, 1060-1068 (2013).
15. Friedland, J.C., Lee, M.H. & Boettiger, D. Mechanically activated integrin switch controls alpha5beta1 function. *Science* **323**, 642-644 (2009).
16. Ye, F. *et al.* The Mechanism of Kindlin-Mediated Activation of Integrin alphaIIb beta3. *Current biology : CB* **23**, 2288-2295 (2013).
17. Calderwood, D.A., Campbell, I.D. & Critchley, D.R. Talins and kindlins: partners in integrin-mediated adhesion. *Nature reviews. Molecular cell biology* **14**, 503-517 (2013).
18. Ussar, S., Wang, H.V., Linder, S., Fassler, R. & Moser, M. The Kindlins: subcellular localization and expression during murine development. *Experimental cell research* **312**, 3142-3151 (2006).
19. Karakose, E., Schiller, H.B. & Fassler, R. The kindlins at a glance. *Journal of cell science* **123**, 2353-2356 (2010).
20. Widmaier, M., Rognoni, E., Radovanac, K., Azimifar, S.B. & Fassler, R. Integrin-linked kinase at a glance. *Journal of cell science* **125**, 1839-1843 (2012).
21. Ye, F. *et al.* Recreation of the terminal events in physiological integrin activation. *The Journal of cell biology* **188**, 157-173 (2010).
22. Meves, A., Stremmel, C., Bottcher, R.T. & Fassler, R. beta1 integrins with individually disrupted cytoplasmic NPxY motifs are embryonic lethal but partially active in the epidermis. *The Journal of investigative dermatology* **133**, 2722-2731 (2013).
23. Bunch, T.A. Integrin alphaIIb beta3 activation in Chinese hamster ovary cells and platelets increases clustering rather than affinity. *The Journal of biological chemistry* **285**, 1841-1849 (2010).

24. Bachir, A.I. *et al.* Integrin-Associated Complexes Form Hierarchically with Variable Stoichiometry in Nascent Adhesions. *Current biology : CB* (2014).
25. Lawson, C. *et al.* FAK promotes recruitment of talin to nascent adhesions to control cell motility. *The Journal of cell biology* **196**, 223-232 (2012).
26. Zhang, X. *et al.* Talin depletion reveals independence of initial cell spreading from integrin activation and traction. *Nature cell biology* **10**, 1062-1068 (2008).
27. Takagi, J., Erickson, H.P. & Springer, T.A. C-terminal opening mimics 'inside-out' activation of integrin alpha5beta1. *Nature structural biology* **8**, 412-416 (2001).
28. Pankov, R. *et al.* Integrin dynamics and matrix assembly: tensin-dependent translocation of alpha(5)beta(1) integrins promotes early fibronectin fibrillogenesis. *The Journal of cell biology* **148**, 1075-1090 (2000).
29. Shi, Q. & Boettiger, D. A novel mode for integrin-mediated signaling: tethering is required for phosphorylation of FAK Y397. *Mol Biol Cell* **14**, 4306-4315 (2003).
30. Hyduk, S.J. *et al.* Talin-1 and kindlin-3 regulate alpha4beta1 integrin-mediated adhesion stabilization, but not G protein-coupled receptor-induced affinity upregulation. *Journal of immunology* **187**, 4360-4368 (2011).
31. Huang, J. *et al.* Impact of order and disorder in RGD nanopatterns on cell adhesion. *Nano letters* **9**, 1111-1116 (2009).
32. Rossier, O. *et al.* Integrins beta1 and beta3 exhibit distinct dynamic nanoscale organizations inside focal adhesions. *Nature cell biology* **14**, 1057-1067 (2012).
33. Paszek, M.J. *et al.* The cancer glycocalyx mechanically primes integrin-mediated growth and survival. *Nature* **511**, 319-325 (2014).
34. Huet-Calderwood, C. *et al.* Differential binding to the ILK complex determines kindlin isoform adhesion localization and integrin activation. *Journal of cell science* (2014).
35. Schlaepfer, D.D., Mitra, S.K. & Ilic, D. Control of motile and invasive cell phenotypes by focal adhesion kinase. *Biochimica et biophysica acta* **1692**, 77-102 (2004).
36. Bouchard, V. *et al.* Fak/Src signaling in human intestinal epithelial cell survival and anoikis: differentiation state-specific uncoupling with the PI3-K/Akt-1 and MEK/Erk pathways. *Journal of cellular physiology* **212**, 717-728 (2007).
37. Zhang, X., Moore, S.W., Iskratsch, T. & Sheetz, M.P. N-WASP-directed actin polymerization activates Cas phosphorylation and lamellipodium spreading. *Journal of cell science* **127**, 1394-1405 (2014).
38. Brami-Cherrier, K. *et al.* FAK dimerization controls its kinase-dependent functions at focal adhesions. *The EMBO journal* **33**, 356-370 (2014).
39. Sulzmaier, F.J., Jean, C. & Schlaepfer, D.D. FAK in cancer: mechanistic findings and clinical applications. *Nature reviews. Cancer* **14**, 598-610 (2014).
40. Deakin, N.O., Pignatelli, J. & Turner, C.E. Diverse roles for the paxillin family of proteins in cancer. *Genes & cancer* **3**, 362-370 (2012).
41. Nieswandt, B. *et al.* Loss of talin1 in platelets abrogates integrin activation, platelet aggregation, and thrombus formation in vitro and in vivo. *The Journal of experimental medicine* **204**, 3113-3118 (2007).
42. Lefort, C.T. *et al.* Distinct roles for talin-1 and kindlin-3 in LFA-1 extension and affinity regulation. *Blood* **119**, 4275-4282 (2012).
43. Conti, F.J., Monkley, S.J., Wood, M.R., Critchley, D.R. & Muller, U. Talin 1 and 2 are required for myoblast fusion, sarcomere assembly and the maintenance of myotendinous junctions. *Development* **136**, 3597-3606 (2009).
44. Fitzpatrick, P., Shattil, S.J. & Ablooglu, A.J. C-terminal COOH of integrin beta1 is necessary for beta1 association with the kindlin-2 adapter protein. *The Journal of biological chemistry* **289**, 11183-11193 (2014).

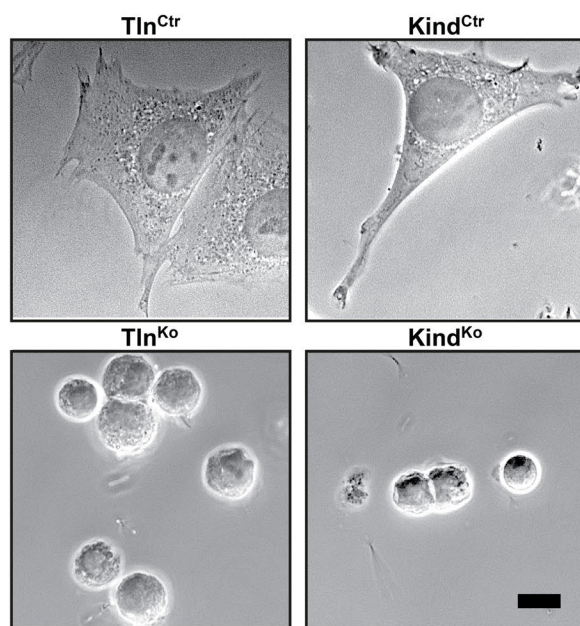
45. Takagi, J., Strokovich, K., Springer, T.A. & Walz, T. Structure of integrin alpha5beta1 in complex with fibronectin. *The EMBO journal* **22**, 4607-4615 (2003).
46. Xie, C. *et al.* Structure of an integrin with an alphaI domain, complement receptor type 4. *The EMBO journal* **29**, 666-679 (2010).
47. Xiong, J.P. *et al.* Crystal structure of the extracellular segment of integrin alpha Vbeta3 in complex with an Arg-Gly-Asp ligand. *Science* **296**, 151-155 (2002).
48. Takagi, J., Petre, B.M., Walz, T. & Springer, T.A. Global conformational rearrangements in integrin extracellular domains in outside-in and inside-out signaling. *Cell* **110**, 599-511 (2002).
49. Zhu, J., Zhu, J. & Springer, T.A. Complete integrin headpiece opening in eight steps. *The Journal of cell biology* **201**, 1053-1068 (2013).
50. Roca-Cusachs, P., Iskratsch, T. & Sheetz, M.P. Finding the weakest link: exploring integrin-mediated mechanical molecular pathways. *Journal of cell science* **125**, 3025-3038 (2012).
51. Deramaudt, T.B. *et al.* Altering FAK-paxillin interactions reduces adhesion, migration and invasion processes. *PloS one* **9**, e92059 (2014).
52. Brown, M.C., Perrotta, J.A. & Turner, C.E. Identification of LIM3 as the principal determinant of paxillin focal adhesion localization and characterization of a novel motif on paxillin directing vinculin and focal adhesion kinase binding. *The Journal of cell biology* **135**, 1109-1123 (1996).
53. Zhu, J. *et al.* Structure of a complete integrin ectodomain in a physiologic resting state and activation and deactivation by applied forces. *Molecular cell* **32**, 849-861 (2008).
54. Rognoni, E. *et al.* Kindlin-1 controls Wnt and TGF-beta availability to regulate cutaneous stem cell proliferation. *Nature medicine* (2014).
55. Fassler, R. & Meyer, M. Consequences of lack of beta 1 integrin gene expression in mice. *Genes & development* **9**, 1896-1908 (1995).
56. Spandidos, A., Wang, X., Wang, H. & Seed, B. PrimerBank: a resource of human and mouse PCR primer pairs for gene expression detection and quantification. *Nucleic acids research* **38**, D792-799 (2010).
57. Ussar, S. *et al.* Loss of Kindlin-1 causes skin atrophy and lethal neonatal intestinal epithelial dysfunction. *PLoS genetics* **4**, e1000289 (2008).
58. Bottcher, R.T. *et al.* Sorting nexin 17 prevents lysosomal degradation of beta1 integrins by binding to the beta1-integrin tail. *Nature cell biology* **14**, 584-592 (2012).
59. Moik, D. *et al.* Mutations in the paxillin-binding site of integrin-linked kinase (ILK) destabilize the pseudokinase domain and cause embryonic lethality in mice. *The Journal of biological chemistry* **288**, 18863-18871 (2013).
60. Takahashi, S. *et al.* The RGD motif in fibronectin is essential for development but dispensable for fibril assembly. *The Journal of cell biology* **178**, 167-178 (2007).
61. Czuchra, A., Meyer, H., Legate, K.R., Brakebusch, C. & Fassler, R. Genetic analysis of beta1 integrin "activation motifs" in mice. *The Journal of cell biology* **174**, 889-899 (2006).
62. van de Linde, S. *et al.* Direct stochastic optical reconstruction microscopy with standard fluorescent probes. *Nature protocols* **6**, 991-1009 (2011).
63. Ovesny, M., Krizek, P., Borkovec, J., Svindrych, Z. & Hagen, G.M. ThunderSTORM: a comprehensive ImageJ plug-in for PALM and STORM data analysis and super-resolution imaging. *Bioinformatics* **30**, 2389-2390 (2014).
64. Friedrichs, J., Helenius, J. & Muller, D.J. Quantifying cellular adhesion to extracellular matrix components by single-cell force spectroscopy. *Nature protocols* **5**, 1353-1361 (2010).
65. Te Riet, J. *et al.* Dynamic coupling of ALCAM to the actin cortex strengthens cell adhesion to CD6. *Journal of cell science* **127**, 1595-1606 (2014).

66. Schubert, R. *et al.* Assay for characterizing the recovery of vertebrate cells for adhesion measurements by single-cell force spectroscopy. *FEBS letters* **588**, 3639-3648 (2014).
67. Hutter, J.L. & Bechhoefer, J. Calibration of Atomic-Force Microscope Tips. *Review of Scientific Instruments* **64**, 1868-1873 (1993).
68. Azioune, A., Carpi, N., Tseng, Q., They, M. & Piel, M. Protein micropatterns: A direct printing protocol using deep UVs. *Methods in cell biology* **97**, 133-146 (2010).
69. Byun, J. *et al.* Automated tool for the detection of cell nuclei in digital microscopic images: application to retinal images. *Molecular vision* **12**, 949-960 (2006).

Figure 1



**C**



**E**

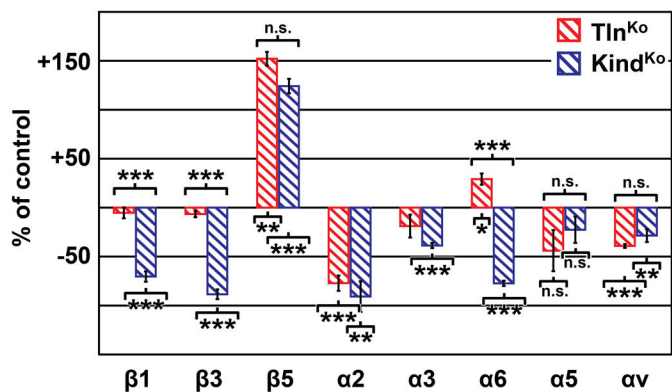


**Figure 2**

Widmaier et al.

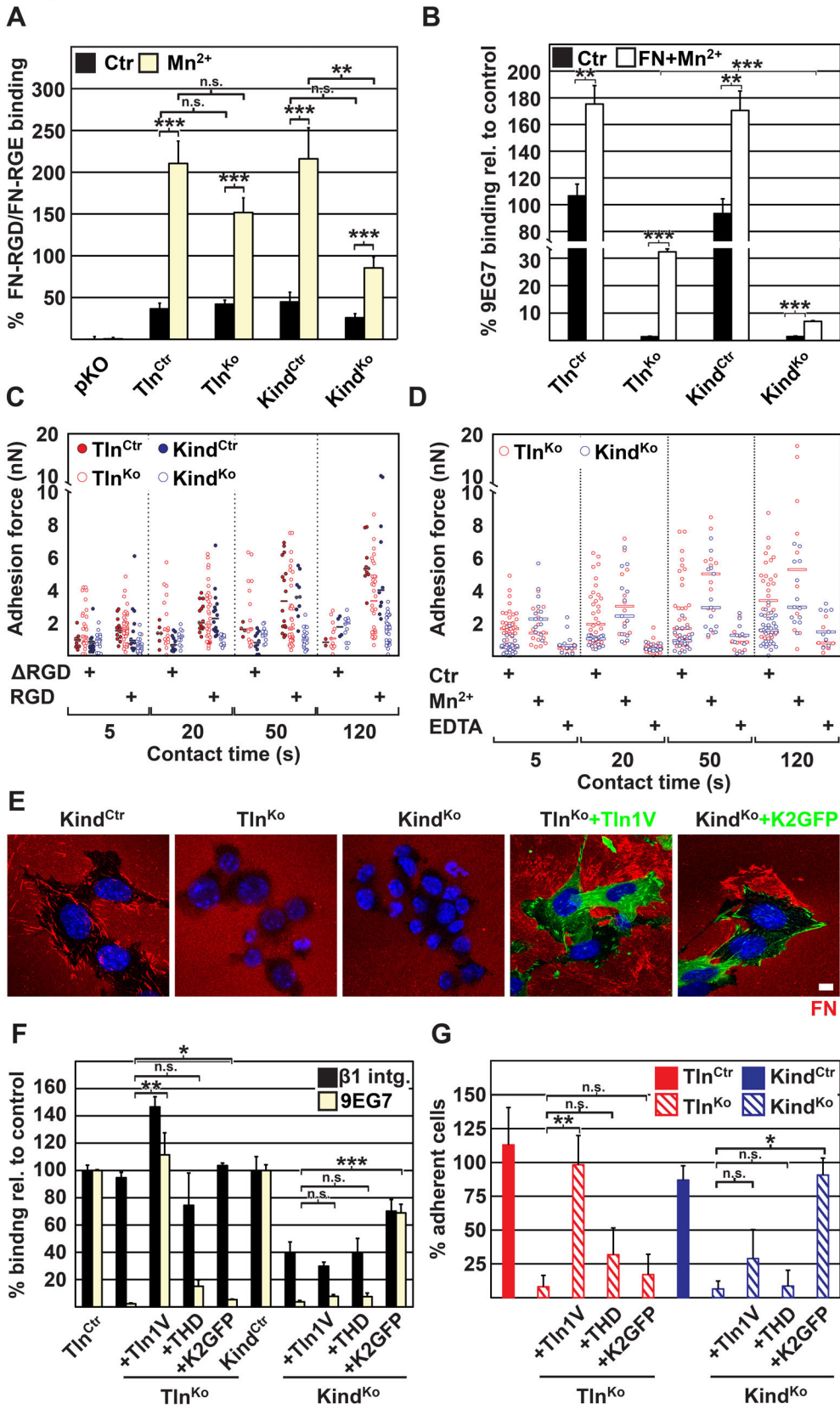


Figure 3

Widmaier et al.

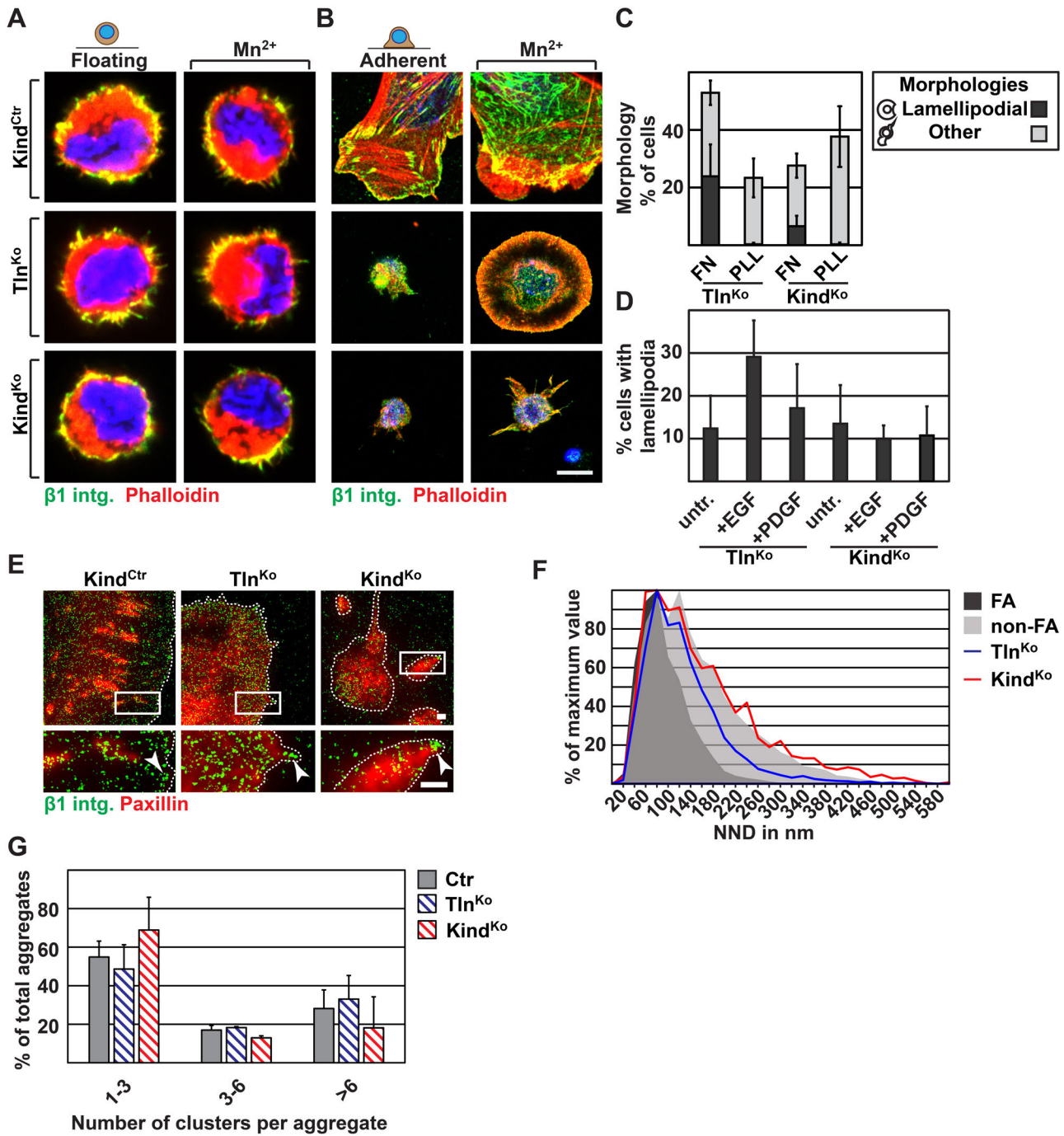


Figure 4

Widmaier et al.

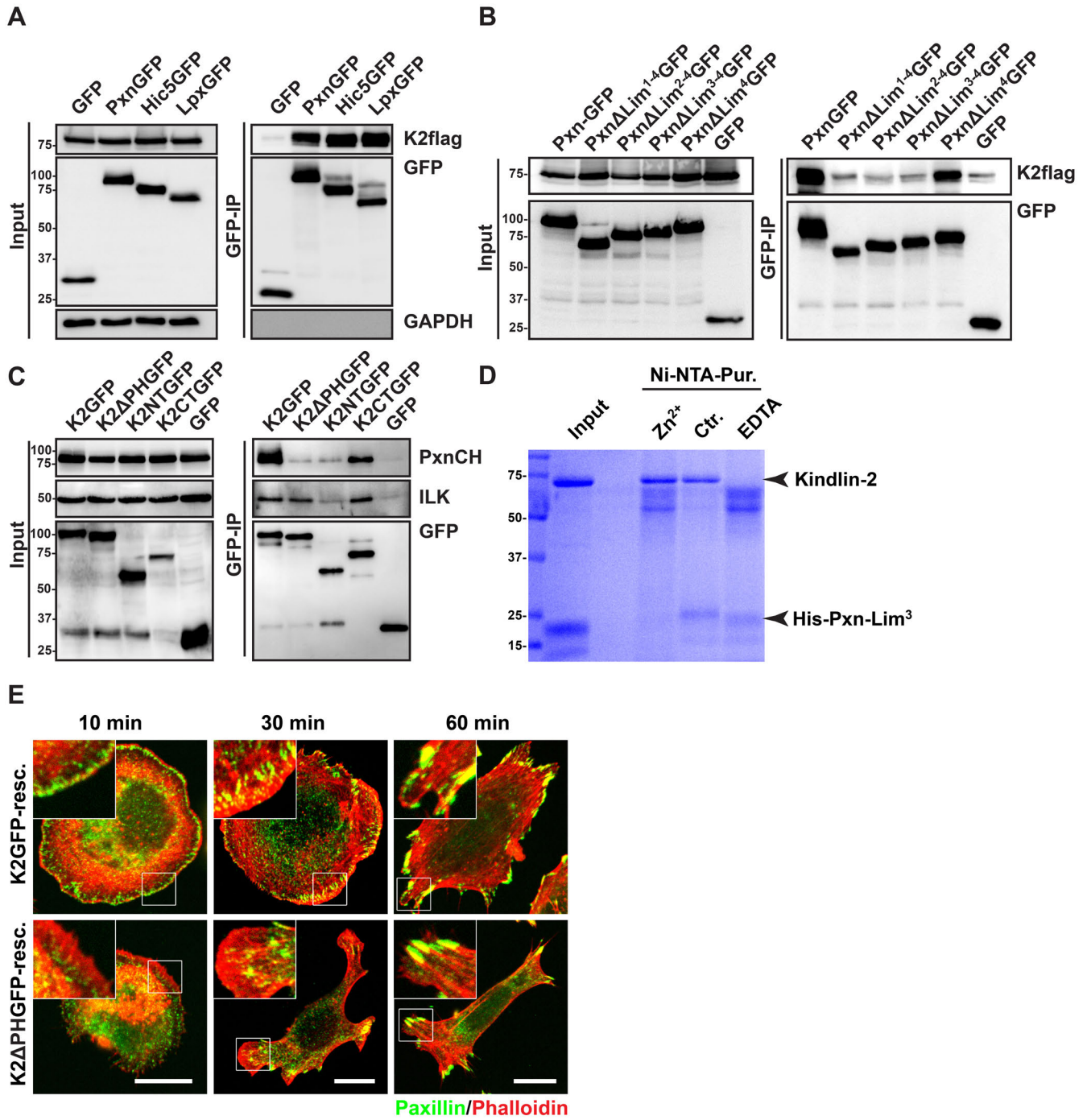


Figure 5

Widmaier et al.

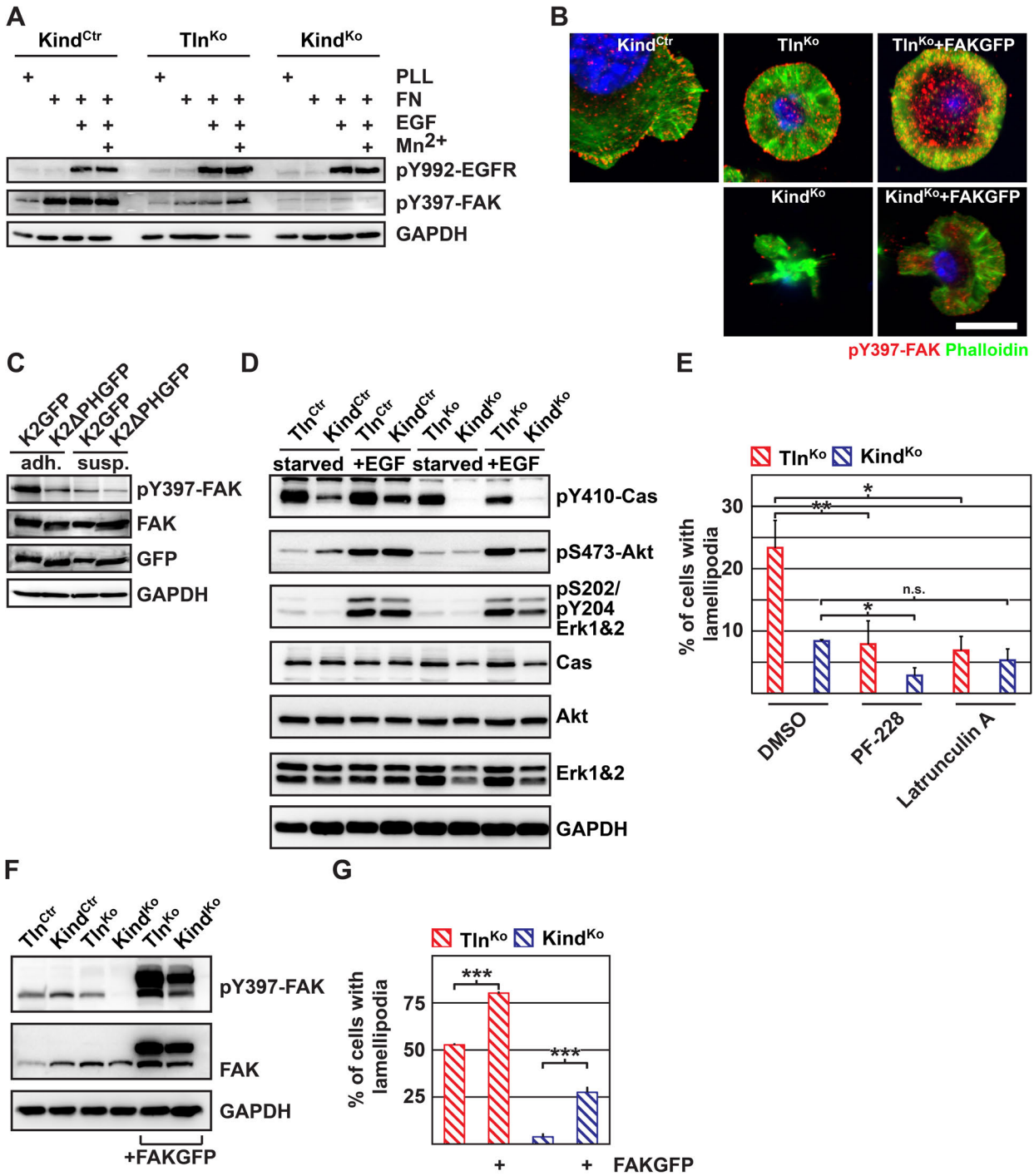


Figure 6

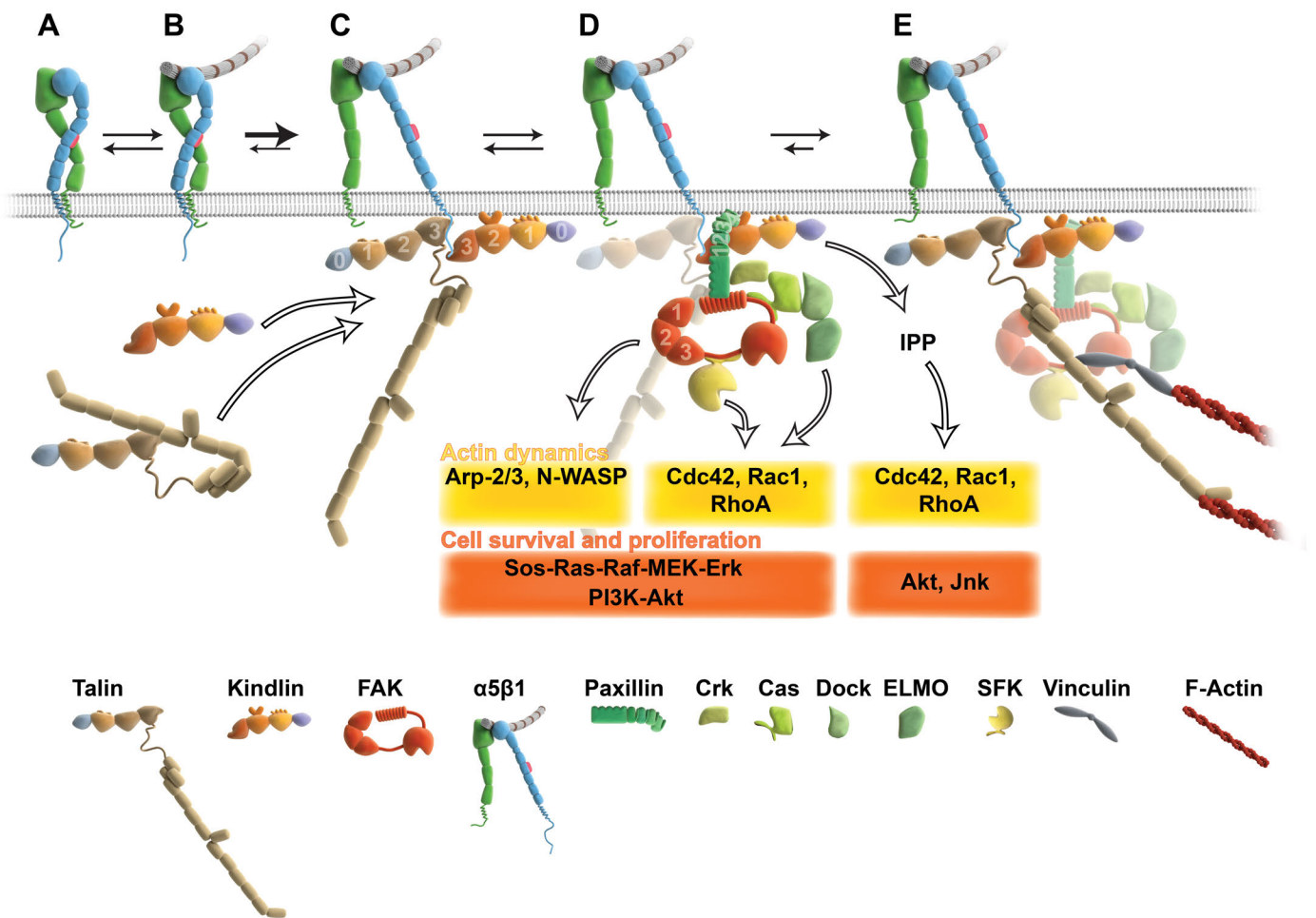


Figure S1

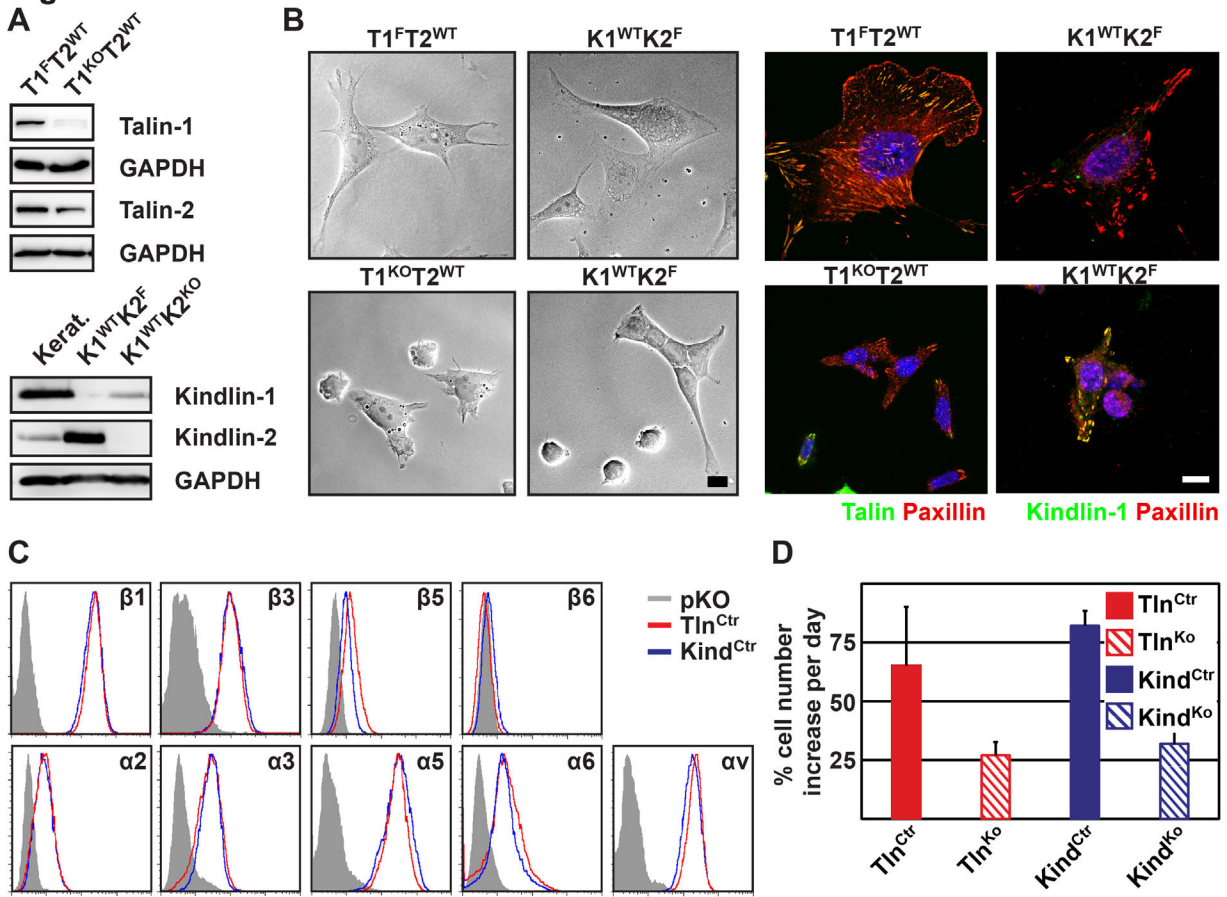


Figure S2

Widmaier et al.

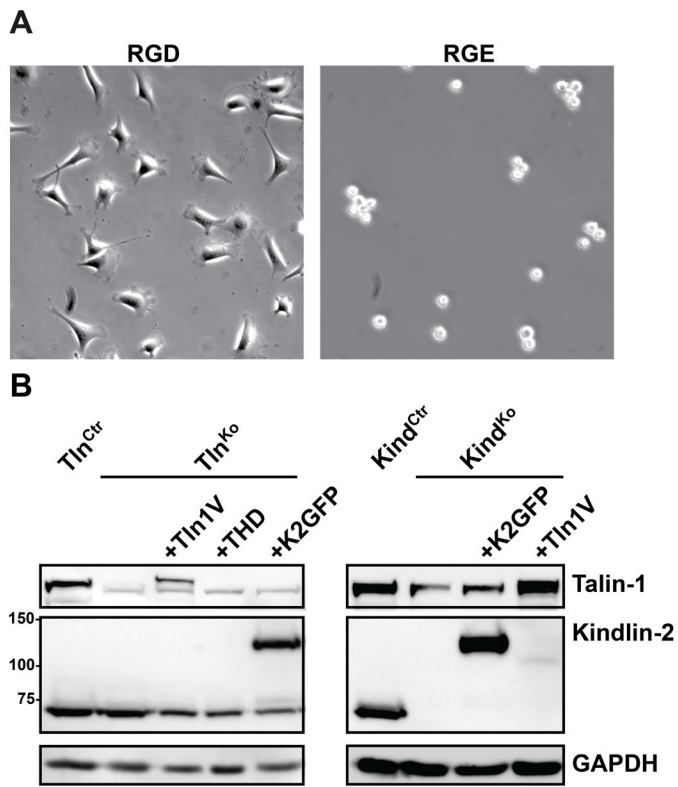
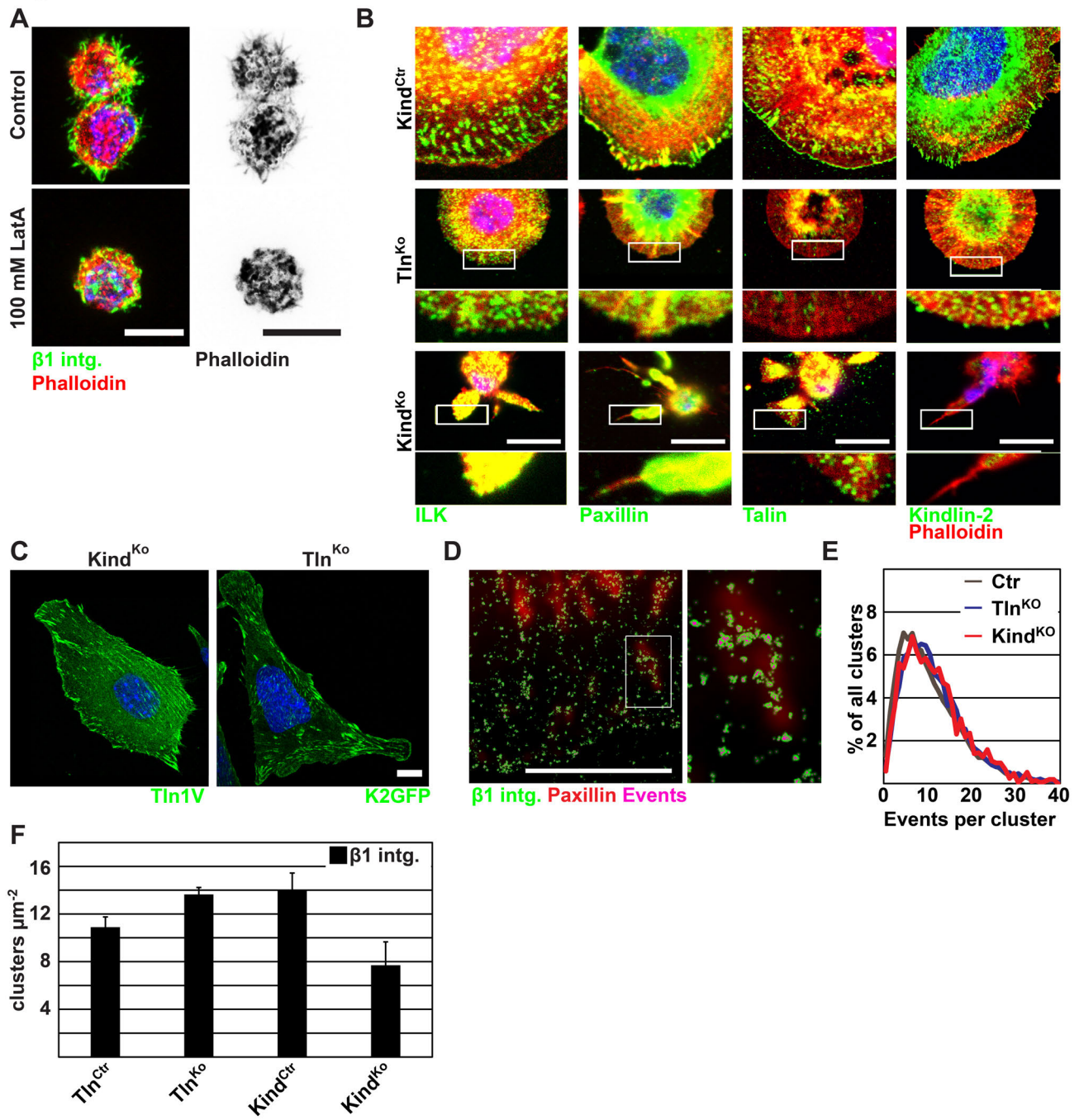
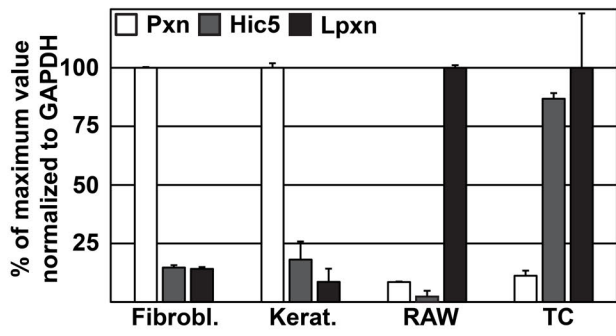


Figure S3

Widmaier et al.



A



B

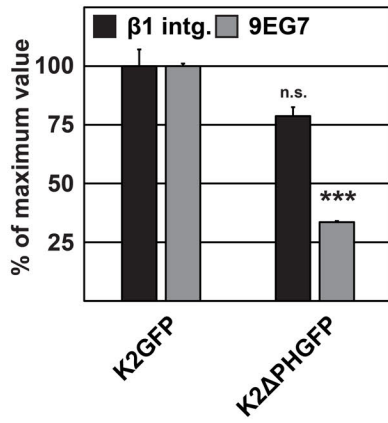
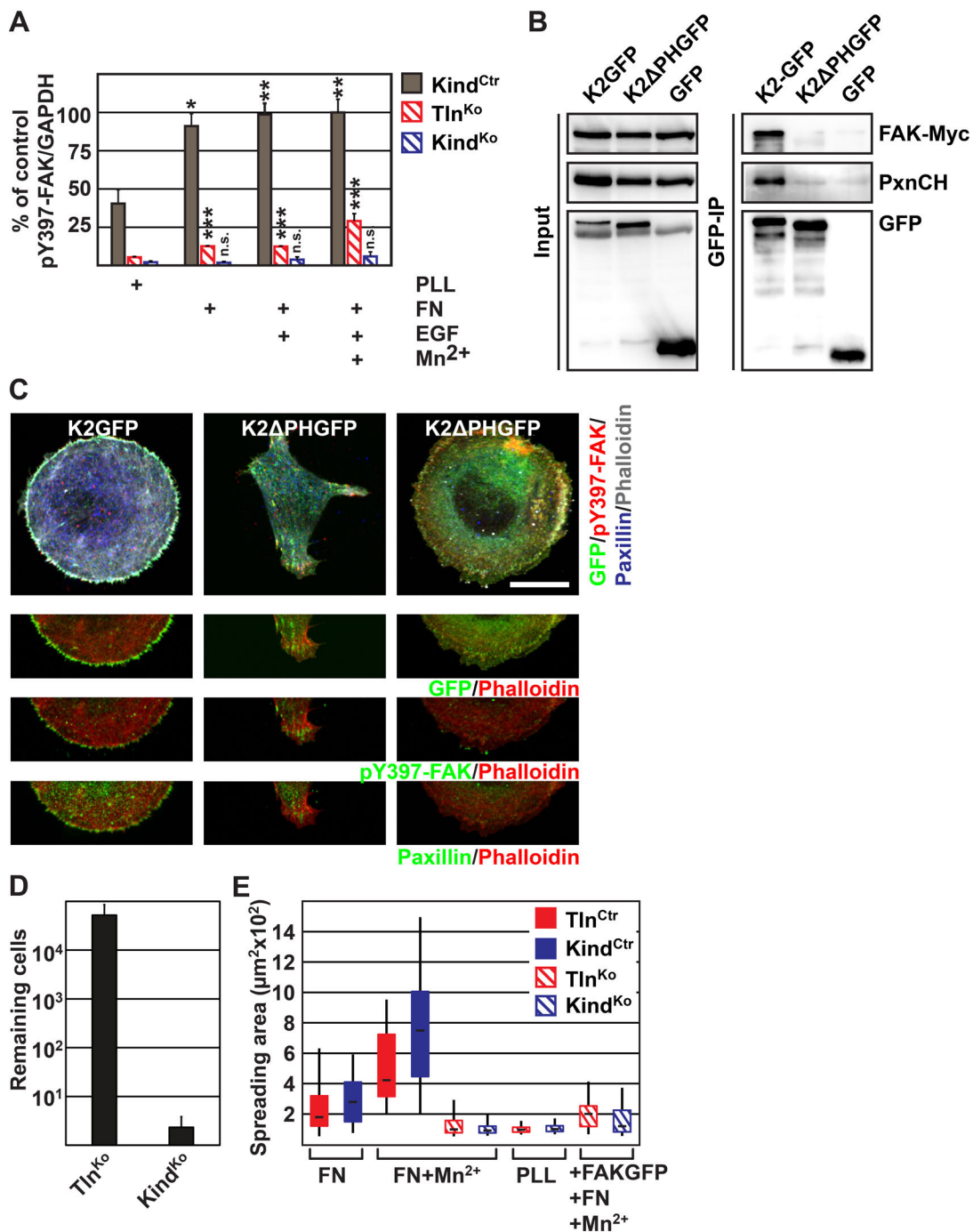


Figure S5



# Integrin-linked kinase at a glance

Moritz Widmaier, Emanuel Rognoni, Korana Radovanac, S. Babak Azimifar and Reinhard Fässler\*

Max Planck Institute of Biochemistry, Department of Molecular Medicine, Am Klopferspitz 18, D-82152 Martinsried, Germany

\*Author for correspondence (faessler@biochem.mpg.de)

Journal of Cell Science 125, 1839–1843  
© 2012. Published by The Company of Biologists Ltd  
doi: 10.1242/jcs.093864

Integrins are a large family of cell–extracellular matrix (ECM) and cell–cell adhesion molecules that regulate development and tissue homeostasis by controlling cell migration, survival, proliferation and differentiation (Hynes,

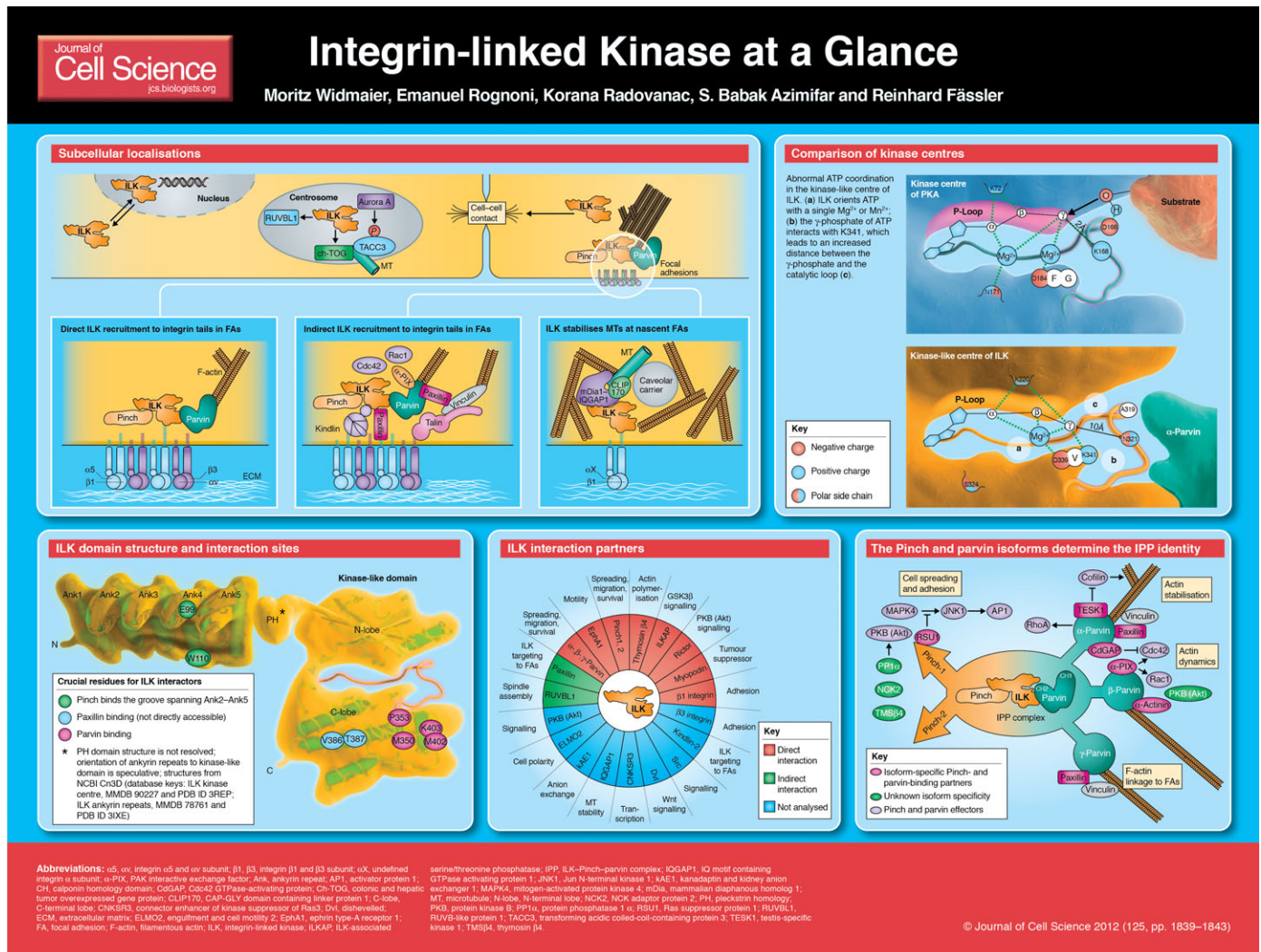
2002). They are non-covalently associated heterodimers consisting of  $\alpha$ - and  $\beta$ -subunits. On the cell surface, integrins exist in a conformation with either high (active) or low (inactive) ligand affinity. Upon activation (inside-out signalling) (Moser et al., 2009), integrins cluster and form nascent focal adhesions, which eventually mature into focal adhesions (FAs) (outside-in signalling) (Legate et al., 2009; Geiger and Yamada, 2011). Major functions of integrins in FAs include their ability to link the ECM to the actin cytoskeleton and to fine tune growth factor receptor signalling (Legate et al., 2009).

Given that integrins lack intrinsic enzymatic activity, their signalling crucially depends on recruiting adaptor and signalling proteins (Schiller et al., 2011). One of the best described of these proteins is integrin-linked

kinase (ILK), which is directly recruited to  $\beta 1$  and  $\beta 3$  integrin cytoplasmic domains. Since its discovery 15 years ago (Hannigan et al., 1996), ILK has been shown to play crucial roles in actin rearrangement, cell polarisation, spreading, migration, proliferation and survival (Legate et al., 2006). Despite its predominant localisation in FAs, ILK has also been shown to reside in cell–cell adhesion sites, in centrosomes and in the nucleus. Here, we summarise the functional properties of ILK and highlight the recent evidence demonstrating that ILK serves as a scaffold protein rather than a kinase.

## ILK and the Pinch–parvin complex

In vivo studies have revealed that ILK is a ubiquitously expressed protein, whose predominant function is to organise the actin cytoskeleton during invertebrate and vertebrate development and homeostasis. In



*Caenorhabditis elegans*, the ILK orthologue PAT-4 localises to integrins at muscle attachment sites. Deletion of the *pat-4* gene causes a 'paralysed at two-fold-stage' (PAT) phenotype that is characterised by muscle detachment through defective integrin-actin linkage and early lethality (Mackinnon et al., 2002). In *Drosophila melanogaster*, a germline deletion of ILK leads to muscle detachment and lethality (Zervas et al., 2001). Mice lacking ILK die during the peri-implantation stage owing to a failure to organise the F-actin cytoskeleton in epiblast cells (Sakai et al., 2003). In addition to the constitutive deletion, the mouse ILK-encoding gene has been deleted in several organs and cell types using the *Cre/loxP* recombination system. The outcome of these studies has been extensively reviewed elsewhere (Rooney and Streuli, 2011; Ho and Bendeck, 2009; Hannigan et al., 2007; Wickström et al., 2010b).

Structurally, ILK has three different domains: five ankyrin repeats at the N-terminus, followed by a pleckstrin homology (PH)-like domain and a kinase-like domain at the C-terminus (Chiswell et al., 2008; Yang et al., 2009) (see poster). Although ILK was shown to directly interact with integrin cytoplasmic tails, it appears that the recruitment of ILK to integrins depends, at least in some cells, on kindlin-2 (also known as Fermt2 and Plekhc1) (Montanez et al., 2008; Chen et al., 2008),  $\alpha$ -parvin (Fukuda et al., 2009) or paxillin (Nikolopoulos and Turner, 2001). Structural studies of ILK have revealed, however, that the proposed paxillin-interacting residues are buried within a polypeptide fold and thus are not directly accessible (Fukuda et al., 2009), suggesting that these residues indirectly contribute to paxillin binding. Before the recruitment of ILK to FAs, ILK forms a ternary complex with the two adaptor proteins Pinch and parvin (termed the IPP complex). Although it is not understood how the IPP complex forms, its formation ensures the stability of the individual components and their faithful targeting to the adhesion site (Zhang et al., 2002; Fukuda et al., 2003a). Mammals have two Pinch genes (Pinch-1 and Pinch-2; also known as *LIMS1* and *LIMS2*, respectively), which encode proteins consisting of five cysteine-rich, zinc-binding LIM domains followed by a nuclear export signal. The first LIM domain of Pinch-1 and -2 binds to a concave surface that extends from the

second to the fifth ankyrin repeat of ILK (Chiswell et al., 2008; Yang et al., 2009) (see poster). The three mammalian parvin isoforms ( $\alpha$ -,  $\beta$ - and  $\gamma$ -parvin) are composed of an N-terminal polypeptide followed by two calponin homology (CH) domains, the second of which binds to the kinase-like domain of ILK (Tu et al., 2001; Fukuda et al., 2009) (see poster). As ILK can only bind one Pinch and one parvin isoform at the same time (Chiswell et al., 2008; Montanez et al., 2009), ILK is capable of being part of several distinct IPP complexes, each resulting in different signalling outputs (see poster and below).

The parvin proteins can interact directly with F-actin (Legate et al., 2006) or they can recruit actin-binding proteins, such as  $\alpha$ -actinin – shown for  $\beta$ -parvin (Yamaji et al., 2004) – or vinculin, an interaction mediated through paxillin (Turner, 2000), which has been shown for  $\alpha$ - and  $\gamma$ -parvin (Yoshimi et al., 2006). In addition, they control actin regulatory proteins such as testicular protein kinase 1 (TESK1), which can bind  $\alpha$ -parvin and promote F-actin polymerisation through phosphorylation of cofilin (LaLonde et al., 2005). By contrast,  $\beta$ -parvin regulates actin dynamics through PAK-interactive exchange factor alpha ( $\alpha$ -PIX, encoded by *ARHGEF6*), a guanidine exchange factor (GEF) for Rac1 and Cdc42 (Mishima et al., 2004). Finally,  $\alpha$ -parvin has been shown to inhibit G-proteins by recruiting Cdc42 GTPase-activating protein (CdGAP, also known as RHG31 and Kiaa1204, and encoded by *ARHGAP31*) to FAs (LaLonde et al., 2006), and to negatively regulate Rho-associated protein kinase (ROCK)-driven contractility in vascular smooth muscle cells (Montanez et al., 2009).

Pinch-1 binds the Ras suppressor protein 1 (RSU1), which is important for integrin-mediated cell adhesion and spreading (Kadmas et al., 2004; Ito et al., 2010). RSU1 is a negative regulator of growth-factor-induced Jun N-terminal kinase 1 (JNK1, also known as MAPK8) (Kadmas et al., 2004). Taken together these findings suggest that the assembly of distinct IPP complexes in a given cell, together with the differential expression patterns of Pinch and parvin isoforms, provides a means for multiple alternative signalling outputs (see poster).

### Emerging functions of ILK

The most prominent subcellular localisation of ILK is in integrin adhesion sites. In recent years it has been reported

that ILK is also present in additional subcellular regions and compartments where it might exert integrin-independent functions.

### Functions in microtubule trafficking networks

Keratinocytes, and probably other cells, employ ILK to capture microtubule (MT) tips to connect them to the cortical actin network (see poster). ILK-mediated MT capture occurs exclusively in nascent FAs and is mediated by recruitment of the large scaffold protein IQ-motif-containing GTPase-activating protein 1 (IQGAP1) (Wickström et al., 2010a). The capture of MT tips can be achieved either directly through binding of IQGAP1 to the MT tip protein CLIP170 (cytoplasmic linker protein 170; also known as CLIP1), or indirectly through IQGAP1-mediated recruitment of mammalian diaphanous homolog 1 (mDia1; also known as DRF1), which is also able to stabilise MTs. As both IQGAP1 and mDia1 are also able to bind F-actin, the ILK–IQGAP1–mDia1 complex connects MTs with actin tracks at  $\beta$ 1-integrin-containing nascent adhesion sites (Wickström et al., 2010a) (see poster). Exocytotic carriers that are transported on MT tracks require a switch from MT-based to actin-based motility at the plasma membrane to pass through the cortical F-actin network and finally fuse with the plasma membrane. Thus, the connection of both networks by the ILK–IQGAP1–mDia1 complex at nascent adhesion sites is essential for the exocytosis of caveolar carriers (Wickström et al., 2010a). Consequently, ILK not only contributes to epithelial cell polarisation through actin remodelling, but also through vesicular trafficking and MT organisation.

### Nuclear functions

Despite its prominent localisation in different integrin adhesion sites, ILK has also been observed in the nucleus of several cell lines, including COS-1 cells (Chun et al., 2005), MCF-7 cells (Acconcia et al., 2007), HeLa cells and keratinocytes (Nakrieko et al., 2008a) (see poster). The nuclear function of ILK, however, is still not well understood. In keratinocytes, nuclear ILK has been shown to induce DNA synthesis (Nakrieko et al., 2008a) and, in MCF-7 cells, it has been found to control the expression of the connector enhancer of kinase suppressor of Ras3 (*CNKSR3*) gene (Acconcia et al., 2007). It is known that *CNKSR3* regulates the

epithelial Na<sup>+</sup> channel (ENaC) through inhibition of the MAPK kinase MEK1 (Ziera et al., 2009). However, the significance of ILK-regulated *CMSKR3* expression is not understood.

It is also not well understood how ILK translocates into the nucleus. For example, it is not known whether the nuclear import of ILK depends on its N-terminus (Acconcia et al., 2007) or on a C-terminal nuclear localisation signal (Chun et al., 2005). The nuclear export of ILK requires the kinase-like domain (Acconcia et al., 2007; Nakrieko et al., 2008a) and is apparently controlled by the nuclear export factor CRM1, integrin-linked kinase-associated serine and threonine phosphatase 2C (ILKAP) and p21-activated kinase 1 (PAK1) (Acconcia et al., 2007; Nakrieko et al., 2008a).

#### Organisation of cell–cell contacts

ILK has been shown to serve as a scaffold for promoting the formation of cell–cell contacts (see poster) and the recruitment of tight junction proteins (Vespa et al., 2003; Vespa et al., 2005). Following treatment of cultured keratinocytes with Ca<sup>2+</sup>, they undergo differentiation. This process is accompanied by the translocation of ILK from FAs to cell–cell adhesion sites (Vespa et al., 2003). This translocation is known to require the N-terminal ankyrin repeats (Vespa et al., 2003); however, it is unclear whether Pinch-1 or -2 translocate together with ILK. In contrast to these *in vitro* findings, deletion of the *Ilk* gene in mouse keratinocytes neither affects cell–cell adhesion nor barrier function in the epidermis, but severely impairs keratinocyte migration on and adhesion to the epidermal–dermal basal membrane (BM), resulting in skin blistering, epidermal hyperthickening and hair loss (Lorenz et al., 2007; Nakrieko et al., 2008b).

#### Centrosome functions

A proteomic search for new ILK-interacting proteins identified a number of proteins, including several centrosome- and mitotic-spindle-associated proteins, such as  $\alpha$ - and  $\beta$ -tubulin, the tubulin-binding proteins RUVBL1 and colonic and hepatic tumor overexpressed gene protein (ch-TOG, also known as CKAP5) (Dobrev et al., 2008) (see poster). Although ILK probably binds these proteins in an indirect manner (Fielding et al., 2008), it colocalises with them in centrosomes from interphase and mitotic cells where it has an essential

role in controlling centrosome function during mitotic spindle organisation and centrosome clustering (Fielding et al., 2008; Fielding et al., 2011). The organisation of the mitotic spindle requires the kinase Aurora A and the association of ch-TOG with the centrosomal transforming acidic coiled-coil-containing protein 3 (TACC3), which in turn promotes the polymerisation and stabilisation of centrosomal MTs (Barr and Gergely, 2007). In ILK-depleted cells, Aurora A kinase, although active, is unable to phosphorylate and thus activate TACC3, resulting in disruption of mitotic spindles. Similarly, the clustering of supernumerary centrosomes in cancer cells is also achieved by the TACC3–ch-TOG complex in an ILK- and Aurora-A-dependent manner (Fielding et al., 2011). ILK associates with ch-TOG, but not with TACC3 or Aurora A. Therefore, it is not clear how ILK supports the phosphorylation of TACC3 by Aurora A. Similarly, it is also unclear how ILK is recruited to centrosomes. The centrosomal localisation of ILK requires RUVBL1 expression and occurs without the known ILK-binding partners,  $\alpha$ -parvin and Pinch (Fielding et al., 2008). Finally, it is also not known why the treatment of cells with QLT-0267, a small chemical compound that binds to the ATP-binding site of ILK, is as effective as siRNA-mediated depletion of ILK in blocking the association of TACC3 with Aurora A (Fielding et al., 2008). The mechanistic interpretation of this work is based on the assumption that ILK acts as a kinase, which has been disproved by genetic and structural studies (see below). A potential explanation for the inhibitory effect of QLT-0267 could be an impairment of the stability of ILK (see the next section).

#### The kinase controversy

The experimental evidence that the kinase-like domain of ILK lacks catalytic activity is overwhelming (Wickström et al., 2010b). Although ILK was initially identified by Dedhar and colleagues as a serine/threonine kinase (Hannigan et al., 1996), it lacks several important motifs that are conserved in most kinases (Hanks et al., 1988) (see poster). Furthermore, genetic studies in flies, worms and mice have demonstrated that the putative kinase activity is not required for development and homeostasis (Zervas et al., 2001; Mackinnon et al., 2002; Lange et al., 2009). Despite this compelling evidence, many papers have been and are still

published claiming that ILK is a bona fide kinase, with only marginal evidence at best.

The crystallisation of kinase-like domain of ILK in complex with the CH domain of  $\alpha$ -parvin and its comparison to the kinase domain of protein kinase A (PKA) has provided a mechanistic explanation for why the kinase function of ILK is not executed (Fukuda et al., 2009). The catalytic activity of a kinase depends on a coordinated interplay of the N- and C-lobes and the catalytic loop of the kinase domain with the substrate and ATP. The N- and C-lobes and the catalytic loop of ILK show major differences to those of bona fide kinases that render the ‘kinase’ of ILK non functional: (1) The catalytic loop lacks important acidic and positively charged residues. The acidic residue (D166 in PKA), which polarises the hydroxyl group of the substrate and accepts its proton, is replaced in ILK with the uncharged alanine residue (A319) (Fukuda et al., 2009). (2) The positively charged residue in the catalytic loop (K168 in PKA), which stabilises the intermediate state of the phosphoryl transfer reaction by neutralizing the negative charge of the  $\gamma$ -ATP phosphoryl group, is replaced in ILK by N321 resulting in a misrouting of ATP to the C-lobe. (3) In the N-lobe, the ATP-binding p-loop captures ATP at a too great distance from the active centre (10 Å), which precludes its movement towards the catalytic loop, and the lysine residue K220 contacts the  $\alpha$ - and  $\gamma$ -ATP phosphoryl groups instead of the  $\alpha$ - and  $\beta$ -phosphoryl groups resulting in an aberrant ATP orientation. (4) Furthermore, the C-lobe of ILK chelates ATP with only one instead of the expected two metal ions. The metal ion is bound by the aspartate residue (D339) of the DVK motif of ILK (a DFG motif in PKA), whereas the second potential metal-binding residue (S324) remains unoccupied. Another divergence from bona fide kinases is the coordination of the  $\gamma$ -ATP phosphoryl-group by the lysine residue (K341) of the DVK motif of the N-lobe, which usually is mediated by the catalytic loop (Fukuda et al., 2009). Nevertheless, despite this structural evidence, dissenting views are still expressed and the controversy rages on (Hannigan et al., 2011).

Thermodynamic and structural analysis of ILK mutants has revealed that the K220A and K220M mutations, previously described as affecting kinase function, destabilise the global ILK structure

(Fukuda et al., 2011), thus reducing ILK stability and the binding of interaction partners such as  $\alpha$ -parvin. This observation provides an explanation for the severe kidney defects observed in mice which either lack  $\alpha$ -parvin expression or carry K220A or K220M mutations in ILK (Lange et al., 2009).

### Redefining the role of ILK in cancer

ILK is overexpressed in many types of cancer, and it has been reported that its depletion or inhibition with the small molecule inhibitor QLT-0267 inhibits anchorage-independent growth, cell cycle progression and invasion (Hannigan et al., 2005). The oncogenic effects of ILK have been attributed for the most part to the catalytic activity of the kinase domain resulting in the activation of protein kinase B (PKB, also known as Akt) and glycogen synthase kinase-3 beta (GSK3 $\beta$ ), which in turn regulates the stability of proto-oncogenic  $\beta$ -catenin (Hannigan et al., 2005). The recent findings showing that mammalian ILK lacks catalytic activity and serves as a scaffold protein in FAs of mammalian cells (Lange et al., 2009; Fukuda et al., 2009) raise the question of how ILK mediates its oncogenic potential despite this functional twist.

One possibility is that ILK controls the activity of oncogenes, such as PKB by controlling their subcellular localisation. For example, the ILK-binding partners  $\alpha$ - and  $\beta$ -parvin induce the recruitment of PKB to the plasma membrane where PKB mediates its oncogenic activity (Fukuda et al., 2003b; Kimura et al., 2010). An alternative possibility is that ILK and ILK-interacting protein(s) regulate oncogenic kinases by controlling the activity of phosphatases. This has been shown for Pinch-1, which binds to and inhibits protein phosphatase 1 $\alpha$  (PP1 $\alpha$ ) resulting in sustained PKB phosphorylation and activity (Eke et al., 2010). Consequently, reducing the amounts of the IPP complex in FAs will concomitantly result in an increased PP1 $\alpha$  activity and decreased PKB function. It is also conceivable that ILK exerts its oncogenic function through its ability to cluster supernumerary centrosomes in cancer cells, thereby preventing their genomic instability and death (Fielding et al., 2011). Finally, ILK might also promote oncogenesis by regulating gene expression in the nucleus or by modulating the assembly of ECM proteins, as shown for fibronectin (Wu et al., 1998), which has

been reported to affect cancer development and invasion (Akiyama et al., 1995).

### Outlook and perspectives

ILK research has been significantly advanced in the past years by the resolution the long-lasting debate regarding the catalytic activity of ILK and by identifying novel functions for ILK, many of which occur outside of FAs. However, most of the emerging functions of ILK (e.g. in the nucleus, at cell-cell adhesion sites and in the centrosome) have only been studied in cultured cells thus far and still await confirmation in vivo.

In addition, several basic functions of ILK in FAs are still unresolved, including the mechanism(s) of the recruitment of ILK to FAs, the role of ILK in FA maturation and as a potential stretch sensor (Bendig et al., 2006), and the turnover and modifications of ILK, to name a few. Whether the recruitment of ILK to FAs occurs through a direct association with the integrin cytoplasmic domains or indirectly, e.g. through binding to kindlins (Montanez et al., 2008) or paxillin (Nikolopoulos and Turner, 2001) is currently unclear. In this regard, it is also not known whether ILK binds or associates with all  $\beta$ -integrin tails or whether this association is more selective. A co-crystallisation of the kinase-like domain of ILK with  $\beta$ -integrin tails should help to answer some of these questions. Similarly, a structural analysis of the predicted PH domain of ILK would clarify whether it adopts a classical PH fold, as predicted in the original publication (Hannigan et al., 1996), or a different motif, whose function would then have to be determined. Zebrafish studies point to a stretch-sensing function for ILK in cardiomyocytes (Bendig et al., 2006). This observation raises the question of whether mechanical stress sensing by ILK is restricted to cardiomyocytes or whether it also occurs in other cells, and of how ILK is executing this function at the molecular level. Finally, it will be important to re-evaluate the role of ILK in cancer. Ideally, these experiments should be performed in an unbiased manner with tumour models in mice (e.g. colon cancer and mammary cancer models) that lack ILK expression, and are complemented by sophisticated in vitro studies with cells derived from the tumours.

It is obvious that despite the rapid progress in ILK research, many questions are still unanswered. Recent advances in imaging and proteomics combined with

genetics, cell biology and biochemistry will make the years to come exciting for all ILK aficionados.

### Acknowledgements

We thank Kyle Legate and Roy Zent for careful reading of the manuscript and Max Iglesias for help with preparation of the art work.

### Funding

The ILK work in the Fässler laboratory is supported by the Tiroler Zukunftsstiftung and the Max Planck Society.

A high-resolution version of the poster is available for downloading in the online version of this article at [jcs.biologists.org](http://jcs.biologists.org). Individual poster panels are available as JPEG files at <http://jcs.biologists.org/lookup/suppl/doi:10.1242/jcs.093864/-DC1>

### References

- Acconcia, F., Barnes, C. J., Singh, R. R., Talukder, A. H. and Kumar, R. (2007). Phosphorylation-dependent regulation of nuclear localization and functions of integrin-linked kinase. *Proc. Natl. Acad. Sci. USA* **104**, 6782-6787.
- Akiyama, S. K., Olden, K. and Yamada, K. M. (1995). Fibronectin and integrins in invasion and metastasis. *Cancer Metastasis Rev.* **14**, 173-189.
- Barr, A. R. and Gergely, F. (2007). Aurora-A: the maker and breaker of spindle poles. *J. Cell Sci.* **120**, 2987-2996.
- Bendig, G., Grimmmer, M., Huttner, I. G., Wessels, G., Dahme, T., Just, S., Trano, N., Katus, H. A., Fishman, M. C. and Rottbauer, W. (2006). Integrin-linked kinase, a novel component of the cardiac mechanical stretch sensor, controls contractility in the zebrafish heart. *Genes Dev.* **20**, 2361-2372.
- Chen, K., Tu, Y., Zhang, Y., Blair, H. C., Zhang, L. and Wu, C. (2008). PINCH-1 regulates the ERK-Bim pathway and contributes to apoptosis resistance in cancer cells. *J. Biol. Chem.* **283**, 2508-2517.
- Chiswell, B. P., Zhang, R., Murphy, J. W., Boggon, T. J. and Calderwood, D. A. (2008). The structural basis of integrin-linked kinase-PINCH interactions. *Proc. Natl. Acad. Sci. USA* **105**, 20677-20682.
- Chun, J., Hyun, S., Kwon, T., Lee, E. J., Hong, S. K. and Kang, S. S. (2005). The subcellular localization control of integrin linked kinase 1 through its protein-protein interaction with caveolin-1. *Cell. Signal.* **17**, 751-760.
- Dobrev, I., Fielding, A., Foster, L. J. and Dedhar, S. (2008). Mapping the integrin-linked kinase interactome using SILAC. *J. Proteome Res.* **7**, 1740-1749.
- Eke, I., Koch, U., Hehlhans, S., Sandfort, V., Stanchi, F., Zips, D., Baumann, M., Shevchenko, A., Pilarsky, C., Haase, M. et al. (2010). PINCH1 regulates Akt1 activation and enhances radioresistance by inhibiting PP1 $\alpha$ . *J. Clin. Invest.* **120**, 2516-2527.
- Fielding, A. B., Dobrev, I., McDonald, P. C., Foster, L. J. and Dedhar, S. (2008). Integrin-linked kinase localizes to the centrosome and regulates mitotic spindle organization. *J. Cell Biol.* **180**, 681-689.
- Fielding, A. B., Lim, S., Montgomery, K., Dobrev, I. and Dedhar, S. (2011). A critical role of integrin-linked kinase, ch-TOG and TACC3 in centrosome clustering in cancer cells. *Oncogene* **30**, 521-534.
- Fukuda, K., Gupta, S., Chen, K., Wu, C. and Qin, J. (2009). The pseudoactive site of ILK is essential for its binding to  $\alpha$ -Parvin and localization to focal adhesions. *Mol. Cell* **36**, 819-830.
- Fukuda, K., Knight, J. D. R., Piszczek, G., Kothary, R. and Qin, J. (2011). Biochemical, proteomic, structural, and thermodynamic characterizations of integrin-linked kinase (ILK): cross-validation of the pseudokinase. *J. Biol. Chem.* **286**, 21886-21895.

- Fukuda, T., Chen, K., Shi, X. and Wu, C. (2003a). PINCH-1 is an obligate partner of integrin-linked kinase (ILK) functioning in cell shape modulation, motility, and survival. *J. Biol. Chem.* **278**, 51324-51333.
- Fukuda, T., Guo, L., Shi, X. and Wu, C. (2003b). CH-ILKBP regulates cell survival by facilitating the membrane translocation of protein kinase B/Akt. *J. Cell Biol.* **160**, 1001-1008.
- Geiger, B. and Yamada, K. M. (2011). Molecular architecture and function of matrix adhesions. *Cold Spring Harb. Perspect. Biol.* **3**, a005033.
- Hanks, S. K., Quinn, A. M. and Hunter, T. (1988). The protein kinase family: conserved features and deduced phylogeny of the catalytic domains. *Science* **241**, 42-52.
- Hannigan, G., Troussard, A. A. and Dedhar, S. (2005). Integrin-linked kinase: a cancer therapeutic target unique among its ILK. *Nat. Rev. Cancer* **5**, 51-63.
- Hannigan, G. E., Leung-Hageteijn, C., Fitz-Gibbon, L., Coppolino, M. G., Radeva, G., Filmus, J., Bell, J. C. and Dedhar, S. (1996). Regulation of cell adhesion and anchorage-dependent growth by a new beta 1-integrin-linked protein kinase. *Nature* **379**, 91-96.
- Hannigan, G. E., Coles, J. G. and Dedhar, S. (2007). Integrin-linked kinase at the heart of cardiac contractility, repair, and disease. *Circ. Res.* **100**, 1408-1414.
- Hannigan, G. E., McDonald, P. C., Walsh, M. P. and Dedhar, S. (2011). Integrin-linked kinase: not so 'pseudo' after all. *Oncogene* **30**, 4375-4385.
- Ho, B. and Bendeck, M. P. (2009). Integrin linked kinase (ILK) expression and function in vascular smooth muscle cells. *Cell Adhes. Migr.* **3**, 174-176.
- Hynes, R. O. (2002). Integrins: bidirectional, allosteric signaling machines. *Cell* **110**, 673-687.
- Ito, S., Takahara, Y., Hyodo, T., Hasegawa, H., Asano, E., Hamaguchi, M. and Senga, T. (2010). The roles of two distinct regions of PINCH-1 in the regulation of cell attachment and spreading. *Mol. Biol. Cell* **21**, 4120-4129.
- Kadrmans, J. L., Smith, M. A., Clark, K. A., Pronovost, S. M., Muster, N., Yates, J. R., 3rd and Beckerle, M. C. (2004). The integrin effector PINCH regulates JNK activity and epithelial migration in concert with Ras suppressor 1. *J. Cell Biol.* **167**, 1019-1024.
- Kimura, M., Murakami, T., Kizaka-Kondoh, S., Itoh, M., Yamamoto, K., Hojo, Y., Takano, M., Kario, K., Shimada, K. and Kobayashi, E. (2010). Functional molecular imaging of ILK-mediated Akt/PKB signaling cascades and the associated role of beta-parvin. *J. Cell Sci.* **123**, 747-755.
- LaLonde, D. P., Brown, M. C., Bouverat, B. P. and Turner, C. E. (2005). Actopaxin interacts with TESK1 to regulate cell spreading on fibronectin. *J. Biol. Chem.* **280**, 21680-21688.
- LaLonde, D. P., Grubinger, M., Lamarche-Vane, N. and Turner, C. E. (2006). CdGAP associates with actopaxin to regulate integrin-dependent changes in cell morphology and motility. *Curr. Biol.* **16**, 1375-1385.
- Lange, A., Wickström, S. A., Jakobson, M., Zent, R., Sainio, K. and Fässler, R. (2009). Integrin-linked kinase is an adaptor with essential functions during mouse development. *Nature* **461**, 1002-1006.
- Legate, K. R., Montañez, E., Kudlacek, O. and Fässler, R. (2006). ILK, PINCH and parvin: the tIPP of integrin signalling. *Nat. Rev. Mol. Cell Biol.* **7**, 20-31.
- Legate, K. R., Wickström, S. A. and Fässler, R. (2009). Genetic and cell biological analysis of integrin outside-in signaling. *Genes Dev.* **23**, 397-418.
- Lorenz, K., Grashoff, C., Torka, R., Sakai, T., Langhein, L., Bloch, W., Aumailley, M. and Fässler, R. (2007). Integrin-linked kinase is required for epidermal and hair follicle morphogenesis. *J. Cell Biol.* **177**, 501-513.
- Mackinnon, A. C., Qadota, H., Norman, K. R., Moerman, D. G. and Williams, B. D. (2002). C. elegans PAT-4/ILK functions as an adaptor protein within integrin adhesion complexes. *Curr. Biol.* **12**, 787-797.
- Mishima, W., Suzuki, A., Yamaji, S., Yoshimi, R., Ueda, A., Kaneko, T., Tanaka, J., Miwa, Y., Ohno, S. and Ishigatsubo, Y. (2004). The first CH domain of affixin activates Cdc42 and Rac1 through alphaPIX, a Cdc42/Rac1-specific guanine nucleotide exchanging factor. *Genes Cells* **9**, 193-204.
- Montanez, E., Ussar, S., Schifferer, M., Bösl, M., Zent, R., Moser, M. and Fässler, R. (2008). Kindlin-2 controls bidirectional signaling of integrins. *Genes Dev.* **22**, 1325-1330.
- Montanez, E., Wickström, S. A., Altstätter, J., Chu, H. and Fässler, R. (2009). Alpha-parvin controls vascular mural cell recruitment to vessel wall by regulating RhoA/ROCK signalling. *EMBO J.* **28**, 3132-3144.
- Moser, M., Legate, K. R., Zent, R. and Fässler, R. (2009). The tail of integrins, talin, and kindlins. *Science* **324**, 895-899.
- Nakrieko, K. A., Vespa, A., Mason, D., Irvine, T. S., D'Souza, S. J. and Dagnino, L. (2008a). Modulation of integrin-linked kinase nucleo-cytoplasmic shuttling by ILKAP and CRM1. *Cell Cycle* **7**, 2157-2166.
- Nakrieko, K. A., Welch, I., Dupuis, H., Bryce, D., Pajak, A., St Arnaud, R., Dedhar, S., D'Souza, S. J. and Dagnino, L. (2008b). Impaired hair follicle morphogenesis and polarized keratinocyte movement upon conditional inactivation of integrin-linked kinase in the epidermis. *Mol. Biol. Cell* **19**, 1462-1473.
- Nikolopoulos, S. N. and Turner, C. E. (2001). Integrin-linked kinase (ILK) binding to paxillin LD1 motif regulates ILK localization to focal adhesions. *J. Biol. Chem.* **276**, 23499-23505.
- Rooney, N. and Streuli, C. H. (2011). How integrins control mammary epithelial differentiation: a possible role for the ILK-PINCH-Parvin complex. *FEBS Lett.* **585**, 1663-1672.
- Sakai, T., Li, S., Docheva, D., Grashoff, C., Sakai, K., Kostka, G., Braun, A., Pfeifer, A., Yurchenko, P. D. and Fässler, R. (2003). Integrin-linked kinase (ILK) is required for polarizing the epiblast, cell adhesion, and controlling actin accumulation. *Genes Dev.* **17**, 926-940.
- Schiller, H. B., Friedel, C. C., Boulegue, C. and Fässler, R. (2011). Quantitative proteomics of the integrin adhesome show a myosin II-dependent recruitment of LIM domain proteins. *EMBO Rep.* **12**, 259-266.
- Tu, Y., Huang, Y., Zhang, Y., Hua, Y. and Wu, C. (2001). A new focal adhesion protein that interacts with integrin-linked kinase and regulates cell adhesion and spreading. *J. Cell Biol.* **153**, 585-598.
- Turner, C. E. (2000). Paxillin interactions. *J. Cell Sci.* **113**, 4139-4140.
- Vespa, A., Darmon, A. J., Turner, C. E., D'Souza, S. J. and Dagnino, L. (2003). Ca<sup>2+</sup>-dependent localization of integrin-linked kinase to cell junctions in differentiating keratinocytes. *J. Biol. Chem.* **278**, 11528-11535.
- Vespa, A., D'Souza, S. J. and Dagnino, L. (2005). A novel role for integrin-linked kinase in epithelial sheet morphogenesis. *Mol. Biol. Cell* **16**, 4084-4095.
- Wickström, S. A., Lange, A., Hess, M. W., Polleux, J., Spatz, J. P., Krüger, M., Pfaller, K., Lambacher, A., Bloch, W., Mann, M. et al. (2010a). Integrin-linked kinase controls microtubule dynamics required for plasma membrane targeting of caveolae. *Dev. Cell* **19**, 574-588.
- Wickström, S. A., Lange, A., Montanez, E. and Fässler, R. (2010b). The ILK/PINCH/parvin complex: the kinase is dead, long live the pseudokinase! *EMBO J.* **29**, 281-291.
- Wu, C., Keightley, S. Y., Leung-Hageteijn, C., Radeva, G., Coppolino, M., Goicoechea, S., McDonald, J. A. and Dedhar, S. (1998). Integrin-linked protein kinase regulates fibronectin matrix assembly, E-cadherin expression, and tumorigenicity. *J. Biol. Chem.* **273**, 528-536.
- Yamaji, S., Suzuki, A., Kanamori, H., Mishima, W., Yoshimi, R., Takasaki, H., Takabayashi, M., Fujimaki, K., Fujisawa, S., Ohno, S. et al. (2004). Affixin interacts with alpha-actinin and mediates integrin signaling for reorganization of F-actin induced by initial cell-substrate interaction. *J. Cell Biol.* **165**, 539-551.
- Yang, Y., Wang, X., Hawkins, C. A., Chen, K., Vaynberg, J., Mao, X., Tu, Y., Zuo, X., Wang, J., Wang, Y. X. et al. (2009). Structural basis of focal adhesion localization of LIM-only adaptor PINCH by integrin-linked kinase. *J. Biol. Chem.* **284**, 5836-5844.
- Yoshimi, R., Yamaji, S., Suzuki, A., Mishima, W., Okamura, M., Obana, T., Matsuda, C., Miwa, Y., Ohno, S. and Ishigatsubo, Y. (2006). The gamma-parvin-integrin-linked kinase complex is critically involved in leukocyte-substrate interaction. *J. Immunol.* **176**, 3611-3624.
- Zervas, C. G., Gregory, S. L. and Brown, N. H. (2001). Drosophila integrin-linked kinase is required at sites of integrin adhesion to link the cytoskeleton to the plasma membrane. *J. Cell Biol.* **152**, 1007-1018.
- Ziera, T., Irlbacher, H., Fromm, A., Latouche, C., Krug, S. M., Fromm, M., Jaisser, F. and Borden, S. A. (2009). Cnksr3 is a direct mineralocorticoid receptor target gene and plays a key role in the regulation of the epithelial sodium channel. *FASEB J.* **23**, 3936-3946.
- Zhang, Y., Chen, K., Tu, Y., Velyvis, A., Yang, Y., Qin, J. and Wu, C. (2002). Assembly of the PINCH-ILK-CH-ILKBP complex precedes and is essential for localization of each component to cell-matrix adhesion sites. *J. Cell Sci.* **115**, 4777-4786.

# Loss of Kindlin-1 Causes Skin Atrophy and Lethal Neonatal Intestinal Epithelial Dysfunction

Siegfried Ussar<sup>1</sup>, Markus Moser<sup>1</sup>, Moritz Widmaier<sup>1</sup>, Emanuel Rognoni<sup>1</sup>, Christian Harrer<sup>1,2</sup>, Orsolya Genzel-Boroviczeny<sup>2</sup>, Reinhard Fässler<sup>1\*</sup>

<sup>1</sup> Department of Molecular Medicine, Max-Planck Institute of Biochemistry, Martinsried, Germany, <sup>2</sup> Division of Neonatology, Perinatal Center, Children's Hospital, Ludwig-Maximilians University, Munich, Germany

## Abstract

Kindler Syndrome (KS), characterized by transient skin blistering followed by abnormal pigmentation, skin atrophy, and skin cancer, is caused by mutations in the FERMT1 gene. Although a few KS patients have been reported to also develop ulcerative colitis (UC), a causal link to the FERMT1 gene mutation is unknown. The FERMT1 gene product belongs to a family of focal adhesion proteins (Kindlin-1, -2, -3) that bind several  $\beta$  integrin cytoplasmic domains. Here, we show that deleting Kindlin-1 in mice gives rise to skin atrophy and an intestinal epithelial dysfunction with similarities to human UC. This intestinal dysfunction results in perinatal lethality and is triggered by defective intestinal epithelial cell integrin activation, leading to detachment of this barrier followed by a destructive inflammatory response.

**Citation:** Ussar S, Moser M, Widmaier M, Rognoni E, Harrer C, et al. (2008) Loss of Kindlin-1 Causes Skin Atrophy and Lethal Neonatal Intestinal Epithelial Dysfunction. *PLoS Genet* 4(12): e1000289. doi:10.1371/journal.pgen.1000289

**Editor:** Veronica van Heyningen, Medical Research Council Human Genetics Unit, United Kingdom

**Received:** May 16, 2008; **Accepted:** November 3, 2008; **Published:** December 5, 2008

**Copyright:** © 2008 Ussar et al. This is an open-access article distributed under the terms of the Creative Commons Attribution License, which permits unrestricted use, distribution, and reproduction in any medium, provided the original author and source are credited.

**Funding:** This work was supported by the BMBF, the Austrian Science Foundation (SFB021) and the Max Planck Society.

**Competing Interests:** The authors have declared that no competing interests exist.

\* E-mail: faessler@biochem.mpg.de

## Introduction

Kindler Syndrome (KS; OMIM:173650) is a rare, recessive genodermatosis caused by mutations in the FERMT1 gene (C20ORF42/KIND1) [1,2]. KS patients suffer from varying skin abnormalities that occur at distinct phases of their life [3]. Skin blisters develop and disappear after birth, followed by skin atrophy, pigmentation defects and finally skin cancer. The severity of the individual symptoms varies extensively among individual patients. FERMT1 mutations are distributed along the entire gene and can give rise to different truncated Kindlin-1 proteins [4]. Interestingly, the different courses of the KS cannot be linked to mutations within specific regions of the FERMT1 gene [3] suggesting that additional environmental and/or genetic factors contribute to the disease course.

Kindlin-1 belongs to a novel family of cytoplasmic adaptor proteins consisting of three members (Kindlin-1-3) [5]. Kindlins are composed of a central FERM (band 4.1, ezrin, radixin, moesin) domain, which is disrupted by a pleckstrin homology (PH) domain. They localize to cell-matrix adhesion sites (also called focal adhesions, FAs) where they regulate integrin function. In line with the role of Kindlins in integrin function, keratinocytes from KS patients and Kindlin-1-depleted keratinocytes display impaired cell adhesion and delayed cell spreading [6,7]. The mechanism how Kindlin-1 regulates integrin function is not understood and controversial. Kindlin-2 (Fermt2) and Kindlin-3 (Fermt3) were shown to bind to the membrane distal NxxY motif of  $\beta 1$  (Itgb1) and  $\beta 3$  (Itgb3) integrin cytoplasmic domains. This binding, in concert with Talin (Tln1) recruitment to the membrane proximal NPxY motif, leads to the activation (inside-out signaling) of  $\beta 1$  and  $\beta 3$  class integrins enabling them to bind to their ligands. Following ligand binding, Kindlin-2 and Kindlin-3 stay in matrix adhesion

sites where they link the ECM to the actin cytoskeleton by recruiting ILK and Migfilin (Fblim1) to FAs (outside-in signaling). Consistent with this adaptor function of Kindlins, keratinocytes from KS patients and keratinocytes depleted of Kindlin-1 display impaired cell adhesion and delayed cell spreading [6,7]. Importantly, however, Kindlin-1 was reported to have different properties than Kindlin-2 and -3, since it was shown to bind like Talin to the proximal NPxY motif of  $\beta 1$  integrin tails [6].

The Kindlins have a specific expression pattern. Kindlin-1 is expressed in epithelial cells, while Kindlin-2 is expressed almost ubiquitously. They are both found at integrin adhesion sites and/or cadherin-based cell-cell junctions. Kindlin-3 is exclusively expressed in hematopoietic cells, where it controls a variety of functions ranging from integrin signaling in platelets [8] to stabilizing the membrane cytoskeleton in mature erythrocytes [9].

Although the FERMT1 gene is expressed in epithelial cells of almost all tissues and organs [5], only abnormalities of the skin and the oral mucosa are associated with KS. Recently it has been reported, however, that some KS patients also develop ulcerative colitis (UC) [4,10,11], which together with Crohn's disease belongs to idiopathic inflammatory bowel disease.

UC usually occurs in the second or third decade of life, although the incidence in pediatric patients is steadily rising [12,13]. UC is restricted to the colon and is characterized by superficial ulcerations of the mucosa. It is currently believed that the mucosal ulcerations are triggered by the release of a complex mixture of inflammatory mediators leading to severe inflammation and subsequent epithelial cell destruction [12]. In line with this paradigm a large number of murine colitis models occur when the innate or adaptive immune response is altered [12]. Genetic linkage analysis in man led to the identification of several susceptibility loci [14,15].

## Author Summary

Mutations in FERMT1, coding for the Kindlin-1 protein, cause Kindler Syndrome in humans, characterized by skin blistering, atrophy, and cancer. Recent reports showed that some Kindler Syndrome patients additionally suffer from ulcerative colitis. However, it is unknown whether this is caused by loss of Kindlin-1 or by unrelated abnormalities such as infections or additional mutations. We ablated the *Fermt1* gene in mice to directly analyze the pathological consequences and the molecular mode of action of Kindlin-1. Kindlin-1-deficient mice develop a severe epidermal atrophy, but lack blisters. All mutant mice die shortly after birth from a dramatic, shear force-induced detachment of intestinal epithelial cells followed by a profound inflammation and organ destruction. The intestinal phenotype is very similar to, although more severe than, the one observed in Kindler Syndrome patients. In vitro studies revealed that impaired integrin activation, and thus impaired adhesion, to the extracellular matrix of the intestinal wall causes intestinal epithelial cell detachment. Therefore, we demonstrate that intestinal epithelial cells require adhesive function of integrins to resist the shear force applied by the stool. Furthermore, we provide evidence that the colitis associated with Kindler Syndrome is caused by a dysfunction of Kindlin-1 rather than by a Kindlin-1-independent event.

In line with the UC disease course most of the KS patients develop their first UC symptoms in adulthood. Interestingly, however, one of them suffered from a severe neonatal form of UC and was diagnosed with a null mutation in the FERMT1 gene after developing trauma-induced skin blistering [10]. Since only a few KS patients were reported to develop intestinal symptoms, it is

currently debated whether UC development in these patients is directly linked to FERMT1 gene mutations or secondarily caused by a microbial infection or an abnormal inflammatory response.

In this study we directly investigated the role of Kindlin-1 in vivo by generating mice carrying a constitutive null mutation in the Kindlin-1 gene. We demonstrate that Kindlin-1 deficient mice develop skin atrophy and a lethal intestinal epithelial dysfunction, resembling the reported UC in KS patients. The intestinal epithelial dysfunction is caused by defective intestinal epithelial integrin activation leading to extensive epithelial detachment followed by a severe inflammatory reaction.

## Results

### Loss of Kindlin-1 Leads to a Lethal Intestinal Epithelial Dysfunction

To unravel the consequences of loss of Kindlin-1 in vivo, we established a mouse strain with a disrupted *Fermt1* gene, leading to a complete loss of Kindlin-1 mRNA and protein (Figure 1A–C). Heterozygous Kindlin-1 mice (*Kindlin-1*<sup>+/-</sup>) had no phenotype and were fertile. Kindlin-1-deficient mice (*Kindlin-1*<sup>-/-</sup>) were born with a normal Mendelian ratio (29.6% +/+; 44.1% +/-; 26.3% -/-; n = 203 at P0) and appeared normal at birth. Two days postnatal (P2), all *Kindlin-1*<sup>-/-</sup> mice analyzed so far were dehydrated (Figure 1D), failed to thrive (Figure 1E) and died between P3–P5 (Figure 1E). Blood glucose and triglyceride levels of *Kindlin-1*<sup>-/-</sup> mice were normal suggesting a normal absorption of nutrients in the small intestine (Figure S1). Their urine showed an increased osmolarity and protein content further pointing to severe dehydration (Figure 1F, Figure S2A and B). Histology of *Kindlin-1*<sup>-/-</sup> kidneys at P3 revealed normal morphology of glomeruli and tubular systems (Figure S2C). Thus, these findings suggest that the peri-natal lethality is not caused by a renal dysfunction.

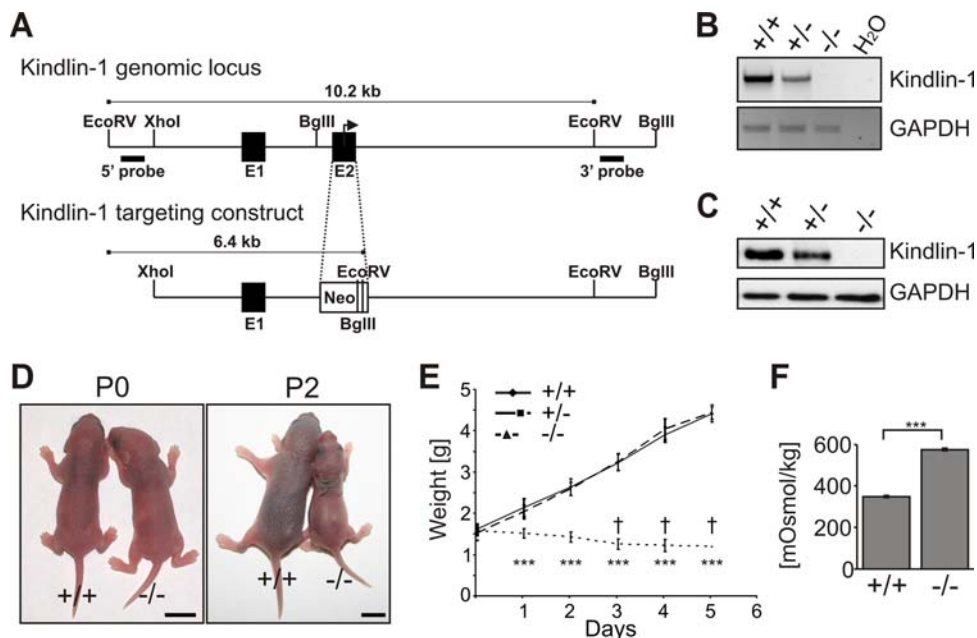


**Figure 1. Loss of Kindlin-1 results in early postnatal lethality.** (A) The *Fermt1* gene was disrupted by replacing the ATG start codon containing exon 2 with a neomycin resistance cassette. (B) Kindlin-1 mRNA levels were determined by PCR from cDNAs derived from P3 kidneys. (C) Loss of Kindlin-1 protein was confirmed by western blotting in colonic IEC lysates. (D) Pictures from newborn (P0) and two day old mice (P2). Scale bars represent 5mm. (E) Weight curve of *Kindlin-1*<sup>-/-</sup> (n = 8) and control littermates (+/+; n = 8; +/-; n = 9) where a † indicates when mice died. \*\*\* indicates a P-value < 0.0001. Error bars show standard deviations. (F) Osmolarity of P2 *Kindlin-1*<sup>-/-</sup> and control (+/+) urine (n = 3 per genotype). Error bars show standard deviations. \*\*\* indicates a P-value < 0.0001. doi:10.1371/journal.pgen.1000289.g001

Next we analyzed whether skin abnormalities caused the perinatal lethality. Although Kindlin-1<sup>-/-</sup> mice showed features of KS like skin atrophy and reduced keratinocyte proliferation (Figure 2A and B), adhesion of basal keratinocytes to the basement membrane (BM) was unaltered (Figure 2A and Figure S3). Histology of backskin sections from different developmental stages revealed normal keratinocyte differentiation (Figure S4), normal development of the epidermal barrier (Figure S5A and Figure 2C and D), and comparable epidermal thickness at E18.5 and P0 (Figure S5B). In line with the progressing proliferation defect quantified by the number of keratinocytes positive for the cell cycle marker Ki67 (Mki67), a reduction of the epidermal thickness was first observed at P1 (Figure S5B). Interestingly despite the mild in vivo phenotype, Kindlin-1<sup>-/-</sup> keratinocytes displayed severe adhesion and spreading defects in culture (Figure S6A and B) further indicating that Kindlin-1<sup>-/-</sup> keratinocytes from mouse and man display similar defects [7].

These results indicated that another defect is responsible for their perinatal lethality. When the stomach and the intestine of Kindlin-1<sup>-/-</sup> mice were examined, they were swollen and filled with milk and gas (Figure 3A) suggesting severe intestinal dysfunction might be the cause of death. The presence of milk in the stomach together with the normal histology of the oral and esophageal mucosa suggested that the lethality is not caused by impaired feeding (Figure S7). At P2, the terminal ileum and colon were shortened and swollen and strictures were evident in the distal colon, which are signs of acute inflammation (Figure 3B). By P3, when the majority of mutant mice were dying, more than 80%

of the colonic epithelium was detached (Figure 3C and Figure S8A–C), became apoptotic (Figure S9) and infiltrated by macrophages, granulocytes (Mac-1; Itgam staining) and T cells (Thy staining) (Figure 3D). The shortened colon was neither a consequence of increased apoptosis, which was only seen in detached epithelium, nor a result of reduced intestinal epithelial cell (IEC) proliferation (Figure S9).

The epithelial detachment and severe inflammation extended into the ileum (Figure 3C). In contrast, the proximal small intestine (duodenum and jejunum) had no evidence of IEC detachment or inflammation (Figure 4). The phenotype of Kindlin-1<sup>-/-</sup> mice for the most part phenocopied the intestinal disease observed in the patient with a complete loss of Kindlin-1 [10].

### Kindlin-1 Is Required for Intestinal Epithelial Cell Adhesion

To define the cell type affected by loss of Kindlin-1 we localized Kindlin-1 in the normal intestine by immunostaining. Similar to the situation in man [4], Kindlin-1 is present throughout the cytoplasm of IECs of the colon and at the basolateral sites of both IECs of the colon (Figure 5A) and the small intestine (Figure 5B). The anti-Kindlin-1 polyclonal antibody produced some weak unspecific background signals in the intestinal mesenchyme of wild type and Kindlin-1<sup>-/-</sup> mice (Figure 5B). Kindlin-2 was exclusively found in cell-cell contacts and did not change its distribution in the absence of Kindlin-1 (Figure 5C and D). Focal adhesion (FA) components such as Talin and Migfilin as well as

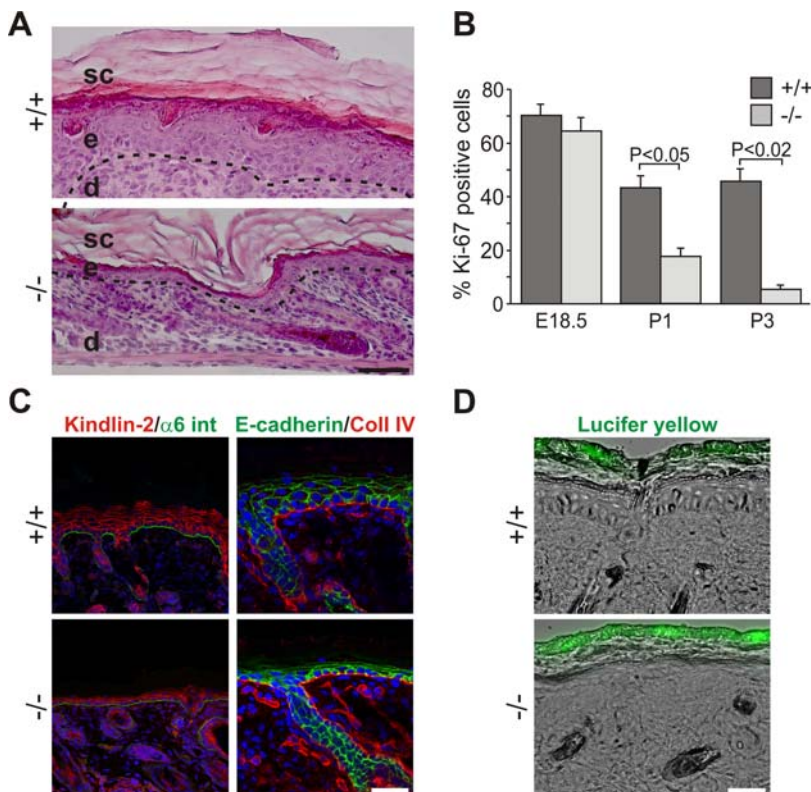


**Figure 2. Atrophy and reduced proliferation in Kindlin-1<sup>-/-</sup> skin.** (A) H&E stainings from P3 backskin show severe epidermal atrophy in Kindlin-1<sup>-/-</sup> mice. The BM is indicated by a dashed line and separates the epidermis (e) from the dermis (d). sc: stratum corneum. Scale bar indicates 50  $\mu$ m. (B) Percentage of Ki67-positive interfollicular keratinocytes, indicating proliferating cells, at different ages (n = 7 per genotype). Error bars show standard errors of the mean. (C) Kindlin-2 (red; co-stained with  $\alpha$ 6 integrin ( $\alpha$ 6 int; in green) and E-cadherin (green, co-stained with Collagen IV (Coll IV) in red) staining of P3 backskin sections. Nuclei are shown in blue. Scale bar indicates 10  $\mu$ m. (D) FITC-Lucifer yellow stain of P3 backskin overlaid with DIC. Lack of lucifer yellow dye penetration shows normal skin barrier in Kindlin-1<sup>-/-</sup> mice. Scale bar indicates 50  $\mu$ m. doi:10.1371/journal.pgen.1000289.g002

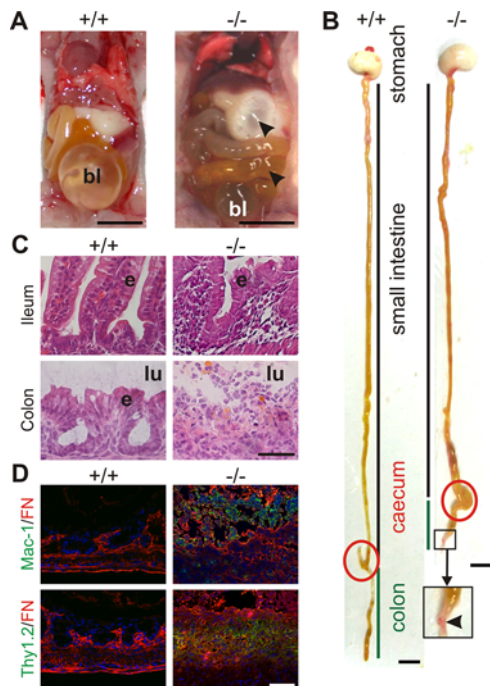


**Figure 3. Severe inflammation and epithelial detachment in *Kindlin-1*<sup>-/-</sup> colon.** (A) Opened abdomen with intestine from P2 mice. Arrowheads indicate air in the stomach and small intestine of *Kindlin-1*<sup>-/-</sup> mice. bl; bladder. Scale bar represents 5 mm. (B) Whole gut preparations from P2 mice. Scale bar represents 5 mm. Arrowhead indicates a stricture in the distal colon. The caecum is highlighted with a red circle and the colon is marked with a green line. (C) H&E staining of P3 colon and ileum. *Kindlin-1*<sup>-/-</sup> mice show complete absence of colonic epithelium (e), exposure of the submucosa to the intestinal lumen (lu) and severe inflammation in colon and ileum. Scale bar represents 50  $\mu$ m. (D) Macrophage and granulocyte infiltrations in P3 colon shown with Mac-1 staining in green. T-cell infiltrates in P3 colon shown with Thy1.2 staining in green. Fibronectin (FN) is stained in red. Scale bar represents 50  $\mu$ m.  
doi:10.1371/journal.pgen.1000289.g003

filamentous actin (F-actin) were expressed normally in *Kindlin-1*<sup>-/-</sup> colonic epithelium that was still adhering to the BM (Figure 5C and data not shown).

Next we determined the time point when mutant mice began developing intestinal abnormalities. At E18.5 the ileum and colon of *Kindlin-1*<sup>-/-</sup> mice were histologically normal and electron microscopy revealed an intact epithelium and basement mem-

brane (BM) (Figure 6A). Shortly after birth (P0), wild-type and *Kindlin-1*<sup>-/-</sup> mice began to suckle and accumulated milk in their stomachs. Within the first hours after birth nursed *Kindlin-1*<sup>-/-</sup> mice contained colostrum in the intestinal lumen and displayed extensive epithelial cell detachment (Figure 6B; see Colon P0) without infiltrating immune cells (Figure 6B and C) in the distal colon. No epithelial detachment occurred when *Kindlin-1*<sup>-/-</sup> mice were delivered by Caesarean section and incubated in a heated and humidified chamber for up to 7 hours (Figure 6B Colon CS) indicating that mechanical stress applied by stool caused IEC detachment. However, inflammatory infiltrates were clearly visible between the detached epithelial cells and the underlying mesenchyme at around 12 hours after birth in fed mice (Figure 6B; see Colon P0.5) and further increased during the following day (Figure 6D). The steady immune cell infiltrate was accompanied with increased expression of the proinflammatory cytokines TNF- $\alpha$  (Tnf) and IL-6 (Il6) and a reduction in goblet cell mucins (Figure 6D and E). The wide range of TNF- $\alpha$  and IL-6 expression levels in *Kindlin-1*<sup>-/-</sup> mice likely reflects the different severities of inflammation at the time tissues were prepared.

Although inflammation extended into the ileum at P2 and P3 (Figure 3B and C), the epithelial cells of the ileum were never detached suggesting that *Kindlin-1*<sup>-/-</sup> mice develop a so-called backwash ileitis caused by stool “washed back” from the colon and subsequently expands proximally.

### Kindlin-1 Controls Activation of Integrins

An important question is how *Kindlin-1* deficiency leads to detachment of intestinal epithelial cells. One potential explanation could be loss of support by a disrupted BM as reported for skin of KS patients [1,2,3]. Moreover, it is known that BM digestion and epithelial detachment in inflammatory bowel disease (IBD) can be triggered via the secretion of MMPs by epithelial and/or infiltrating immune cells [17]. This possibility could be excluded, since *Kindlin-1*<sup>-/-</sup> mice at P1 showed a continuous BM with all major components present, both in areas of the colon where IECs were still adherent as well as in areas where IECs were detached (Figure 7A). Interestingly, also the skin of *Kindlin-1*<sup>-/-</sup> mice showed a normal BM distribution by immunostaining (Figure S3).

An alternative explanation for the IEC detachment could be a reduction of integrin levels, or a dysfunction of integrins, similar to that reported for *Kindlin-3*-deficient platelets [8] and *Kindlin-2*-deficient primitive endoderm [18]. The normal distribution of  $\beta$ 1 integrin (Figure 7B) and the comparable levels of  $\beta$ 1 and  $\alpha$ v (Itgav)

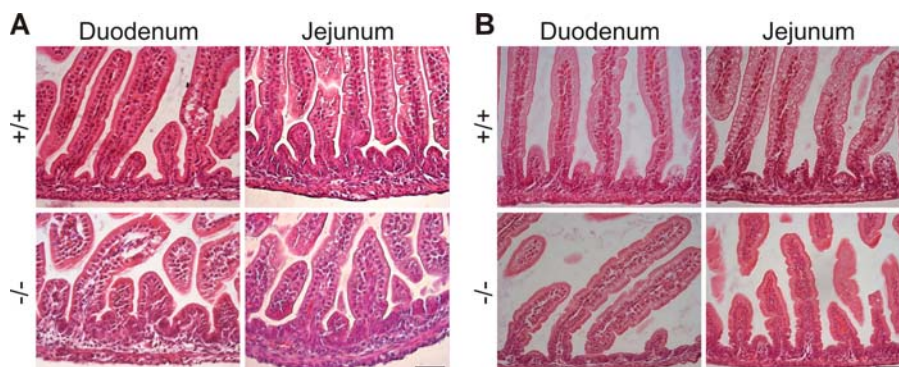


**Figure 4. Normal duodenum and jejunum in *Kindlin-1*<sup>-/-</sup> mice.** H&E stainings of (A) P1 and (B) P3 duodenal and jejunal sections reveal a normal histology of the *Kindlin-1*<sup>-/-</sup> small intestine. Scale bar represents 50  $\mu$ m.  
doi:10.1371/journal.pgen.1000289.g004

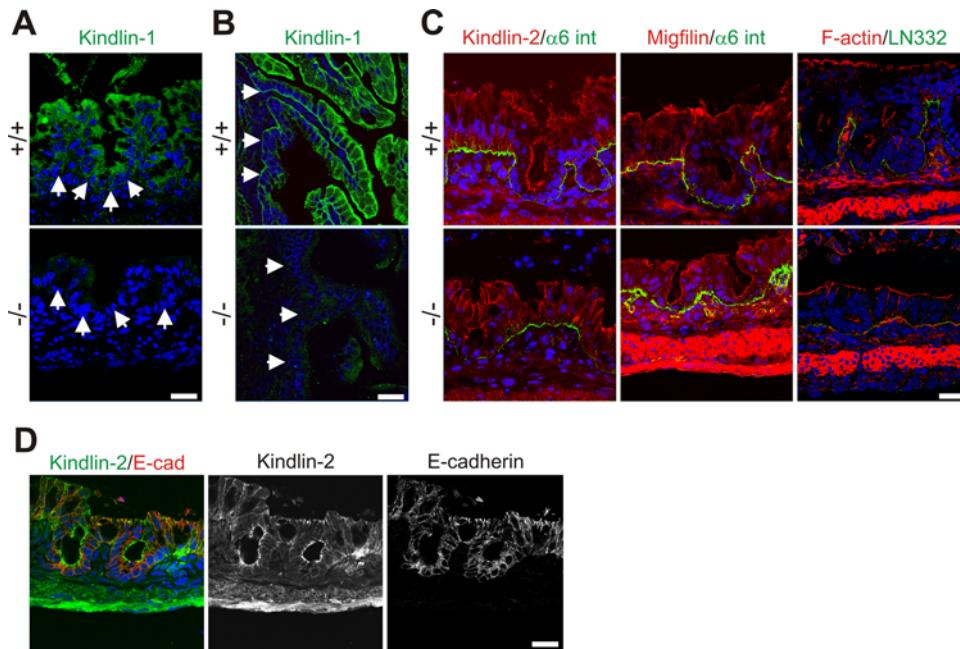


**Figure 5. Kindlin-1 localization in mouse intestine.** (A) Immunofluorescence staining of Kindlin-1 in neonatal colon. Arrows indicate BM. (B) Immunofluorescence staining of P1 ileum for Kindlin-1. Arrows indicate the BM. (C) Immunofluorescence staining of P1 colon for Kindlin-2, Migfilin, F-actin (red),  $\alpha 6$  integrin ( $\alpha 6$  int; green) and Laminin-332 (LN332; green). (D) Immunofluorescence staining of colon for Kindlin-2 (green) and E-cadherin (E-cad; red). All scale bars represent 10  $\mu\text{m}$ . doi:10.1371/journal.pgen.1000289.g005

integrins (Figure 7C and D and data not shown) excluded a defect in expression and/or translocation of integrins to the plasma membrane. Flow cytometry of primary IECs with the monoclonal antibody 9EG7, which recognizes an activation-associated epitope on the  $\beta 1$  integrin subunit, showed significantly reduced binding (Figure 8A) suggesting that loss of Kindlin-1 decreases activation (inside-out signaling) of  $\beta 1$  integrins. Primary keratinocytes from Kindlin-1<sup>-/-</sup> mice also showed normal localization (Figure S10A) and surface expression of  $\beta 1$  integrins (Figure S10B). Interestingly, 9EG7 staining revealed reduced, although not statistically significant, activation of  $\beta 1$  integrins in these cells (Figure S10C).

Since it is difficult to culture and maintain primary murine IECs, we depleted Kindlin-1 in a human colon carcinoma cell line (HT-29) using RNAi (HT-29siKind1; Figure 8B) to show that integrin-mediated cell adhesion and shear stress induced detachment were also perturbed in a colon cell line. HT-29siKind1 cells were unable to adhere to Fibronectin (FN; Fn1) and showed strongly reduced adhesion to Laminin-332 and Collagen IV (Figure 8C) and easily detached from FN upon exposure to low (0.5 dyn/cm<sup>2</sup>) as well as high shear stress (up to 4 dyn/cm<sup>2</sup>; Figure S11). The remaining adhesion to Laminin-332 and Collagen IV is likely mediated by other Laminin- and Collagen-binding receptors on colonic epithelial cells such as  $\alpha 6\beta 4$  integrins (Itga6, Itgb4) and discoidin domain receptors [19,20], which are both known to function independent of Laminin and Collagen binding  $\beta 1$  integrins [21].

These findings indicate that (i) loss of Kindlin-1 impairs integrin activation, which compromises adhesion of colonic epithelial cells, that (ii) Kindlin-2 cannot rescue Kindlin-1 loss in colonic epithelial cells, and that (iii) the residual IEC adhesion to Laminin and Collagen is suspended by shear forces exerted for example, by the feces.

It has been reported that Kindlin-1 associates with the membrane proximal NPxY motif of  $\beta 1$  and  $\beta 3$  integrins [6]. This

observation, however, is in contrast with observations made with Kindlin-2 and -3, both of which bind the membrane distal NxxY motifs of  $\beta 1$  and  $\beta 3$  integrins to trigger their activation [8,18,22]. To explore the mechanism whereby Kindlin-1 induces integrin activation, we performed pull down experiments with recombinant GST-tagged cytoplasmic  $\beta$  integrin tails in IEC and keratinocyte lysates. The results confirmed that Kindlin-1 associated with the cytoplasmic domains of  $\beta 1$  and  $\beta 3$  (Figure 8D). Since substitutions of the tyrosine residues in the proximal NPxY motifs with alanine ( $\beta 1$ Y788A;  $\beta 3$ Y747A) allowed Kindlin-1 binding, while tyrosine to alanine substitutions in the distal NxxY motif of  $\beta 1$  and  $\beta 3$  integrin tails ( $\beta 1$ Y800A;  $\beta 3$ Y759A) abolished Kindlin-1 binding, we conclude that the binding and functional properties are conserved among all Kindlins. This was further confirmed with direct binding assays, which showed that the recombinant His-tagged C-terminal FERM domain of Kindlin-1 (aa 471–677) containing the phosphotyrosine binding (PTB) motif bound GST-tagged  $\beta 1$  but not the Y800A mutated  $\beta 1$  integrin cytoplasmic tail (Figure 8E).

It is well established that Talin can induce activation of integrins, and for a long time it was believed that it is sufficient for the execution of this task. This important function of Talin was discovered by overexpressing Talin or its FERM domain in CHO cells stably expressing the human platelet integrin  $\alpha \text{IIb}\beta 3$  (Itga2b, Itgb3) [23], which shifted the inactive conformation of  $\alpha \text{IIb}\beta 3$  integrin to a high affinity state, as demonstrated by increased binding of the PAC1 antibody recognizing activation associated epitopes on  $\alpha \text{IIb}\beta 3$  integrin (Figure 8F). In contrast to Talin, overexpression of Kindlin-1 failed to trigger activation of  $\alpha \text{IIb}\beta 3$  integrin in these cells (Figure 8F). Interestingly, as described for Kindlin-2 [18,22], overexpression of both the Talin FERM domain and Kindlin-1 doubled PAC1 binding when compared with cells expressing only the Talin FERM domain (Figure 8F). The synergism between Talin and Kindlin-1 depends on a Kindlin-1 and  $\beta$  integrin tail interaction, as a PTB mutant of

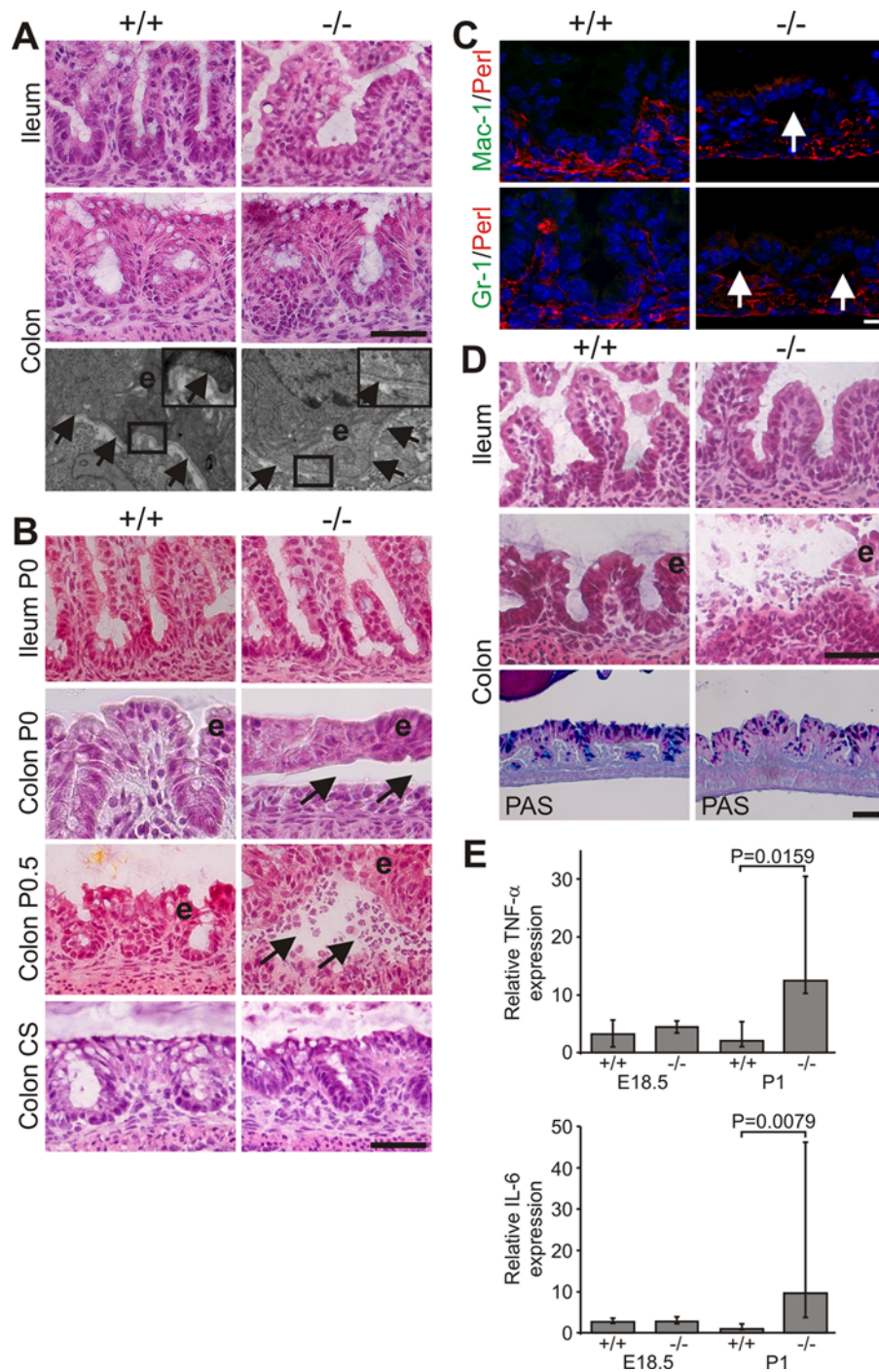


**Figure 6. Progressive epithelial dysfunction in Kindlin-1<sup>-/-</sup> mice.** (A) Normal morphology of IECs and BM at E18.5. Shown are H&E stainings of the ileum and colon and electron microscopy pictures at 12000 $\times$  magnification from the colon. The boxed enlargement shows the BM, e: epithelium. Arrows point to the BM. (B) Colonic IEC (e) detachment at P0 (Colon P0, around 5–6 hours after birth) that becomes infiltrated by immune cells around 12 hours after birth (Colon P0.5). In mice delivered by Caesarean section (CS) and kept unfed for 7 hours no epithelial cell detachment can be observed. Arrows indicate blister. (C) IEC detachment but no macrophage (Mac-1) and granulocyte (GR-1) infiltrations at P0 (Mac-1 and GR-1 in green; Perlecan (Perl) indicating BM in red). Arrows indicate IEC detachment. (D) Immune cell infiltrations in the lumen of the colon and floating epithelial sheets (e) in the colonic lumen at P1. PAS staining shows reduced goblet cell mucins in Kindlin-1<sup>-/-</sup> colonic epithelium. Scale bars in A, B and D represent 50  $\mu$ m and in C 10  $\mu$ m. (E) Median of Real Time PCR results from whole colon mRNA at E18.5 (n=2 per genotype) and P1 (n=5 per genotype) for TNF- $\alpha$  and IL-6. Error bars show range. The P value was determined using a Mann-Whitney test. doi:10.1371/journal.pgen.1000289.g006

Kindlin-1 (QW611/612AA) failed to bind  $\beta$  integrin tails (Figure 8G) and the synergistic effect with Talin was lost (Figure 8F). These findings suggest that Kindlin-1 is not sufficient

for integrin activation but is required for inducing Talin-mediated integrin activation. This notion was confirmed with CHO cells, in which endogenous Kindlin-2 levels were depleted by RNAi

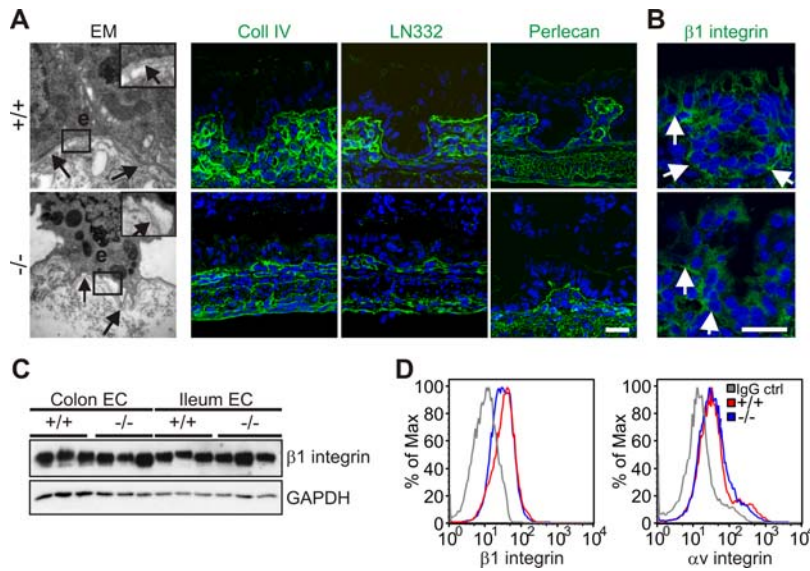


**Figure 7. Normal BM composition and integrin localization in P1 colon.** (A) Electron micrograph at 12000 $\times$  magnification shows detachment of colonic IECs from the BM at P1. Arrows point to the BM. The boxed enlargement shows the BM, e: epithelium. Cryo-sections from the colon of P1 *Kindlin-1*<sup>+/+</sup> and *Kindlin-1*<sup>-/-</sup> mice stained for Collagen IV (Coll IV), Laminin-332 (LN332) and Perlecan. The staining of them shows a normal distribution and localization in *Kindlin-1*<sup>-/-</sup> colon. Scale bar represents 10  $\mu$ m. (B)  $\beta 1$  integrin staining of P1 colon. Arrows indicate the BM. Scale bar represents 10  $\mu$ m. (C) Western blot from IECs for  $\beta 1$  integrin. (D)  $\beta 1$  and  $\alpha v$  integrin FACS profile on primary IECs. doi:10.1371/journal.pgen.1000289.g007

(Figure 8H). Furthermore, overexpressing Talin failed to induce integrin activation in these cells, but expression of Kindlin-1 restored this function (Figure 8I).

These findings show (i) that Kindlin-1 and -2 require Talin for integrin activation, (ii) that Talin requires Kindlins for integrin activation, and (iii) that Kindlin-1 and Kindlin-2 have redundant functions *in vitro* as both Kindlin-1 and -2 are recruited to FAs where they exert similar functions on integrin cytoplasmic tails. However, *in vivo* this is not the case as Kindlin-2 is recruited to cell-cell contacts in IECs and apparently does not compensate Kindlin-1 loss.

## Discussion

In the present study we show that a null mutation in the *Fermt1* gene gives rise to skin atrophy and an acute and fulminant, neonatal intestinal epithelial dysfunction. We demonstrate that the primary defect is a loss of the intestinal epithelial barrier that secondarily leads to inflammatory cell infiltrates and the development of a severe colitis. Furthermore, we show that loss of the intestinal epithelial barrier is caused by a severe adhesion defect of intestinal epithelial cells to the underlying BM, which in turn is caused by the inability of integrins to become activated and to bind BM components. It is possible that in addition to defective integrin activation and epithelial detachment, Kindlin-1 exerts other yet unidentified functions that could contribute to the phenotype in *Kindlin-1*<sup>-/-</sup> mice.

Kindler syndrome (KS) is thought to be primarily a skin disease with a disease course that is characterized by epidermal atrophy and followed by epidermal blistering, pigmentation defects and skin cancer. The complex disease syndrome is difficult to diagnose at the disease onset due to similarities with other forms of skin blistering diseases (also called epidermolysis bullosa; EB) that are caused by mutations in keratin and BM genes [24]. Recent case reports showed that KS may involve more organs than only the skin, as several KS patients also suffer from intestinal symptoms. One patient with a severe form of KS developed a severe postnatal

UC. Interestingly, this patient was diagnosed with a null mutation in the *FERMT1* gene after developing trauma-induced skin blistering [10]. In line with this severe UC case of KS, we found that the null mutation of the *Fermt1* gene in mice also leads to a dramatic and lethal intestinal epithelial dysfunction very shortly after birth. Lethality is usually not seen in KS patients, which is most likely due to the immaturity of the murine intestine at birth, making it more vulnerable to injury [25].

The intestinal epithelial dysfunction of *Kindlin-1*-deficient mice is characterized by flat and superficial ulcerations in the colon, as the epithelium detaches from an intact BM. The defects begin in the rectum and extend along the entire colon finally leading to a severe pancolitis. The ulcerations and epithelial cell detachments are restricted to the colon, although the ileum shows signs of a secondary inflammation at later stages of the disease. *In vitro* studies with primary IECs from *Kindlin-1*<sup>-/-</sup> mice and *Kindlin-1*-depleted HT-29 cells showed that the cell detachment is caused by impaired activation of integrins leading to weak adhesion of IECs to the underlying BM. Mechanistically Kindlin-1 requires direct binding to the  $\beta 1$  and  $\beta 3$  integrin cytoplasmic domains to promote the activation of the two integrin subfamilies. These biochemical and functional properties are conserved among the three members of the Kindlin family. Kindlin-2-mediated binding and activation of  $\beta 1$  and  $\beta 3$  integrins critically support the attachment of endoderm and epiblast cells to the underlying BM in peri-implantation embryos [18], while Kindlin-3 plays a central role for the activation of platelet integrins [8]. The findings of this report also demonstrate that Talin function crucially depends on the activity of Kindlin-1. Depletion of Kindlin-2 (the only Kindlin expressed in CHO cells) completely prevents overexpressed Talin from activating integrins. Re-expression of either Kindlin in *Kindlin-2*-depleted CHO cells, however, recovers the ability of Talin to trigger the activation of integrins. It will be important to next investigate how Kindlins become activated and why Kindlin-2 is unable to take over the function of Kindlin-1 in Kindler Syndrome and *Kindlin-1*-deficient mice.

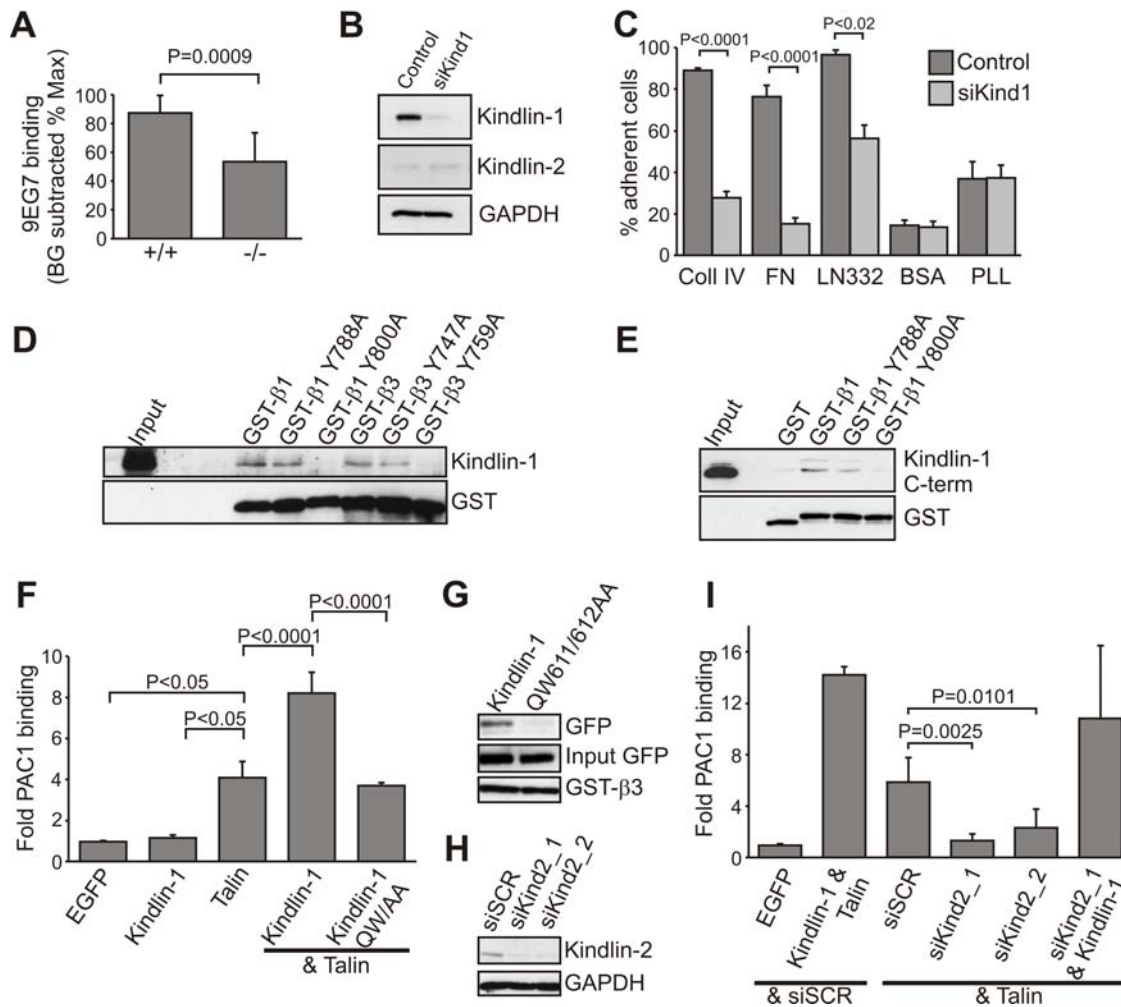


**Figure 8. Kindlin-1 association with  $\beta$  integrins is required for Talin-mediated integrin activation.** (A) Kindlin-1 IECs display significantly reduced 9EG7 binding (active  $\beta 1$  integrin). The 9EG7 binding was quantified by subtracting background (BG) values from mean fluorescence intensity (MFI) values and normalized to total  $\beta 1$  integrin expression ( $n = 8$  mice per genotype). Error bars show standard deviations. (B) Western blot from HT-29 cells expressing a control siRNA or a siRNA directed against hKindlin-1 (siKind1) for Kindlin-1 and Kindlin-2. GAPDH was used to show equal loading. (C) Adhesion assay of control and Kindlin-1-depleted HT-29 cells on the indicated substrates ( $n = 5$ ). Shown are mean values, error bars show standard errors of the mean. Coll IV, Collagen IV; FN, Fibronectin; LN332, Laminin-332; PLL, Poly-L lysine. (D) Kindlin-1 pull-down from IEC lysates using GST-tagged cytoplasmic  $\beta$  integrin tails. (E) Direct interaction of Kindlin-1 with  $\beta 1$  integrin cytoplasmic tails. His-tagged Kindlin-1 C-terminus was coprecipitated with GST-tagged  $\beta 1$  integrin cytoplasmic tails, but not with GST alone or an Y800A mutant form of  $\beta 1$  integrin. (F) Quantification of  $\alpha 11\beta 3$  integrin activation, as measured by activation specific antibody PAC1 in CHO cells using flow cytometry ( $n = 9$ ). Shown are mean values, error bars show standard deviations. (G) Pull-down with GST-tagged cytoplasmic  $\beta 3$  integrin tail from CHO cells transiently transfected with the indicated EGFP-constructs. (H) Western blot of CHO cells 24 hours after transfection with the indicated siRNAs. (siSCR: scrambled; siKind2\_1 and siKind2\_2: Kindlin-2 specific siRNAs) (I) Quantification of  $\alpha 11\beta 3$  integrin activation in CHO cells transfected with the indicated cDNA constructs and/or siRNAs ( $n = 8$ ). Shown are mean values, error bars show standard deviations. doi:10.1371/journal.pgen.1000289.g008

The conclusion that the observed phenotype is triggered by IEC detachment rather than by a primary inflammatory defect in Kindlin-1 deficient mice is based on the observation that epithelial cell detachment always occurred prior to immune cell infiltration. We would therefore, argue that the detachment of IECs resembles an intestinal wound, which secondarily triggers a strong wound healing response leading to immune cell infiltrates and release of a cytokine storm. In line with this hypothesis, epithelial cell detachment and induction of inflammatory reactions can be completely prevented when Kindlin-1 pups are delivered by Caesarian section and subsequently incubated in a humidified and temperature controlled chamber. Mechanical stress applied by the colostrum is likely inducing the detachment of the weakly adhering epithelial cells in the colon. The vast majority of mouse models

reported to develop colitis so far have an abnormal immune system [12,26]. This fact as well as the identification of several susceptibility loci in human patients [14,15] led to the conclusion that defects in the immune system are of central importance for UC development. Severe adhesion defects of IECs leading to a massive wound response may represent an alternative etiology for UC development.

Although adhesion is severely compromised in the colon of Kindlin-1-deficient mice, they are born without skin blisters. This is in line with KS patients, who are also born without skin blisters even when they are delivered by the vaginal route but develop blisters postnatally at trauma prone sites. Interestingly, Kindlin-1 deficient mice did not show defective adhesion of basal keratinocytes to the BM even after application of mechanical stress. The different severity of the adhesion defect in skin and

colon could be reflected by the functional properties of the distinct set of integrins expressed in the two organs and the absence of classical hemidesmosomes in intestinal epithelial cells [27].

Another pronounced skin defect in Kindlin-1-deficient mice as well as KS patients is skin atrophy, which seems to be due to reduced proliferation of interfollicular keratinocytes. This finding raises several questions; first, regarding the mechanism underlying the molecular control of cell proliferation by Kindlin-1. The mechanism is unknown and could result from a diminished cross talk between integrin and growth factor signaling. Second, it is also unclear how a molecular player that supports proliferation is giving rise to cancer at a later stage. It is possible that the localization of Kindlins in different cellular compartments, i.e. cell-matrix adhesion sites, cell-cell adhesion sites and in certain instances in the nucleus, equips them with different functions that become evident at different time points in life.

Kindlin-1 and -2 are co-expressed in epidermal cells as well as epithelial cells of the colon. Interestingly, we found that Kindlin-2 cannot compensate Kindlin-1 function in vivo, neither in the colon nor in skin. Since Kindlin-2 normally localizes to cell-cell adhesions in both cell types and does not translocate to integrin adhesion sites in mutant intestinal and epidermal epithelial cells, it is unable to compensate for the loss of Kindlin-1, although both Kindlins are capable of performing the same tasks at the integrin tails *ex vivo* and in vitro [27]. Hence, a therapeutic strategy to reroute some of the Kindlin-2 from cell-cell to the integrin adhesion sites may represent a promising approach to prevent ulceration in KS patients with severe UC.

## Materials and Methods

### Mouse Strains

The Kindlin-1<sup>-/-</sup> mice were obtained by replacing the ATG-containing exon 2 with a neomycin resistance cassette (detailed information on the cloning of the targeting construct can be obtained from [Faessler@biochem.mpg.de](mailto:Faessler@biochem.mpg.de)). The construct was electroporated into R1 embryonic stem (ES) cells (passage 15) and homologous recombination was verified with southern blots. Genomic DNA was digested with EcoRV, blotted and then hybridized with a 5' probe or digested with BglII, blotted and hybridized with a 3' probe (Figure 1A). Targeted ES cells were injected into blastocysts and transferred into foster mice. Mice were housed in a special pathogen free mouse facility. All animal experiments have been approved by the local authorities.

### Histology, Immunohistochemistry, and Immunofluorescence Stainings

For H&E stainings intestinal segments were either PFA fixed and embedded in paraffin, or frozen on dry-ice in cryo-matrix (Thermo). Immunohistochemistry of paraffin embedded sections was carried out as previously described [5]. Sections of 8 μm thickness were prepared and stained following routine protocols. Cryo sections were fixed in 4% PFA/PBS except for the Kindlin-1 staining where sections were fixed with 1:1 methanol/acetone at -20°C. Subsequently tissue sections were blocked with 3% BSA/PBS, incubated with primary antibodies in a humidity chamber over night at 4°C, with fluorescently labeled secondary antibodies for 1 h at RT and finally mounted in Elvanol. Pictures were taken with a Leica DMIRE2 confocal microscope with a 100× or 63× NA 1.4 oil objective.

### GST-Pull Downs

Recombinant GST-β1, β1Y788A, β1Y800A, β3, β3Y747A, β3Y759A cytoplasmic tails were expressed and purified from *E.coli*

under non denaturing conditions. 5 μg of recombinant tails were incubated with 500 μg IEC lysate (in 50 mM Tris pH 7.4, 150 mM NaCl, 1 mM EDTA, 1% Triton-X-100) overnight. GST-constructs were precipitated with glutathione beads (Novagen). Subsequent western blots were probed for Kindlin-1 and GST.

### Antibodies

A polyclonal peptide antibody against Kindlin-1 was raised against the peptide YFKNKELEQGEPIEK as previously described [5].

The following antibodies were used at the given concentration indicated for western blot (W), immunoprecipitation (IP), immunofluorescence (IF), immunohistochemistry (IHC): Kindlin-1 (W: 1:5000, IF cells: 1:200, IF tissue: 1:1000), Kindlin-2 (W: 1:1000, IF cells: 1:200, IF tissue: 1:200), E-cadherin (Cdh1; Zymed, W: 1:5000), Migfilin (W: 1:5000, IF cells: 1:100, IF tissue: 1:100), GAPDH (Chemicon; W: 1:10000), phalloidin Tritc (Sigma; IF cells: 1:800, IF tissue: 1:800), Mac-1 (EuroBioscience; IF tissue: 1:100), GR-1 (Ly6g; eBioscience; IF tissue: 1:100), Thy1.2 (PharMingen; IF tissue: 1:100), GST (Novagen; W: 1:10000), His (CellSignaling; W: 1:1000), PAC1 (BD; FACS: 1:100), α6 integrin (Itga6; PharMingen; IF tissue: 1:100), CollagenIV (a gift from Dr. Rupert Timpl; IF tissue: 1:100), Laminin-332 (a gift from Dr. Monique Aumelley; IF tissue: 1:200), Perlecan (Hspq2; a gift from Dr. Rupert Timpl; IF tissue: 1:100), β1 integrin (Chemicon; WB: 1:3000, IF tissue: 1:600), 9EG7 (PharMingen; FACS: 1:100), EGFP (Abcam; WB: 1:10000), β1 integrin (PharMingen; FACS: 1:200), αv integrin (PharMingen; FACS: 1:200), Keratin10 (Krt10; Covance; IHC: 1:600), Keratin14 (Krt14; Covance; IHC: 1:600), Loricrin (Lor; Covance; IHC: 1:500) Ki67 (Dianova; IHC: 1:50), cCaspase3 (CellSignaling, IHC: 1:100).

### Caesarean Section

Pregnant mice were sacrificed by cervical dislocation when embryos were at E18.5–E19 of gestation. The uterus was removed and cut open. Embryos were taken out and the umbilical cord was cut. Mice were subsequently dried and kept in an incubator at 37°C and high humidity.

### Real Time PCR

Total RNA from whole colons was extracted with a PureLink Micro to Midi RNA extraction kit (Invitrogen) following the manufacturers instructions. cDNA was prepared using the iScript cDNA Synthesis Kit (Biorad). Real Time PCR using a Sybr Green ready mix (Biorad) was performed in an iCycler (Biorad). Each sample was measured in triplicates and values were normalized to GAPDH. Following primers were used; TNFα fwd: AAAATTC-GAGTGACAAGCCTGTAGC, TNFα rev: GTGGGTGAG-GAGCACGTAG. IL-6 fwd: CTATACCACTTCACAAGTCG-GAGG IL-6 rev: TGCACAACCTCTTTCTCATTTCC. RT-PCR for Kindlin-1 and GAPDH was performed as previously described [5].

### Isolation of IECs

Neonatal mouse intestine was removed and flushed with 1 ml PBS. The intestine was longitudinally cut open, rinsed with PBS and incubated for 40 min. in IEC isolation buffer (130 mM NaCl, 10 mM EDTA, 10 mM Hepes pH 7.4, 10% FCS and 1 mM DTT) at 37°C on a rotor. The epithelium was shaken off and pelleted by centrifugation at 2000rpm for 5 min. For WB analysis cells were washed once with PBS and subsequently lysed. For flow cytometry cells were washed once with PBS and trypsinized with

2× trypsin (GIBCO) for 10 min. at 37°C. Trypsin was inactivated with DMEM containing 10%FCS. A single cell suspension was prepared by passing cells through a cell strainer (BD).

### Isolation of Keratinocytes

Primary keratinocytes were isolated from P3 mice as described previously [28]. Cells were cultured on a mixture of Coll (Cohesion) and 10 µg/ml FN (Invitrogen) coated plastic dishes in keratinocyte growth medium containing 8% chelated FCS (Invitrogen) and 45 µM Ca<sup>2+</sup>.

### Flow Cytometry

IEC's and keratinocytes were stained with 9EG7 antibody in Tris buffered saline [29]. For the PAC1 binding assay CHO cells were stained for 40 min. at RT as described previously [23]. Cells were gated for viability by excluding propidium iodide-positive cells. CHO cells transfected with EGFP-tagged constructs were additionally gated for highly EGFP-positive cells. Measurements were performed with a FACS Calibur (BD) and data evaluation was done with FlowJo software.

### Constructs

The EGFP-Kindlin-1 expression plasmid was previously described [5]. The cDNA encoding His-Kindin-1 C-terminus (aa 471–677) was amplified by PCR and cloned into the pQE-70 vector (Qiagen). The Kindlin-1 PTB mutation QW611/612AA was introduced with a site directed mutagenesis kit (Stratagene) following the manufacturers recommendations. All EGFP constructs were cloned into the pEGFP-C1 vector (Clontech) and subsequently sequenced. EGFP-Talin head was previously described [8].

### Cell Culture

CHO and HT-29 cells were maintained in DMEM containing penicillin/streptomycin, non-essential amino-acids and 10% or 20% FCS, respectively (GIBCO). Cells were transfected with 2 µg of each DNA in six well plates using Lipofectamine 2000 following the manufacturers' instructions (Invitrogen).

### RNAi

To deplete Kindlin-1 constitutively from HT-29 cells, an shDNA corresponding to the cDNA sequence GTAAGT CCTGGTTTATACA of hKindlin-1 and a control cDNA with the sequence AGCAGTGCATGTATGCTTC were cloned into the pSuperRetro vector (OligoEngine). Viral particles were prepared as described previously [30]. HT-29 cells were infected and subsequently selected with 2mg/l puromycin. Transient knockdown of Kindlin-2 from CHO cells was achieved by transfection of the siRNAs; Kind2\_1: GCCUCAAGCUCUUCUUGAUdTdT and Kind2\_2: CUCUGGACGGGAUAAGGAUdTdT, and a control siRNA (purchased from Sigma) using Lipofectamine 2000 (Invitrogen), following the manufacturers instructions. Cells were harvested and assayed 24 hours after transfection.

### Adhesion Assay

The adhesion assays were performed as previously described [29], using 40000 cells per well in serum free DMEM (HT-29) or MEM (primary keratinocytes).

### Osmolarity

Osmolarity was measured from 50 µl urine using an Osmomat 030 from Gonotec.

### X-Gal Barrier Assay

Embryonic skin barrier formation was determined as previously described [31].

### Shear Stress Assay

Slides with a 1 µm diameter (ibidi BioDiagnostics) were coated overnight with 5 µg/ml FN and then blocked with 1% BSA. 100.000 cells were seeded onto the slides and incubated for 2.5 hours in a cell culture incubator. Cells were subsequently exposed to increasing amounts of shear force in two minute intervals (as indicated in the Figure S11) and pictures were taken every second.

### Co-Immunoprecipitation

CHO cells were transiently transfected with the indicated EGFP constructs. Approximately 1mg of protein lysate was immunoprecipitated using the µMACS Epitope Tag Protein Isolation Kit for EGFP tags (Miltenyi Biotec) following the manufacturers instructions.

### Electron Microscopy

Electron microscopy was performed as previously described [29].

### Statistical Analysis

Analyses were performed with GraphPad Prism. If not mentioned otherwise in the figure legends, Gaussian distribution of datasets was determined by a D'Agostino & Pearson omnibus normality test. If samples were not Gaussian distributed a Mann-Whitney test was performed. Gaussian distributed samples were either compared with a one way ANOVA and a Tukey's multiple comparison post test or an unpaired two-tailed t-test.

### Supporting Information

**Figure S1** Normal triglyceride and glucose levels in the blood of P3 Kindlin-1<sup>-/-</sup> mice. Triglyceride (n=7 per genotype) and glucose (n=5 per genotype) levels from total blood at P3. The differences are statistically insignificant. Shown are mean values, error bars show standard deviations.

Found at: doi:10.1371/journal.pgen.1000289.s001 (0.5 MB TIF)

**Figure S2** Normal kidney morphology in Kindlin-1<sup>-/-</sup> mice. (A) Coomassie stained gel of 10 µl urine from P2 and P3 control and Kindlin-1<sup>-/-</sup> mice. (B) Quantification of total protein in urine from Kindlin-1<sup>+/+</sup>, Kindlin-1<sup>+/-</sup> and Kindlin-1<sup>-/-</sup> mice at P1 (n=14/7/6) and P3 (n=20/20/9). Error bars show standard deviation. (C) H&E staining of P3 Kindlin-1<sup>+/+</sup> and Kindlin-1<sup>-/-</sup> kidneys. Kindlin-1<sup>-/-</sup> kidneys do not show altered glomeruli and collecting duct morphology. Scale bar represents 200 µm. Enlargements show glomeruli (A1, A3) and collecting ducts (A2, A4). Scale bar represents 50 µm.

Found at: doi:10.1371/journal.pgen.1000289.s002 (8.6 MB TIF)

**Figure S3** Normal BM composition and deposition in P3 Kindlin-1<sup>-/-</sup> backskin. P3 backskin of wild type and Kindlin-1<sup>-/-</sup> mice was stained for the BM components Laminin-332 (LN332; red), Collagen IV (Coll IV; red) and Fibronectin (FN; red) and co-stained with α6 or β4 integrin marking (green) the basal site of basal keratinocytes. The stainings reveal no differences in BM deposition and composition or α6 and or β4 integrin localization between control and Kindlin-1<sup>-/-</sup> littermates. Scale bar indicates 30 µm.

Found at: doi:10.1371/journal.pgen.1000289.s003 (9.8 MB TIF)

**Figure S4** Normal skin differentiation. P3 backskin of control and Kindlin-1<sup>-/-</sup> mice was stained for epidermal differentiation markers Keratin14, Keratin10 and Loricrin (red) and co-stained with  $\alpha 6$  integrin (green) to mark basal keratinocytes. The stainings show no difference in the differentiation pattern of Kindlin-1<sup>-/-</sup> keratinocytes. Scale bar indicates 10  $\mu$ m.

Found at: doi:10.1371/journal.pgen.1000289.s004 (8.4 MB TIF)

**Figure S5** Normal skin development. (A) Normal X-Gal staining in E17 Kindlin-1<sup>-/-</sup> embryos indicating normal barrier formation during development. Scale bar indicates 5 mm. (B) H&E staining of back skin from control and Kindlin-1<sup>-/-</sup> littermates of different age. In Kindlin-1<sup>-/-</sup> mice the epidermal (e) thickness at E18.5 and P0 is normal but clear epidermal atrophy is seen at P1. Scale bar indicates 50  $\mu$ m. (d): dermis.

Found at: doi:10.1371/journal.pgen.1000289.s005 (8.5 MB TIF)

**Figure S6** Altered adhesion and spreading of Kindlin-1<sup>-/-</sup> keratinocytes. (A) Adhesion assay of control and Kindlin-1<sup>-/-</sup> keratinocytes on LN332, Laminin-332; Coll IV, Collagen IV; FN, Fibronectin; PLL, Poly-L lysine (n = 3). Shown are mean values, error bars show standard error of the mean. (B) Cell area measured upon spreading on 5  $\mu$ g/ml Fibronectin at the indicated time-points using MetaMorph software (n = 30 cells per genotype from 3 independent experiments). Shown are mean values, error bars show standard deviation (\*\*\*) p < 0.0001.

Found at: doi:10.1371/journal.pgen.1000289.s006 (0.8 MB TIF)

**Figure S7** Oral and oesophageal mucosa in Kindlin-1<sup>-/-</sup> mice. Histology of the oral mucosa and the oesophagus of P3 Kindlin-1<sup>+/+</sup> and Kindlin-1<sup>-/-</sup> mice did not reveal an abnormal morphology. Scale bar represents 50  $\mu$ m.

Found at: doi:10.1371/journal.pgen.1000289.s007 (8.1 MB TIF)

**Figure S8** Progressive epithelial loss in Kindlin-1<sup>-/-</sup> colons. (A) Quantification of the extent of intact colonic epithelium at P1 and P3 (n = 3 per genotype and age). Error bars show range. (B) Overview of an H&E picture of a P3 control and Kindlin-1<sup>-/-</sup> colon. The Kindlin-1<sup>-/-</sup> colon shows a complete absence of colonic epithelium (black arrowheads), while the epithelium in the caecum is still present (white arrowheads). Scale bars show 500  $\mu$ m. (C) Magnifications of the boxed areas shown in B.

Found at: doi:10.1371/journal.pgen.1000289.s008 (7.7 MB TIF)

**Figure S9** Normal IEC proliferation but detachment induced apoptosis. P1 colons from wild type and Kindlin-1<sup>-/-</sup> mice were

DAB stained for cleaved Caspase-3 to determine apoptosis and Ki67 stained to show proliferating IECs. Apoptosis occurs in detached epithelium of Kindlin-1<sup>-/-</sup> mice. In areas of still adhering epithelium the number of proliferating IECs is similar between wild type and Kindlin-1<sup>-/-</sup> mice. Scale bar indicates 50  $\mu$ m.

Found at: doi:10.1371/journal.pgen.1000289.s009 (8.7 MB TIF)

**Figure S10**  $\beta 1$  integrin activation in Kindlin-1<sup>-/-</sup> keratinocytes. (A) Immunofluorescence staining for  $\beta 1$  integrin (green) and Laminin-332 (LN332; red) from P3 backskin shows normal localization of  $\beta 1$  integrin in Kindlin-1<sup>-/-</sup> backskin. (B) FACS quantification of  $\beta 1$  integrin expression of freshly isolated control and Kindlin-1<sup>-/-</sup> keratinocytes at P2 shows unaltered  $\beta 1$  integrin expression on basal keratinocytes. Error bars show range (n = 4) (C) 9EG7 FACS quantification of these keratinocytes shows no significant reduction in  $\beta 1$  integrin activation. Error bars show range (n = 4).

Found at: doi:10.1371/journal.pgen.1000289.s010 (8.0 MB TIF)

**Figure S11** Shear induced detachment of Kindlin-1 depleted HT-29 cells. Control and Kindlin-1 depleted HT-29 (siKind1) cells were plated on Fibronectin-coated flow chamber slides and exposed to increasing shear forces as indicated in the figure. Control cells did not detach from the matrix while Kindlin-1 depleted cells were unable to resist low or high shear forces (compare lane 1 (0dyn/cm<sup>2</sup>) with lane 2 (0,5dyn/cm<sup>2</sup>)). Scale bar indicates 50  $\mu$ m.

Found at: doi:10.1371/journal.pgen.1000289.s011 (9.0 MB TIF)

## Acknowledgements

We would like to thank Wilhelm Bloch for electron microscopy, Reinhart Kluge for blood parameter measurements, Klaus-Peter Janssen for IL-6 and TNF $\alpha$  primers, Julia Schlehe, Sara Wickström, Mercedes Costell, Ralph Boettcher, Anika Lange, Ambra Pozzi, and Roy Zent for critical reading of the manuscript and Simone Bach and Melanie Ried for excellent technical assistance.

## Author Contributions

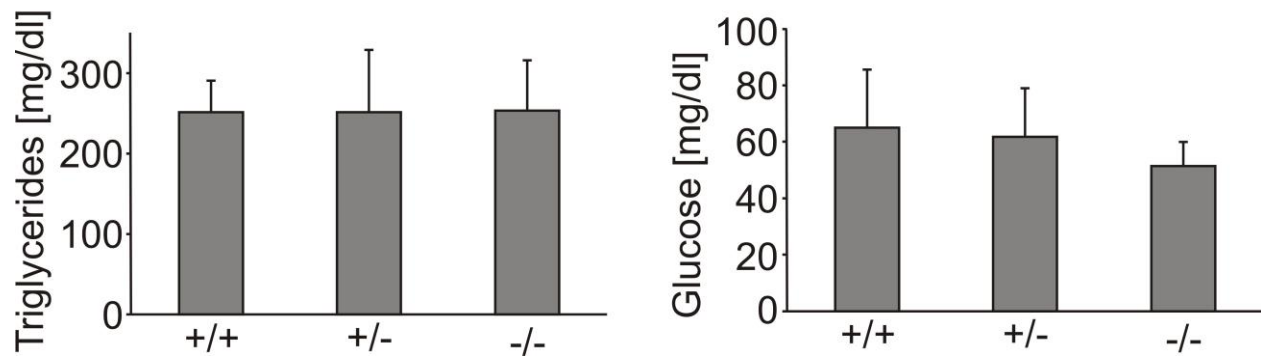
Conceived and designed the experiments: SU MM RF. Performed the experiments: SU MW ER CH. Analyzed the data: SU RF. Contributed reagents/materials/analysis tools: OGB. Wrote the paper: SU RF.

## References

- Siegel DH, Ashton GH, Penagos HG, Lee JV, Feiler HS, et al. (2003) Loss of kindlin-1, a human homolog of the *Caenorhabditis elegans* actin-extracellular-matrix linker protein UNC-112, causes Kindler syndrome. *Am J Hum Genet* 73: 174–187.
- Jobard F, Bouadjar B, Caux F, Hadj-Rabia S, Has C, et al. (2003) Identification of mutations in a new gene encoding a FERM family protein with a pleckstrin homology domain in Kindler syndrome. *Hum Mol Genet* 12: 925–935.
- Lai-Cheong JE, Liu L, Sethuraman G, Kumar R, Sharma VK, et al. (2007) Five new homozygous mutations in the KIND1 gene in Kindler syndrome. *J Invest Dermatol* 127: 2268–2270.
- Kern JS, Herz C, Haan E, Moore D, Nottelmann S, et al. (2007) Chronic colitis due to an epithelial barrier defect: the role of kindlin-1 isoforms. *J Pathol* 213: 462–470.
- Ussar S, Wang HV, Linder S, Fassler R, Moser M (2006) The Kindlins: subcellular localization and expression during murine development. *Exp Cell Res* 312: 3142–3151.
- Kloeker S, Major MB, Calderwood DA, Ginsberg MH, Jones DA, et al. (2004) The Kindler syndrome protein is regulated by transforming growth factor-beta and involved in integrin-mediated adhesion. *J Biol Chem* 279: 6824–6833.
- Herz C, Aumailley M, Schulte C, Schlotzer-Schrehardt U, Bruckner-Tuderman L, et al. (2006) Kindlin-1 is a phosphoprotein involved in regulation of polarity, proliferation, and motility of epidermal keratinocytes. *J Biol Chem* 281: 36082–36090.
- Moser M, Nieswandt B, Ussar S, Pozgajova M, Fassler R (2008) Kindlin-3 is essential for integrin activation and platelet aggregation. *Nat Med* 14: 325–330.
- Kruger M, Moser M, Ussar S, Thievsen I, Lubert CA, et al. (2008) SILAC mouse for quantitative proteomics uncovers kindlin-3 as an essential factor for red blood cell function. *Cell* 134: 353–364.
- Sadler E, Klausegger A, Muss W, Deinsberger U, Pohla-Gubo G, et al. (2006) Novel KIND1 gene mutation in Kindler syndrome with severe gastrointestinal tract involvement. *Arch Dermatol* 142: 1619–1624.
- Freeman EB, Kogmeier J, Martinez AE, Mellerio JE, Haynes L, et al. (2008) Gastrointestinal complications of epidermolysis bullosa in children. *Br J Dermatol*.
- Xavier RJ, Podolsky DK (2007) Unravelling the pathogenesis of inflammatory bowel disease. *Nature* 448: 427–434.
- Podolsky DK (2002) Inflammatory bowel disease. *N Engl J Med* 347: 417–429.
- Fisher SA, Tremelling M, Anderson CA, Gwilliam R, Bumpstead S, et al. (2008) Genetic determinants of ulcerative colitis include the ECM1 locus and five loci implicated in Crohn's disease. *Nat Genet* 40: 710–712.
- Franke A, Balschun T, Karlsen TH, Hedderich J, May S, et al. (2008) Replication of signals from recent studies of Crohn's disease identifies previously unknown disease loci for ulcerative colitis. *Nat Genet* 40: 713–715.
- Mudter J, Neurath MF (2007) Il-6 signaling in inflammatory bowel disease: pathophysiological role and clinical relevance. *Inflamm Bowel Dis* 13: 1016–1023.

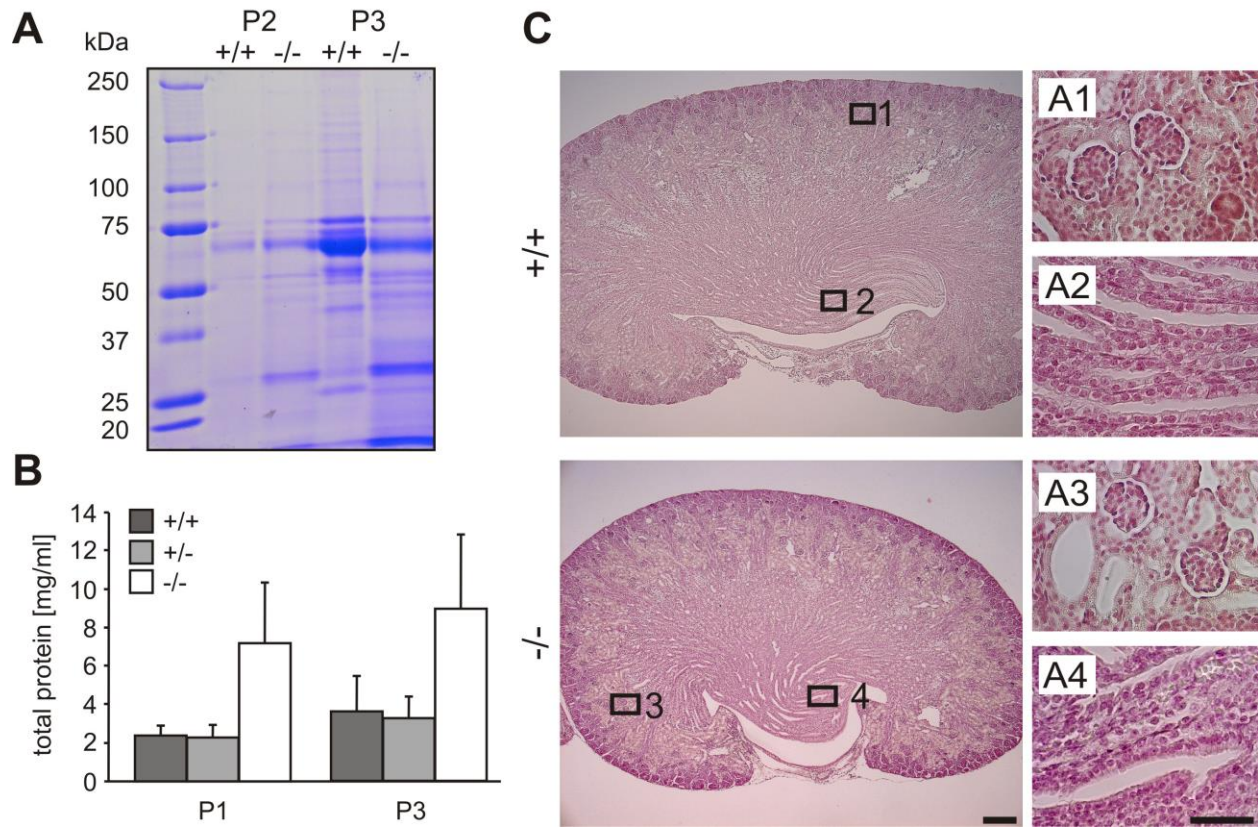
17. Medina C, Radomski MW (2006) Role of matrix metalloproteinases in intestinal inflammation. *J Pharmacol Exp Ther* 318: 933–938.
18. Montanez E, Ussar S, Schifferer M, Bosl M, Zent R, et al. (2008) Kindlin-2 controls bidirectional signaling of integrins. *Genes Dev* 22: 1325–1330.
19. Vogel W, Gish GD, Alves F, Pawson T (1997) The discoidin domain receptor tyrosine kinases are activated by collagen. *Mol Cell* 1: 13–23.
20. Alves F, Vogel W, Mossie K, Millauer B, Hofler H, et al. (1995) Distinct structural characteristics of discoidin I subfamily receptor tyrosine kinases and complementary expression in human cancer. *Oncogene* 10: 609–618.
21. Vogel W, Brakebusch C, Fassler R, Alves F, Ruggiero F, et al. (2000) Discoidin domain receptor 1 is activated independently of beta(1) integrin. *J Biol Chem* 275: 5779–5784.
22. Ma YQ, Qin J, Wu C, Plow EF (2008) Kindlin-2 (Mig-2): a co-activator of beta3 integrins. *J Cell Biol* 181: 439–446.
23. O'Toole TE, Katagiri Y, Faull RJ, Peter K, Tamura R, et al. (1994) Integrin cytoplasmic domains mediate inside-out signal transduction. *J Cell Biol* 124: 1047–1059.
24. Aumailley M, Has C, Tunggal L, Bruckner-Tuderman L (2006) Molecular basis of inherited skin-blistering disorders, and therapeutic implications. *Expert Rev Mol Med* 8: 1–21.
25. Hauck AL, Swanson KS, Kenis PJ, Leckband DE, Gaskins HR, et al. (2005) Twists and turns in the development and maintenance of the mammalian small intestine epithelium. *Birth Defects Res C Embryo Today* 75: 58–71.
26. Kang SS, Bloom SM, Norian LA, Geske MJ, Flavell RA, et al. (2008) An antibiotic-responsive mouse model of fulminant ulcerative colitis. *PLoS Med* 5: e41.
27. Fontao L, Stutzmann J, Gendry P, Launay JF (1999) Regulation of the type II hemidesmosomal plaque assembly in intestinal epithelial cells. *Exp Cell Res* 250: 298–312.
28. Romero MR, Carroll JM, Watt FM (1999) Analysis of cultured keratinocytes from a transgenic mouse model of psoriasis: effects of suprabasal integrin expression on keratinocyte adhesion, proliferation and terminal differentiation. *Exp Dermatol* 8: 53–67.
29. Czuchra A, Meyer H, Legate KR, Brakebusch C, Fassler R (2006) Genetic analysis of beta1 integrin “activation motifs” in mice. *J Cell Biol* 174: 889–899.
30. Massoumi R, Chmielarska K, Hennecke K, Pfeifer A, Fassler R (2006) Cylid inhibits tumor cell proliferation by blocking Bcl-3-dependent NF-kappaB signaling. *Cell* 125: 665–677.
31. Patel S, Xi ZF, Seo EY, McGaughey D, Segre JA (2006) Klf4 and corticosteroids activate an overlapping set of transcriptional targets to accelerate in utero epidermal barrier acquisition. *Proc Natl Acad Sci U S A* 103: 18668–18673.

**Figure S1**



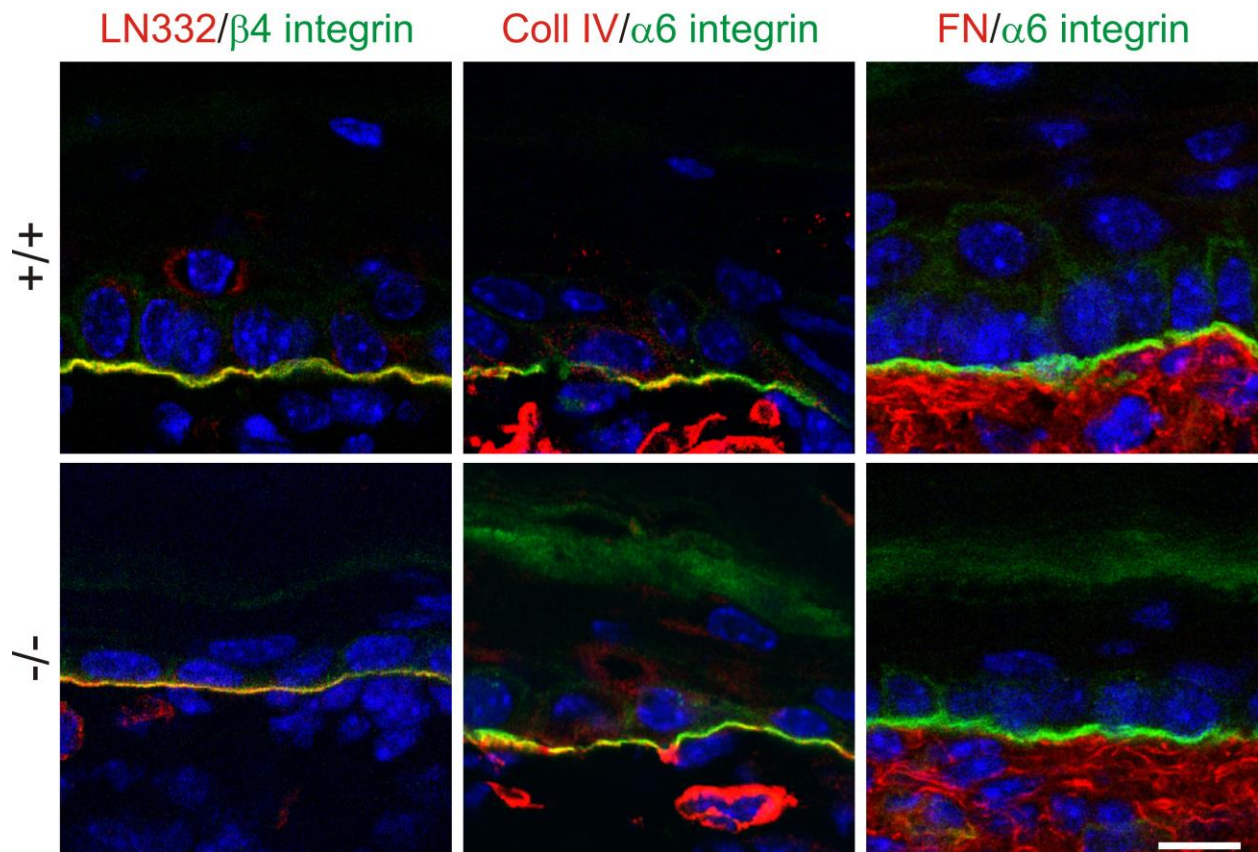
Normal triglyceride and glucose levels in the blood of P3 Kindlin-1<sup>-/-</sup> mice. Triglyceride (n = 7 per genotype) and glucose (n = 5 per genotype) levels from total blood at P3. The differences are statistically insignificant. Shown are mean values, error bars show standard deviations.

**Figure S2**



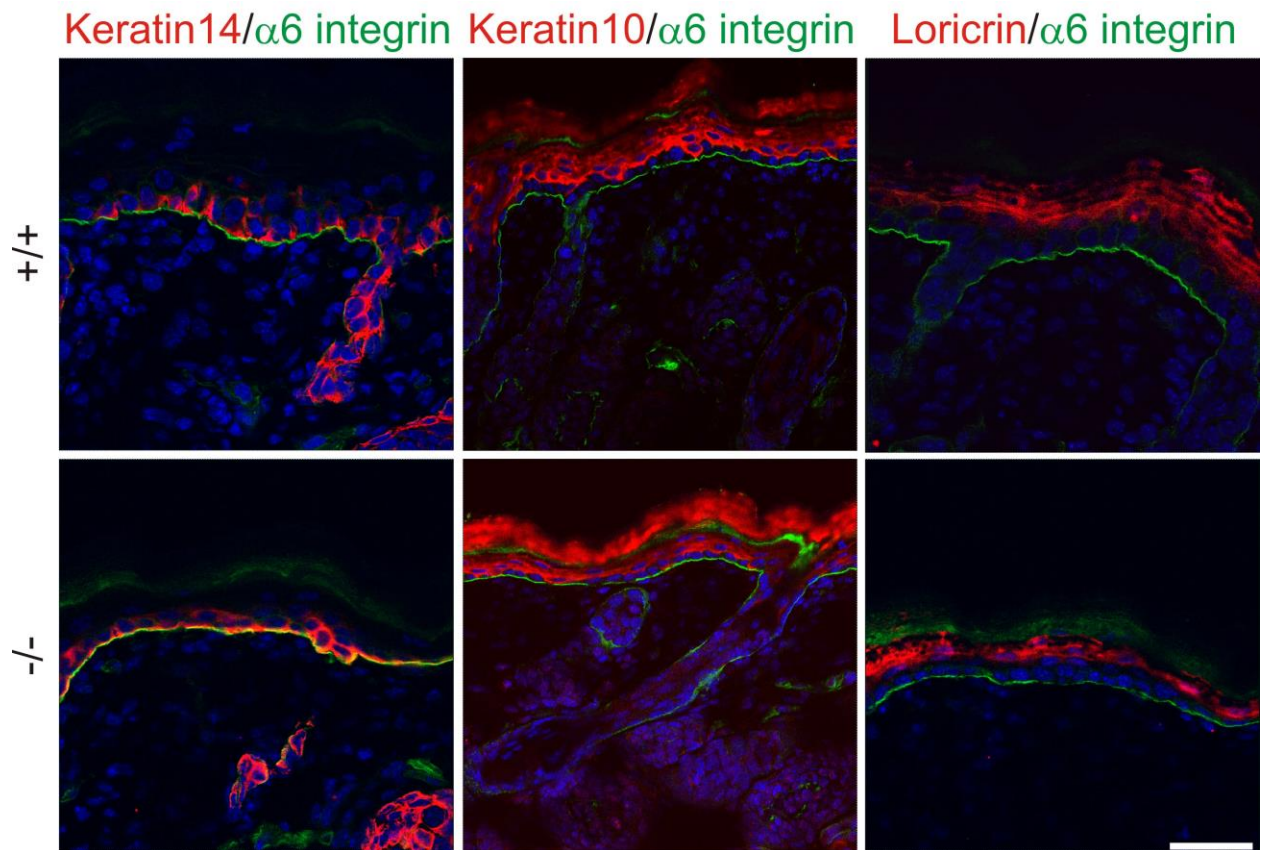
Normal kidney morphology in *Kindlin-1*<sup>-/-</sup> mice. (A) Coomassie stained gel of 10  $\mu$ l urine from P2 and P3 control and *Kindlin-1*<sup>-/-</sup> mice. (B) Quantification of total protein in urine from *Kindlin-1*<sup>+/+</sup>, *Kindlin-1*<sup>+/-</sup> and *Kindlin-1*<sup>-/-</sup> mice at P1 (n = 14/7/6) and P3 (n = 20/20/9). Error bars show standard deviation. (C) H&E staining of P3 *Kindlin-1*<sup>+/+</sup> and *Kindlin-1*<sup>-/-</sup> kidneys. *Kindlin-1*<sup>-/-</sup> kidneys do not show altered glomeruli and collecting duct morphology. Scale bar represents 200  $\mu$ m. Enlargements show glomeruli (A1, A3) and collecting ducts (A2, A4). Scale bar represents 50  $\mu$ m.

Figure S3



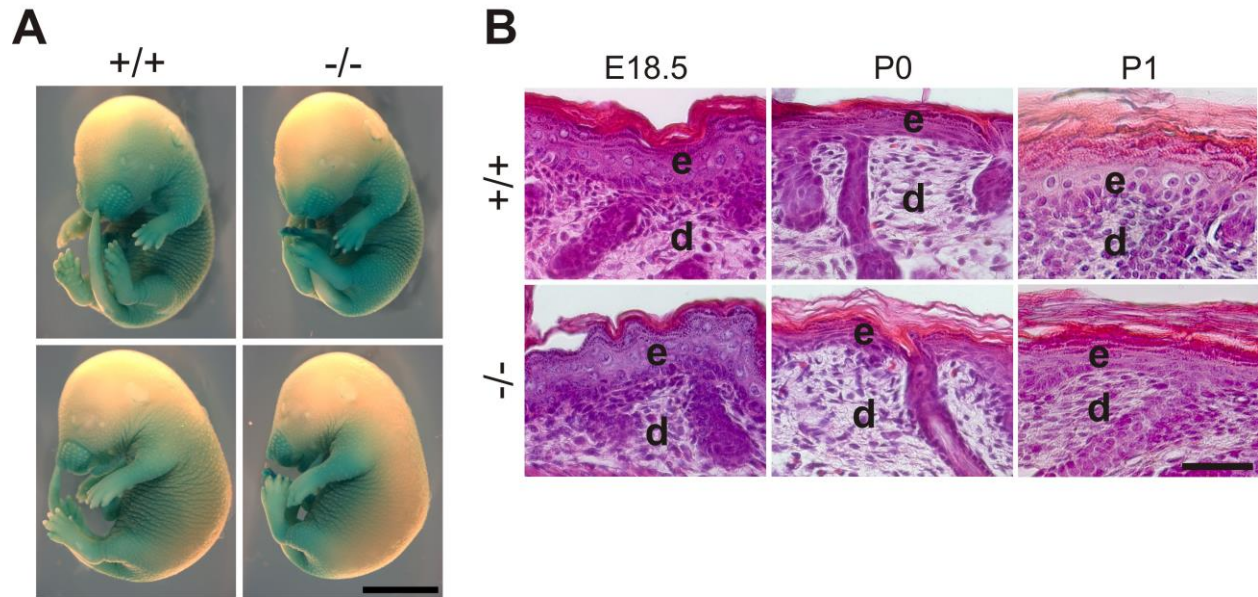
Normal BM composition and deposition in P3 Kindlin-1<sup>-/-</sup> backskin. P3 backskin of wild type and Kindlin-1<sup>-/-</sup> mice was stained for the BM components Laminin-332 (LN332; red), Collagen IV (Coll IV; red) and Fibronectin (FN; red) and co-stained with  $\alpha$ 6 or  $\beta$ 4 integrin marking (green) the basal site of basal keratinocytes. The stainings reveal no differences in BM deposition and composition or  $\alpha$ 6 and or  $\beta$ 4 integrin localization between control and Kindlin-1<sup>-/-</sup> littermates. Scale bar indicates 30  $\mu$ m.

Figure S4



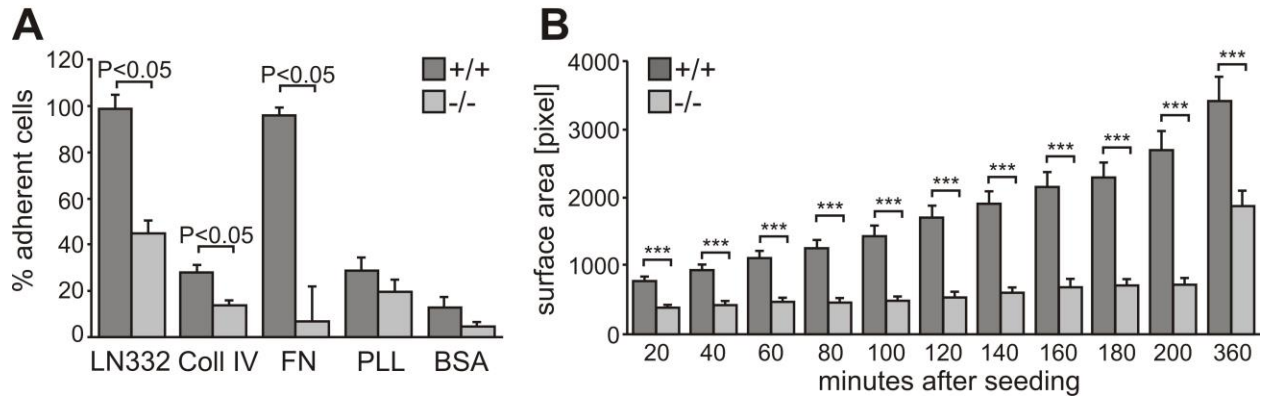
Normal skin differentiation. P3 backskin of control and Kindlin-1<sup>-/-</sup> mice was stained for epidermal differentiation markers Keratin14, Keratin10 and Loricrin (red) and co-stained with  $\alpha$ 6 integrin (green) to mark basal keratinocytes. The stainings show no difference in the differentiation pattern of Kindlin-1<sup>-/-</sup> keratinocytes. Scale bar indicates 10  $\mu$ m.

**Figure S5**



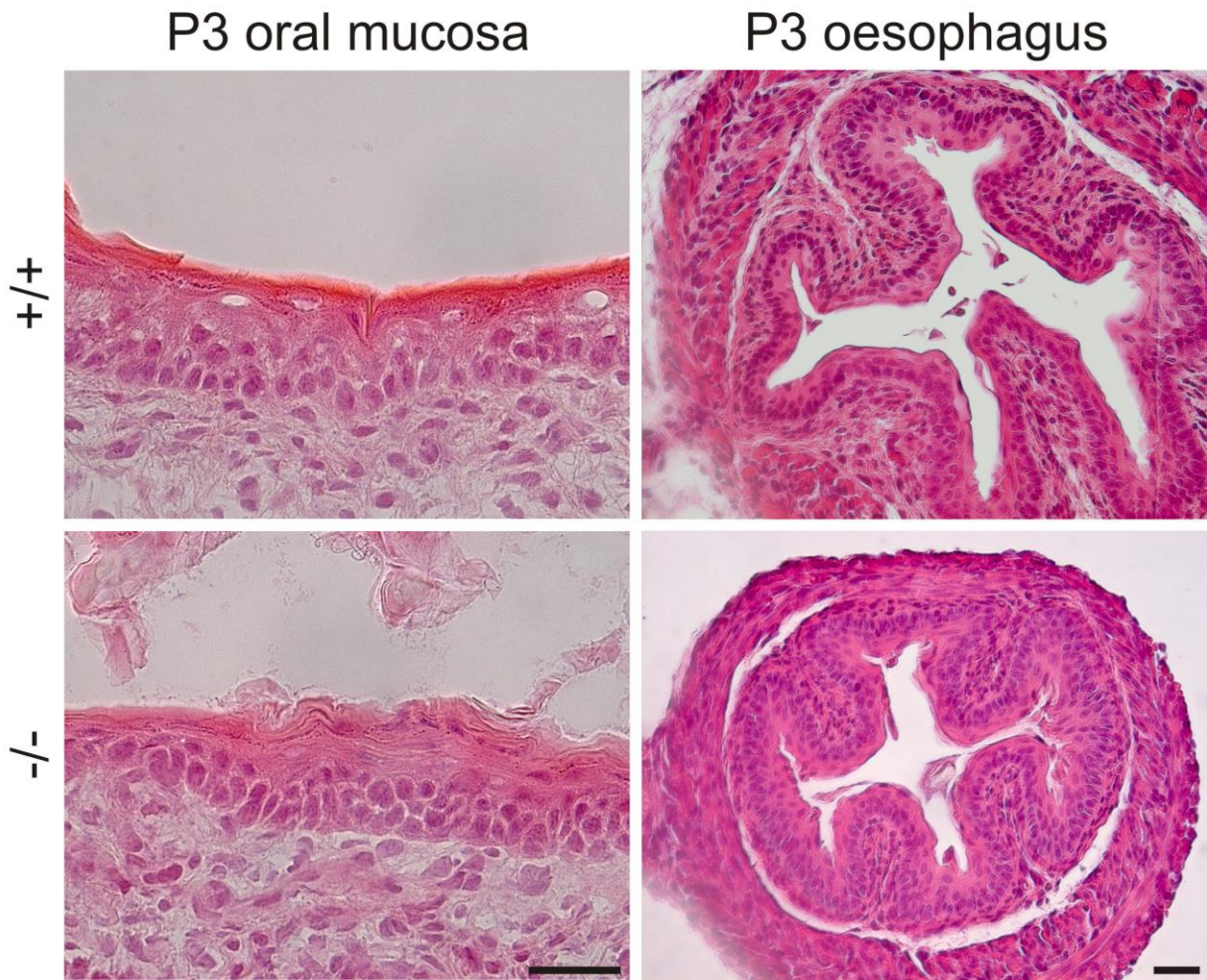
Normal skin development. (A) Normal X-Gal staining in E17 *Kindlin-1*<sup>-/-</sup> embryos indicating normal barrier formation during development. Scale bar indicates 5 mm. (B) H&E staining of back skin from control and *Kindlin-1*<sup>-/-</sup> littermates of different age. In *Kindlin-1*<sup>-/-</sup> mice the epidermal (e) thickness at E18.5 and P0 is normal but clear epidermal atrophy is seen at P1. Scale bar indicates 50  $\mu$ m. (d): dermis.

**Figure S6**



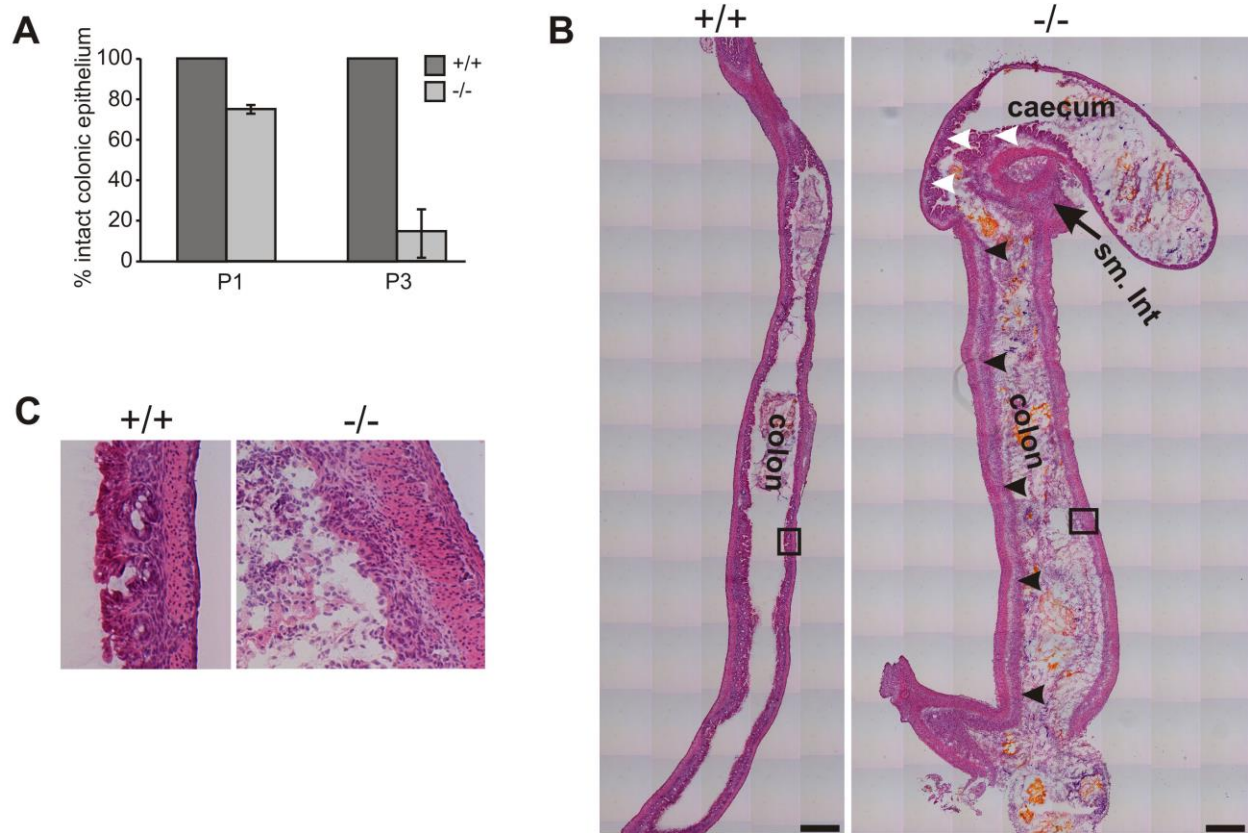
Altered adhesion and spreading of Kindlin-1<sup>-/-</sup> keratinocytes. (A) Adhesion assay of control and Kindlin-1<sup>-/-</sup> keratinocytes on LN332, Laminin-332; Coll IV, Collagen IV; FN, Fibronectin; PLL, Poly-L lysine (n = 3). Shown are mean values, error bars show standard error of the mean. (B) Cell area measured upon spreading on 5 µg/ml Fibronectin at the indicated time-points using MetaMorph software (n = 30 cells per genotype from 3 independent experiments). Shown are mean values, error bars show standard deviation (\*\*\*) p<0.0001).

Figure S7



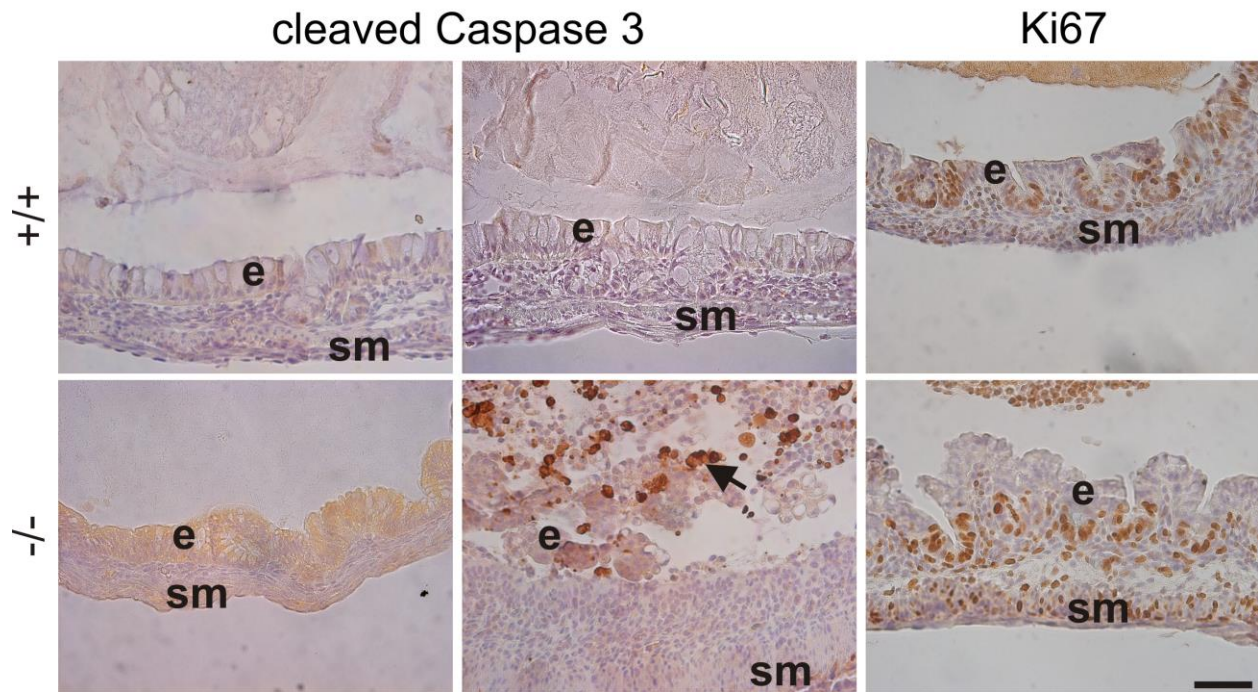
Oral and oesophageal mucosa in Kindlin-1<sup>-/-</sup> mice. Histology of the oral mucosa and the oesophagus of P3 Kindlin-1<sup>+/+</sup> and Kindlin-1<sup>-/-</sup> mice did not reveal an abnormal morphology. Scale bar represents 50  $\mu$ m.

**Figure S8**



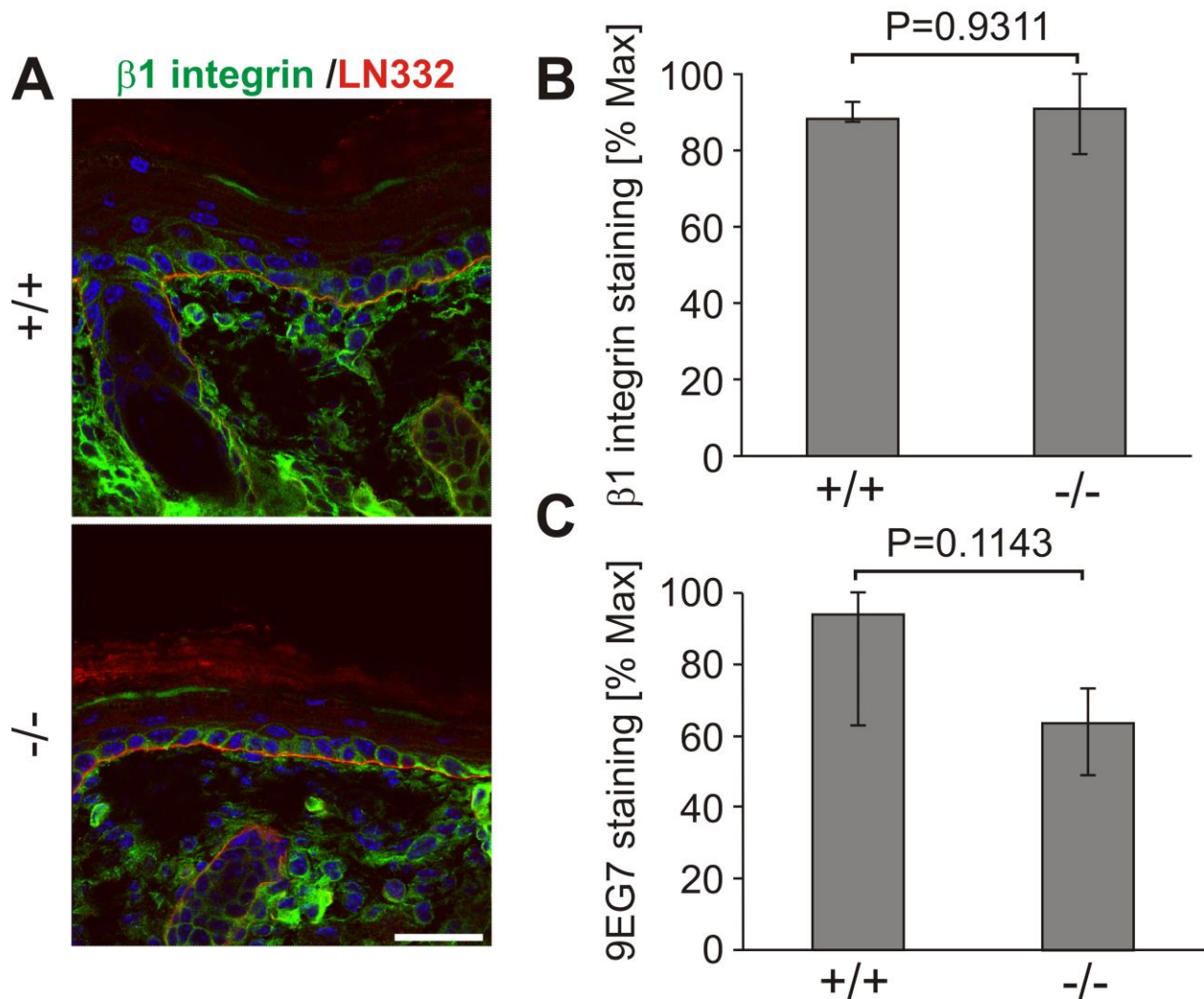
Progressive epithelial loss in Kindlin-1<sup>-/-</sup> colons. (A) Quantification of the extent of intact colonic epithelium at P1 and P3 (n = 3 per genotype and age). Error bars show range. (B) Overview of an H&E picture of a P3 control and Kindlin-1<sup>-/-</sup> colon. The Kindlin-1<sup>-/-</sup> colon shows a complete absence of colonic epithelium (black arrowheads), while the epithelium in the caecum is still present (white arrowheads). Scale bars show 500  $\mu$ m. (C) Magnifications of the boxed areas shown in B.

**Figure S9**



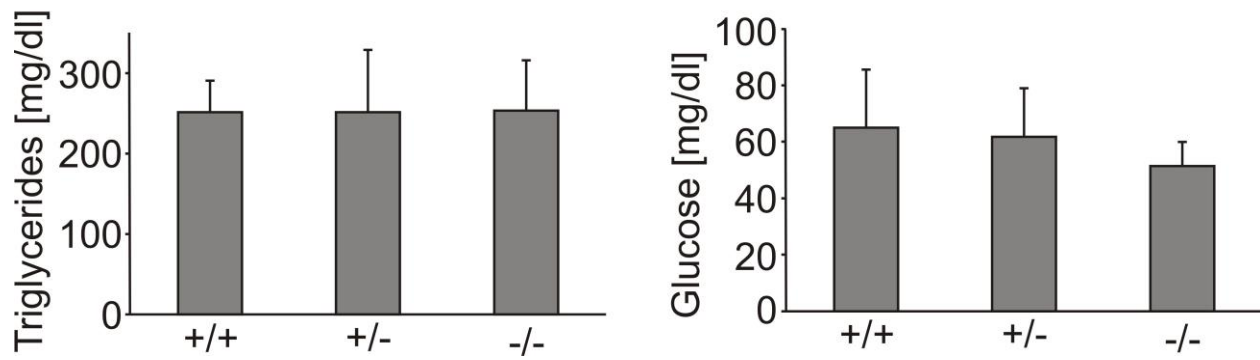
Normal IEC proliferation but detachment induced apoptosis . P1 colons from wild type and Kindlin-1<sup>-/-</sup> mice were DAB stained for cleaved Caspase-3 to determine apoptosis and Ki67 stained to show proliferating IECs. Apoptosis occurs in detached epithelium of Kindlin-1<sup>-/-</sup> mice. In areas of still adhering epithelium the number of proliferating IECs is similar between wild type and Kindlin-1<sup>-/-</sup> mice. Scale bar indicates 50  $\mu$ m.

Figure S10



$\beta 1$  integrin activation in Kindlin-1<sup>-/-</sup> keratinocytes. (A) Immunofluorescence staining for  $\beta 1$  integrin (green) and Laminin-332 (LN332; red) from P3 backskin shows normal localization of  $\beta 1$  integrin in Kindlin-1<sup>-/-</sup> backskin. (B) FACS quantification of  $\beta 1$  integrin expression of freshly isolated control and Kindlin-1<sup>-/-</sup> keratinocytes at P2 shows unaltered  $\beta 1$  integrin expression on basal keratinocytes. Error bars show range (n = 4) (C) 9EG7 FACS quantification of these keratinocytes shows no significant reduction in  $\beta 1$  integrin activation. Error bars show range (n = 4).

**Figure S11**



Shear induced detachment of Kindlin-1 depleted HT-29 cells. Control and Kindlin-1 depleted HT-29 (siKind1) cells were plated on Fibronectin-coated flow chamber slides and exposed to increasing shear forces as indicated in the figure. Control cells did not detach from the matrix while Kindlin-1 depleted cells were unable to resist low or high shear forces (compare lane 1 (0dyn/cm<sup>2</sup>) with lane 2 (0,5dyn/cm<sup>2</sup>). Scale bar indicates 50  $\mu$ m.

# Kindlin-1 controls Wnt and TGF- $\beta$ availability to regulate cutaneous stem cell proliferation

Emanuel Rognoni<sup>1</sup>, Moritz Widmaier<sup>1</sup>, Madis Jakobson<sup>1</sup>, Raphael Ruppert<sup>1</sup>, Siegfried Ussar<sup>1</sup>, Despoina Katsoukri<sup>1</sup>, Ralph T Böttcher<sup>1</sup>, Joey E Lai-Cheong<sup>2,3</sup>, Daniel B Rifkin<sup>4</sup>, John A McGrath<sup>3</sup> & Reinhard Fässler<sup>1</sup>

Kindlin-1 is an integrin tail binding protein that controls integrin activation. Mutations in the *FERMT-1* gene, which encodes for Kindlin-1, lead to Kindler syndrome in man, which is characterized by skin blistering, premature skin aging and skin cancer of unknown etiology. Here we show that loss of Kindlin-1 in mouse keratinocytes recapitulates Kindler syndrome and also produces enlarged and hyperactive stem cell compartments, which lead to hyperthickened epidermis, ectopic hair follicle development and increased skin tumor susceptibility. Mechanistically, Kindlin-1 controls keratinocyte adhesion through  $\beta_1$ -class integrins and proliferation and differentiation of cutaneous epithelial stem cells by promoting  $\alpha_v\beta_6$  integrin-mediated transforming growth factor- $\beta$  (TGF- $\beta$ ) activation and inhibiting Wnt- $\beta$ -catenin signaling through integrin-independent regulation of Wnt ligand expression. Our findings assign Kindlin-1 the previously unknown and essential task of controlling cutaneous epithelial stem cell homeostasis by balancing TGF- $\beta$ -mediated growth-inhibitory signals and Wnt- $\beta$ -catenin-mediated growth-promoting signals.

Kindler syndrome (KS) is an autosomal-recessive disease caused by loss-of-function mutations in the *FERMT-1* gene, which encodes Kindlin-1. The skin is the principal affected organ in individuals with KS and displays trauma-induced blisters, photosensitivity, pigmentation defects and increased risk for malignancies<sup>1,2</sup>.

The Kindlins belong to a family of evolutionary conserved proteins, which are found primarily at cell-matrix adhesion sites, where they bind the cytoplasmic tail of  $\beta$  subunit-containing integrins and increase integrin affinity for ligands (also called integrin activation)<sup>3–5</sup>. In addition, they are also present at cell-cell adhesion sites, in the cytoplasm and in the nucleus, where their functions are unknown<sup>6,7</sup>. Epidermal and hair follicle (HF) keratinocytes express Kindlin-1 and Kindlin-2. However, despite their striking sequence similarity, Kindlin-1 and Kindlin-2 cannot compensate for each other, indicating that they have specialized functions<sup>3,8</sup>.

Epidermal keratinocytes express several integrins, most notably members of the  $\beta_1$  subunit-containing subfamily<sup>9</sup>. Keratinocytes of the HF bulge express high levels of  $\beta_1$  and  $\alpha_v\beta_6$  integrin<sup>10</sup>. The HF bulge harbors dormant stem cells (SCs) that periodically become activated to sustain the hair cycle<sup>11,12</sup>. The alternation of bulge SC activation and dormancy is regulated by a tight interplay of antagonistic signaling pathways. SC dormancy is achieved by bone morphogenic protein (BMP) and TGF- $\beta$  signaling, whereas SC activation is elicited by shutting down BMP and TGF- $\beta$  signaling and activating canonical Wnt- $\beta$ -catenin signaling. Perturbations of these cell growth-regulating signaling pathways or of integrin signaling can profoundly alter SC homeostasis and tumor incidence<sup>13–16</sup>. It has been shown, for

example, that increased integrin expression or activity is associated with an increased risk for squamous cell carcinoma<sup>16–18</sup>. Conversely, loss of  $\beta_1$  subunit-containing integrin expression in skin (M. Sibilica, Medical University of Vienna, Austria, personal communication) or other tissues such as the mammary gland markedly reduces tumor susceptibility<sup>19</sup>. Moreover, it has been shown recently that Kindlin-2 can stabilize  $\beta$ -catenin and induce Wnt signaling in certain tumor cell lines<sup>20</sup>. It is therefore enigmatic why patients with KS suffer from an increased tumor risk<sup>2,21,22</sup> despite Kindlin-1 loss and compromised integrin functions in their keratinocytes<sup>3,23,24</sup>. This discrepancy suggests that Kindlin-1 harbors potent tumor-suppressor function(s) in keratinocytes that operate independently of the abundant and oncogenic  $\beta_1$ -class integrins. In this study we identified oncogenic signaling pathways that are tightly controlled by Kindlin-1.

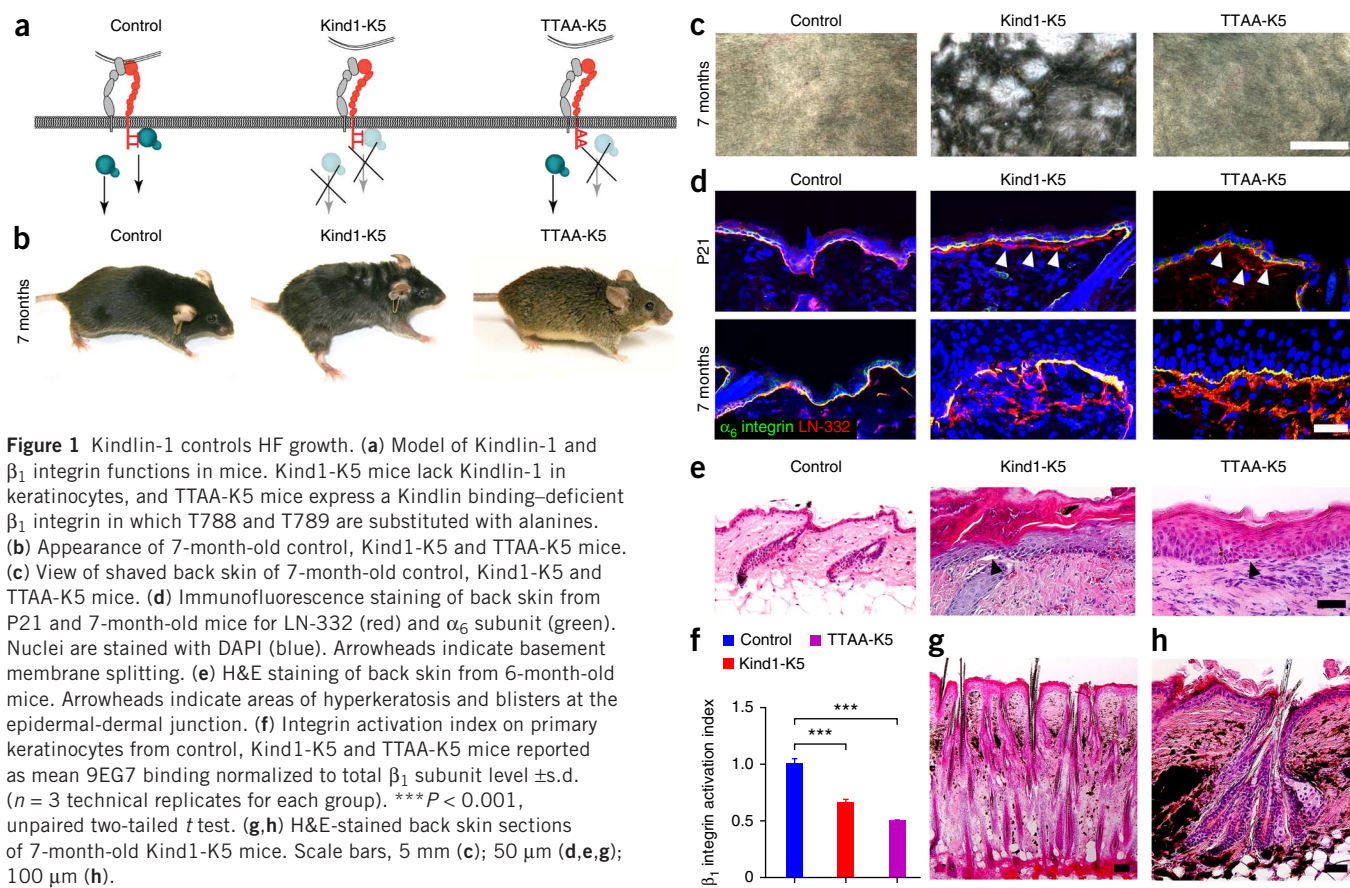
## RESULTS

### Kindlin-1 loss in epidermis and HFs leads to KS-like defects

To circumvent the lethal ulcerative colitis of a constitutive *Fermt-1* gene ablation<sup>3</sup>, we efficiently deleted the *Fermt-1* gene in keratinocytes by breeding mice with floxed *Fermt-1* with Keratin-5 (K5)-Cre transgenic mice<sup>25</sup> (resulting in Kind1-K5 mice; **Fig. 1a–c** and **Supplementary Fig. 1a–c**). Kindlin-1 loss persisted and did not affect Kindlin-2 expression in these mice (**Supplementary Fig. 1b**). Heterozygous Kind1-K5 mice or mice with homozygous floxed *Fermt-1* used as control strains had no apparent phenotype. Homozygous Kind1-K5 mice were born within the expected Mendelian ratio, were fertile and gained weight normally (**Supplementary Fig. 1d**).

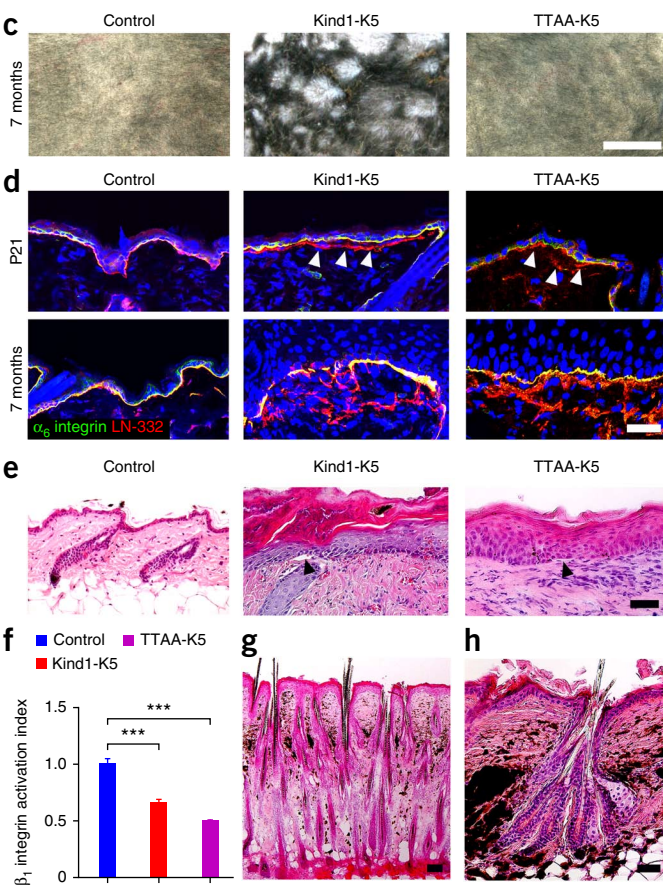
<sup>1</sup>Department of Molecular Medicine, Max Planck Institute of Biochemistry, Martinsried, Germany. <sup>2</sup>Department of Dermatology, King Edward VII Hospital, Windsor, UK. <sup>3</sup>St. John's Institute of Dermatology, King's College London (Guy's Campus), London, UK. <sup>4</sup>New York University, Langone School of Medicine, New York, New York, USA. Correspondence should be addressed to R.F. (faessler@biochem.mpg.de).

Received 14 November 2013; accepted 3 February 2014; published online 30 March 2014; doi:10.1038/nm.3490



The first histologic phenotype emerged at around postnatal day (P) 21 in the back skin of Kind1-K5 mice, with basement membrane splitting, small blisters at the dermal-epidermal junction and aberrant accumulation of F-actin and cell-cell adhesion proteins at the basal side of basal keratinocytes (Fig. 1d,e and Supplementary Fig. 1e). We also observed the same defects in mice expressing Kindlin binding-deficient  $\beta_1$  subunits in keratinocytes (Fig. 1a) due to substitutions of T788 and T789 to alanine in the  $\beta_1$  subunit cytoplasmic domain (TTAA-K5 mice)<sup>26</sup>, indicating that they are caused by malfunctioning  $\beta_1$ -class integrins (Fig. 1f). The blisters and basement membrane defects triggered a regenerative response with granulocyte, monocyte and T cell infiltrates in the dermis of the back skin of Kind1-K5 and TTAA-K5 mice (Supplementary Fig. 1f–h).

At P60, Kind1-K5 mice showed progressive melanin deposits, first in the tail and then in the entire back skin (Fig. 1g,h and Supplementary Fig. 1i), resembling poikiloderma in KS. At around 3 months of age, Kind1-K5 mice developed an irregular hair coat with small patches of densely clustered hair (Fig. 1b) that increased in size with age and appeared as meanders on the shaved back skin (Fig. 1c). At 6–8 months of age, Kind1-K5 mice began to lose hair, and patches with dense hair and alopecia alternated on their hair coat (Supplementary Fig. 1j). TTAA-K5 mice developed neither pigmentation defects nor densely packed hairs (Fig. 1b,c,e). Kind1-K5 mice also developed areas of atrophy next to areas of hyperkeratosis in the tail and back skin, whereas TTAA-K5 mice displayed hyperkeratotic areas only (Fig. 1e and Supplementary Fig. 2a). Although the number of Ki67-positive cells was higher in the epidermis of Kind1-K5 and TTAA-K5 mice compared to control littermates (Supplementary Fig. 2b–d), keratinocyte differentiation and apoptosis were unaffected in both mouse strains (Supplementary Fig. 2e–i).



These results show that Kindlin-1 deletion in the mouse epidermis recapitulates human KS and additionally induces an aberrant hair coat, which does not develop in TTAA-K5 mice, indicating that the aberrant hair coat is caused by Kindlin-1-specific and  $\beta_1$  class- and inflammation-independent mechanisms.

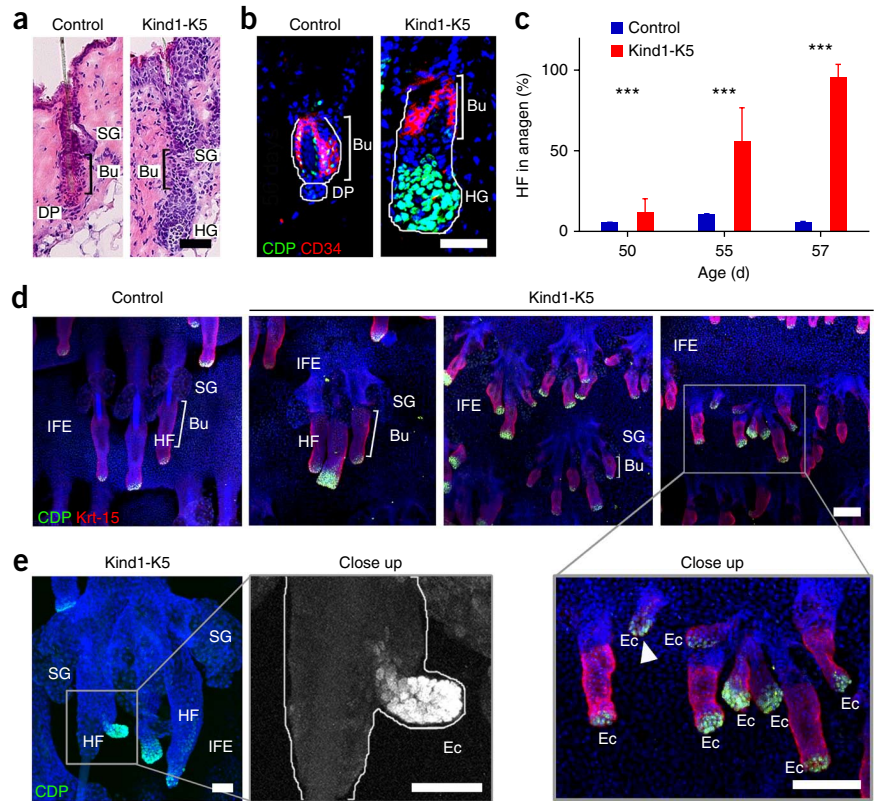
### Kindlin-1 loss disturbs the hair cycle and induces ectopic HFs

Back skin histology of 6-month-old Kind1-K5 mice revealed two different HF abnormalities: (i) areas with isolated and densely packed HFs (Fig. 1g) separated by 1–15 interfollicular epithelium (IFE) cells compared to the  $37 \pm 10$  (mean  $\pm$  s.d.,  $n = 4$  mice per genotype) IFE cells observed between control HFs, and (ii) HFs with multiple hair shafts and bulges that clustered together and contained hair strands exiting the skin through a single hair canal (Fig. 1h).

A detailed hair cycle analysis revealed that HF morphogenesis and the first hair cycle proceeded normally in the skin of Kind1-K5 mice (Supplementary Fig. 3a). At P50, HFs from control and Kind1-K5 mice entered telogen (resting phase of the hair cycle). Whereas HFs from control mice remained in a long telogen until P80 before a new hair cycle was initiated (Supplementary Fig. 3a), HFs from Kind1-K5 mice immediately re-entered anagen (growth phase of the hair cycle) (Fig. 2a–c), which was visible by the formation of a hair germ and the expression of the transcription factor CCAAT displacement protein (CDP)<sup>27</sup>. We never observed premature anagen induction in TTAA-K5 mice (Supplementary Fig. 3b).

Whole-mount staining of the tail epidermis at P80 showed HFs from control mice with prominent sebaceous glands, normal-sized Keratin-15 (Krt-15)-positive bulges and small hair germs with few CDP<sup>+</sup> cells (Fig. 2d). The tail skin of Kind1-K5 mice contained small ectopic HFs originating from pre-existing HFs and the IFE (Fig. 2d,e).

**Figure 2** Premature anagen induction and ectopic HF development in skin from Kind1-K5 mice. **(a)** H&E-stained back skin sections of P56 mice. **(b)** Immunostaining of HFs from P56 mice for CD34 (red) and CDP (green). Nuclei are stained with DAPI (blue). **(c)** The percentage of anagen HFs at the indicated time points (mean  $\pm$  s.d.,  $n = 4$  mice per genotype,  $\geq 8$  10 $\times$  objective fields were counted). \*\*\* $P < 0.001$ , unpaired two-tailed  $t$  test. **(d)** Immunostaining of tail epidermal whole mounts for CDP (green), Krt-15 (red) and DAPI (blue) of P80 mice. Of note, there is ectopic HF growth in the IFE of Kind1-K5 mice. **(e)** Ectopic HF outgrowth from a pre-existing HF of tail whole mount skin in a 6-month-old Kind1-K5 mouse stained for CDP (green) and DAPI (blue). Scale bars, 50  $\mu$ m (**a,b**); 100  $\mu$ m (**d,e**). Bu, bulge; SG, sebaceous gland; HG, hair germ; DP, dermal papilla; Ec, ectopic HF.



Ectopic HF- and IFE-derived HFs were also present in the back skin of Kind1-K5 mice and expressed the dermal papilla marker alkaline phosphatase (**Supplementary Fig. 3c,d**). Of note, whereas HF numbers increased after P50 in the back skin of Kind1-K5 mice, their number began declining after 1 year of age (**Supplementary Fig. 3i**).

These findings show that Kindlin-1 deficiency leads to a premature onset of anagen, the formation of ectopic HFs in the IFE and from pre-existing HFs and a decline in HF numbers at old age.

### Kindlin-1 regulates cutaneous epithelial SC homeostasis

The ectopic HFs in Kind1-K5 mice pointed to a perturbed SC homeostasis. The epidermis contains different SC populations that reside in different niches<sup>11</sup>. Whereas bulge SCs express CD34, Krt-15, nephronectin (Npnt)<sup>28</sup> and high levels of  $\alpha_6$  integrin (**Fig. 3a**), reliable mouse IFE SC markers are still missing<sup>11,29</sup>. Immunostaining revealed higher numbers of CD34<sup>+</sup> bulge cells in back skin (**Supplementary Fig. 3e**) and enlarged Krt-15<sup>+</sup> bulges in tail whole mounts of Kind1-K5 mice at P80 compared to controls (**Fig. 3b** and **Supplementary Fig. 3f**). Krt-15<sup>+</sup> cells were also present in the infundibulum and IFE of Kind1-K5 mice (**Fig. 3b**) but were not present in control mice. Npnt expression expanded into the sebaceous gland, the infundibulum and the outer root sheath (**Fig. 3b,c**), and Npnt mRNA levels were higher in FACS-sorted bulge and infundibulum-junctional zone cells of Kind1-K5 mice compared to controls (**Supplementary Fig. 3h**). Also, the leucine-rich repeats and immunoglobulin-like domains 1 (Lrig1)-positive SC population of the infundibulum-junctional zone<sup>30</sup> extended toward the infundibulum and lower hair shaft of back and tail skin HFs of Kind1-K5 mice (**Fig. 3d** and **Supplementary Fig. 3g**).

Despite normal hair cycles and hair counts until P50 (**Supplementary Fig. 3a,i**), FACS quantifications of keratinocytes from mouse skin at P40 revealed significantly more SCs in the bulge, upper isthmus and infundibulum-junctional zone of Kind1-K5 mice compared to controls (**Fig. 3e,f**). A time-course analysis showed that the expansion of the SC compartments was already visible at P21, peaked at P50–P80 and then began declining to become markedly smaller in 12-month-old Kind1-K5 mice (**Fig. 3g** and **Supplementary Table 1**).

In line with normal hair coat development, SC subpopulations were unaffected in TTA-K5 mice, at least until 1 year of age (**Supplementary Fig. 3j**).

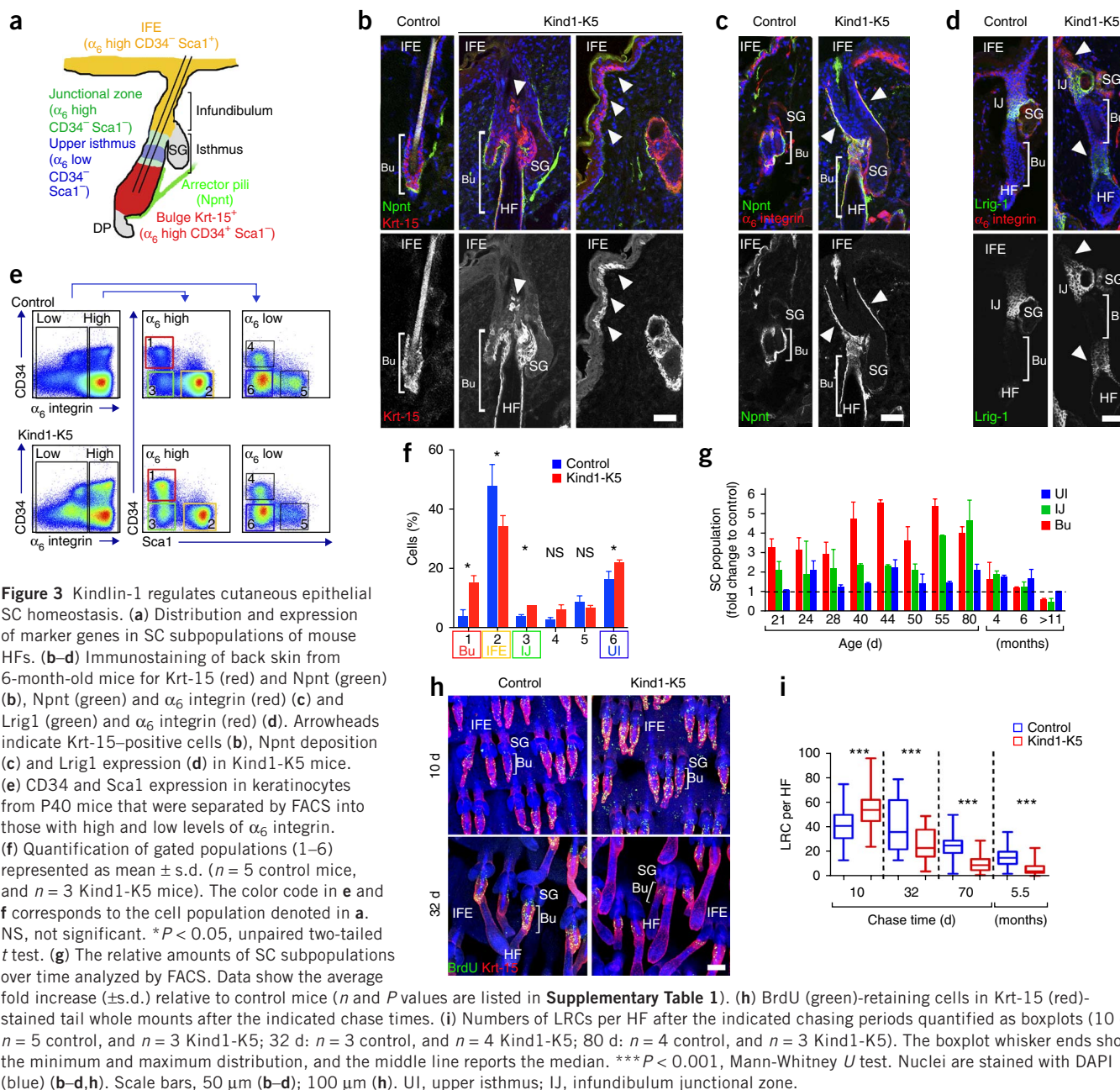
To test whether elevated proliferation caused the enlarged bulges, we performed BrdU label-retaining cell (LRC) assays. After 10 days of chase, significantly more bulge cells were BrdU<sup>+</sup> in tail whole mounts of Kind1-K5 mice compared to controls, whereas after 32 days, 70 days and 5.5 months, significantly fewer bulge cells were BrdU<sup>+</sup> in Kind1-K5 mice (**Fig. 3h,i**).

These findings demonstrate that Kindlin-1 deficiency elevates cutaneous epithelial SC proliferation, numbers and compartments in a  $\beta_1$  class-independent manner.

### Kindlin-1 triggers $\alpha_v\beta_6$ integrin-mediated TGF- $\beta$ release in skin

To determine whether Kindlin-1 loss alters integrin surface levels, we analyzed integrin profiles on primary keratinocytes using FACS. The levels of  $\beta_1$  and  $\beta_4$  integrin subunits were slightly lower and the levels of  $\beta_5$  and  $\beta_8$  integrin subunits were slightly higher in cells from Kind1-K5 mice compared to controls. Detection of  $\beta_3$  integrin subunits was not evident in either genotype. We also noted clearly elevated  $\beta_6$  subunit levels in Kindlin-1-deficient keratinocytes (**Fig. 4a**), as were *Itgb6* (encoding the  $\beta_6$  integrin subunit) mRNA levels in FACS-sorted cutaneous SCs (**Supplementary Fig. 4a**). Immunostaining showed  $\beta_6$  subunit expression extending from the bulge and outer root sheath to the infundibulum and IFE of Kind1-K5 mice (**Fig. 4b**).

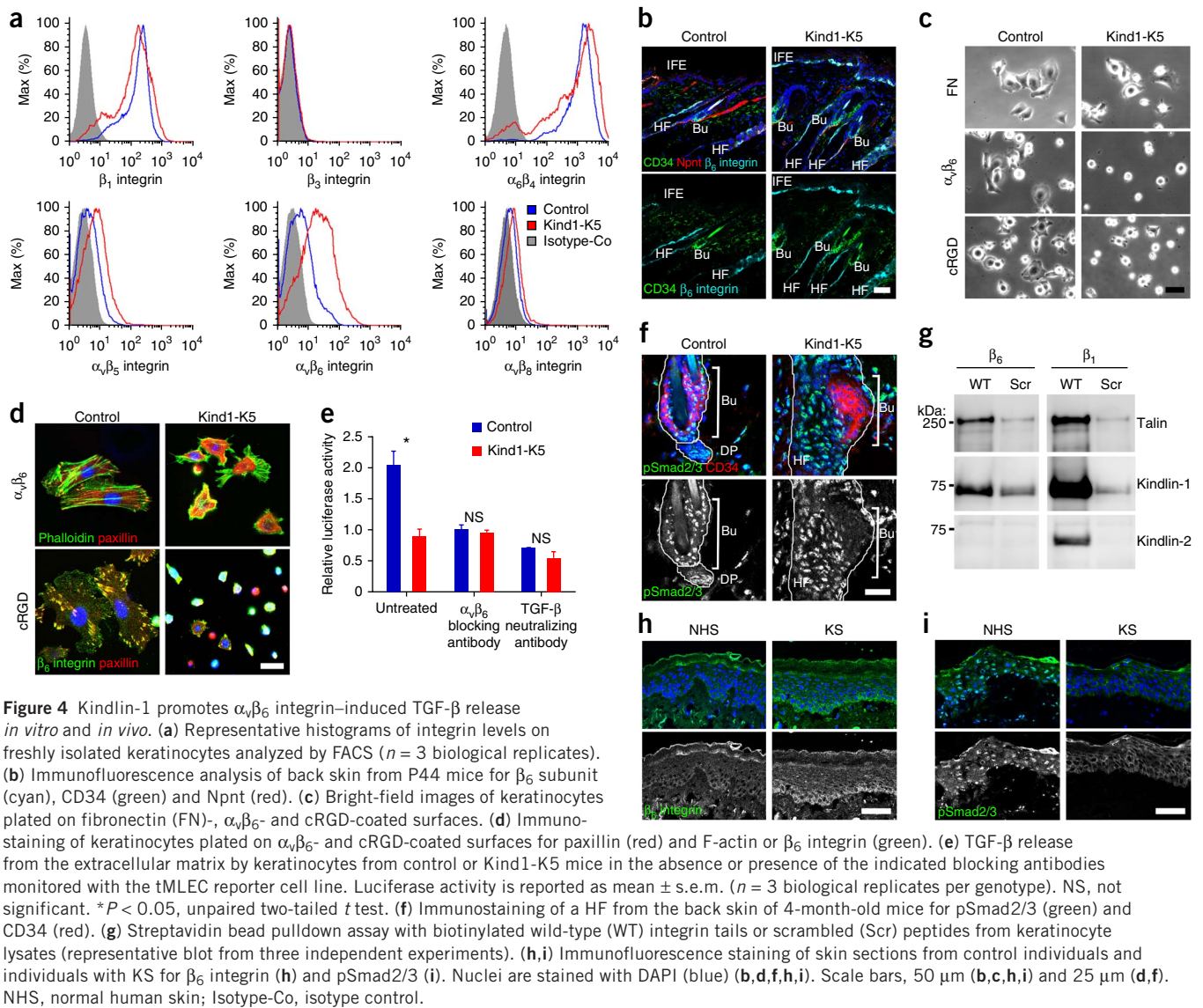
Next we investigated  $\beta_6$  subunit-dependent cell spreading and focal adhesion formation. Although keratinocytes from Kind1-K5 mice spread normally on fibronectin, they displayed severely impaired adhesion, spreading, clustering of paxillin in focal adhesion-like structures and assembly of F-actin stress fibers when plated on surfaces coated with  $\alpha_v\beta_6$ -specific antibodies or  $\alpha_v$ -specific peptidomimetic cyclic RGD (cRGD) (**Fig. 4c,d** and **Supplementary Fig. 4b,c**),



indicating that  $\alpha_v\beta_6$  integrins in keratinocytes from Kind1-K5 mice are nonfunctional. We confirmed the  $\alpha_v\beta_6$  specificity of these defects by treating keratinocytes from control mice with the  $\beta_6$ -blocking antibody 10D5, which phenocopied the spreading defects of Kindlin-1–deficient cells on cRGD surfaces (**Supplementary Fig. 4d**).

Active  $\alpha_v\beta_6$  integrins can release TGF- $\beta$  from the latency associated protein (LAP)<sup>31</sup>, which in turn suppresses the proliferation of bulge SCs<sup>10,12,32,33</sup>. We tested  $\alpha_v\beta_6$ -dependent TGF- $\beta$  release by seeding keratinocytes together with transformed mink lung epithelial cells (tMLECs), which are able to report TGF- $\beta$ -induced luciferase on a latent TGF- $\beta$  binding protein-1 (LTBP-1)–LAP–TGF- $\beta$ 1–rich matrix<sup>34</sup> (**Fig. 4e**). Keratinocytes from control mice efficiently induced the luciferase reporter, which could be inhibited with the  $\alpha_v\beta_6$  blocking antibody 10D5 or the TGF- $\beta$  neutralizing antibody 1D11. In sharp contrast, keratinocytes from Kind1-K5 mice were

unable to release TGF- $\beta$ , confirming that their  $\alpha_v\beta_6$  integrins are nonfunctional (**Fig. 4e**). In line with this *in vitro* result, TGF- $\beta$  signaling was also severely impaired in bulge cells of Kind1-K5 mice *in vivo*, in which phosphorylated Smad2 and Smad3 (pSmad2/3) was detectable neither before nor after premature anagen induction (**Fig. 4f** and **Supplementary Fig. 4g**). Signaling by BMP through phosphorylation of Smad1, Smad5 and Smad8 (pSmad1/5/8), which also suppresses bulge cell proliferation<sup>35,36</sup>, was unaffected (**Supplementary Fig. 4h**). Treatment of Kindlin-1–deficient keratinocytes with soluble TGF- $\beta$ 1 induced robust Smad2 phosphorylation and reduced cell proliferation (**Supplementary Fig. 4e,f**), indicating that TGF- $\beta$ 1 signals are efficiently transduced. The severe dysfunction of  $\alpha_v\beta_6$  integrins was not compensated by Kindlin-2 because of the inability of Kindlin-2 to bind  $\beta_6$  tails (**Fig. 4g**). Most notably, subjects with KS showed a similar TGF- $\beta$  defect as Kind1-K5 mice, with elevated expression



of  $\beta_6$  subunits and reduced nuclear pSmad2/3 in large areas of basal epidermal keratinocytes (Fig. 4h,i), whereas pSmad1/5/8 was unaffected (Supplementary Fig. 4i).

These findings indicate that Kindlin-1 is essential for  $\beta_6$  subunit-containing integrin-mediated cell adhesion, cell spreading and TGF- $\beta$  release required for SC quiescence.

#### Kindlin-1 curbs Wnt- $\beta$ -catenin signaling in skin

Premature anagen induction, ectopic HF development and expansion of SC compartments also develop in mice with elevated Wnt- $\beta$ -catenin signaling in keratinocytes<sup>37–40</sup>, and reduced HF spacing and aberrant hair orientation occur in mice overexpressing the  $\beta$ -catenin cofactor Lef1 (ref. 41) or mice with increased Notch signaling<sup>42</sup>. In the skin of control mice,  $\beta$ -catenin levels were high at cell-cell junctions, low in the nucleus and absent at the basal side of basal keratinocytes. In contrast, in the epidermis of Kind1-K5 mice,  $\beta$ -catenin also accumulated at basal sides of basal keratinocytes, in the nuclei of a large number of IFE cells and in catagen HFs (Fig. 5a and Supplementary Fig. 5d). Furthermore, Kind1-K5 mice showed  $\beta$ -catenin in the nuclei of developing hair germs during premature anagen

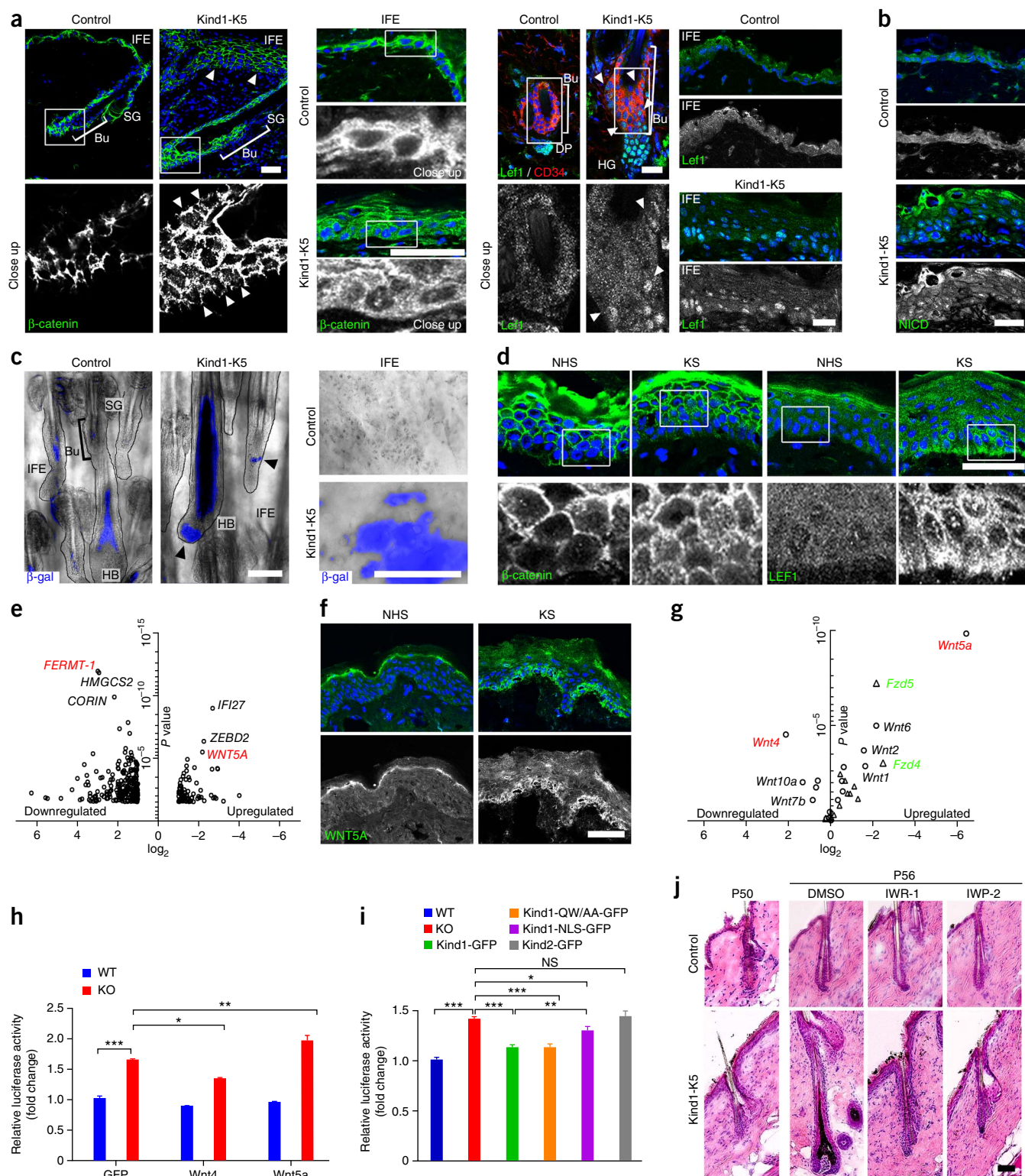
induction (Supplementary Fig. 5a,b) and extended Lef1 expression from the normal site in hair germs to the bulge and IFE at all stages analyzed (Fig. 5a and Supplementary Fig. 5a,c,d). Notably, at P50, shortly before bulges from Kind1-K5 mice induced premature anagen, they showed high nuclear Lef1 levels, indicating a premature onset of Wnt signaling. In control mice, Lef1 was absent in telogen bulges and became highly expressed in the nuclei of hair germ cells and weakly expressed in the cytoplasm of IFE cells (Fig. 5a and Supplementary Fig. 5a). The numbers of nuclear Notch effector Notch intracellular domain (NICD)-containing cells and NICD-induced *Hes1* mRNA levels were unaltered in hair germs and the pericortex, but both were higher in the IFE of Kind1-K5 mice compared to controls at all time points analyzed (Fig. 5b and Supplementary Fig. 5e–g).

Next we determined Wnt- $\beta$ -catenin signaling by intercrossing Kind1-K5 and control mice with TOPgal reporter mice, which express  $\beta$ -galactosidase under a TCF-Lef-controlled minimal c-Fos promoter<sup>43</sup>. In HFs from control mice, TOPgal activities were high in the pericortex during anagen, low during catagen and lost in telogen, with some residual activity in club hairs. In Kind1-K5 mice, the high TOPgal activity in the pericortex and bulb of anagen HFs persisted

throughout catagen, decreased in telogen (Fig. 5c and Supplementary Fig. 5i) and was strongly re-induced in the following anagen stage (Supplementary Fig. 5h). Furthermore, we observed a patch-like distribution of TOPgal in the IFE of Kind1-K5 mice, which was absent in controls (Fig. 5c). Notably, the IFE of humans with KS showed similar abnormalities in  $\beta$ -catenin–LEF1 expression, with weak nuclear  $\beta$ -catenin expression in the basal cell layer and a patch-like distribution

of nuclear LEF1, whereas normal human skin contained  $\beta$ -catenin exclusively in cell-cell contacts and LEF1 in the cytoplasm (Fig. 5d and Supplementary Fig. 5j).

These findings demonstrate that loss of Kindlin-1 induces nuclear translocation of  $\beta$ -catenin–Lef1 in KS and mouse skin, leading to elevated Wnt– $\beta$ -catenin signaling and premature anagen onset of HFs in Kind1-K5 mice.



### Kindlin-1 regulates Wnt ligand expression

To find an explanation for the increased Wnt- $\beta$ -catenin signaling in the absence of Kindlin-1, we compared the skin transcriptome between healthy individuals and subjects with KS using microarray analyses. As we expected, *FERMT-1* expression was absent in skin from subjects with KS, and the levels of mRNAs encoding inflammatory proteins were high (Fig. 5e; the complete list is given in Supplementary Table 2). Unexpectedly, the levels of several Wnt signaling components, most notably *WNT5A*, were high in individuals with KS compared to healthy individuals (Fig. 5e). Immunostaining confirmed the aberrant expression of *WNT5A* in basal keratinocytes of individuals with KS (Fig. 5f). Quantitative PCR (qPCR) and *in situ* hybridization of tail whole mounts from Kind1-K5 mice corroborated high *Wnt5a* mRNA levels in hair bulbs, ectopic HFs and patches of the IFE, which overlapped with high TOPgal activities (Fig. 5g and Supplementary Fig. 6a–c). qPCR of all known Wnt ligands and receptors revealed that the levels of several canonical (*Wnt1*, *Wnt2b*, *Wnt3a* and *Wnt9b*) and noncanonical (*Wnt6* and *Wnt2*) Wnts were also significantly higher in keratinocytes from Kind1-K5 mice compared to controls, whereas the levels of *Wnt4*, *Wnt7a*, *Wnt9a*, *Wnt10a* and *Wnt16* were significantly lower (Fig. 5g and Supplementary Table 3). The expression of several Frizzled (Fzd) receptors was higher in Kind1-K5 mice compared to controls, most notably *Fzd4* and *Fzd5* and to a lesser extent the Fzd co-receptor *Lrp6*. We also performed qPCR of FACS-sorted bulge cells and *in situ* hybridization of tail whole mounts from Kind1-K5 mice and confirmed the high *Fzd4* mRNA levels and patch-like expression of *Fzd4* in the IFE (Supplementary Fig. 6d,e).

Transfection of Kindlin-1-deficient keratinocytes with SuperTOPFlash reporter revealed that the elevated Wnt signaling was cell autonomous (Fig. 5h,i) and that *Lef1* was limiting the extent of Wnt signaling (Supplementary Fig. 6f). Overexpression of *Wnt4*, which triggers translocation of  $\beta$ -catenin to cell-cell junctions, thereby preventing nuclear accumulation of  $\beta$ -catenin and Wnt- $\beta$ -catenin signaling<sup>44</sup>, decreased SuperTOPFlash activity in Kindlin-1-deficient keratinocytes compared to GFP-transfected controls (Fig. 5h). Overexpression of *Wnt5a*, which together with *Lrp5* and *Fzd4* efficiently activates the canonical Wnt- $\beta$ -catenin signaling pathway<sup>45</sup>, further increased the activity of the SuperTOPFlash reporter in Kindlin-1-deficient cells but not in control cells in which *Fzd4* expression was low (Fig. 5h and Supplementary Fig. 6d,e).

Re-expression of similar quantities of Kindlin-1-GFP or the integrin binding-deficient Kindlin-1<sup>Q611A,W612A</sup>-GFP but not Kindlin-2 attenuated the increased SuperTOPFlash activities and

levels of *Wnt4* and *Wnt5a* in Kindlin-1-deficient keratinocytes (Fig. 5i and Supplementary Fig. 6g–j), indicating that inhibition of Wnt- $\beta$ -catenin signaling is Kindlin-1 specific and does not require integrin binding. To exclude a role for nuclear Kindlin-1, we expressed Kindlin-1-GFP fused to two SV40 nuclear localization signals (NLSs) in Kind1-null cells. Although most of the protein localized to the nucleus, the elevated SuperTOPFlash activity was only partially rescued (Fig. 5i), probably because of Kind1-NLS-GFP spillovers into the cytoplasm (Supplementary Fig. 6j).

To corroborate that elevated Wnt protein secretion and high Wnt- $\beta$ -catenin signaling underlie premature HF anagen induction in Kind1-K5 mice, we treated them at P49, shortly before telogen onset (Fig. 5j and Supplementary Fig. 7a), with IWP-2, which blocks Wnt protein secretion by inhibiting porcupine-mediated palmitoylation of Wnts<sup>46</sup>, or with IWR-1, which inhibits tankyrases, thereby stabilizing the  $\beta$ -catenin destruction complex<sup>46,47</sup>. Both compounds efficiently blocked premature anagen induction in Kind1-K5 mice and decreased SuperTOPFlash activities *in vitro* (Fig. 5j and Supplementary Fig. 7a,b). In line with previous reports<sup>42</sup>, inhibition of Wnt signaling also reduced aberrant Notch activities in Kind1-K5 keratinocytes *in vitro* and *in vivo*, which in turn normalized *Wnt4* levels<sup>48</sup> (Supplementary Fig. 7c–g).

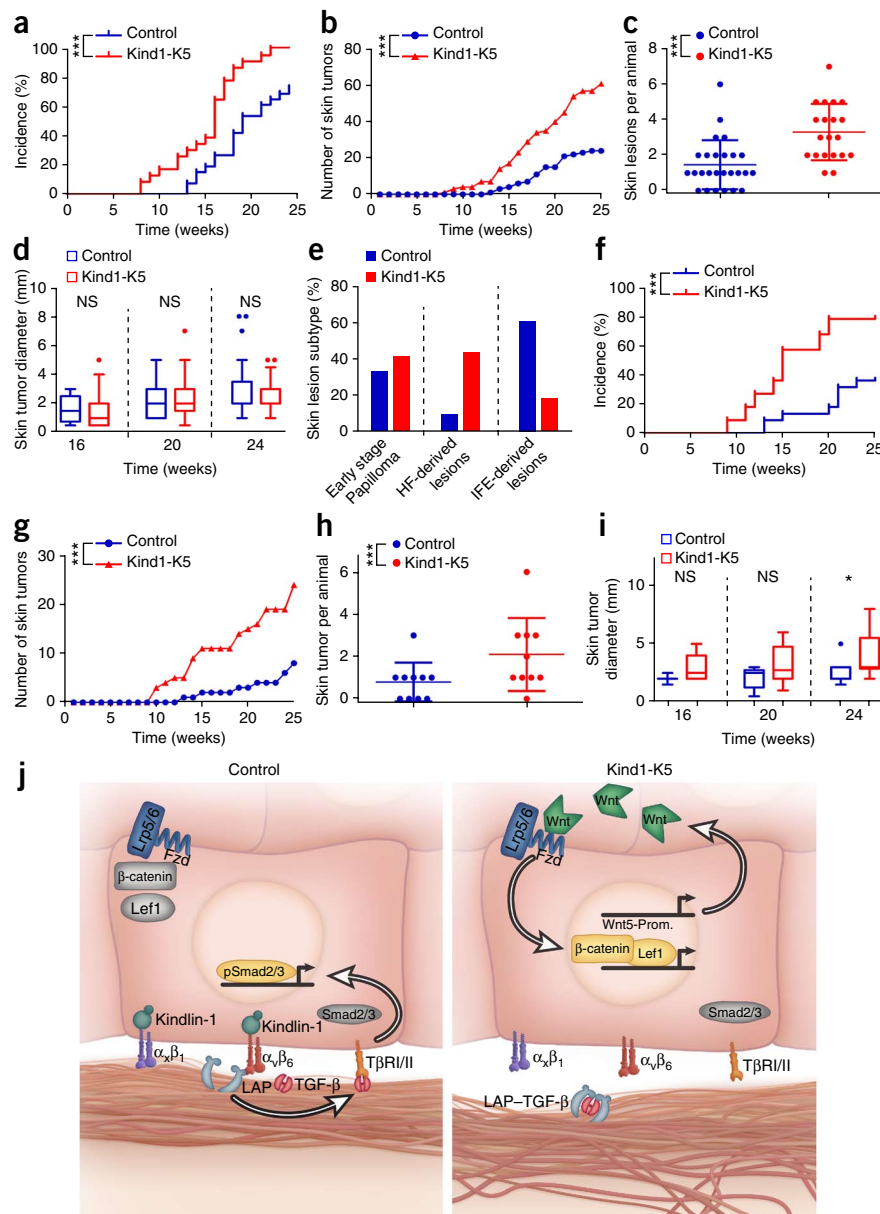
Together these findings demonstrate that Kindlin-1 inhibits Wnt- $\beta$ -catenin signaling by regulating the transcription of Wnt ligands and receptors in a cell-autonomous and integrin-independent manner.

### Loss of Kindlin-1 increases skin tumor susceptibility

The low TGF- $\beta$  levels and augmented Wnt signaling in humans with KS and Kind1-K5 mice are oncogenic threats<sup>49,50</sup>. To test this hypothesis, we used the two-stage carcinogenesis protocol and treated mice with 7,12-dimethylbenz[a]anthracene (DMBA) and 12-*O*-tetradecanoylphorbol-13-acetate (TPA) for 25 weeks. Kind1-K5 mice developed tumors earlier and had more tumors than control mice (Fig. 6a–c). Of note, tumor sizes were similar between Kind1-K5 and control mice (Fig. 6d), which could be due to different skin lesion subtypes. Indeed, histology of the tumor lesions revealed that hyperkeratotic and exophytic papillomas dominated in control mice, whereas HF-derived trichofolliculoma-like lesions, sebaceous papillomas, mixed papillomas and basal cell carcinoma-like lesions dominated in Kind1-K5 mice (Fig. 6e and Supplementary Fig. 8a). In line with uncurbed Wnt signaling, we observed more cells with nuclear  $\beta$ -catenin and *Lef1* expression in tumors from Kind1-K5 mice (Supplementary Fig. 8b–d).

**Figure 5** Kindlin-1 controls Wnt- $\beta$ -catenin signaling. (a) Immunofluorescence staining for  $\beta$ -catenin (green) in HFs (P44) (left) and the IFE (P55) (middle) and for *Lef1* and CD34 (red) in HFs and the IFE (4 months) (right) from control and Kind1-K5 mice. Arrowheads indicate aberrant  $\beta$ -catenin (left) or *Lef1* (right) localization. (b) IFE immunofluorescence staining for NICD (green) from P44 control and Kind1-K5 mice. (c) TOPgal reporter activity in tail HFs (left) and the IFE (right) from 3-month-old control and Kind1-K5 mice. Arrowheads indicate HFs with abnormal TOPgal activity.  $\beta$ -gal,  $\beta$ -galactosidase. (d) Immunofluorescence staining of human skin from control individuals and individuals with KS for  $\beta$ -catenin (left) and *LEF1* (right). (e) Skin gene expression profile of NHS ( $n = 3$ ) and KS ( $n = 3$ ) assessed with microarray and shown as a volcano plot. Genes with at least twofold change in KS were plotted according to the  $\log_2$  fold change (x axis) and the  $\log_{10}$   $P$  value (y axis), unpaired two-tailed  $t$  test. (f) Immunofluorescence staining for *WNT5A* (green) in the skin of control individuals and individuals with KS. (g) Volcano plot of the qPCR-determined gene expression profile of keratinocytes from control and Kind1-K5 mice. Mean expressions relative to *Gapdh* of Wnt ligands (circle, red) and receptors (triangle, green) were plotted according to the  $\log_2$  fold change (x axis) and  $\log_{10}$   $P$  value (y axis) ( $n = 3$  biological replicates per genotype; the  $\pm$  s.e.m. values are listed in Supplementary Table 3). (h) Transient overexpression of GFP, *Wnt4* and *Wnt5a* in floxed keratinocytes (WT) and Kindlin-1-deficient keratinocytes previously treated with adenovirus expressing Cre recombinase (KO) expressing the TOPFlash reporter. Values are corrected for the *Renilla* control and are represented as mean  $\pm$  s.e.m. fold increase relative to WT cells ( $n = 5$  WT and KO biological replicates). \* $P < 0.05$ , \*\* $P < 0.01$ , unpaired two-tailed  $t$  test. (i) TOPFlash reporter activity in KO cells stably re-expressing Kindlin-1-GFP, integrin binding-deficient Kindlin-1<sup>Q611A,W612A</sup>-GFP (Kind1-QW/AA-GFP), NLS-tagged Kindlin-1-GFP or Kindlin-2-GFP. Values are corrected for the *Renilla* control, are represented as fold increase relative to WT cells and are reported as mean  $\pm$  s.e.m. ( $n = 21$  WT and KO;  $n = 13$  Kind1-GFP;  $n = 9$  Kind1-QW/AA-GFP;  $n = 5$  Kind1-NLS-GFP and Kind2-GFP; all biological replicates). NS, not significant. \* $P < 0.05$ , \*\* $P < 0.01$ , \*\*\* $P < 0.001$ , unpaired two-tailed  $t$  test. (j) H&E staining of control and Kind1-K5 mice at 1 d (P50) and after treatment (P56) with the indicated Wnt inhibitor. Nuclei are stained with DAPI (blue) (a,b,d,f). All scale bars, 50  $\mu$ m.

**Figure 6** Loss of Kindlin-1 increases skin tumor incidence. (a–e) Two-stage carcinogenesis ( $n = 26$  control mice and  $n = 23$  Kind1-K5 mice). (a–c) Tumor incidence ( $P$  value by log-rank test) (a), burden ( $P$  value by log-rank test) (b) and skin lesions per animal (reported as mean  $\pm$  s.d.,  $P$  value by Mann-Whitney  $U$  test) after 25 weeks of treatment (c). \*\*\* $P < 0.001$ . (d) Tumor growth reported by diameter shown in a boxplot, where the whisker ends are at the 1.5-interquartile range, and the middle lines represent the median. NS, not significant;  $P$  values by Mann-Whitney  $U$  test. (e) The percentage of skin lesion subtypes from control ( $n = 25$  lesions) and Kind1-K5 ( $n = 47$  lesions) mice that were staged by histology and immunofluorescence analysis (Supplementary Fig. 8a). (f–i) One-stage carcinogenesis with DMBA ( $n = 10$  control mice and  $n = 10$  Kind1-K5 mice monitored as in a–d). (f–i) Tumor incidence ( $P$  value by log-rank test) (f), skin lesion number ( $P$  value by Wilcoxon  $t$  test) (g), frequency (reported as mean  $\pm$  s.d.,  $P$  value by Mann-Whitney  $U$  test) (h) and size (reported as boxplot, where the whisker ends are at the 1.5-interquartile range, and the middle lines represent the median;  $P$  value by Mann-Whitney  $U$  test) (i). NS, not significant. \* $P < 0.05$ , \*\*\* $P < 0.001$ . (j) Molecular functions of Kindlin-1. In normal cells (left), Kindlin-1 activates  $\beta_1$ -class integrins and  $\alpha_v\beta_6$  integrin to facilitate adhesion and TGF- $\beta$  liberation from LAP, respectively. Free TGF- $\beta$  activates T $\beta$ R1/II, leading to nuclear translocation of pSmad2/3, which promotes SC quiescence. In Kindlin-1-deficient cells (right), activation of  $\beta_1$ -class integrins and  $\alpha_v\beta_6$  is impaired, leading to adhesion defects and loss of TGF- $\beta$ -mediated SC quiescence. In addition, dysregulated Wnt ligand expression leading to elevation of Wnt5a levels leads to canonical Wnt- $\beta$ -catenin signaling through the Lrp5/6–Fzd4 complex. Wnt5-Prom, Wnt5 promoter.



A single DMBA treatment induced more and slightly larger tumors in Kind1-K5 mice compared to controls (Fig. 6f–i), indicating that the hyperproliferative state of keratinocytes in Kind1-K5 mice was sufficient to promote tumor development. Furthermore, the tumors in the Kind1-K5 mice originated primarily from HFs and sebaceous glands containing hyperactive SCs.

## DISCUSSION

Loss-of-function mutations in the *FERMT-1* gene cause KS, which is characterized by skin blistering at birth, premature skin aging, pigmentation defects and increased incidence of skin cancer. The ability of Kindlin-1 to activate integrins and link them to the F-actin cytoskeleton explains the development of skin blisters and basement membrane splitting followed by an inflammatory response. However, the notion that skin tumor development is promoted by hyperactive integrins and inhibited by compromised integrins indicates that Kindlin-1 loss activates oncogenic functions, inhibits tumor-suppressor functions or both. The task of this study was to identify such pathway(s).

Deletion of Kindlin-1 in skin epithelial cells with the K5-Cre driver line leads to small skin blistering, basement membrane defects,

chronic skin inflammation, progressive pigmentation defects and skin atrophy and is hence similar to KS. Unexpectedly, Kind1-K5 mice also develop enlarged cutaneous epithelial SC compartments, hyperactive bulge SCs, distorted HF cycles and ectopic HFs (Supplementary Fig. 8e). In line with high SC proliferation, treatment with both DMBA and TPA as well as with DMBA only induces a significantly higher tumor incidence and tumor burden in Kind1-K5 mice. Moreover, the majority of the tumors are basal cell carcinoma- and trichofolliculoma-like lesions, suggesting that the tumors originate predominantly from HF bulge SCs.

In search for a mechanistic explanation for the dysregulated SC and tumor cell proliferation in Kind1-K5 mice, we identified two Kindlin-1-regulated signaling pathways with opposing functions on bulge SC quiescence (Fig. 6j). Kindlin-1 binding to the cytoplasmic tail of  $\beta_6$  subunit-containing integrin<sup>51</sup> triggers  $\alpha_v\beta_6$  integrin binding to the RGD motif of LAP, thereby liberating TGF- $\beta$  and inducing TGF- $\beta$  receptor signaling and cutaneous epithelial SC quiescence. These findings are supported by a report showing that loss of  $\beta_6$

subunit-containing integrin impairs TGF- $\beta$  signaling and elevates bulge SC activity *in vivo*<sup>32</sup>.

Despite the sequence similarities of Kindlin-1 and Kindlin-2 (ref. 52) and their expression in keratinocytes from control and Kind1-K5 mice, Kindlin-2 can only partially compensate for Kindlin-1 at  $\beta_1$  subunit-containing integrin adhesion sites. Furthermore, Kindlin-2 is unable to bind  $\beta_6$  subunit tails, which prevents it from releasing TGF- $\beta$ 1 and suppressing SC proliferation. Interestingly, other TGF- $\beta$  isoforms such as TGF- $\beta$ 2 activate HF stem cells by antagonizing BMP in the bulge<sup>53</sup>. In contrast to LAP1, however, LAP2 lacks the  $\alpha\beta_6$ -binding RGD motif<sup>54</sup>, and hence the release of TGF- $\beta$ 2 and BMP signaling are not affected by Kindlin-1 loss.

It is particularly interesting that high Kindlin-1 levels have also been associated with high TGF- $\beta$ 1 signaling in metastatic breast cancers<sup>55</sup>. Although it was not investigated how Kindlin-1 regulates TGF- $\beta$ 1 signaling, this observation, together with our findings, suggests that different tumor stages may benefit from different Kindlin-1 levels: in early stage tumors, low TGF- $\beta$  signaling supports tumor growth, whereas in late stage tumors, high TGF- $\beta$  signaling promotes the epithelial-to-mesenchymal transition and metastatic progression<sup>56</sup>. If this is the case, subjects with KS suffering from an increased tumor risk may be protected from metastasis.

We also found elevated Wnt- $\beta$ -catenin signaling in cutaneous epithelial cells of Kind1-K5 mice and the epidermis of subjects with KS, which is inevitably associated with a high tumor risk and severe SC and hair cycle defects<sup>13,50</sup>. The defect leads to ectopic HF formation and aberrant hair cycling and is due to aberrant expression of several Wnt ligands, most notably Wnt5a, which probably act in an auto-crine manner. Notably, chemical compounds that inhibit Wnt protein secretion or Wnt- $\beta$ -catenin signaling prevent the hair cycle and Wnt signaling defects in keratinocytes from Kind1-K5 mice.

Wnt5a is best known for the ability to activate the noncanonical Wnt signaling pathway. However, Wnt5a can also elicit canonical Wnt- $\beta$ -catenin signaling. The decision of which signaling pathway is induced is dictated by the type of cell surface receptor to which Wnt5a is binding: Wnt5a binding to the Ror2 receptor tyrosine kinase inhibits the transcriptional activity of  $\beta$ -catenin and thus canonical signaling, whereas Wnt5a binding to Fzd4 and the Lrp5/6 co-receptors leads to  $\beta$ -catenin stabilization and canonical Wnt signaling<sup>45</sup>. Interestingly, Wnt- $\beta$ -catenin signaling can activate Notch<sup>42</sup>, which is also elevated in keratinocytes from Kind1-K5 mice and may contribute at least in part to the Kind1-K5 mouse phenotype, for example, by suppressing *Wnt4* expression<sup>48</sup> and the recruitment of  $\beta$ -catenin to cell-cell junctions<sup>44</sup>. Clearly, the dysregulated expression of Wnt proteins and their receptors in Kind1-K5 mice strongly suggests that Kindlin-1 safeguards the skin and HFs against an overshooting activation of the important and at the same time potentially harmful canonical Wnt- $\beta$ -catenin signals.

In summary, our results show that Kindlin-1 loss results in a combination of defects caused by the dysregulation of distinct pathways: the compromised  $\beta_1$  integrins impair adhesion and induce an inflammatory response, the impaired TGF- $\beta$  liberation from LAP leads to HF SC hyperproliferation, and the increased Wnt signaling abrogates the resting phase of the hair cycle, expands the SC compartments and, together with impaired TGF- $\beta$  signaling and inflammation, contributes to the increased tumor risk. The high epithelial SC activity eventually leads to SC exhaustion and skin atrophy later in life, which is another hallmark of KS. It is also conceivable that the ability of Kindlin-1 to shuttle between integrin sites, where it mediates adhesion, migration and TGF- $\beta$  release, and the cytoplasm, where it

curbs Wnt- $\beta$ -catenin signaling, may also contribute to physiologic SC homeostasis and hair development (Fig. 6j); mobilization of bulge SCs has little or no integrin-ligand engagement and therefore uses Kindlin-1 to prevent Wnt- $\beta$ -catenin signaling and their activation. Once activated bulge SCs move to the hair germ, they engage integrins to ensure downward growth and therefore have less Kindlin-1 in the cytoplasm to inhibit Wnt- $\beta$ -catenin signaling.

## METHODS

Methods and any associated references are available in the [online version of the paper](#).

*Note: Any Supplementary Information and Source Data files are available in the online version of the paper.*

## ACKNOWLEDGMENTS

We thank J. Polleux for generating gold nanoarrays, S. Bach for expert technical assistance, C. Mein (Barts and the London Genome Centre) for generating the human microarray data and R. Zent and R. Paus for carefully reading the manuscript. We thank M. Aumailley (University of Cologne), R. Grosschedl (Max Planck Institute (MPI) Immunobiology), S. Violette (Biogen Idec), D. Sheppard (University of California, San Francisco) and M. Wegner (University of Erlangen) for providing antibodies and I. Thesleff (University of Helsinki), R. Kageyama (Kyoto University), A. Kispert (University of Hannover) and J. Behrens (University of Erlangen) for sending essential constructs. This work was funded by the US National Institutes of Health (CA034282) to D.B.R., the Wellcome Trust (PhD studentship to J.E.L.-C.) and the UK National Institute for Health Research (NIHR) Biomedical Research Centre based at Guy's and St. Thomas' National Health Service Foundation Trust and King's College London to J.A.M., the Advanced European Research Council (ERC) Grant (ERC Grant Agreement 322652) and the Max Planck Society to R.F.

## AUTHOR CONTRIBUTIONS

R.F. initiated the project. R.F. and E.R. designed the experiments and wrote the paper. E.R., D.K., M.W., M.J., R.R., S.U., R.T.B. and J.E.L.-C. performed experiments. E.R., M.W., M.J. and R.F. analyzed data. D.B.R. and J.A.M. provided important reagents and/or analytical tools. All authors read and approved the manuscript.

## COMPETING FINANCIAL INTERESTS

The authors declare no competing financial interests.

Reprints and permissions information is available online at <http://www.nature.com/reprints/index.html>.

- Meves, A., Stremmel, C., Gottschalk, K. & Fässler, R. The Kindlin protein family: new members to the club of focal adhesion proteins. *Trends Cell Biol.* **19**, 504–513 (2009).
- Lai-Cheong, J.E. *et al.* Kindler syndrome: a focal adhesion genodermatosis. *Br. J. Dermatol.* **160**, 233–242 (2009).
- Ussar, S. *et al.* Loss of Kindlin-1 causes skin atrophy and lethal neonatal intestinal epithelial dysfunction. *PLoS Genet.* **4**, e1000289 (2008).
- Montanez, E. *et al.* Kindlin-2 controls bidirectional signaling of integrins. *Genes Dev.* **22**, 1325–1330 (2008).
- Moser, M., Nieswandt, B., Ussar, S., Pozgajova, M. & Fässler, R. Kindlin-3 is essential for integrin activation and platelet aggregation. *Nat. Med.* **14**, 325–330 (2008).
- Dowling, J.J., Vreede, A.P., Kim, S., Golden, J. & Feldman, E.L. Kindlin-2 is required for myocyte elongation and is essential for myogenesis. *BMC Cell Biol.* **9**, 36 (2008).
- Lai-Cheong, J.E., Ussar, S., Arita, K., Hart, I.R. & McGrath, J.A. Colocalization of kindlin-1, kindlin-2, and migfilin at keratinocyte focal adhesion and relevance to the pathophysiology of Kindler syndrome. *J. Invest. Dermatol.* **128**, 2156–2165 (2008).
- He, Y., Esser, P., Heinemann, A., Bruckner-Tuderman, L. & Has, C. Kindlin-1 and -2 have overlapping functions in epithelial cells implications for phenotype modification. *Am. J. Pathol.* **178**, 975–982 (2011).
- Watt, F.M. Role of integrins in regulating epidermal adhesion, growth and differentiation. *EMBO J.* **21**, 3919–3926 (2002).
- Tumbar, T. *et al.* Defining the epithelial stem cell niche in skin. *Science* **303**, 359–363 (2004).
- Watt, F.M. & Jensen, K.B. Epidermal stem cell diversity and quiescence. *EMBO Mol. Med.* **1**, 260–267 (2009).
- Woo, W.M. & Oro, A.E. SnapShot: hair follicle stem cells. *Cell* **146**, 334–334 (2011).

13. Arwert, E.N., Hoste, E. & Watt, F.M. Epithelial stem cells, wound healing and cancer. *Nat. Rev. Cancer* **12**, 170–180 (2012).
14. Alonso, L. & Fuchs, E. Stem cells in the skin: waste not, Wnt not. *Genes Dev.* **17**, 1189–1200 (2003).
15. Watt, F.M. & Fujiwara, H. Cell–extracellular matrix interactions in normal and diseased skin. *Cold Spring Harb. Perspect. Biol.* **3**, a005124 (2011).
16. Janes, S.M. & Watt, F.M. New roles for integrins in squamous-cell carcinoma. *Nat. Rev. Cancer* **6**, 175–183 (2006).
17. Evans, R.D. *et al.* A tumor-associated  $\beta 1$  integrin mutation that abrogates epithelial differentiation control. *J. Cell Biol.* **160**, 589–596 (2003).
18. Ferreira, M., Fujiwara, H., Morita, K. & Watt, F.M. An activating  $\beta 1$  integrin mutation increases the conversion of benign to malignant skin tumors. *Cancer Res.* **69**, 1334–1342 (2009).
19. White, D.E. *et al.* Targeted disruption of  $\beta 1$ -integrin in a transgenic mouse model of human breast cancer reveals an essential role in mammary tumor induction. *Cancer Cell* **6**, 159–170 (2004).
20. Yu, Y. *et al.* Kindlin 2 forms a transcriptional complex with  $\beta$ -catenin and TCF4 to enhance Wnt signalling. *EMBO Rep.* **13**, 750–758 (2012).
21. Arita, K. *et al.* Unusual molecular findings in Kindler syndrome. *Br. J. Dermatol.* **157**, 1252–1256 (2007).
22. Emanuel, P.O., Rudikoff, D. & Phelps, R.G. Aggressive squamous cell carcinoma in Kindler syndrome. *Skinmed* **5**, 305–307 (2006).
23. Lai-Cheong, J.E. *et al.* Loss-of-function FERMT1 mutations in kindler syndrome implicate a role for fermitin family homolog-1 in integrin activation. *Am. J. Pathol.* **175**, 1431–1441 (2009).
24. Has, C. *et al.* Kindlin-1 is required for RhoGTPase-mediated lamellipodia formation in keratinocytes. *Am. J. Pathol.* **175**, 1442–1452 (2009).
25. Brakebusch, C. *et al.* Skin and hair follicle integrity is crucially dependent on  $\beta 1$  integrin expression on keratinocytes. *EMBO J.* **19**, 3990–4003 (2000).
26. Böttcher, R.T. *et al.* Sorting nexin 17 prevents lysosomal degradation of  $\beta 1$  integrins by binding to the  $\beta 1$ -integrin tail. *Nat. Cell Biol.* **14**, 584–592 (2012).
27. Braun, K.M. *et al.* Manipulation of stem cell proliferation and lineage commitment: visualisation of label-retaining cells in wholemounts of mouse epidermis. *Development* **130**, 5241–5255 (2003).
28. Fujiwara, H. *et al.* The basement membrane of hair follicle stem cells is a muscle cell niche. *Cell* **144**, 577–589 (2011).
29. Alonso, L. & Fuchs, E. Stem cells of the skin epithelium. *Proc. Natl. Acad. Sci. USA* **100** (suppl. 1), 11830–11835 (2003).
30. Jensen, K.B. *et al.* Lrig1 expression defines a distinct multipotent stem cell population in mammalian epidermis. *Cell Stem Cell* **4**, 427–439 (2009).
31. Munger, J.S. *et al.* The integrin  $\alpha 5\beta 6$  binds and activates latent TGF $\beta 1$ : a mechanism for regulating pulmonary inflammation and fibrosis. *Cell* **96**, 319–328 (1999).
32. Xie, Y., McElwee, K.J., Owen, G.R., Häkkinen, L. & Larjava, H.S. Integrin  $\beta 6$ -deficient mice show enhanced keratinocyte proliferation and retarded hair follicle regression after depilation. *J. Invest. Dermatol.* **132**, 547–555 (2012).
33. Li, L. & Bhatia, R. Stem cell quiescence. *Clin. Cancer Res.* **17**, 4936–4941 (2011).
34. Annes, J.P., Chen, Y., Munger, J.S. & Rifkin, D.B. Integrin  $\alpha 5\beta 6$ -mediated activation of latent TGF- $\beta$  requires the latent TGF- $\beta$  binding protein-1. *J. Cell Biol.* **165**, 723–734 (2004).
35. Kobiela, K., Stokes, N., de la Cruz, J., Polak, L. & Fuchs, E. Loss of a quiescent niche but not follicle stem cells in the absence of bone morphogenetic protein signaling. *Proc. Natl. Acad. Sci. USA* **104**, 10063–10068 (2007).
36. Zhang, J. *et al.* Bone morphogenetic protein signaling inhibits hair follicle anagen induction by restricting epithelial stem/progenitor cell activation and expansion. *Stem Cells* **24**, 2826–2839 (2006).
37. Gat, U., DasGupta, R., Degenstein, L. & Fuchs, E. *De novo* hair follicle morphogenesis and hair tumors in mice expressing a truncated  $\beta$ -catenin in skin. *Cell* **95**, 605–614 (1998).
38. Lo Celso, C., Prowse, D.M. & Watt, F.M. Transient activation of  $\beta$ -catenin signaling in adult mouse epidermis is sufficient to induce new hair follicles but continuous activation is required to maintain hair follicle tumours. *Development* **13**, 1787–1799 (2004).
39. Lowry, W.E. *et al.* Defining the impact of  $\beta$ -catenin/Tcf transactivation on epithelial stem cells. *Genes Dev.* **19**, 1596–1611 (2005).
40. Silva-Vargas, V. *et al.*  $\beta$ -catenin and Hedgehog signal strength can specify number and location of hair follicles in adult epidermis without recruitment of bulge stem cells. *Dev. Cell* **9**, 121–131 (2005).
41. Zhou, P., Byrne, C., Jacobs, J. & Fuchs, E. Lymphoid enhancer factor 1 directs hair follicle patterning and epithelial cell fate. *Genes Dev.* **9**, 700–713 (1995).
42. Estrach, S. *et al.* Jagged 1 is a  $\beta$ -catenin target gene required for ectopic hair follicle formation in adult epidermis. *Development* **133**, 4427–4438 (2006).
43. DasGupta, R. & Fuchs, E. Multiple roles for activated LEF/TCF transcription complexes during hair follicle development and differentiation. *Development* **126**, 4557–4568 (1999).
44. Bernard, P., Fleming, A., Lacombe, A., Harley, V.R. & Vilain, E. Wnt4 inhibits  $\beta$ -catenin/TCF signalling by redirecting  $\beta$ -catenin to the cell membrane. *Biol. Cell* **100**, 167–177 (2008).
45. Mikels, A.J. & Nusse, R. Purified Wnt5a protein activates or inhibits  $\beta$ -catenin–TCF signaling depending on receptor context. *PLoS Biol.* **4**, e115 (2006).
46. Chen, B. *et al.* Small molecule-mediated disruption of Wnt-dependent signaling in tissue regeneration and cancer. *Nat. Chem. Biol.* **5**, 100–107 (2009).
47. Huang, S.M. *et al.* Tankyrase inhibition stabilizes axin and antagonizes Wnt signalling. *Nature* **461**, 614–620 (2009).
48. Devgan, V., Mammucari, C., Millar, S.E., Brisken, C. & Dotto, G.P. p21WAF1/Cip1 is a negative transcriptional regulator of Wnt4 expression downstream of Notch1 activation. *Genes Dev.* **19**, 1485–1495 (2005).
49. Guasch, G. *et al.* Loss of TGF $\beta$  signaling destabilizes homeostasis and promotes squamous cell carcinomas in stratified epithelia. *Cancer Cell* **12**, 313–327 (2007).
50. Beronja, S. *et al.* RNAi screens in mice identify physiological regulators of oncogenic growth. *Nature* **501**, 185–190 (2013).
51. Bandyopadhyay, A., Rothschild, G., Kim, S., Calderwood, D.A. & Raghavan, S. Functional differences between kindlin-1 and kindlin-2 in keratinocytes. *J. Cell Sci.* **125**, 2172–2184 (2012).
52. Ussar, S., Wang, H.V., Linder, S., Fässler, R. & Moser, M. The Kindlins: subcellular localization and expression during murine development. *Exp. Cell Res.* **312**, 3142–3151 (2006).
53. Oshimori, N. & Fuchs, E. Paracrine TGF- $\beta$  signaling counterbalances BMP-mediated repression in hair follicle stem cell activation. *Cell Stem Cell* **10**, 63–75 (2012).
54. Annes, J.P. *et al.* Making sense of latent TGF $\beta$  activation. *J. Cell Sci.* **116**, 217–224 (2003).
55. Sin, S. *et al.* Role of the focal adhesion protein kindlin-1 in breast cancer growth and lung metastasis. *J. Natl. Cancer Inst.* **103**, 1323–1337 (2011).
56. Chaudhury, A. & Howe, P.H. The tale of transforming growth factor- $\beta$  (TGF $\beta$ ) signaling: a soigné enigma. *IUBMB Life* **61**, 929–939 (2009).

## ONLINE METHODS

**Mouse strains.** The conditional *Fermt-1<sup>lox/flox</sup>* mice carry a *loxP*-flanked ATG-containing exon 2 (Supplementary Fig. 1a) and were generated by electroporation of R1 embryonic stem cells using standard procedures<sup>57</sup>. Homologous recombination was verified with Southern blots, and positive embryonic stem cell clones were used to generate chimeric mice. Mice were crossed with transgenic mice carrying a deleter-flp recombinase to remove the neomycin cassette and with mice carrying deleter-Cre (to confirm the null phenotype) or K5-Cre transgenes, respectively<sup>58</sup>. For all animal studies, transgenic mice were backcrossed eight times to C57BL/6 mice. The TTAA-K5 transgenic mice were obtained through an intercross of mice carrying alanine substitutions of T788 and T789 in the cytoplasmic domain of  $\beta_1$  integrin<sup>26</sup> with *Itgb1*-floxed mice and K5-Cre transgenic mice. The TOPgal Wnt reporter mice<sup>43</sup> were intercrossed with Kind1-K5 mice. For all *in vivo* experiments, genders were distributed randomly between the genotypes. Mice were housed in a special pathogen-free mouse facility, and all animal experiments were carried out according to the rules of and approved by the government of Upper Bavaria.

**DMBA and TPA tumor experiment.** Cutaneous two-stage chemical carcinogenesis was performed as previously described<sup>59</sup> using topical applications of 100 nmol (25  $\mu$ g) DMBA (Sigma) in 100  $\mu$ l of acetone and twice weekly applications of 10 nmol (6.1  $\mu$ g) TPA (Sigma) in 200  $\mu$ l of acetone or only acetone for 25 weeks. The tumor model was terminated after 25 weeks of TPA promotion because of the critical skin health condition of Kind1-K5 mice. For tumor experiments, control animals were treated with acetone or TPA only. For all animal studies, 7-week-old mice were randomized after genotyping, and sample size was estimated by nonparametric Wilcoxon test (*U* test). The number and size of tumors were recorded once per week after the start of promotion (week 0). All mice were euthanized at the end of the experiment. Skin lesions were analyzed by histology and graded as described previously<sup>59–61</sup>.

**Subjects with KS.** Individuals with KS gave their informed written consent under protocols approved by St. Thomas' Hospital Ethics Committee (COREC number 06/Q0702/154), and the study was conducted according to the Declaration of Helsinki Principles. For immunofluorescence (IF) analysis, biopsies were taken from age- and site-matched controls (NHS) and subjects with KS with the following mutations: KS patient 1 (3-year-old Indian girl; homozygous nonsense mutation *+/+ p.Glu516X*) and KS patient 2 (22-year-old Panamanian woman; homozygous nonsense mutation *+/+ p.Arg271X*).

RNA for microarray analysis was isolated from upper-arm biopsies taken from three subjects with KS; KS patient A, a 22-year-old Omani woman with the homozygous nonsense mutation *+/+ p.Arg271X*; KS patient B, a 7-year-old Indian girl with the homozygous nonsense mutation *+/+ p.Try616X*; and KS patient C, a 19-year-old Omani woman with the nonsense mutation *+/+ p.Try616X*. Control skin RNA was isolated from four age-, site- and sex-matched biopsies.

**Gene expression microarray.** Total RNA was extracted using the RNeasy Fibrous Tissue Mini kit (Qiagen), and quantity and quality were measured on a Nanodrop spectrophotometer (Nanodrop, Wilmington, DE, USA). For whole-genome Illumina expression analysis, total RNA from each skin biopsy was hybridized to an Illumina Human-Ref-6 v2 BeadChip expression array (Illumina, San Diego, CA, USA). The Illumina HumanRef-6 v2 BeadChips were scanned with an Illumina Bead Array Reader confocal scanner.

The microarray data analysis was performed using Illumina's BeadStudio Data Analysis Software (Illumina). The expression signals for all genes from each individual were grouped in KS and NHS and averaged. In order to identify statistically significant differentially regulated genes, a prefiltering set was determined for significantly higher ( $\geq 2$ -fold change) and lower ( $\leq 0.5$ -fold change) expression intensity between KS and NHS skin samples. Bonferroni's correction was applied to each *P* value to obtain an adjusted *P* value to identify differentially expressed mRNAs with high statistical significance (Supplementary Table 2). The microarray data have been submitted to NCBI under the GEO accession number GSE47642.

**FACS analysis.** FACS analysis and sorting was performed as previously described<sup>62</sup>. A suspension of primary keratinocytes in FACS-PBS (PBS with

1% BSA) was incubated for 1 h with primary antibodies on ice and then washed twice with FACS-PBS. Cell viability was assessed by 7-aminoactinomycin labeling (BD Biosciences) or ethidium monoazide staining (Invitrogen). FACS analysis was carried out using a FACSCantoTMII cytometer (BD Biosciences) and cell sorting with an AriaFACSII high-speed sorter (BD Biosciences), both of which were equipped with FACS DiVa software (BD Biosciences). Purity of the sorted cells was determined by post-sort FACS analysis and typically exceeded 95%. Integrin surface FACS analysis of primary keratinocytes was carried out as previously described<sup>63</sup>. Data analysis was conducted using the FlowJo program (version 9.4.10).

**Real-time PCR and Notch target gene inhibition.** Total RNA from total skin or FACS-sorted keratinocytes was extracted with the RNeasy Mini extraction kit (Qiagen) following the manufacturer's instructions. For Notch target gene inhibition analysis, cells were plated on fibronectin- and collagen I-coated six-well plates (1.2  $\times 10^6$  cells per well) and were treated the next day with 2.5  $\mu$ M N-[N-(3,5-difluorophenacetyl)-L-alanyl]-S-phenylglycine t-butyl ester (DAPT; Selleckchem, S2215) in full keratinocyte growth medium (KGM) for 24 h before total RNA isolation. cDNA was prepared with an iScript cDNA Synthesis Kit (Biorad). Real-time PCR was performed with an iCycler (Biorad). Each sample was measured in triplicate, and values were normalized to *Gapdh*. The PCR primers used are listed in Supplementary Table 4.

**Antibodies and inhibitors.** The following antibodies or molecular probes were used at the indicated concentrations for western blot (W), IF, immunohistochemistry (IHC) or flow cytometry (FACS): Kindlin-1 (home made<sup>3</sup>; W: 1:5,000, IF of tissue: 1:1,000), Kindlin-2 (Sigma; K3269; W: 1:1,000), talin (Sigma; 8D4; W: 1:1,000), GAPDH (Calbiochem; 6C5; W: 1:10,000), phalloidin-Alexa 488 (Invitrogen; A12379; IF tissue: 1:500; IF of cells: 1:800), integrin  $\alpha_M$  (Mac-1) (eBioscience; M1/70; IF of tissue: 1:200), GR1 (Ly6g) (eBioscience; RB6-8C5; IF of tissue: 1:200), CD4 (PharMing; H129.19; IF of tissue: 1:200), CD19 (PharMing; 1D3; IF of tissue: 1:200), integrin  $\alpha_x$  (CD11c) (BD Bioscience; HL3; IF of tissue: 1:200), desmoplakin (Fritzgerald Industries International; 20R-DP002; IF tissue: 1:500), integrin  $\alpha_6$  (Itga6) (PharMingen; GoH3; IF of tissue: 1:200, FACS: 1:500), laminin-332 (a gift from M. Aumailley, University of Cologne, Germany; IF of tissue: 1:500), Keratin-10 (Krt-10) (Covance; PRB-159P; IHC: 1:600), Keratin-15 (Krt-15) (a gift from R. Grosschedl; MPI Immunobiology, Freiburg, Germany; IF: 1:500), Lef1 (a gift from R. Grosschedl, MPI Immunobiology, Freiburg, Germany; IF of tissue: 1:500), Loricrin (Lor) (Covance; PRB-145P; IF: 1:500), Ki67 (Dianova; M7249; IHC: 1:100), cleaved caspase-3 (Asp175, cCaspase3) (Cell Signaling; 9661; IF of tissue: 1:200), CD34 (BD Bioscience; RAM34; IF of tissue: 1:200, FACS: 1:100), Sca1 (BioLegend; D7; IF of tissue: 1:200, FACS: 1:200), Lrig1 (R&D Systems, AF3688; IF: 1:500), BrdU (Abcam; ab6326; IF: 1:500), Keratin-5 (Krt-5) (Covance; PRB-160P; IF: 1:1,000), Keratin-6 (Krt-6) (Covance; PRB-169; IF: 1:500), CDP (Santa Cruz; sc-13024; IF: 1:500), integrin  $\beta_1$  (BD Biosciences; Ha2/5; FACS: 1:200), integrin  $\beta_3$  (BD Bioscience; 2C3.G2; FACS: 1:200), integrin  $\beta_4$  (BD Biosciences; 346-11A; FACS: 1:200), integrin  $\beta_6$  CH2A1 (Itgb6) (a gift from S. Violette, Biogen Idec; IF of mouse tissue: 1:500), integrin  $\beta_6$  (Itgb6) (Chemicon; 10D5; IF of human tissue: 1:200, FACS: 1:200, IF of cells: 1:500), integrin  $\beta_5$  (Itgb5) (a gift from D. Sheppard, University of California, USA; FACS: 1:200), integrin  $\beta_8$  (Itgb8) (Santa Cruz; sc-25714; FACS: 1:200), paxillin (BD Bioscience; 610051; IF: 1:500); pSMAD2/3 (Santa Cruz, sc11769; IF: 1:200), pSmad2 (Millipore; AB3849; W: 1:2,000), total Smad2/3 (Santa Cruz; sc-8332; W: 1:1,000), pSMAD1/5/8 (Millipore; AB3848; IF of tissue: 1:200), Sox9 (a gift from M. Wegner, University of Erlangen, Germany; IF of tissue: 1:500), trichohyalin (AE15) (Abcam; ab58755; IF of tissue: 1:500), activated Notch1 (NICD) (Abcam, ab8925; IF of tissue: 1:200) and pan-laminin (Sigma; L9393; IF of tissue: 1:500). The following secondary antibodies were used: goat anti-rabbit Alexa 488 (A11008), goat anti-human Alexa 488 (A11013), goat anti-mouse Alexa 488 (A11029), donkey anti-goat Alexa 488 (A11055), goat anti-guinea pig Alexa 594 (A11076), goat anti-mouse Alexa 546 (A11003), goat anti-rabbit Alexa 546 (A11010) (all from Invitrogen; FACS: 1:500, IF: 1:500), streptavidin-Cy5 (Dianova; 016170084; FACS: 1:400), goat anti-rat horseradish peroxidase (HRP) (Dianova; 712035150; W: 1:10,000), goat anti-mouse HRP (172-1011) and goat anti-rabbit HRP (172-1019) (all from Biorad; W: 1:10,000). For mouse monoclonal primary antibodies the M.O.M. (Mouse on Mouse) kit

(Vector Labs) was used according to the manufacturer's protocol. Mast cells were stained for mast cell heparin with avidin-FITC (Invitrogen; 43-4411; IF of tissue: 1:100) as previously described<sup>64</sup>. Nuclei were stained with DAPI (Sigma).

The Notch signaling inhibitor DAPT (Selleckchem; S2215) was dissolved in ethanol at 25  $\mu\text{g } \mu\text{l}^{-1}$ . The Wnt inhibitors IWP-2 (Calbiochem; 681671) and IWR-1 (Sigma; I0161) were dissolved in DMSO at 2.5  $\mu\text{g } \mu\text{l}^{-1}$  (IWP-2) or 10  $\mu\text{g } \mu\text{l}^{-1}$  (IWR-1).

**BrdU labeling.** The LRC assay was performed as previously described<sup>27</sup>. Briefly, 10-day-old mice were injected four times with 50 mg  $\text{kg}^{-1}$  body weight BrdU every 12 h to label mitotic cells, and then mice were maintained for the indicated chase periods. To determine LRCs per HF bulge, tail epidermal whole mounts were prepared,  $z$  projections were acquired using a Leica SP5 confocal microscope (20 $\times$  objective), and BrdU-positive cells were counted from  $\geq 30$  HFs per animal from different whole mounts.

**Cell culture.** The TGF- $\beta$  reporter cell line tMLEC and LTBP1-TGF- $\beta$  matrix-producing CHO-LTBP1 cells were used as described previously<sup>34</sup>. Primary keratinocytes were isolated at P21 or at the indicated time points as described previously<sup>65</sup>. To generate clonal keratinocyte cell lines, primary cells from *Fermt1*<sup>fllox/fllox</sup> mice were spontaneously immortalized, single clones were picked, and Kindlin-1 ablation was induced by transient transfection with an adenovirus expressing Cre recombinase. Keratinocytes were cultured in KGM containing 8% chelated FCS (Invitrogen) and 45  $\mu\text{M}$   $\text{Ca}^{2+}$  in a 5%  $\text{CO}_2$  humidified atmosphere on plastic dishes coated with a mixture of 30  $\mu\text{g } \text{ml}^{-1}$  collagen I (Advanced BioMatrix) and 10  $\mu\text{g } \text{ml}^{-1}$  fibronectin (Invitrogen).

**Inhibition of premature anagen induction and increased Notch signaling.** At telogen onset (P49), back skin of control and Kind1-K5 mice was shaved, and 100  $\mu\text{l}$  of 200  $\mu\text{M}$  IWR-1 or IWP-2 (diluted in PBS) was subcutaneously injected every 24 h into a marked skin region. 100  $\mu\text{l}$  DMSO diluted in PBS was used for control experiments. At P56, the treated back skin was isolated, sectioned and stained with H&E. Ten serially sectioned HFs per animal were counted. To analyze Notch signaling, back skin sections were stained for NICD, and NICD-positive nuclei were quantified.

**Constructs and transfections.** Wnt4 expression constructs were gifts from A. Kispert (University of Hannover, Germany), and the human  $\beta$ -catenin expression construct was a gift from J. Behrens (University of Erlangen, Germany). Human WNT5A (ID18032), LEF1 (ID16709), pHes1-luc (ID43806), SuperTOPFlash (ID17165) and FOPFlash (ID12457) reporter plasmids were purchased from Addgene. The pEGFP-C1 expression vector was acquired from Clontech.

GFP-tagged Kindlin-1, Kindlin-2 and Kindlin-1-QWAA expression constructs were described previously<sup>3</sup>, and the Kindlin1-NLS construct was generated by fusing SV40 NLS motifs to the N terminus of Kindlin-1. The expression cassettes were driven by a CAG promoter and flanked by two inverted terminal repeat sites recognized by sleeping beauty transposase 100 $\times$  (SB100 $\times$ )<sup>66</sup> and transiently co-transfected with the SB100 $\times$  vector in a 1:1 ratio using Lipofectamine 2000 (Invitrogen) following the manufacturer's instructions. After two passages, cells stably expressing the GFP fusion protein were FACS sorted for equal expression levels, which was further confirmed by western blotting.

**Histology and immunostainings.** Small pieces from back skin were either fixed in paraformaldehyde (PFA) and embedded in paraffin or frozen on dry ice in cryo-matrix (Thermo) and sectioned. Tail skin whole mounts were prepared and immunostained as described<sup>27</sup>. Immunohistochemistry (H&E, DAB, Oil Red O, alkaline phosphatase (AP) and  $\beta$ -gal) of skin sections and tail whole mounts and immunofluorescence staining of tissue sections were carried out as described<sup>25</sup>. To better visualize the blue  $\beta$ -gal stain, the epidermal whole mount was overlaid with a grayscale image. Immunostaining of human skin sections for  $\beta_6$  integrin followed published protocols<sup>67</sup>.

HF bulge sizes were quantified in epidermal tail whole mounts stained for Krt-15, and  $z$  projections were collected with a confocal microscope using a 20 $\times$  objective. The length and diameter of a Krt-15-positive bulge area was measured with the ImageJ software (version 1.41n), and bulge volumes were calculated using the circular cylinder formula ( $v = \pi \times r^2 \times h$ , where  $v$  is the

volume,  $r$  is the radius, and  $h$  is the height). The HF numbers were quantified in serial sections of comparable back skin regions from at least three mice per genotype and the indicated ages. HFs per 10 $\times$  objective field of H&E-stained sections were counted. HFs in anagen and early HF development were staged as described previously<sup>68,69</sup>.

Images were collected by confocal microscopy (DMIRE2 or SP5, Leica) with a 10 $\times$ , 20 $\times$  numerical aperture (NA) 1.4 or 40 $\times$  oil objective using Leica Confocal software (version 2.5 build 1227) or by bright field microscopy (Axioskop, Carl Zeiss with a 10 $\times$  NA 0.3, 20 $\times$  NA 0.5 or 40 $\times$  NA 0.75 objective) and DC500 camera with IM50 software (Leica).

**In situ hybridization.** Antisense riboprobes for mouse *Fzd4* (SpeI-EcoRI fragment of mouse FZD4 3' untranslated region), *Wnt5a* (gift from I. Thesleff, University of Helsinki, Finland) and *Hes1* (gift from R. Kageyama, Kyoto University, Japan) were synthesized with T7 RNA polymerase (New England BioLabs) and DIG (digoxigenin) RNA Labeling Mix according to the manufacturer's instructions (Roche). Isolated tail skin epidermis was fixed in 4% PFA in PBS, washed in PBS for 5 min twice and then washed twice for 15 min in PBS with 0.1% active diethylpyrocarbonate followed by 15 min equilibration in 5 $\times$  saline-sodium citrate (SSC). Samples were first prehybridized for 1 h at 58  $^{\circ}\text{C}$  in 50% formamide, 5 $\times$  SSC and 40  $\mu\text{g } \text{ml}^{-1}$  salmon sperm DNA, then hybridized for 16 h at 58  $^{\circ}\text{C}$  with 400  $\text{ng } \text{ml}^{-1}$  of DIG-labeled probe in prehybridization mix and washed twice for 30 min in 2 $\times$  SSC at room temperature, followed by a 60-min wash at 65  $^{\circ}\text{C}$  in 2 $\times$  SSC and then a 60-min wash at 65  $^{\circ}\text{C}$  in 0.2 $\times$  SSC. The tissues were washed in Tris-buffered saline (TBS) for 5 min three times, blocked in 0.5% blocking reagent (Roche) in 0.1% Tween 20 and TBS (TBST) for 90 min at room temperature and then incubated in 1:5,000-diluted anti-DIG AP (Roche) in 0.5% blocking reagent in TBST at 4  $^{\circ}\text{C}$  overnight. After three 60-min washes in TBST, tissues were incubated in NTMT (100 mM NaCl, 100 mM Tris, pH 9.5, 50 mM  $\text{MgCl}_2$  and 0.1% Tween 20) for 10 min at room temperature. Color was developed using BM Purple AP substrate precipitating reagent (Roche) at 37  $^{\circ}\text{C}$ . The reaction was stopped for 15 min with TE buffer (10 mM Tris and 1 mM EDTA, pH 8.0), and samples were mounted with 70% glycerol.

**Peptide pulldowns.** Pulldowns were performed with  $\beta_1$  WT tail peptide (HDDR EFAKFEKEKMNAKWDGTGENPIYKSAVTTVVPKYEGK-OH),  $\beta_1$  scrambled peptide (EYEFEPDKVDGTGAKGTMAKNEKKFRNYTVHNIWESRKV AP-OH),  $\beta_6$  WT tail peptide (HDRKEVAKFEAERSKAKWQTGTNPLYRGST STFKNVTYKHREKHKAGLSSDG-OH) and  $\beta_6$  scrambled peptide (KTDHAV QGDKKLSHKKNRGTSKATFPKVRHYETEEWAALESYGSRFTKNSR-OH). All peptides were desthiobiotinylated. Before use, peptides were immobilized on 35  $\mu\text{l}$  Dynabeads MyOne Streptavidine C1 (10 mg  $\text{ml}^{-1}$ ; Invitrogen) for 3 h at 4  $^{\circ}\text{C}$ .

Keratinocytes were lysed on ice in Mammalian Protein Extraction Reagent (Thermo Scientific), and 1 mg of cell lysate was incubated with the indicated peptides for 4 h at 4  $^{\circ}\text{C}$ . After three washes with lysis buffer, the beads were boiled in SDS-PAGE sample buffer, and the supernatant was loaded on 8% SDS-PAGE gels.

**Preparation of  $\alpha_v\beta_6$  antibody-coated coverslips.** Antibody coating was carried out as described<sup>70</sup>. Briefly, glass slides (24 mm  $\times$  24 mm; Menzel) were sterilized, coated with collagen I (Advanced BioMatrix) for 1 h at 37  $^{\circ}\text{C}$ , air dried, covered with nitrocellulose dissolved in methanol and air dried again. Slides were incubated with  $\alpha_v\beta_6$ -specific antibody (10D5; 10  $\mu\text{g } \text{ml}^{-1}$ ; Chemicon) diluted in PBS overnight at 4  $^{\circ}\text{C}$  in a humidity chamber, washed once with PBS and blocked with 1% BSA for 1 h at room temperature.

**Generation of dense gold nanoarrays functionalized with cRGD.** In a typical synthesis, 7 mg  $\text{ml}^{-1}$  of polystyrene<sub>154</sub>-block-poly(2-vinylpyridine)<sub>33</sub> (PS<sub>154</sub>-*b*-P2VP<sub>33</sub>; Polymer Source) was dissolved at room temperature in *p*-xylene (Sigma) and stirred for 2 d. Hydrogen tetrachloroaurate (III) trihydrate ( $\text{HAuCl}_4 \cdot 3\text{H}_2\text{O}$ ; Sigma) was added to the block co-polymer solution (1  $\text{HAuCl}_4$  per 2 P2VP units) and stirred for 2 d in a sealed glass vessel. Glass coverslips (Carl Roth) were cleaned in a piranha solution for at least 2 h and rinsed extensively with MilliQ water and dried under a stream of nitrogen. Micellar monolayers were prepared by dip coating a glass coverslip into previously prepared solutions with a constant

velocity equal to 24 mm min<sup>-1</sup>. The dip-coated glass slides were exposed to oxygen plasma (150 W, 0.15 mbar, 45 min; PVA TEPLA 100 Plasma System). To prevent nonspecific protein adsorption or cell binding, the glass background was covalently modified with silane-terminated polyethylene glycol (PEG; molecular weight 2,000) (ref. 71). Thiol-terminated cRGD was synthesized as described before<sup>72</sup>. The gold nanoparticles were then functionalized with this ligand by incubating the PEG-functionalized substrates in 100 µl of a 50 µM aqueous solution. The substrates were then rinsed thoroughly, incubated overnight with water and finally dried with nitrogen.

**Spreading assay.** A single-cell suspension with  $1.0 \times 10^5$  cells per well in a six-well plate was plated in serum-free KGM (1% BSA and 1% penicillin-streptomycin) on fibronectin-coated glass coverslips (10 µg ml<sup>-1</sup> fibronectin in PBS for 1 h at room temperature) or the indicated substrates for 3 h at 37 °C. Cells were imaged by a bright-field Axiovert 40 CFL microscope (20× objective; Carl Zeiss) and a CV640 camera (Prosilica) before fixation in 4% PFA-PBS and immunostaining with the indicated antibodies. The spreading area was quantified after staining with phalloidin-Alexa 488 (Invitrogen) with an AxioImager Z1 microscope (20× objective; Carl Zeiss) using the ImageJ software (Version 1.41n).

**TGF-β stimulation assays.** Keratinocytes were starved for several hours and stimulated with 5 ng ml<sup>-1</sup> recombinant human TGF-β1 (PEROTech) in serum-free KGM for the indicated times, lysed and analyzed by western blotting. TGF-β-modulated proliferation was determined in 70% confluent keratinocytes that were cultured in six-well plates, incubated for 8 h with 10 µM 5-ethynyl-2'-deoxyuridine (EdU; Invitrogen) and the indicated concentrations of TGF-β1 and analyzed with the Click-iT EdU Alexa Fluor488 Flow Cytometry Assay kit (Invitrogen).

**TGF-β release assay.** TGF-β release was determined as described<sup>34</sup>. Briefly, CHO-LTBP1 cells were seeded ( $5.0 \times 10^4$  cells per well) for 48 h in a 96-well plate in triplicates to deposit an LTBP1-TGF-β-rich matrix. Cells were then detached with PBS and 15 mM EDTA, and the remaining LTBP1-TGF-β-rich matrix was washed twice with PBS and incubated with keratinocytes ( $2.0 \times 10^4$  cells per well) and tMLEC cells ( $1.5 \times 10^4$  cells per well) in a 100 µl final volume either in the absence or presence of α<sub>v</sub>β<sub>6</sub> integrin-blocking antibody (10D5; 20 µg ml<sup>-1</sup>; Chemicon) or TGF-β neutralizing antibody (1D11; 15 µg ml<sup>-1</sup>; BD Biosciences). The amount of released TGF-β was measured after 16–24 h using a Bright Glo luciferase kit (Promega).

**Wnt and Notch reporter assay.** Cells were plated on fibronectin- and collagen I-coated 12-well plates ( $6.0 \times 10^5$  cells per well) before transient transfection with 0.5 µg of pHes1-luc, SuperTOPFLASH or SuperFOPFLASH reporter, the indicated expression plasmid and 50 ng thymidine kinase-driven *Renilla* (Promega) for controlling the transfection efficiency. The total amount of transfected plasmid DNA was kept constant at 1.5 µg per well using the pEGFP-C1 expression vector as a transfection control (Clontech). After 24 h (Wnt reporter) or 48 h (Notch reporter), luciferase activity was analyzed with a Dual Luciferase reporter assay system (Promega). To determine the effect of Wnt or Notch signaling, cells were treated with the indicated inhibitor 18 h after transfection, and luciferase activity was measured 24 h later.

**Statistical analyses.** Analyses were performed with GraphPad Prism software (version 5.00, GraphPad Software). Experiments were routinely repeated at least three times, and the repeat number was increased according to effect size or sample variation. If not mentioned otherwise in the figure legend, statistical significance (\* $P < 0.05$ ; \*\* $P < 0.01$ ; \*\*\* $P < 0.001$ ; NS, not significant) was determined by unpaired *t* test (for biological effects with assumed normal distribution), Wilcoxon *t* test or Mann-Whitney *U* test. In the boxplots, the middle line represents the median, the box ends represent the 25th and 75th percentiles, the whisker ends show the minimum and maximum distribution or are at the 1.5-interquartile range, and outliers are shown as dots, as indicated in the figure legend. Unbiased and reproducible identification of cells with positive nuclear staining for β-catenin, Lef1 and NICD was ensured by quantification of nuclear staining intensities with ImageJ tool (version 1.41n).

57. Fässler, R. & Meyer, M. Consequences of lack of β1 integrin gene expression in mice. *Genes Dev.* **9**, 1896–1908 (1995).
58. Ramirez, A. *et al.* A keratin K5Cre transgenic line appropriate for tissue-specific or generalized Cre-mediated recombination. *Genesis* **39**, 52–57 (2004).
59. Abel, E.L., Angel, J.M., Kiguchi, K. & DiGiovanni, J. Multi-stage chemical carcinogenesis in mouse skin: fundamentals and applications. *Nat. Protoc.* **4**, 1350–1362 (2009).
60. Kasper, M. *et al.* Wounding enhances epidermal tumorigenesis by recruiting hair follicle keratinocytes. *Proc. Natl. Acad. Sci. USA* **108**, 4099–4104 (2011).
61. Sundberg, J.P., Sundberg, B.A. & Beamer, W.G. Comparison of chemical carcinogen skin tumor induction efficacy in inbred, mutant, and hybrid strains of mice: morphologic variations of induced tumors and absence of a papillomavirus cocarcinogen. *Mol. Carcinog.* **20**, 19–32 (1997).
62. Jensen, K.B., Driskell, R.R. & Watt, F.M. Assaying proliferation and differentiation capacity of stem cells using disaggregated adult mouse epidermis. *Nat. Protoc.* **5**, 898–911 (2010).
63. Lorenz, K. *et al.* Integrin-linked kinase is required for epidermal and hair follicle morphogenesis. *J. Cell Biol.* **177**, 501–513 (2007).
64. Kunder, C.A. *et al.* Mast cell-derived particles deliver peripheral signals to remote lymph nodes. *J. Exp. Med.* **206**, 2455–2467 (2009).
65. Montanez, E. *et al.* Analysis of integrin functions in peri-implantation embryos, hematopoietic system, and skin. *Methods Enzymol.* **426**, 239–289 (2007).
66. Mâtès, L. *et al.* Molecular evolution of a novel hyperactive Sleeping Beauty transposase enables robust stable gene transfer in vertebrates. *Nat. Genet.* **41**, 753–761 (2009).
67. Brown, J.K. *et al.* Integrin-α<sub>v</sub>β<sub>6</sub>, a putative receptor for foot-and-mouth disease virus, is constitutively expressed in ruminant airways. *J. Histochem. Cytochem.* **54**, 807–816 (2006).
68. Müller-Röver, S. *et al.* A comprehensive guide for the accurate classification of murine hair follicles in distinct hair cycle stages. *J. Invest. Dermatol.* **117**, 3–15 (2001).
69. Paus, R. *et al.* A comprehensive guide for the recognition and classification of distinct stages of hair follicle morphogenesis. *J. Invest. Dermatol.* **113**, 523–532 (1999).
70. Shi, Q. & Boettiger, D. A novel mode for integrin-mediated signaling: tethering is required for phosphorylation of FAK Y397. *Mol. Biol. Cell* **14**, 4306–4315 (2003).
71. Blümmel, J. *et al.* Protein repellent properties of covalently attached PEG coatings on nanostructured SiO<sub>2</sub>-based interfaces. *Biomaterials* **28**, 4739–4747 (2007).
72. Morales-Avila, E. *et al.* Multimeric system of 99mTc-labeled gold nanoparticles conjugated to c[RGDFK(C)] for molecular imaging of tumor α<sub>v</sub>β<sub>3</sub> expression. *Bioconjug. Chem.* **22**, 913–922 (2011).

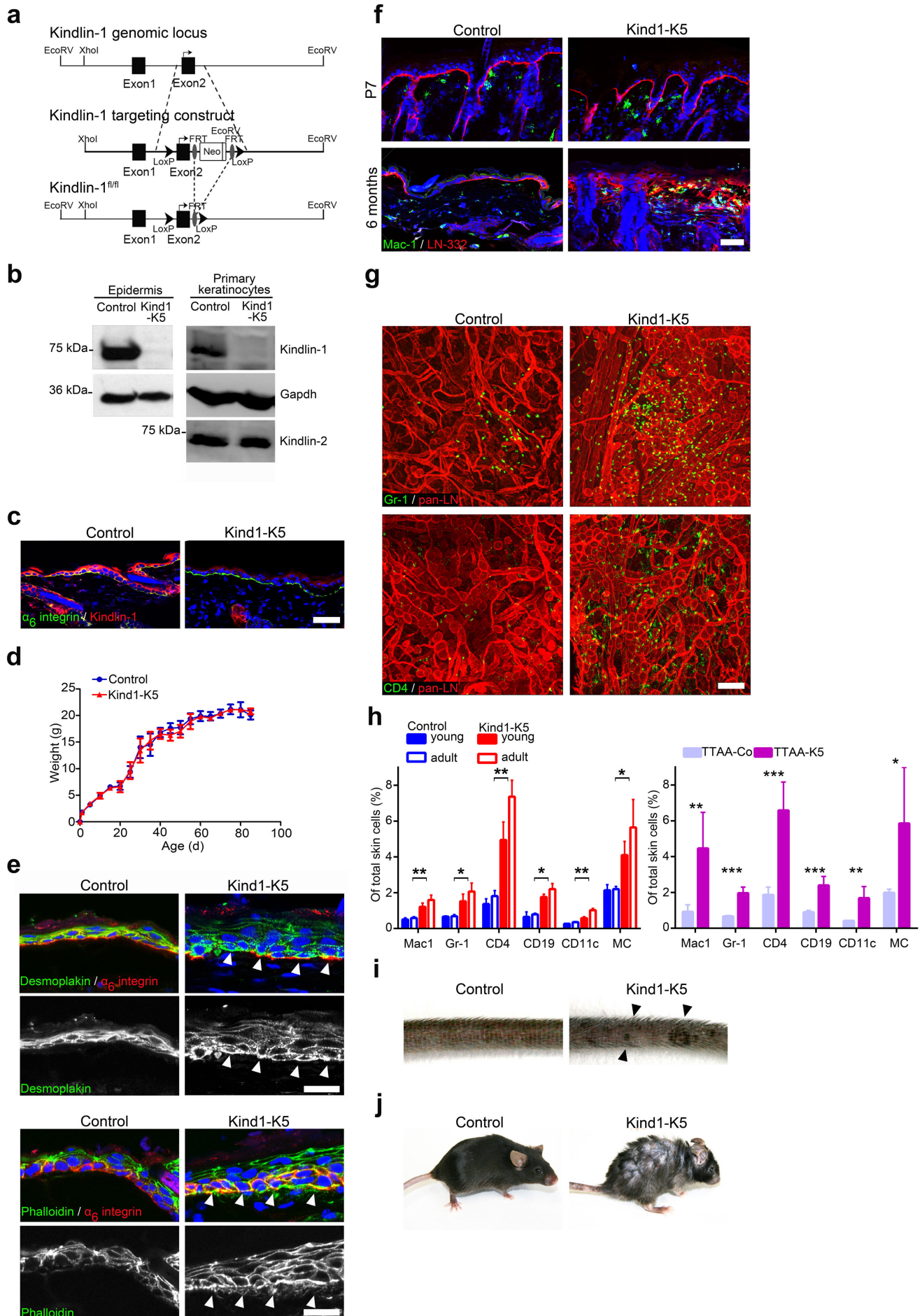
# Supplementary Information

## **Kindlin-1 controls cutaneous epithelial stem cell proliferation by modulating Wnt ligand and TGF $\beta$ availability**

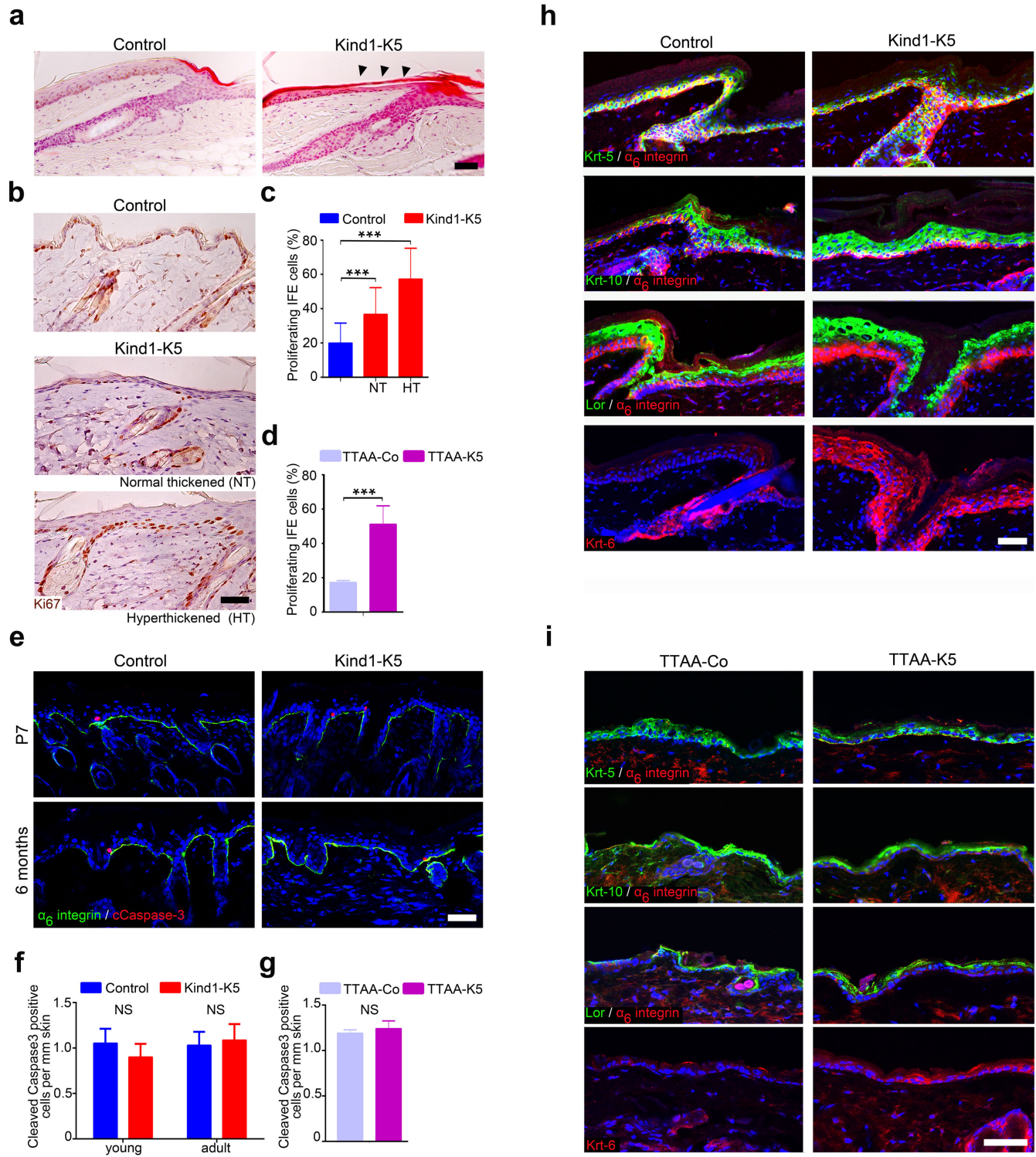
Emanuel Rognoni, Moritz Widmaier, Madis Jakobson, Raphael Ruppert, Siegfried Ussar,  
Despoina Katsougkri, Ralph T. Böttcher, Joey E. Lai-Cheong, Daniel B. Rifkin, John A.  
McGrath, Reinhard Fässler

Supplementary Figure 1–8

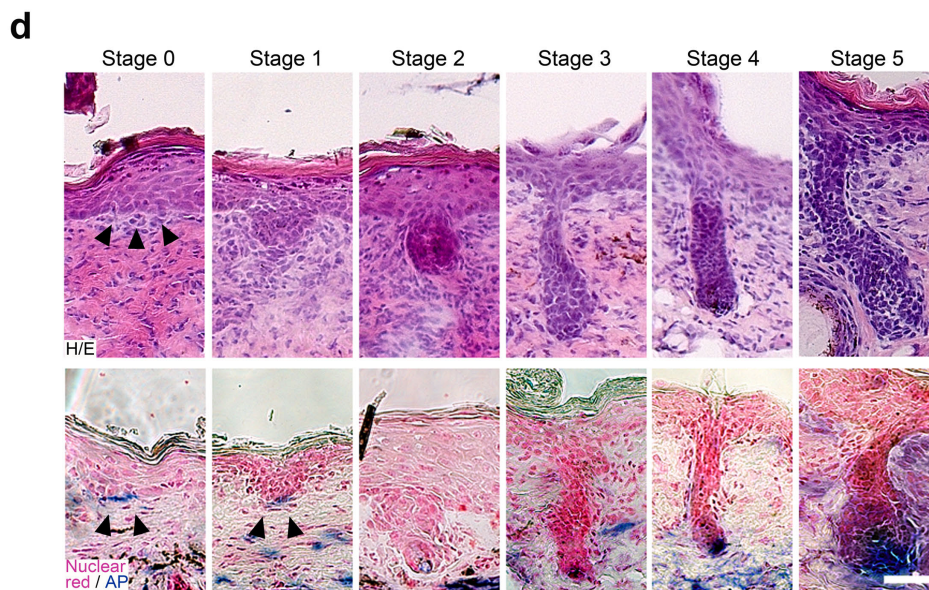
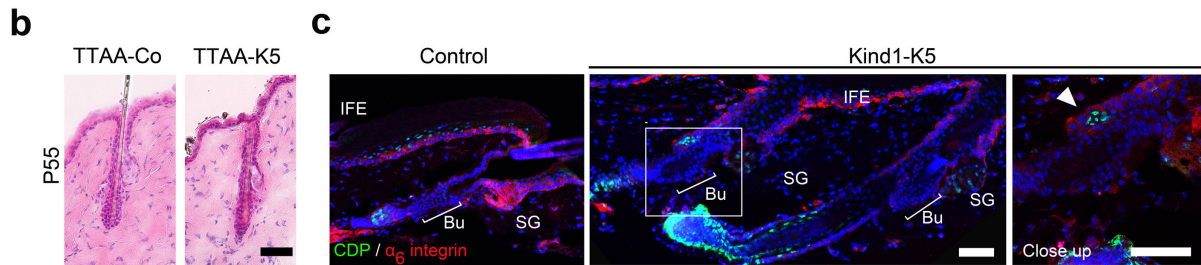
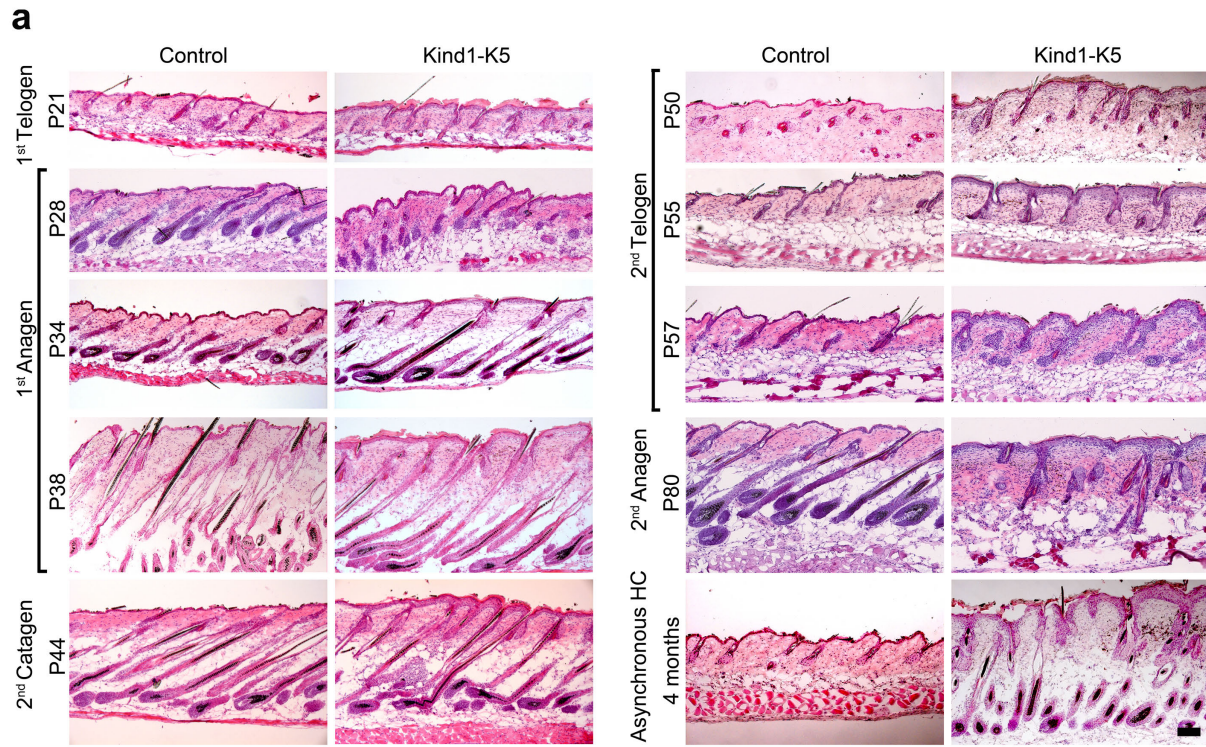
Supplementary Table 1–4

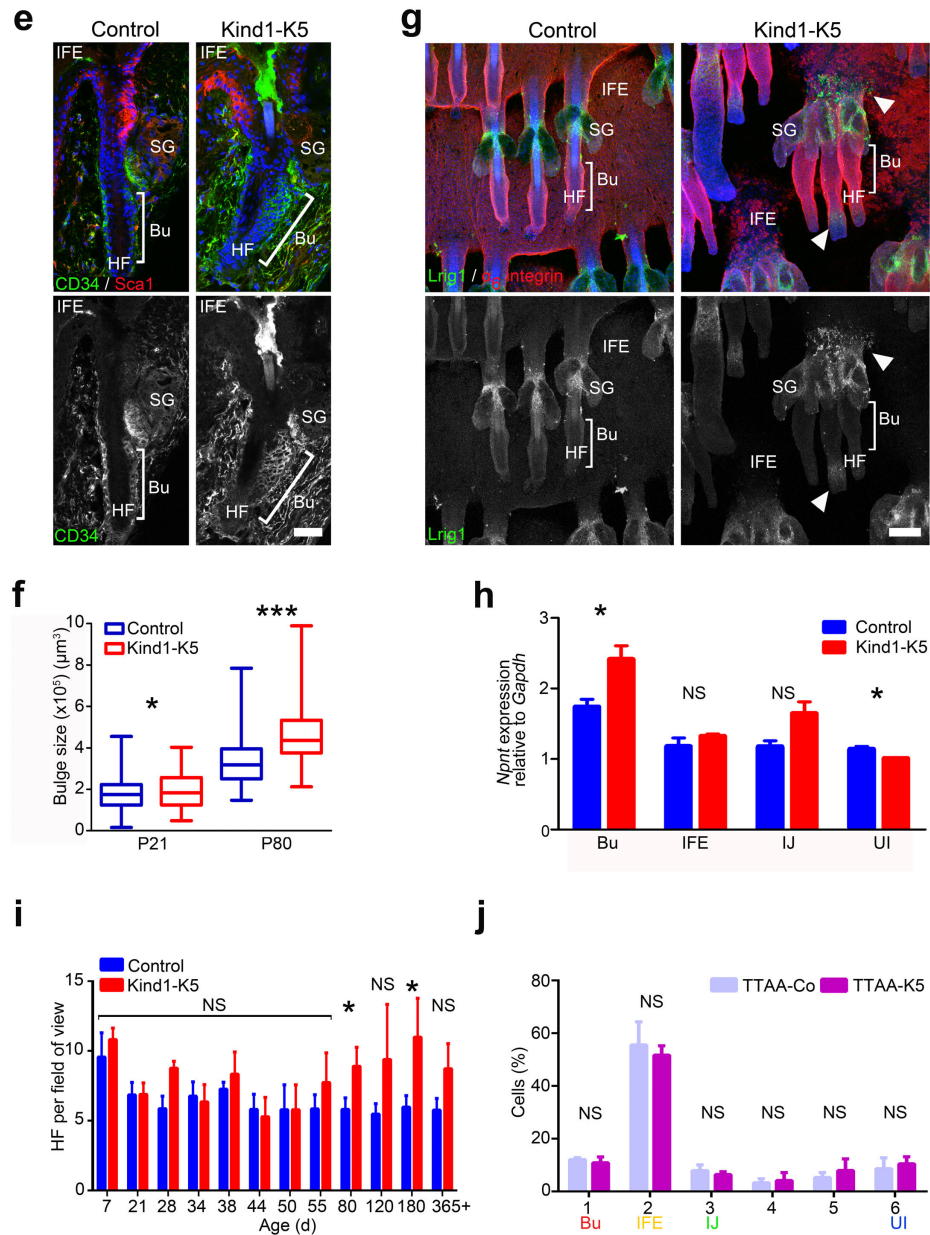


**Supplementary Figure 1** Conditional deletion of Kindlin-1 in skin. (a) Scheme depicting the conditional Kindlin-1 targeting strategy. (b,c) Western blotting of epidermal and primary keratinocyte lysates for Kindlin-1 and -2 (b) and immunofluorescence for Kindlin-1 (red) and  $\alpha_6$  integrin (green) in back skin sections from P21 old mice (c). Nuclei are stained with DAPI (blue). (d) Weight curve of control and Kind1-K5 male littermates reported as mean  $\pm$  SD ( $n=8$  Control; 6 Kind1-K5). (e) Immunofluorescence staining of P44 back skin for Desmoplakin (green) (upper panel) and Phalloidin (green) (lower panel) co-stained for  $\alpha_6$  integrin (red). Arrowheads indicate basal localization. Nuclei are stained with DAPI (blue). (f) Immunofluorescence staining of back skin from P7 and 6 months old mice for LN-332 (red) and Mac-1 (green) detecting macrophage infiltrations. Nuclei are stained with DAPI (blue). (g) Immunofluorescence staining of ear whole mounts from 4 months old mice for Gr-1 (green) staining granulocytes (upper panel) and CD4 (green) staining T cells (lower panel). Blood vessels are stained with pan-LN (red). (h) Number of innate and adaptive immune cells (macrophages: Mac-1, granulocytes: Gr-1, T cells: CD4, B lymphocytes: CD19, dendritic epidermal cells: CD11c, mast cells: MC) in the dermis of Kind1-K5 (left) and TTA-K5 mice (right) quantified as percentage of total skin cells and shown as mean  $\pm$  SD ( $n=4$  per genotype). (i) Pigment deposits in tails from 6 months old Kind-K5 mice (see arrowheads). (j) Appearance of control and Kind1-K5 mice after one year of age. Scale bars indicate 50  $\mu$ m (e,f,g) and 25  $\mu$ m (e).

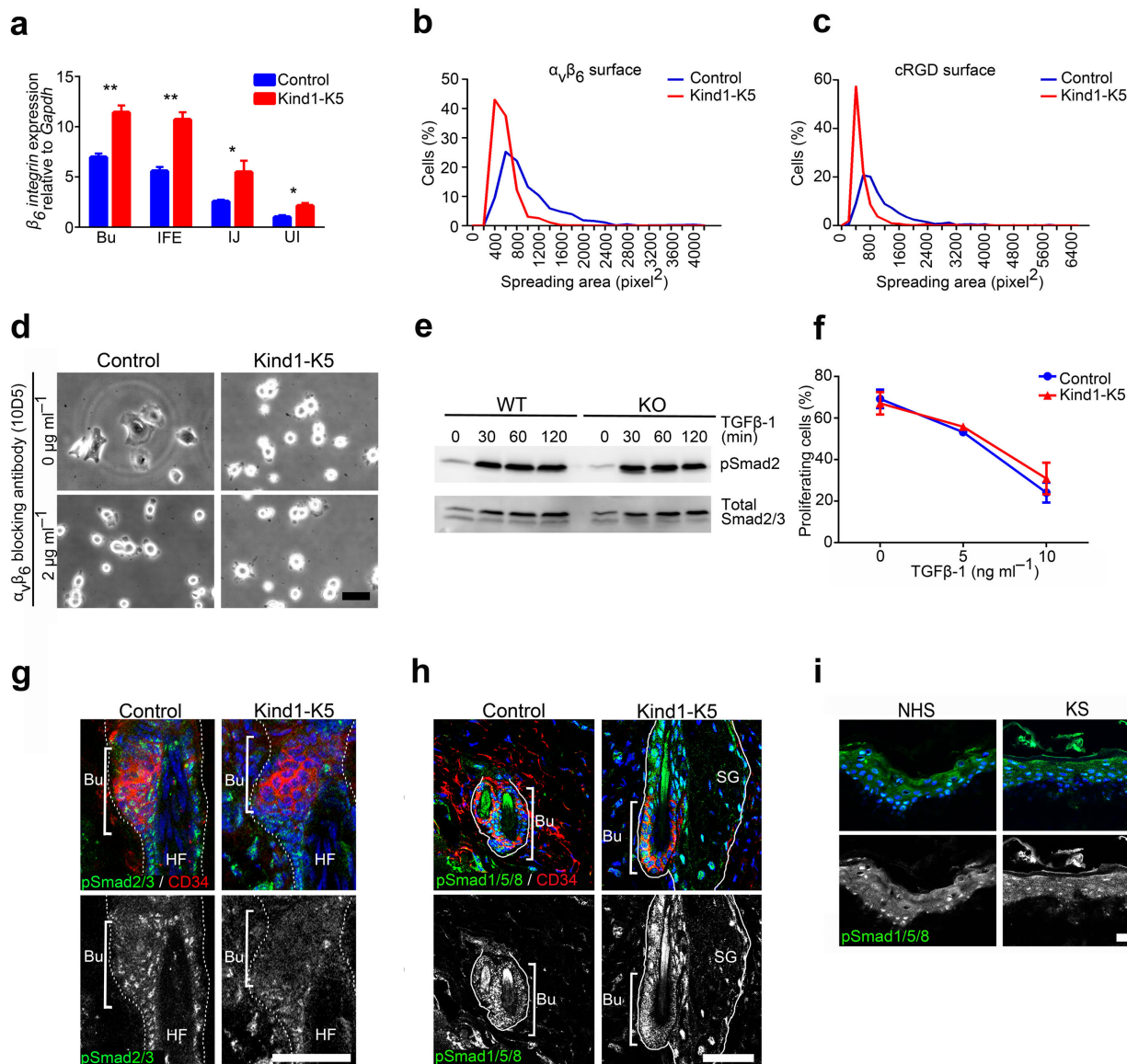


**Supplementary Figure 2** Skin characterization of Kind1-K5 and TTA-K5 mice. **(a)** H/E staining of 6 months old tail skin. Arrowheads indicate atrophic skin areas in Kind1-K5 mice. **(b)** Ki67 staining of back skin sections from 6 months old mice with upper panel showing normal and lower panel hyperthickened epidermis in Kind1-K5 mice. **(c,d)** Ki67-positive Kind1-K5 **(c)** and TTA-K5 **(d)** IFE keratinocytes quantified as percentage of total interfollicular cells and shown as mean  $\pm$  SD ( $n=3$  per genotype,  $\geq 20$  10x objective fields were counted). **(e-g)** Back skin sections from P7 and 6 months old mice, respectively, immunostained for cleaved Caspase-3 (cCaspase-3; red) and  $\alpha_6$  integrin (green) **(e)**, and quantification of cleaved Caspase-3 positive cells per mm IFE in young ( $\leq P21$ ) and adult ( $\geq 3$  months) skin **(f)** or adult skin of TTA-K5 mice **(g)** reported as mean  $\pm$  SD ( $n=5$  young and 4 adult Control; 7 young and 3 adult Kind1-K5 mice, 5 adult TTA-Co and TTA-K5). Nuclei in **(e)** are stained with DAPI (blue). **(h,i)** Differentiation of epidermal keratinocytes in back skin of 10 weeks old Kind1-K5 **(h)** and TTA-K5 **(i)** mice shown with indicated differentiation markers (keratin 5, Krt-5; keratin 10, Krt-10; loricrin, Lor; all in green) and co-stained with  $\alpha_6$  integrin (red). Keratinocyte activation is shown by Krt-6 (red) expression (lower panel). Nuclei are stained with DAPI (blue). All scale bars indicate 50  $\mu$ m.

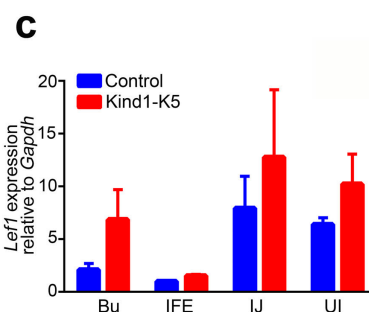
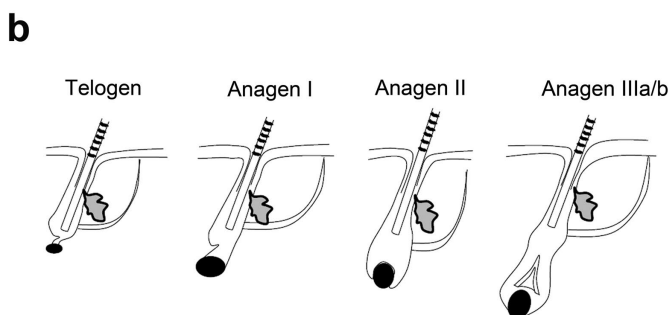
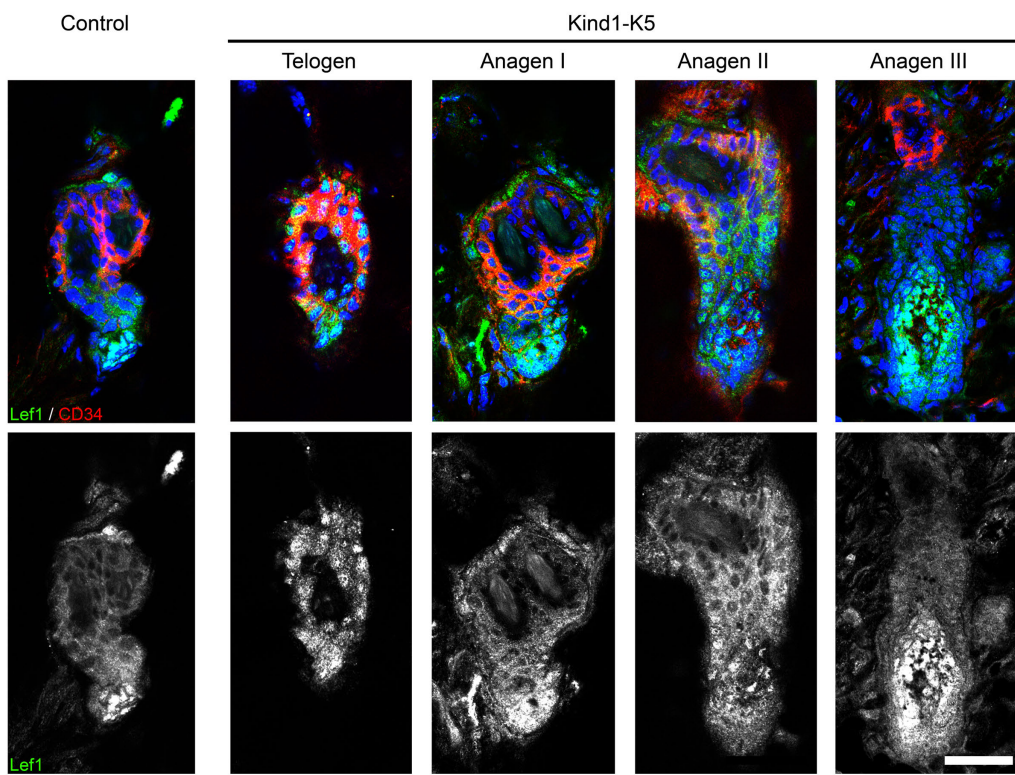
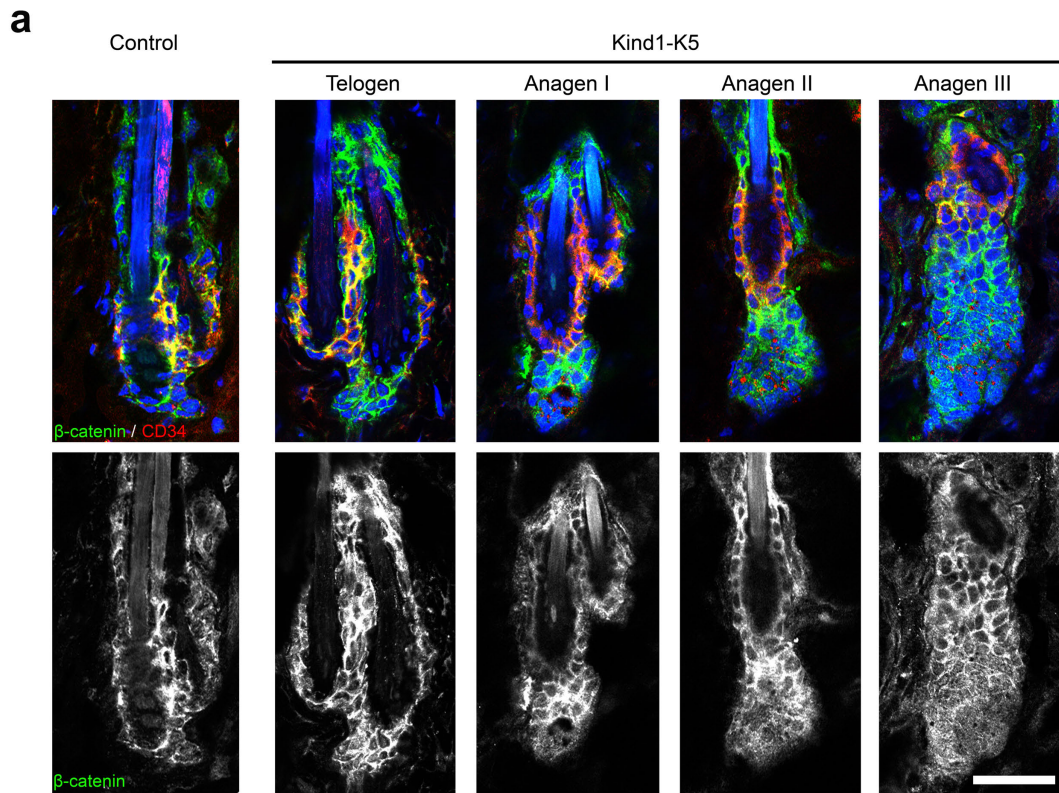


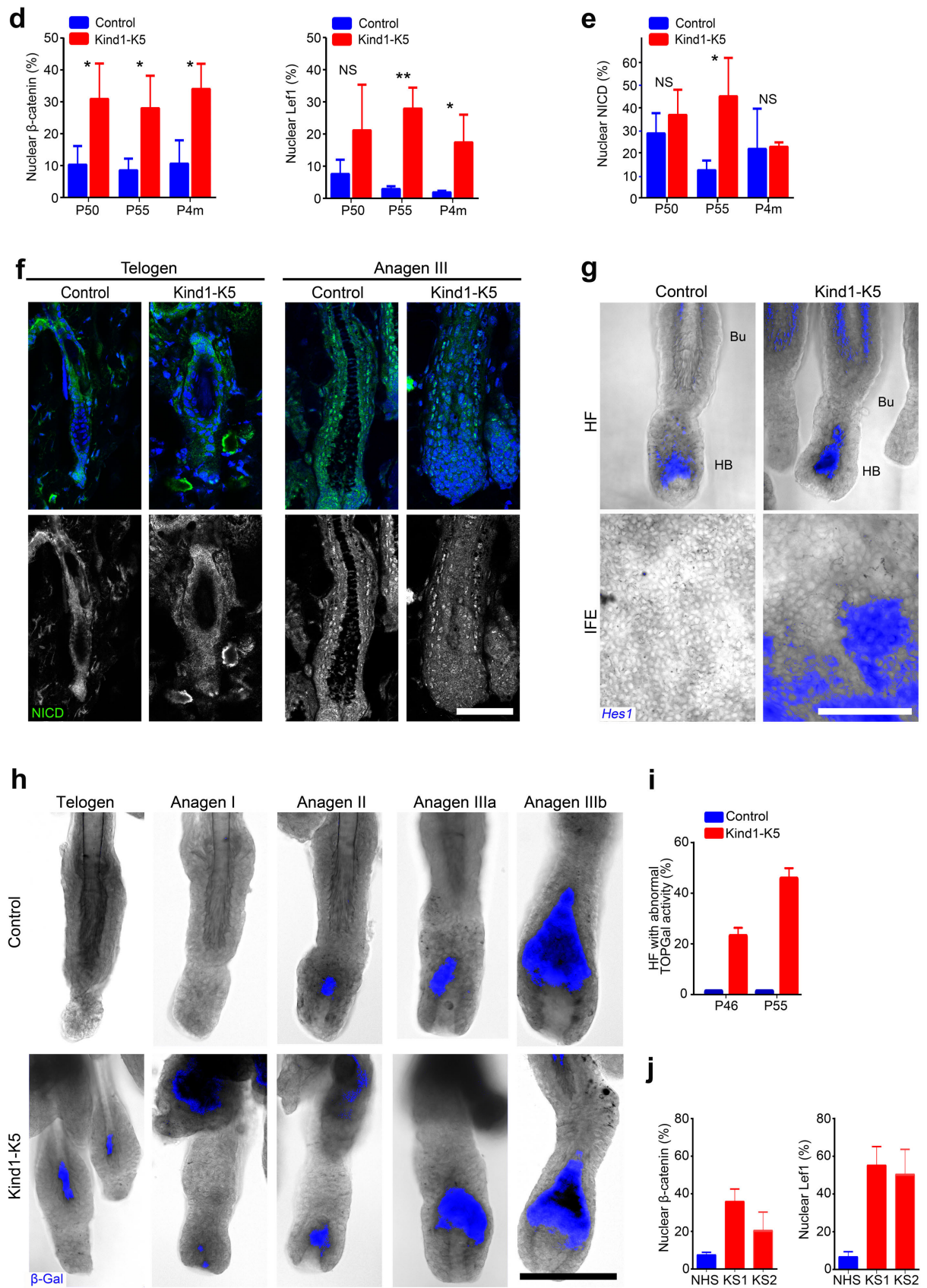


**Supplementary Figure 3** HF and SC compartment analysis in skin from Kind1-K5 and TTA-K5 mice. (a) H/E staining of back skin sections at indicated time points for HC analysis. (b) H/E staining of P55 back skin from TTA-Co and TTA-K5 mice. (c) Immunostaining of back skin from P80 mice for CDP (green) and  $\alpha_6$  integrin (red). Arrowhead in right panel indicates ectopic CDP expression. Nuclei are stained with DAPI (blue). (d) Ectopic HF development in back skin of Kind1-K5 mice analyzed by H/E (upper panel) and alkaline phosphatase (AP) staining (lower panel). HF stages 1–5 were classified as described before<sup>69</sup>; arrowheads indicate early hair germ formation. (e) Immunostaining of P80 back skin HF for CD34 (green) and Sca1 (red). Nuclei are stained with DAPI (blue). (f) Bulge size analysis reported as boxplots (P21  $n=3$  Control; 4 Kind1-K5; P80  $n=5$  per genotype; 20–67 HFs per animal from different whole mounts; boxplot whisker ends show min/max distribution and middle line reports the median). (g) Immunostaining of tail whole mounts from P80 mice for Lrig1 (green) and  $\alpha_6$  integrin (red). Arrowheads indicate ectopic Lrig1 expression. Nuclei are stained with DAPI (blue). (h) FACS-sorted keratinocyte subpopulations from 3 P80 mice per genotype were pooled and transcript levels of *Npnt* analyzed by qPCR. Expression levels are reported as mean  $\pm$  SEM relative to *Gapdh* ( $n=3$  technical replicates). (i) HF numbers in back skin at indicated age are reported as mean  $\pm$  SD ( $n=2-4$  per genotype,  $\geq 10$  10x objective fields were counted). (j) FACS analysis of primary TTA-K5 keratinocytes ( $n=4$  per genotype) described in Fig. 3e,f. The color code corresponds to the cell population denoted in Fig. 3a. Scale bar indicates 50  $\mu\text{m}$  in (a–d) and 100  $\mu\text{m}$  in (e,g). Bu, bulge; SG, sebaceous gland; HF, hair follicle; IFE, interfollicular epidermis; UI, upper isthmus; IJ, interfundibulum junctional zone.

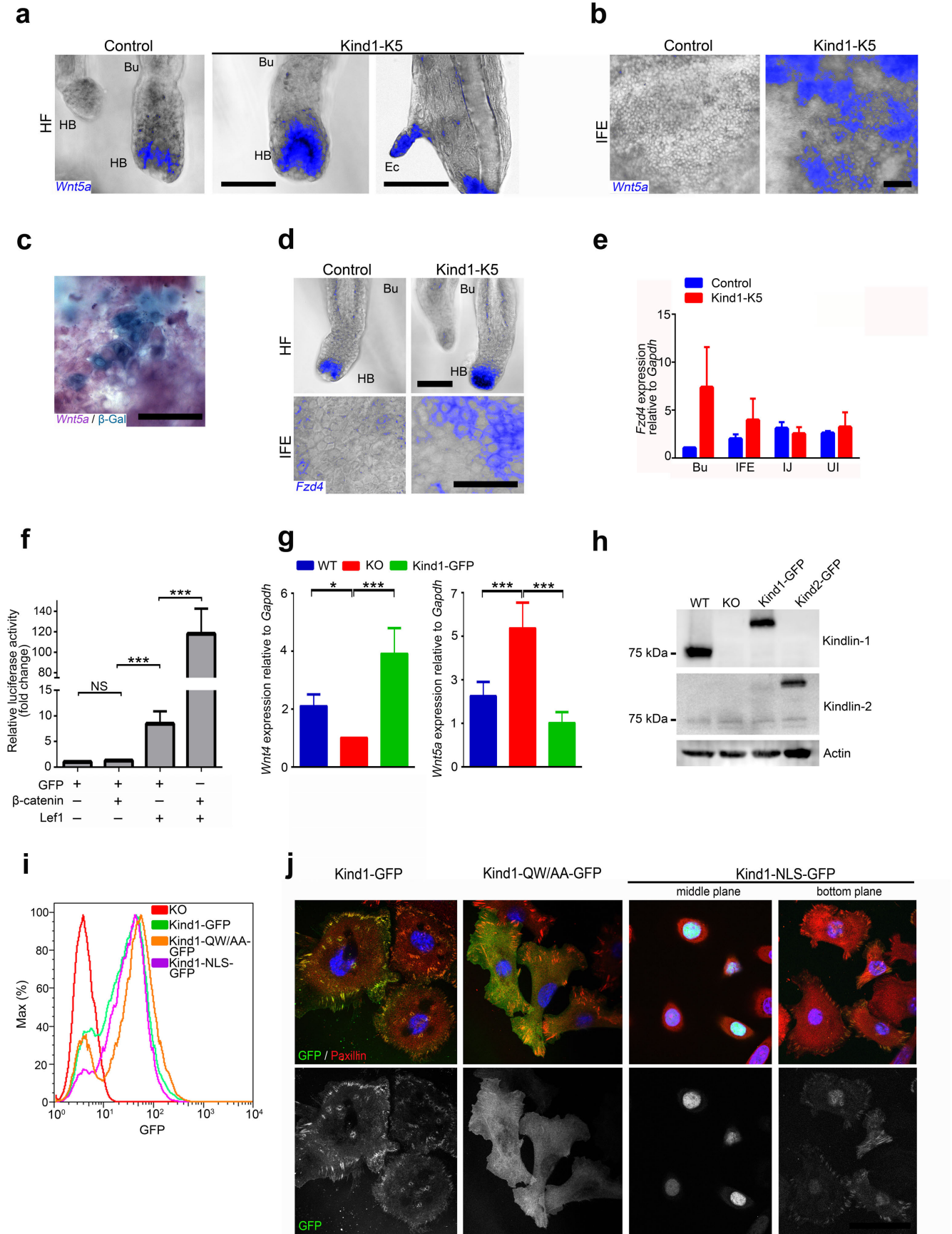


**Supplementary Figure 4** Influence of Kindlin-1 on  $\alpha_v\beta_6$  integrin, TGF $\beta$  and BMP signaling. **(a)** FACS sorted keratinocyte subpopulations from 3 P80 mice per genotype were pooled and transcript levels of  $\beta_6$  *integrin* were analyzed by qPCR. Expression levels are reported as mean  $\pm$  SEM relative to *Gapdh* ( $n=3$  technical replicates). **(b,c)** Representative experiment showing spreading area on anti- $\alpha_v\beta_6$  integrin antibody ( $n=814$  Control and 826 Kind1-K5 cells; **b**) and cRGD-coated (**c**) surfaces ( $n=731$  Control and 694 Kind1-K5 cells) ( $n=3$  biological replicates). **(d)** Spreading of primary keratinocytes on cRGD-coated surfaces in the absence or presence of anti- $\alpha_v\beta_6$  integrin blocking antibody. **(e)** Treatment of keratinocytes with TGF $\beta$ -1 for indicated time points followed by western blot analysis of pSmad2 and total Smad2/3. **(f)** Proliferation analyzed with the EdU incorporation assay after treatment with indicated TGF $\beta$ -1 concentrations reported as mean  $\pm$  SEM ( $n=3$  biological replicates). **(g)** Immunofluorescence staining of P44 back skin HF for pSmad2/3 (green) and CD34 (red). Nuclei are stained with DAPI (blue). **(h)** Immunofluorescence staining of a 6 months old back skin HF for pSmad1/5/8 (green) and CD34 (red). Nuclei are stained with DAPI (blue). **(i)** Immunostaining of biopsy skin sections from healthy (NHS) and individuals with KS for pSmad1/5/8 (green). Nuclei are stained with DAPI (blue). All scale bars indicate 50  $\mu$ m. Bu, bulge; SG, sebaceous gland; IFE, interfollicular epidermis; UI, upper isthmus; IJ, interfundibulum junctional zone.





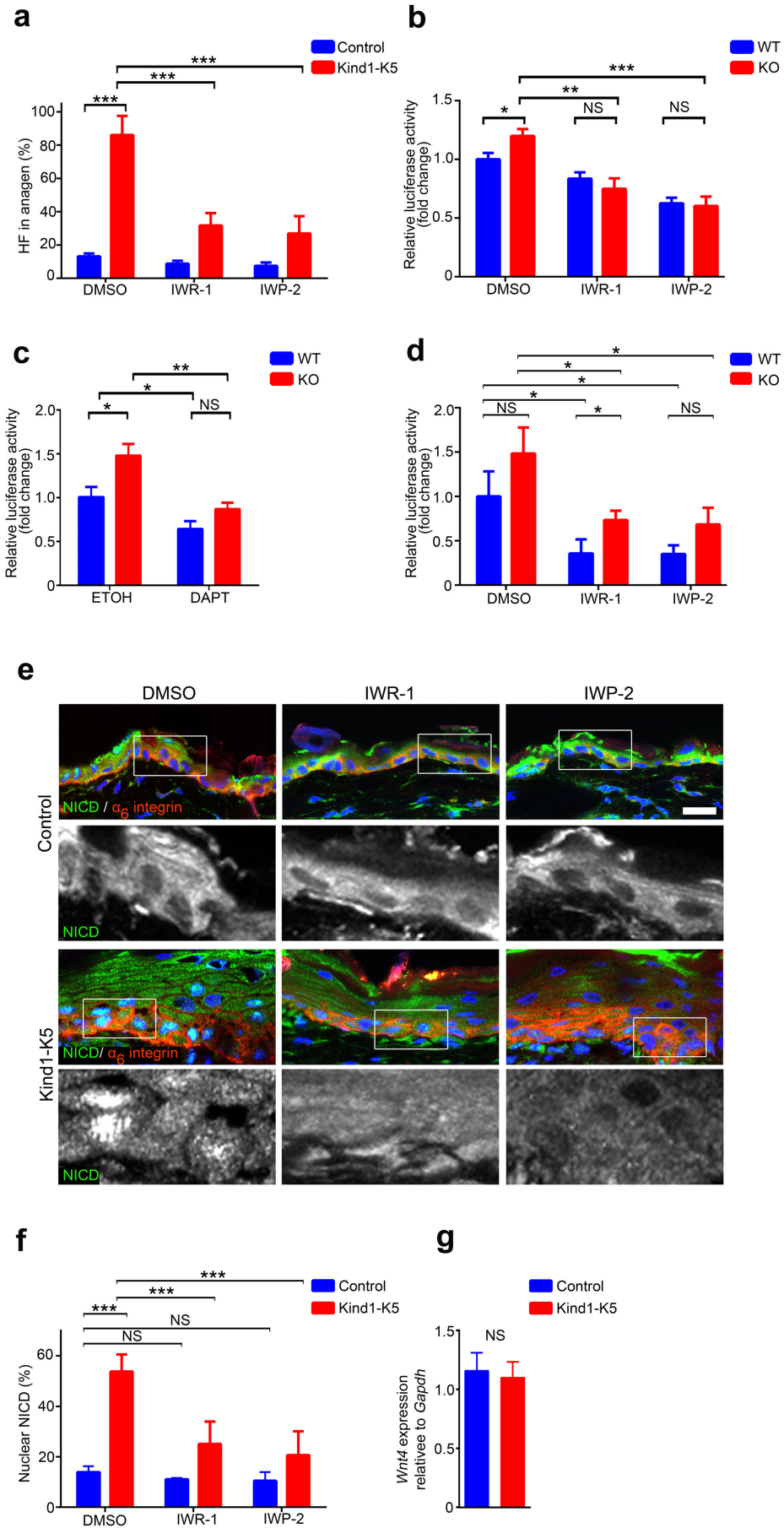
**Supplementary Figure 5** Kindlin-1 loss leads to elevated Wnt- $\beta$ -catenin and Notch signaling in skin. (a) Immunofluorescence staining of back skin from Kind1-K5 mice during premature anagen induction at indicated HC stage (illustrated in b) for  $\beta$ -catenin (upper panel) and Lef1 (green) (lower panel) and co-staining with CD34 (red). Nuclei are stained with DAPI (blue). (b) Scheme of HF during the HC transition from telogen to full anagen. (c) FACS-sorted keratinocyte subpopulations from 3 P80 mice per genotype were pooled and transcript levels of *Lef1* were analyzed by qPCR and shown as mean  $\pm$  SEM relative to *Gapdh* ( $n=3$  technical replicates). (d,e) Percentage of IFE keratinocytes at indicated time points with nuclear  $\beta$ -catenin (d, left), Lef1 (d, right) and NICD (e) reported as mean  $\pm$  SD ( $n=3$  mice per genotype with  $>1000$  IFE cells counted per genotype). (f) Immunofluorescence staining of telogen (left panel) and anagen (right panel) HF from 4 months old mice for NICD (green) and DAPI (blue). (g) *In situ* hybridization of epidermal tail whole mount from 3 months old mice for *Hes1*; the blue *in situ* signal was overlaid with the grayscale images of the HF and IFE. (h) Comparison of TOPGal reporter activity at indicated HC during anagen induction in tail skin from control and Kind1-K5 mice; the blue  $\beta$ -Gal activity was overlaid with a grayscale image of the HF. (i) Percentage of tail skin HFs with abnormal TOPGal activity quantified at indicated time points ( $n=3$  per genotype). (j) Percentage of IFE keratinocytes with nuclear  $\beta$ -catenin (left) and Lef1 (right) in healthy humans (NHS) and subject 1 (KS1) and 2 (KS2) with KS disease reported as mean  $\pm$  SD ( $n=8$  40x field of view,  $>1000$  IFE keratinocytes per subject). Scale bars indicate 50  $\mu\text{m}$  (a) and 100  $\mu\text{m}$  (f-h). Bu, bulge; IFE, interfollicular epidermis; UI, upper isthmus; IJ, interfundibulum junctional zone.



**Supplementary Figure 6** Kindlin-1 controls Wnt- $\beta$ -catenin signaling. (a,b) *In situ* hybridization of epidermal tail whole mount from P48 (HFs) (a) and 4 months (IFE, b and Ec, a) old mice for *Wnt5a*. (c) IFE TOPgal reporter activity overlays with *Wnt5a* expression in 4 months old Kind1-K5 tail epidermal whole mounts. For double labeling  $\beta$ -Gal staining (blue) was developed before epidermal whole mounts were probed for *Wnt5a* (purple). (d) *In situ* hybridization of epidermal tail whole mount from 2 months (HFs) and 8 months (IFE) old mice for *Fzd4*. The blue *in situ* signal was overlaid with the grayscale images of the HF and IFE (a,b,d). (e) FACS-sorted keratinocyte subpopulations from 3 P80 mice per genotype were pooled and transcript levels of *Fzd4* were analyzed by qPCR and shown as mean  $\pm$  SEM relative to *Gapdh* ( $n=3$  technical replicates). (f) TOPFlash activity in keratinocytes from control mice transiently transfected with *Lef1* and  $\beta$ -catenin expression plasmids. Values were corrected for the renilla control, are represented as fold increase relative to lowest value and reported as mean  $\pm$  SEM ( $n=4$  biological replicates). (g) qPCR of *Wnt4* and *Wnt5a* transcript levels in floxed (WT), AdenoCre-treated Kindlin-1 deficient (KO) and Kindlin-1-GFP keratinocytes shown as mean  $\pm$  SEM relative to *Gapdh* ( $n=3$  biological replicates). (h-j) Western blot for Kindlin-1 and 2 (h), FACS analysis for GFP (i) and immunostaining for paxillin (red) and GFP (green) (j) of Kindlin-1 deficient keratinocytes stably transduced with indicated GFP-tagged Kindlin-1 constructs. Nuclei are stained with DAPI (blue). All scale bars indicate 50  $\mu$ m. Bu, bulge; Ec, ectopic hair follicle; HB, hair bulb; HF, hair follicle; IFE, interfollicular epidermis; UI, upper isthmus; IJ, interfundibulum junctional zone.

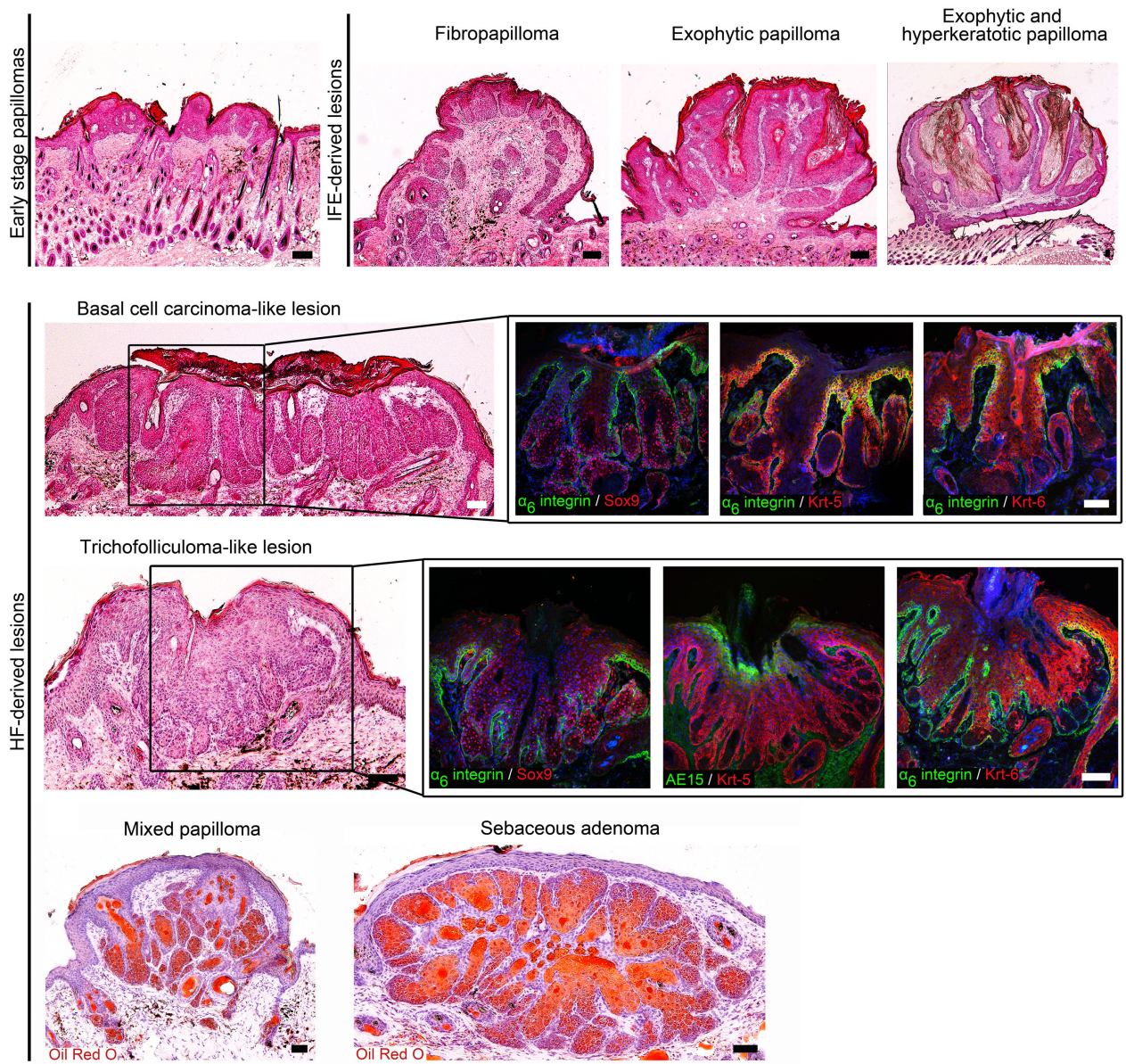
# Supplementary Figure 7

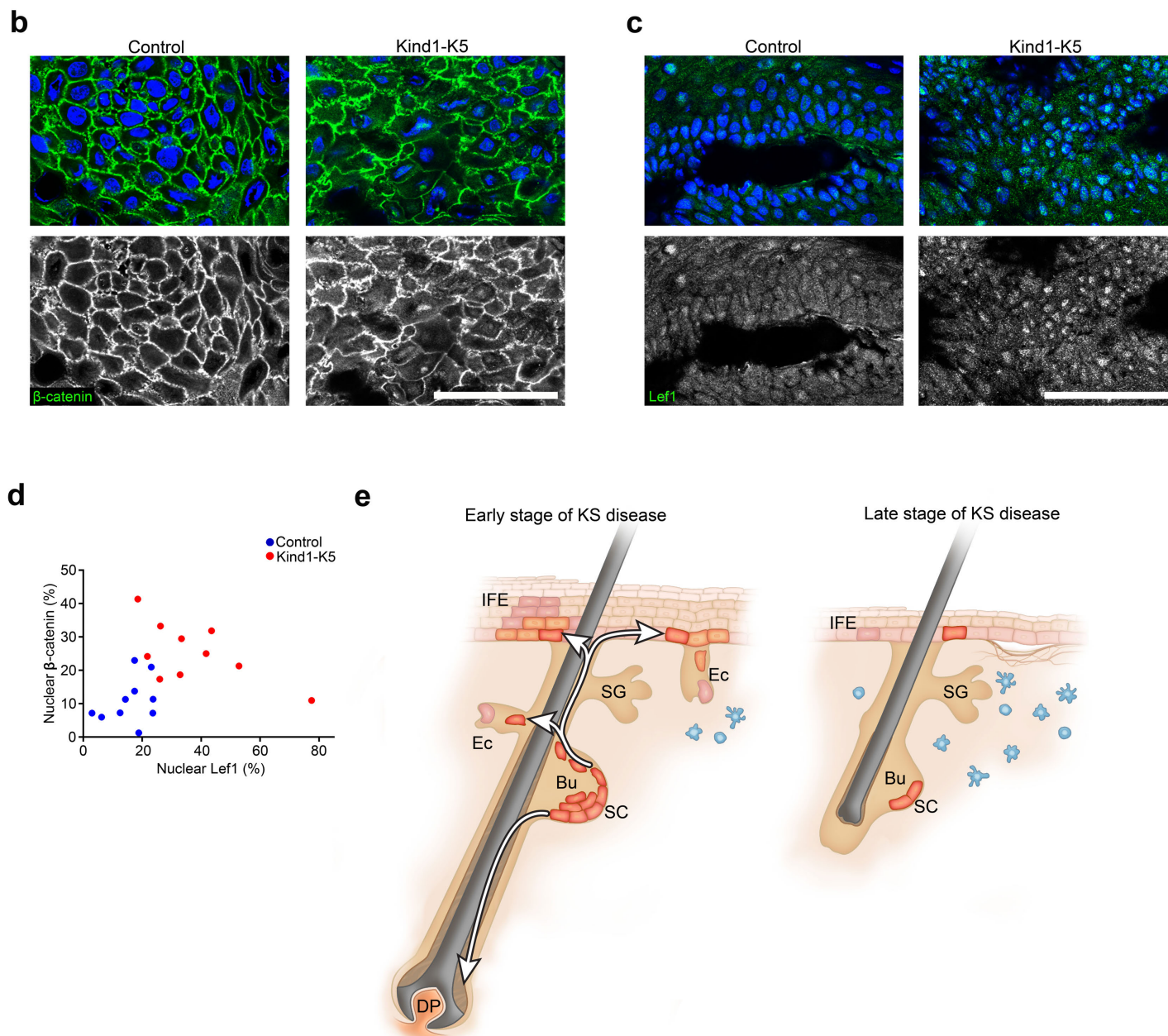
Rognoni et al.



**Supplementary Figure 7** Kindlin-1 loss induced Wnt- $\beta$ -catenin and Notch signaling *in vivo* and *in vitro*. (a) Quantification of inhibition of premature anagen induction reported as percentage of anagen HFs after indicated treatments at P56 (reported as mean  $\pm$  SD,  $n=4$  mice per genotype,  $\geq 8$  10x objective fields were counted). (b–d) TOPFlash and pHes1-Luc reporter assay with floxed (WT) and Adeno-Cre treated Kindlin-1 deficient keratinocyte (KO) lines. Values were corrected for the renilla control, are represented as fold increase relative to WT cells and reported as mean  $\pm$  SEM. (b) TOPFlash reporter activity measured 24 h after treatment with 50  $\mu$ M of indicated Wnt inhibitor ( $n=5$ , all biological replicates). (c,d) pHes1-Luc reporter activity analyzed 24 h after treatment with 2.5  $\mu$ M DAPT (Notch signaling inhibitor) ( $n=4$ , all biological replicates) (c) or with 50  $\mu$ M of indicated Wnt inhibitor ( $n=3$ , all biological replicates) (d). (e) Immunofluorescence staining of back skin for NICD (green) and  $\alpha_6$  integrin (red) after treatment with Wnt inhibitor. Nuclei are stained with DAPI (blue). Scale bar indicates 25  $\mu$ m. (f) Percentage of IFE cells with nuclear NICD in back skin treated with Wnt inhibitors and shown as mean  $\pm$  SD ( $n=4$  per genotype,  $\geq 1000$  IFE keratinocytes counted per mouse). (g) qPCR of *Wnt4* transcript levels in floxed (WT) and AdenoCre-treated Kindlin-1 deficient (KO) keratinocytes treated with 2.5  $\mu$ M DAPT for 24 h shown as mean  $\pm$  SEM expression relative to *Gapdh* ( $n=4$  biological replicates).

**a**





**Supplementary Figure 8** Elevated Wnt-β-catenin signaling in skin tumors from Kind1-K5 mice. (a) Histological analysis of skin lesions after two stage carcinogenesis. H/E staining of representative skin lesions. BCC- and trichofolliculoma-like lesions display characteristic staining for Sox9 (red), Krt-5 (red), Krt-6 (red), AE15 (green) and α<sub>6</sub> integrin (green). Mixed papilloma and sebaceous adenoma were positive for OilRed O. Nuclei are stained with DAPI (blue). (b,c) Tumor sections immunostained for β-catenin (green) (b) and Lef1 (green) (c). Nuclei are stained with DAPI (blue). (d) Percentage of cells with nuclear β-catenin (y-axis) and Lef1 (x-axis) in tumors (n=10 per genotype; ≥ 1500 cells counted per tumor). (e) Model showing early and late cellular consequences of Kindlin-1 deletion in mouse keratinocytes. The early stage shows elevated epithelial SC proliferation and mobilization leading to expanded SC compartments, epidermal hyperthickening, premature HF induction and ectopic HF development from existing HF and IFE (early KS disease stage). The late stage is characterized by an inflammatory response to skin blistering and SC exhaustion leading to a progressive HF loss and skin atrophy. Scale bars indicate 100 μm (a) and 50 μm (b,c). Bu, bulge; SC, stem cell; SG, sebaceous gland; HF, hair follicle, DP, dermal papilla; IFE, interfollicular epidermis; Ec, ectopic HF.

**Supplementary Table 1** *P*-values for relative amount of SC subpopulations over time analyzed by FACS (see **Fig. 3g**). *P*-values were calculated with unpaired t-test. Bu, bulge; UI, upper isthmus; IJ, interfundibulum junctional zone.

Age	N (animal number)		SC compartment		
	Control	Kind1-K5	Bu	IJ	UI
<b>21 d</b>	4	3	<i>P</i> = 0.0004	<i>P</i> = 0.0146	<i>P</i> = 0.9161
<b>24 d</b>	5	3	<i>P</i> = 0.0008	<i>P</i> = 0.3161	<i>P</i> = 0.0082
<b>28 d</b>	5	3	<i>P</i> = 0.0047	<i>P</i> = 0.0874	<i>P</i> = 0.1014
<b>40 d</b>	5	3	<i>P</i> = 0.0008	<i>P</i> < 0.0001	<i>P</i> = 0.0302
<b>44 d</b>	3	3	<i>P</i> = 0.0009	<i>P</i> = 0.0004	<i>P</i> = 0.0182
<b>50 d</b>	5	3	<i>P</i> = 0.0004	<i>P</i> = 0.0032	<i>P</i> = 0.2708
<b>55 d</b>	3	3	<i>P</i> = 0.0012	<i>P</i> < 0.0001	<i>P</i> = 0.0452
<b>80 d</b>	7	4	<i>P</i> < 0.0001	<i>P</i> < 0.0001	<i>P</i> = 0.0003
<b>4 months</b>	4	3	<i>P</i> = 0.2501	<i>P</i> = 0.0074	<i>P</i> = 0.0010
<b>6 months</b>	8	5	<i>P</i> = 0.0863	<i>P</i> = 0.4542	<i>P</i> = 0.0047
<b>&gt;11 months</b>	4	3	<i>P</i> = 0.2265	<i>P</i> = 0.0232	<i>P</i> = 0.3730

**Supplementary Table 2** Microarray data with significant gene expression changes of  $\geq 2$  fold. First sheet shows all genes sorted by the difference score. In the following sheets genes are divided in the indicated categories (Wnt signaling; Inflammation and Wound healing; Proliferation and Cell cycle; Metabolism).

N, NHS skin; K, KS skin; AVG, average; DiffScor, difference score.

**Supplementary Table 3** Wnt ligand and receptor transcript analysis. qPCR of primary keratinocytes for Wnt ligands and Wnt receptors reported as mean  $\pm$  SEM expression relative to *Gapdh* ( $n$ = indicated biological replicates).  $P$ -values were calculated with unpaired t-test. ND, not determined.

Gene Symbol	Control		Kind1-K5		Log <sub>2</sub> fold change	P-value	n
	mean	SEM	mean	SEM			
<i>Wnt1</i>	0.496	0.089	1.50	0.089	1.649	0.001	3
<i>Wnt2</i>	0.506	0.053	1.494	0.053	1.578	$2 \times 10^{-4}$	3
<i>Wnt2b</i>	0.785	0.039	1.215	0.039	0.633	0.001	3
<i>Wnt3</i>	ND		ND		ND		
<i>Wnt3a</i>	0.813	0.054	1.187	0.054	0.550	0.008	3
<i>Wnt4</i>	1.562	0.095	0.438	0.095	-2.088	$3 \times 10^{-5}$	4
<i>Wnt5a</i>	0.024	0.003	1.976	0.003	6.400	$2 \times 10^{-10}$	3
<i>Wnt5b</i>	0.99	0.162	1.012	0.162	0.033	0.885	4
<i>Wnt6</i>	0.366	0.032	1.634	0.032	2.167	$1 \times 10^{-5}$	3
<i>Wnt7a</i>	1.200	0.057	0.800	0.057	-0.589	0.007	3
<i>Wnt7b</i>	1.263	0.158	0.737	0.158	-0.822	0.078	3
<i>Wnt8a</i>	ND		ND		ND		
<i>Wnt8b</i>	ND		ND		ND		
<i>Wnt9a</i>	1.220	0.131	0.780	0.131	-0.667	0.017	3
<i>Wnt9b</i>	1.000	0.256	2.090	0.256	1.067	0.500	3
<i>Wnt10a</i>	1.408	0.122	0.591	0.122	-1.300	0.009	3
<i>Wnt10b</i>	0.877	0.074	1.124	0.074	0.3611	0.077	3
<i>Wnt11</i>	1.107	0.193	0.893	0.193	-0.021	0.326	4
<i>Wnt16</i>	1.209	0.087	0.791	0.087	-0.622	0.027	3
<i>Fzd1</i>	1.064	0.242	0.936	0.242	-0.216	0.721	4
<i>Fzd2</i>	1.065	0.243	0.935	0.243	-0.180	0.726	3
<i>Fzd3</i>	0.364	0.010	1.636	0.010	2.169	$6 \times 10^{-8}$	3
<i>Fzd4</i>	0.378	0.145	1.623	0.145	2.482	0.001	4
<i>Fzd5</i>	0.858	0.123	1.142	0.123	0.433	0.153	4
<i>Fzd6</i>	0.942	0.106	1.058	0.106	0.173	0.468	4
<i>Fzd7</i>	0.642	0.124	1.358	0.124	1.128	0.015	3
<i>Fzd8</i>	0.743	0.134	1.257	0.134	0.813	0.035	4
<i>Fzd9</i>	0.766	0.066	1.234	0.066	0.694	0.007	3
<i>Fzd10</i>	0.983	0.048	1.017	0.048	0.050	0.640	3
<i>Lrp5</i>	1.024	0.079	0.976	0.079	-0.071	0.681	4
<i>Lrp6</i>	0.840	0.048	1.160	0.048	0.470	0.003	4
<i>Ror1</i>	0.690	0.086	1.310	0.086	0.933	0.036	3
<i>Ror2</i>	0.682	0.135	1.318	0.135	1.302	0.067	4

**Supplementary Table 4** List of qPCR oligonucleotides.

<b>Gene Symbol</b>	<b>PCR primer</b>
<i>Gapdh</i>	Fw: TCCTGCACCACCAACTGCTTAGC Rev: TGGATGCAGGGATGATGTTCTGG
<i>Npnt</i>	Fw: ATTGATGAATGTGCGACTGG Rev: CTGCTACACTGGTGCTGTCC
<i>Itgb6</i>	Fw: ATGGGGATTGAGCTGGTCTG Rev: GACAGGTGGGTGAAATTCTCC
<i>Lef1</i>	Fw: TCTGGCTACATAATGATGCCCA Rev: GGACATGCCTTGCTTGGAGTT
<i>Wnt1</i>	Fw: CGACTGATCCGACAGAACCC Rev: CCATTTGCACTCTCGCACA
<i>Wnt2</i>	Fw: CCTCCGAAGTAGTCGGGAATC Rev: GCAGGACTTTAATTCTCCTTGGC
<i>Wnt2b</i>	Fw: AACATCCATTACGGTGTTTCGC Rev: CCTGTGCGTCGGAAGTCTG
<i>Wnt3a</i>	Fw: AATTTGGAGGAATGGTCTCTCGG Rev: CAGCAGGTCTTCACTTCACAG
<i>Wnt4</i>	Fw: GTCAGGATGCTCGGACAACAT Rev: CACGTCTTTACCTCGCAGGA
<i>Wnt5a</i>	Fw: GGACCACATGCAGTACATTGG Rev: CGTCTCTCGGCTGCCTATTT
<i>Wnt5b</i>	Fw: TCCTGGTGGTCACTAGCTCTG Rev: TGCTCCTGATACTGACTGACACA
<i>Wnt6</i>	Fw: GCAAGACTGGGGGTTTCGAG Rev: CCTGACAACCACACTGTAGGAG
<i>Wnt7a</i>	Fw: TGAACTTACACAATAACGAGGCG Rev: GTGGTCCAGCACGTCTTAGT
<i>Wnt7b</i>	Fw: CTTACCTATGCCATCACGG Rev: TGGTTGTAGTAGCCTTGCTTCT
<i>Wnt9a</i>	Fw: GGCCAAGCACACTACAAG Rev: AGAAGAGATGGCGTAGAGGAAA
<i>Wnt9b</i>	Fw: CAGAGAGGCTTTAAGGAGACGG Rev: CCTGGGGAGTCGTCACAAG
<i>Wnt10a</i>	Fw: CAGATCGCCATCCATGAGTG Rev: ACCGCAAGCCTTCAGTTTACC
<i>Wnt10b</i>	Fw: ATCGCCGTTACGAGTGTC Rev: GGAAACC GCGCTTGAGGAT
<i>Wnt11</i>	Fw: ATGCGTCTACACAACAGTGAAG Rev: GTAGCGGGTCTTGAGGTCAG

<i>Wnt16</i>	Fw: GCAGGCTGTCGCCAAGTTA Rev: GTCTGCCTCTGGTCTTTTTCTC
<i>Fzd1</i>	Fw: GAGTTCTGGACCAGTAATCCGC Rev: ATGAGCCCGTAAACCTTGGTG
<i>Fzd2</i>	Fw: CTTCTCGCAAGAGGAGACTCG Rev: GTGGTGACCGTGAAGAAAGTG
<i>Fzd3</i>	Fw: TGATGAGCCATATCCCCGACT Rev: GCCTATGAAATAGCGAGCAAATG
<i>Fzd4</i>	Fw: AACCTCGGCTACAACGTGAC Rev: GGCACATAAACCGAACAAAGGAA
<i>Fzd5</i>	Fw: GAGTCACACCCACTCTACAACA Rev: CGGAATCGTTCCATGTCAATGAG
<i>Fzd6</i>	Fw: TAATGGACACTTTTGGCATC Rev: ATCCAATGTCTCTTGGGACT
<i>Fzd7</i>	Fw: GACCAAGCCATTCTCCGTG Rev: CAGGTAGGGAGCAGTAGGGTA
<i>Fzd8</i>	Fw: CCGCTGGTGGAGATACAGTG Rev: CGGTTGTAGTCCATGCACAG
<i>Fzd9</i>	Fw: CGCACGCACTCTGTATGGAG Rev: GCCGAGACCAGAACACCTC
<i>Fzd10</i>	Fw: CATGCCAACCTGATGGGTC Rev: GCCACCTGAATTTGAACTGCT
<i>Lrp5</i>	Fw: ACGTCCCGTAAGGTTCTCTTC Rev: GCCAGTAAATGTCGGAGTCTAC
<i>Lrp6</i>	Fw: TGCAAACAGACGGGACTTGAG Rev: CGGGGACAATAATCCAGAAACAA
<i>Ror1</i>	Fw: AACCTTGATGAGCCGATGAA Rev: CAGCGGATACTGGGAGGTG
<i>Ror2</i>	Fw: AAGTGGAAGATTCGGAGGCAA Rev: CTTCAGCCACCGCACATTG

# Sorting nexin 17 prevents lysosomal degradation of $\beta_1$ integrins by binding to the $\beta_1$ -integrin tail

Ralph Thomas Böttcher<sup>1,2</sup>, Christopher Stremmel<sup>1,2</sup>, Alexander Meves<sup>1,3</sup>, Hannelore Meyer<sup>1,3</sup>, Moritz Widmaier<sup>1</sup>, Hui-Yuan Tseng<sup>1</sup> and Reinhard Fässler<sup>1,4</sup>

**Integrin functions are controlled by regulating their affinity for ligand, and by the efficient recycling of intact integrins through endosomes. Here we demonstrate that the Kindlin-binding site in the  $\beta_1$ -integrin cytoplasmic domain serves as a molecular switch enabling the sequential binding of two FERM-domain-containing proteins in different cellular compartments. When  $\beta_1$  integrins are at the plasma membrane, Kindlins control ligand-binding affinity. However, when they are internalized, Kindlins dissociate from integrins and sorting nexin 17 (SNX17) is recruited to free  $\beta_1$ -integrin tails in early endosomes to prevent  $\beta_1$ -integrin degradation, leading to their recycling back to the cell surface. Our results identify SNX17 as a  $\beta_1$ -integrin-tail-binding protein that interacts with the free Kindlin-binding site in endosomes to stabilize  $\beta_1$  integrins, resulting in their recycling to the cell surface where they can be reused.**

Integrins are the main family of adhesion molecules mediating cell interactions with the extracellular matrix<sup>1</sup> (ECM). A hallmark of integrins is their ability to tune their affinity for ligand by shifting their extracellular domain between different conformations. Key molecules that increase ligand-binding affinity are the FERM (4.1, ezrin, radixin, moesin)-domain-containing proteins Talins and Kindlins<sup>2,3</sup>. Talins bind the membrane-proximal NPxY motif of  $\beta$ -integrin cytoplasmic tails and Kindlins the membrane-distal NxxY motif and the adjacent threonine residues<sup>4–9</sup>.

Increasing evidence indicates that integrin trafficking through the endosomal pathway affects their function, cell surface distribution, signalling through integrin-associated growth factor receptors and the turnover of ECM proteins such as fibronectin<sup>10,11</sup>. In contrast to the well-established mechanisms for integrin recycling<sup>10,12–14</sup>, the mechanisms for integrin degradation are not well understood. Fibronectin-bound  $\alpha_5\beta_1$  integrin was recently shown to be internalized, sorted into multivesicular endosomes and degraded in lysosomes in a ubiquitin- and endosomal sorting complex required for transport (ESCRT)-dependent manner<sup>15</sup>.

Here, we identified the FERM-domain-containing protein SNX17 as a  $\beta_1$ -tail-binding protein that, following  $\beta_1$ -integrin internalization and Kindlin dislodgement, is recruited to the free  $\beta_1$  tails in early endosomes to prevent  $\beta_1$ -integrin degradation by lysosomes.

## RESULTS

### $\beta_1$ -integrin TT788/789AA and Y795A substitutions cause peri-implantation lethality in mice

Thr 788 and 789 and Tyr 795 in the  $\beta_1$ -integrin tail are required for binding Kindlins<sup>6,9,16</sup>. To investigate their significance *in vivo* they were substituted with alanines in mice. Although mice heterozygous for the mutation were normal, their intercross failed to produce live homozygous offspring (TT/AA: +/+ : 35%, (TT/AA)/+ : 65%, (TT/AA)/(TT/AA): 0%,  $N = 100$ ; Y795A: +/+ : 33%, (Y795A)/+ : 67%, (Y795A)/(Y795A): 0%,  $N = 100$ ). Timed mating revealed severely malformed or resorbed embryos (Fig. 1a,b and Supplementary Fig. S1a) at embryonic day (E) 7.5 (+/+ : 25%, (TT/AA)/+ : 53%, (TT/AA)/(TT/AA): 17%, resorbed: 5%,  $N = 36$ ) characterized by defects in cell polarity, laminin111 deposition and cavitation (Fig. 1b). As the defects of the  $\beta_1$  TT/AA and  $\beta_1$  Y795A were identical, we mainly show results for  $\beta_1$  TT/AA mice and cells.

Embryoid bodies generated from embryonic stem (ES) cells derived from littermate wild-type ( $\beta_1$  wt) and homozygous TT/AA ( $\beta_1$  TT/AA) blastocysts confirmed the *in vivo* findings. After 2–4 days in suspension culture,  $\beta_1$  wt ES cells developed embryoid bodies consisting of an outer primitive endoderm layer, a basement membrane and an undifferentiated core, which converted into a layer of pseudo-stratified primitive ectoderm and a central cavity

<sup>1</sup>Department of Molecular Medicine, Max Planck Institute for Biochemistry, 82152 Martinsried, Germany. <sup>2</sup>These authors contributed equally to this work. <sup>3</sup>Present addresses: Department of Dermatology, Mayo Clinic, Rochester, Minnesota 55905, USA (A.M.); Institute of Medical Microbiology, Immunology and Hygiene, Technical University Munich, 81675 Munich, Germany (H.M.).

<sup>4</sup>Correspondence should be addressed to R.F. (e-mail: Faessler@biochem.mpg.de)

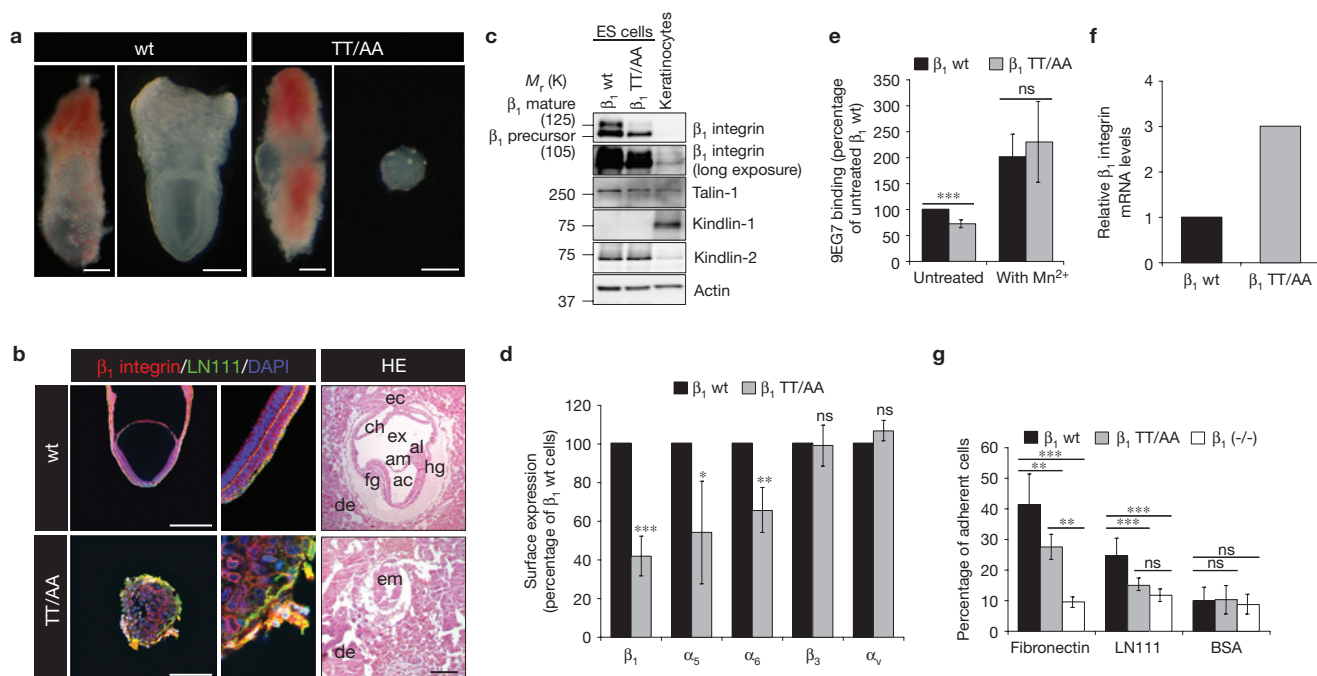


**Figure 1** The  $\beta_1$ -TT/AA-integrin tail mutation leads to severe defects. (a) Bright-field images of E7.5 embryos with and without implantation chamber. Wild type, wt. (b) Left and central panels show whole-mount pictures of E7.5 embryos stained for  $\beta_1$  integrin (red) and laminin111 (green). Nuclei were counterstained with DAPI (blue). Right panels show haematoxylin and eosin (HE) staining of E7.5 embryo sections. em, embryo; de, decidua; ac, amniotic cavity; am, amnion; al, allantois; ch, chorion; ec, ectoplacental cone; fg, foregut; hg, hindgut; ex, exocoelomic cavity. (c) Western blot for  $\beta_1$  integrin, Talin-1, Kindlin-1, Kindlin-2 and actin of embryonic stem (ES) cell lysates, including a control

lane for Kindlin-1 from a wt keratinocyte lysate. (d) Expression of integrin subunits on ES cells determined by FACS (mean  $\pm$  s.d.;  $n = 4$ ; \* $P = 0.0134$ , \*\* $P = 0.0011$ , \*\*\* $P < 0.0001$ ). (e) Integrin activation on ES cells measured by 9EG7 binding and corrected for total  $\beta_1$ -integrin expression (mean  $\pm$  s.d.;  $n = 4$ ; \*\*\* $P = 0.0003$ ). (f) Expression of  $\beta_1$ -integrin mRNA in ES cells measured by quantitative real-time PCR ( $n = 2$ ). (g) Adhesion assay of ES cells on different substrates (mean  $\pm$  s.d.;  $n = 3$ ; \*\* $P < 0.01$  and \*\*\* $P < 0.005$ ).  $P$  values, Student's  $t$ -test; ns, not significant. Scale bars, 100  $\mu$ m. Uncropped images of blots are shown in Supplementary Fig. S6.

on day 4–6 (Supplementary Fig. S1b). In contrast,  $\beta_1$  TT/AA ES cells formed compact aggregates covered by a discontinuous basement membrane and few endoderm cells, which lost their polarized  $\beta$ -catenin, E-cadherin and F-actin distribution, and lacked a central cavity (Supplementary Fig. S1b,c).

$\beta_1$  TT/AA ES cells adhered less to feeder cells (Supplementary Fig. S1d) and had reduced levels of the mature (relative molecular mass, 125,000;  $M_r$  125K)  $\beta_1$  integrin, whereas Kindlin-2 and Talin-1 expression were normal (Fig. 1c). Fluorescence-activated cell sorting (FACS) analysis confirmed reduced  $\beta_1$ -integrin surface levels to about 40% in  $\beta_1$  TT/AA ES cells and revealed decreased levels of  $\alpha_5$  and  $\alpha_6$  integrins, whereas  $\beta_3$  and  $\alpha_v$  levels were unaffected (Fig. 1d). Kindlin-2 binding to the  $\beta_1$ -integrin tail is required for activating the 9EG7 epitope in ES cells<sup>7</sup>. The level of 9EG7 antibody binding to  $\beta_1$  TT/AA was reduced after adjusting to total  $\beta_1$  levels but could be normalized to wt levels with manganese (Fig. 1e). The reduced  $\beta_1$ -TT/AA-integrin levels were not due to insufficient messenger RNA transcription, as we detected increased  $\beta_1$ -integrin mRNA transcript levels in  $\beta_1$  TT/AA ES cells (Fig. 1f). 'Plate-and-wash' adhesion assays revealed a significantly diminished level of attachment of  $\beta_1$  TT/AA ES cells to ECM substrates (Fig. 1g). Similar results were observed in  $\beta_1$  Y795A ES cells (Supplementary Fig. S1e–g).

To determine whether the reduced level of  $\beta_1$  TT/AA and  $\beta_1$  Y795A surface expression occurs in other cell types, we characterized fibroblasts expressing  $\beta_1$  wt,  $\beta_1$  TT/AA or  $\beta_1$  Y795A integrins.

We generated  $\beta_1$ -null fibroblasts from floxed  $\beta_1$  parental cells re-expressing either  $\beta_1$  wt,  $\beta_1$  TT/AA or  $\beta_1$  Y795A complementary DNAs. We also isolated fibroblasts from  $\beta_1$  flox/wt and  $\beta_1$  flox/TT/AA littermates and deleted the floxed alleles by adenoviral Cre transduction (Supplementary Fig. S2a,b). Fibroblasts from both cell systems behaved similarly in all assays. Fibroblasts expressing  $\beta_1$  TT/AA or  $\beta_1$  Y795A integrins showed a reduced level of  $\beta_1$  surface expression despite increased mRNA levels (Supplementary Fig. S2c–f and data not shown). Immunoblotting showed a reduced expression level of the mature ( $M_r$  125K)  $\beta_1$ -TT/AA-integrin polypeptide, whereas the level of immature form ( $M_r$  105K) was increased when compared with cells expressing  $\beta_1$  wt (Supplementary Fig. S2g). In line with our ES cell results, we observed significantly less 9EG7 antibody binding to  $\beta_1$ -TT/AA-expressing fibroblasts (Supplementary Fig. S2h).

These findings show that the TT/AA or Y795A  $\beta_1$  tail substitutions reduce  $\beta_1$  cell-surface levels and suggest defects in integrin processing or turnover.

### The distal NxxY motif and the adjacent TT788/789 control $\beta_1$ -integrin turnover

Surface levels of transmembrane proteins are controlled by the synthesis rate, maturation and export of the polypeptide to the cell surface, internalization, recycling and degradation. To determine whether the TT/AA substitutions alter  $\beta_1$ -integrin maturation in the secretory pathway,  $\beta_1$ -wt- and  $\beta_1$ -TT/AA-expressing fibroblasts were

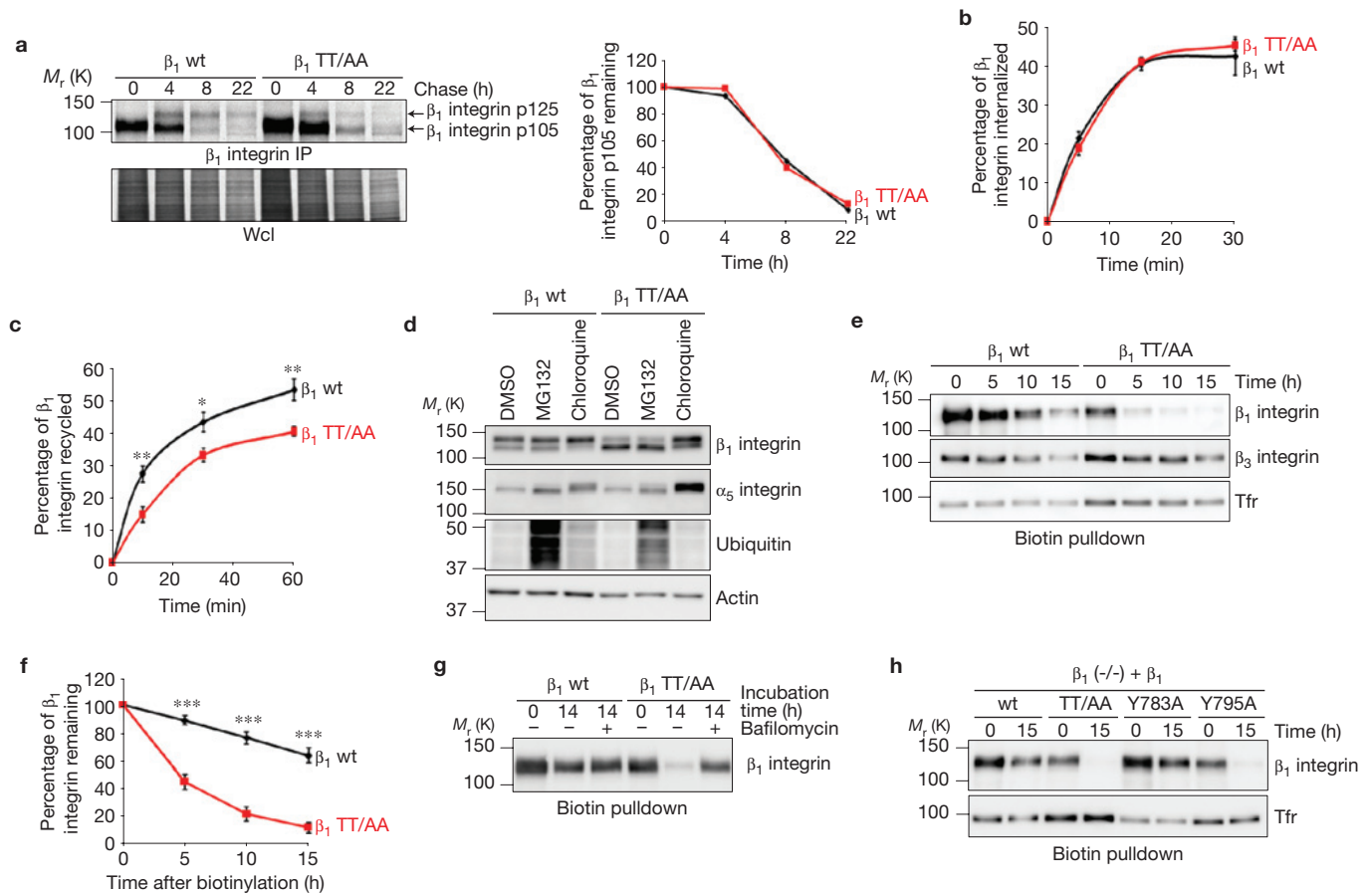


**Figure 2** TT788/789 regulate  $\beta_1$  recycling and degradation. **(a)** Pulse-chase analyses of  $\beta_1$ -integrin maturation in cells expressing wt or  $\beta_1$  TT/AA integrins. Cells were collected and analysed by immunoprecipitation after metabolic labelling with [ $^{35}$ S]methionine/cysteine and chased for the indicated time points. Maturation curves show immature  $\beta_1$  integrin as a percentage of the total  $\beta_1$  integrin (right) and were drawn from densitometric scans of the autoradiograms (left). **(b)** Quantification of  $\beta_1$ -integrin internalization in  $\beta_1$ -wt- and  $\beta_1$ -TT/AA-expressing cells by capture-ELISA (mean  $\pm$  s.d.;  $n = 4$ ). **(c)** Quantification of  $\beta_1$ -integrin recycling in  $\beta_1$ -wt- and  $\beta_1$ -TT/AA-expressing fibroblasts by capture-ELISA (mean  $\pm$  s.d.;  $n = 5$ ; \* $P < 0.05$  and \*\* $P < 0.01$ ). **(d)** Western blot analysis of  $\beta_1$ -wt- and  $\beta_1$ -TT/AA-expressing cells treated with either proteasome (MG132) or

lysosome inhibitor (chloroquine) for 20 h. Actin served as a loading control. **(e,f)** Degradation of cell-surface integrins was determined by biotinylation cell-surface proteins and incubating for the indicated time points, followed by biotin pull-down and western blot analysis **(e)** or quantification by capture-ELISA **(f)** (mean  $\pm$  s.d.;  $n = 4$ ; \*\*\* $P < 0.0001$ ). **(g)** Lysosomal inhibition by bafilomycin prevents degradation of  $\beta_1$  TT/AA integrin. Degradation was measured by surface biotinylation and incubation of the cells for 14 h in the presence or absence of bafilomycin. **(h)** Degradation of  $\beta_1$ -integrin mutants (wt, TT/AA, Y783A and Y795A) was determined by biotinylation cell-surface proteins and incubating for 0 h and 15 h, followed by biotin pull-down and western blot analysis. All  $P$  values, Student's  $t$ -test. Uncropped images of blots are shown in Supplementary Fig. S6.

pulse labelled with [ $^{35}$ S]methionine/cysteine. Owing to the higher  $\beta_1$ -TT/AA-integrin mRNA levels,  $\beta_1$  TT/AA cells expressed more immature  $\beta_1$  integrin in the initial pulse-labelling phase; however, the immature,  $M_r$ 105K-sized  $\beta_1$ -integrin polypeptide disappeared in both cell types with the same kinetics, indicating that the TT/AA mutation does not affect the initial processing of the  $\beta_1$  polypeptide (Fig. 2a). The increased ratio between the  $M_r$ 105K- and the  $M_r$ 125K-sized  $\beta_1$  polypeptides in  $\beta_1$  TT/AA fibroblasts and the increased persistence of the  $M_r$ 125K  $\beta_1$  wt polypeptide indicated marked differences in  $\beta_1$  TT/AA turnover. As integrin turnover is affected by intracellular trafficking, we compared  $\beta_1$  wt and  $\beta_1$  TT/AA internalization and recycling by surface labelling with cleavable biotin. Whereas  $\beta_1$  wt and  $\beta_1$  TT/AA integrins internalized with the same kinetics, the TT/AA substitutions showed a decreased recycling rate back to the plasma membrane (Fig. 2b,c). The similar time constant at the start of recycling together with the significantly different plateaux of recycled  $\beta_1$  wt and

$\beta_1$  TT/AA integrins indicates that the recycling machinery is normal whereas the number of recycling integrins (reflected by the different plateaux) is lower in  $\beta_1$ -TT/AA-expressing cells.

To determine whether reduced recycling of  $\beta_1$  TT/AA to the cell surface results from increased degradation, we treated  $\beta_1$  wt and  $\beta_1$  TT/AA fibroblasts with the lysosomal inhibitor chloroquine or the proteasomal inhibitor MG132. Lysosome inhibition rescued the mature  $\beta_1$  TT/AA to wt levels and stabilized the corresponding  $\alpha_5$  subunit, whereas proteasome inhibition had no effect on  $\beta_1$  TT/AA and  $\alpha_5$  stability (Fig. 2d). We also determined the degradation kinetics of the surface  $\beta_1$  integrins by surface labelling of  $\beta_1$  wt and  $\beta_1$  TT/AA cells with biotin, followed by the measurement of biotinylated proteins after pull-down with streptavidin beads and immunoblotting or capture enzyme-linked immunosorbent assay (ELISA). Whereas  $\beta_1$  wt was slowly degraded with an estimated half-life of over 20 h, degradation of  $\beta_1$  TT/AA occurred quickly with a 4–5 h

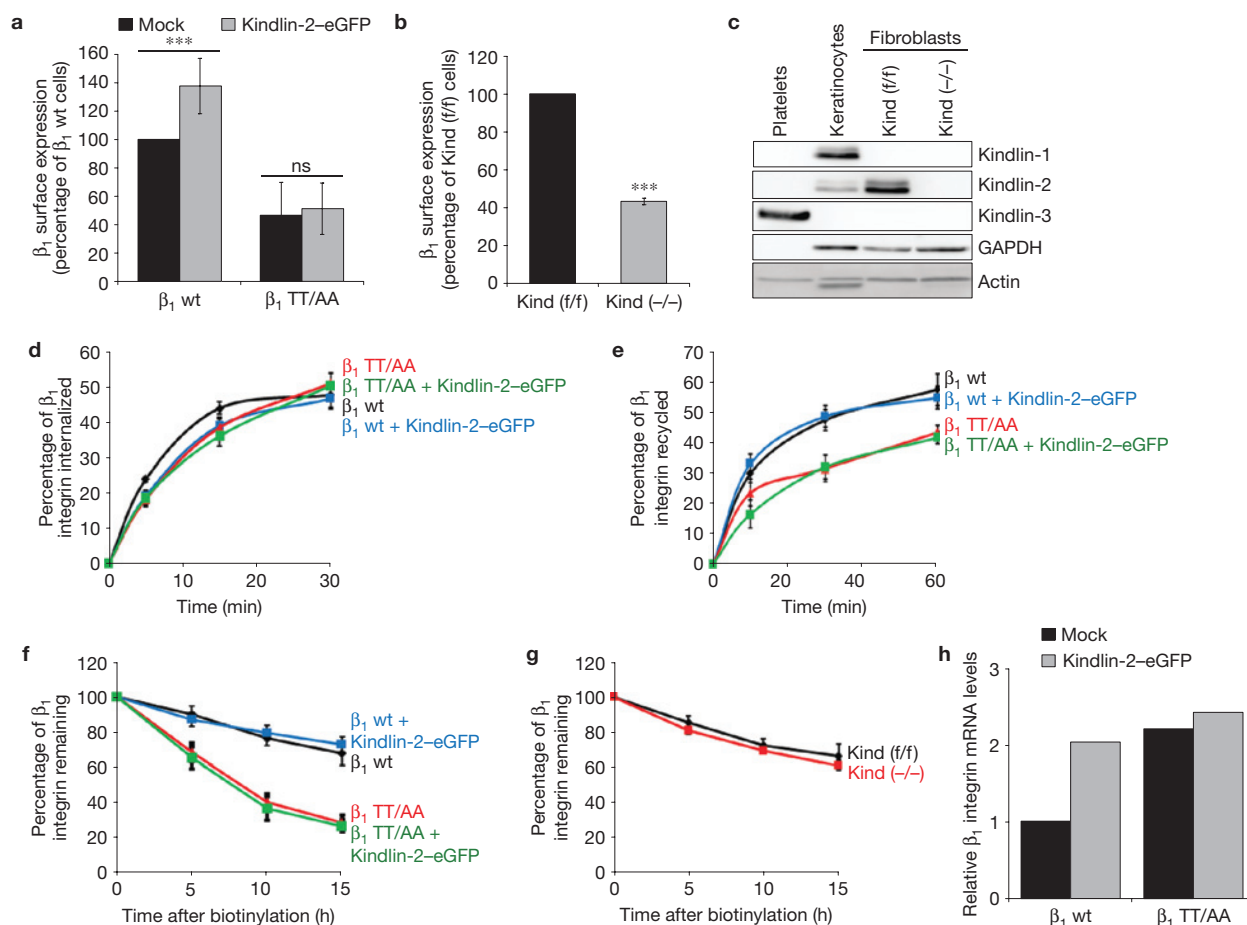


**Figure 3** Kindlin-2-dependent regulation of  $\beta_1$ -integrin surface levels. **(a)**  $\beta_1$  surface expression in  $\beta_1$ -wt- and  $\beta_1$ -TT/AA-expressing fibroblasts after overexpression of Kindlin-2-eGFP determined by FACS (mean  $\pm$  s.d.;  $n = 11$ ; \*\*\* $P < 0.0001$ ; ns, not significant). **(b)**  $\beta_1$  surface levels in control (Kind (f/f)) and Kindlin-1 and -2 double null (Kind (-/-)) fibroblasts determined by FACS (mean  $\pm$  s.d.;  $n = 3$ ; \*\*\* $P < 0.0001$ ). **(c)** Western blot analysis of cell lysates from platelets, keratinocytes and Kind (-/-) fibroblasts with antibodies against the three Kindlin family members. Actin and GAPDH served as loading control. **(d,e)** Quantification of  $\beta_1$ -integrin internalization **(d)** and recycling **(e)** in

$\beta_1$  wt and  $\beta_1$  TT/AA cells with and without Kindlin-2-eGFP overexpression by capture-ELISA (mean  $\pm$  s.e.m.;  $n = 8$  **(d)** and  $n = 10$  **(e)**). **(f,g)** Quantification of surface  $\beta_1$ -integrin stability in Kindlin-2-eGFP-overexpressing **(f)** and Kind (-/-) cells **(g)**. Degradation of cell-surface  $\beta_1$  integrin was determined by biotinylating cell-surface proteins and incubating for the indicated time points, followed by capture-ELISA (mean  $\pm$  s.d.;  $n = 4$  **(f)**;  $n = 3$  **(g)**; ns, not significant). **(h)**  $\beta_1$ -integrin mRNA expression in Kindlin-2-eGFP-overexpressing fibroblasts measured by quantitative real-time PCR ( $n = 2$ ). All  $P$  values, Student's  $t$ -test. Uncropped images of blots are shown in Supplementary Fig. S6

half-life (Fig. 2e,f). This was specific to  $\beta_1$  integrin as the degradation rates of  $\beta_3$  integrin and the transferrin receptor (Tfr) were similar in both cell types (Fig. 2e). Furthermore, bafilomycin rescued the degradation of biotinylated  $\beta_1$  TT/AA, confirming that the instability of  $\beta_1$  TT/AA results from lysosomal degradation (Fig. 2g). To determine whether the  $\beta_1$ -tail NxxY motifs are also required for  $\beta_1$ -integrin stability, we expressed  $\beta_1$  Y783A and  $\beta_1$  Y795A integrins in  $\beta_1$ -null cells. Biotinylated  $\beta_1$  protein was detectable after 15 h in  $\beta_1$ -wt- and  $\beta_1$ -Y783A-expressing cells, but was almost completely degraded in  $\beta_1$ -TT/AA- and  $\beta_1$ -Y795A-expressing cells (Fig. 2h).

These experiments indicate that the TT788/789 and distal NxxY sequence control turnover of surface  $\beta_1$  integrins.

### Kindlin-2 regulates $\beta_1$ surface levels by controlling $\beta_1$ -integrin mRNA levels

As the TT788/789 and the membrane-distal NxxY motif in  $\beta_1$  integrin tails are required for Kindlin binding<sup>6,9,16</sup>, we investigated whether

disrupting this interaction was responsible for the reduced  $\beta_1$  TT/AA surface levels, recycling and stability. As reported, overexpression of Kindlin-2-eGFP in  $\beta_1$  wt cells significantly increased  $\beta_1$ -integrin surface levels<sup>17</sup>, but not in  $\beta_1$ -TT/AA-expressing fibroblasts, probably because their mRNA levels are already upregulated (Fig. 3a). Conversely,  $\beta_1$ -integrin surface levels were significantly diminished in fibroblasts lacking the *kindlin-1* and -2 genes (Fig. 3b,c). Despite increased  $\beta_1$  surface levels in Kindlin-2-overexpressing cells, internalization, recycling (Fig. 3d,e) and stability of surface  $\beta_1$  integrins were normal (Fig. 3f). Furthermore, the degradation of surface  $\beta_1$  integrins was unchanged in fibroblasts lacking Kindlin-1 and -2 (Fig. 3g). Instead, the  $\beta_1$ -integrin mRNA levels were increased in Kindlin-2-eGFP-overexpressing cells (Fig. 3h). Internalization and recycling assays could not be performed with cells lacking Kindlin-1 and -2, as their adhesion to ECM substrates was very weak and cells were lost during the assays. Collectively, these data show that Kindlin-2 increases  $\beta_1$ -integrin surface expression primarily by upregulating  $\beta_1$ -integrin mRNA levels.

### SNX17 interacts with the TT788/789–Y795 motif of the $\beta_1$ cytoplasmic domain

To understand how TT788/789 and the membrane-distal NxxY motif regulate recycling, stability and surface expression of  $\beta_1$  integrins, we screened for new  $\beta_1$ -tail-interacting protein(s) using stable isotope labelling by amino acids in cell culture<sup>18</sup> (SILAC) followed by pulldown experiments with synthesized full-length  $\beta_1$  wt,  $\beta_1$  TT/AA cytoplasmic domain or scrambled peptides (to identify nonspecific interactors) and mass-spectrometry-based proteomics<sup>19</sup>. Among proteins with high light-to-heavy isotope ratios indicative for specific binding, were known  $\beta_1$ -tail-interacting proteins such as Talin-1, Talin-2, Kindlin-2, Dab2 and ILK, and also SNX17 (Fig. 4a and Supplementary Table S1). Only four of these proteins failed to bind when compared with a  $\beta_1$ -TT/AA-integrin tail, and of those Kindlin-2 and SNX17 showed the highest ratios (Fig. 4a). SNX17 belongs to the sorting nexin (SNX) family of adaptor proteins whose hallmark is a phox-homology (PX) domain known to mediate association with phosphatidylinositol-3-monophosphate (PtdIns(3)P)-enriched endosomes<sup>20</sup>. Similarly to Talin and Kindlin, SNX17 contains a FERM domain with a QW motif in the F3 subdomain required in Talin and Kindlin for binding the  $\beta_1$  tail<sup>7,20,21</sup>. SNX17 has been implicated in endocytic trafficking of transmembrane proteins including low-density lipoprotein receptor family members LDLR and LRP1 (refs 22–24), P-selectin<sup>25</sup> and APP (ref. 26).

Consistent with the proteomic data, SNX17 and Kindlin-2 were readily detected in peptide pulldowns with  $\beta_1$  wt but not with  $\beta_1$  TT/AA,  $\beta_1$  Y795A,  $\alpha_5$  or scrambled peptides (Fig. 4b). To determine whether SNX17 directly interacts with the  $\beta_1$ -integrin tail, we performed integrin-tail-peptide-pulldown experiments with recombinant wt GST–SNX17 or GST–SNX17 with a mutated QW motif (GST–SNX17QW/AA). These experiments revealed that SNX17 binds directly to  $\beta_1$  wt but not  $\beta_1$  TT/AA,  $\beta_1$  Y795A or scrambled peptides and showed that the interaction is specific because a QW mutation in the F3 subdomain of SNX17 abolished binding (Fig. 4c). SNX17 and Kindlin-2 share the binding site on the  $\beta_1$ -integrin tail and compete for  $\beta_1$ -integrin-tail binding *in vitro* (Supplementary Fig. S3a). However they do not co-localize in living cells, indicating that they interact with the  $\beta_1$  tail in different subcellular compartments (Fig. 4d). Co-localization studies in living cells revealed that SNX17 partially overlapped with the early endosomal antigen-1 (EEA1), an early endosome marker, as well as with the Tfr, a recycling endosome marker (Fig. 4e, and Supplementary Fig. S3b). No significant co-localization was observed with the lysosomal acid membrane protein 1 (Lamp1) and Rab7 (Fig. 4f and Supplementary Fig. S3c,d). Owing to the lack of suitable antibodies, we employed live-cell microscopy to show co-localization of eGFP-tagged SNX17 with antibody-labelled internalized  $\beta_1$  integrins (Fig. 4g) and with  $\alpha_5$  integrin–eGFP (Supplementary Fig. S3e). We also observed co-localization of SNX17–eGFP with  $\beta_1$  TT/AA-positive endosomes (Supplementary Fig. S3f), which is probably due to the binding of the PX domain to endosomal lipids. 9EG7 antibody labelling revealed the presence of active  $\beta_1$  wt integrins in focal adhesions but not in SNX17–eGFP-positive endosomes (Supplementary Fig. S3g), suggesting that SNX17-bound  $\beta_1$  integrins are in a low-affinity state. To demonstrate interactions of the endogenous proteins, we surface labelled  $\beta_1$  integrins, enriched the endosomal  $\beta_1$ -integrin

pool by inhibiting recycling with primaquine<sup>27</sup> and co-precipitated labelled  $\beta_1$  wt integrins with endogenous SNX17 (Fig. 4h). The interaction was lost in cells expressing  $\beta_1$  TT/AA integrins (Fig. 4h). These findings show that SNX17 is a  $\beta_1$ -integrin-tail-binding protein, that the interaction occurs in endosomes and that the SNX17 and Kindlin-binding site overlap.

### SNX17 is required for $\beta_1$ -integrin recycling and stabilization

To determine whether SNX17 regulates  $\beta_1$ -integrin trafficking and/or degradation we depleted SNX17 by short interfering RNA (siRNA) transfection or by short hairpin RNA (shRNA) retroviral expression (shSNX17-1 and shSNX17-2). SNX17 depletion decreased the mature  $\beta_1$ -integrin pool in whole-cell lysates (Fig. 5a) and reduced the  $\beta_1$  wt surface levels by 40% (Fig. 5b). Bafilomycin treatment rescued the mature  $\beta_1$ -wt-integrin pool, indicating enhanced lysosomal degradation in SNX17-depleted cells (Fig. 5a). Immunoblotting and capture ELISA of surface-biotinylated  $\beta_1$  integrins from control (shCtr) and SNX17-depleted fibroblasts confirmed that  $\beta_1$  wt integrins were degraded in the absence of SNX17 (Fig. 5c,d and Supplementary Fig. S4a). The increased  $\beta_1$ -integrin degradation was specific, as the stability of the Tfr and of the SNX17-binding-deficient  $\beta_1$  TT/AA integrin were unaffected by SNX17 downregulation (Fig. 5c and Supplementary Fig. S4b). Expression of shRNA-resistant wt SNX17 restored stability and  $\beta_1$ -integrin surface levels in SNX17-depleted cells, whereas SNX17QW/AA did not (Fig. 5d–f and Supplementary Fig. S4a). Similarly to  $\beta_1$  TT/AA cells,  $\beta_1$ -wt-integrin internalization was normal in SNX17-depleted cells (data not shown), whereas recycling to the cell surface was significantly impaired (Fig. 5g). Thus, SNX17 promotes recycling of  $\beta_1$  integrins and prevents their degradation.

To monitor  $\beta_1$  wt trafficking in control and SNX17-depleted cells and  $\beta_1$  TT/AA trafficking along the endocytic pathway, we labelled surface  $\beta_1$  integrins with an antibody before internalization. At 10 min after internalization,  $\beta_1$  wt- and  $\beta_1$  TT/AA-positive puncta were evenly distributed in the cytoplasm and localized to the early endosomal compartment (Supplementary Fig. S4c). At 30 min, the internalized  $\beta_1$  wt signal level in control cells was reduced, indicating that  $\beta_1$  wt efficiently recycled to the cell surface. In contrast,  $\beta_1$  TT/AA and  $\beta_1$  wt in SNX17-depleted cells co-localized with Lamp1-positive lysosomes (Supplementary Fig. S4c), supporting the observation that the  $\beta_1$ -tail/SNX17 interaction prevents routing of  $\beta_1$  integrin into the lysosome.

To investigate whether SNX17 controls recycling or degradation of  $\beta_1$  integrins, we performed recycling assays of  $\beta_1$  wt in SNX17-depleted cells and of  $\beta_1$  TT/AA in the presence and absence of bafilomycin. Bafilomycin treatment rescued the recycling rates and the surface levels of  $\beta_1$  TT/AA and  $\beta_1$  wt in SNX17-depleted cells (Fig. 5h and Supplementary Fig. S4d,e). Moreover, internalized  $\beta_1$  TT/AA and  $\beta_1$  wt in SNX17-depleted cells no longer accumulated in the late endosome/lysosome compartments 30 min after internalization (Supplementary Fig. S4c). These findings were corroborated by substituting all lysine residues of the  $\alpha_5$  and  $\beta_1$  tails with arginines ( $\beta_1$  8xKR±TT/AA;  $\alpha_5$  4xKR) to inhibit ubiquitylation and ESCRT-mediated lysosomal degradation. The lysine to arginine substitutions did not affect integrin internalization (data not shown). However, expression of the  $\beta_1$  8xKR+TT/AA

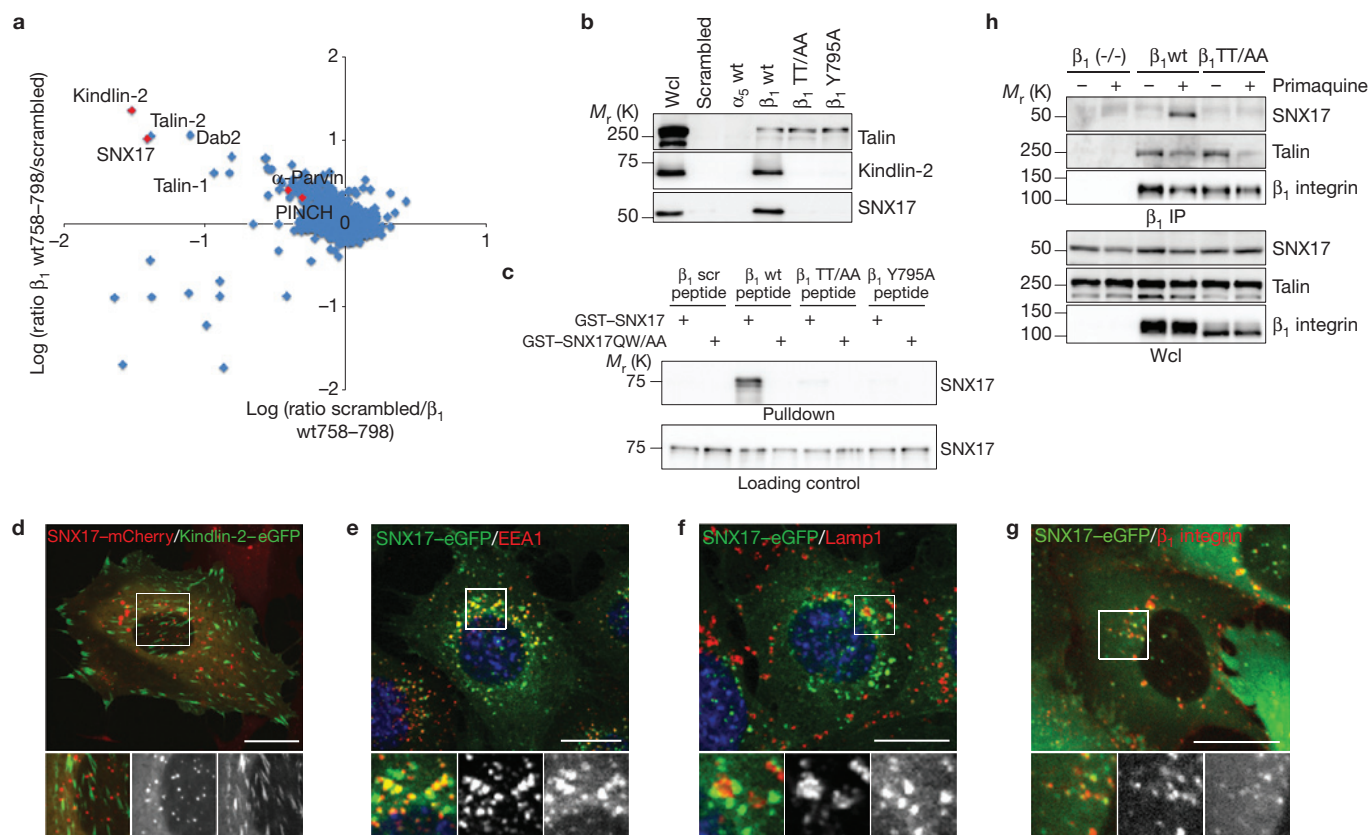


**Figure 4** SNX17 requires TT788/789 for  $\beta_1$ -integrin-tail binding. **(a)** Scatter plot of  $\beta_1$ -wt-tail peptide versus scrambled-peptide pulldown results. The log<sub>2</sub> SILAC ratio of proteins identified with at least 2 unique peptides in each mass spectrometry run is plotted as the forward pulldown (x axis) against the reverse labelling pulldown (y axis). Specific interaction partners show inverse ratios between forward and reverse experiment, grouping them into the upper left quadrant. Red dots indicate those proteins that failed to bind to the  $\beta_1$ -TT/AA-tail peptide in a separate experiment. **(b)** Western blot showing Talin-1, Kindlin-2 and SNX17 binding to the biotinylated peptides indicated. Wcl, whole-cell lysate. **(c)** Streptavidin-bead pulldown assay with the indicated biotinylated  $\beta_1$ -integrin cytoplasmic tail peptides and recombinant GST-tagged SNX17 or a GST-tagged SNX17QW/AA. **(d)** SNX17-mCherry-expressing cells were transfected with Kindlin-2-eGFP and fluorescence distribution was

determined in living cells by spinning-disc confocal microscopy. Stills of movies are shown. **(e, f)** Immunostaining of SNX17-eGFP-expressing cells with EEA1 **(e)** and Lamp1 **(f)** antibodies. Nuclei were counterstained with DAPI (blue). Correlation coefficient 0.300  $\pm$  0.116 (EEA1), -0.457  $\pm$  0.141 (Lamp1); mean  $\pm$  s.d.;  $n = 44$  **(e)**;  $n = 25$  **(f)**. **(g)** Localization of endogenous  $\beta_1$  integrin after surface labelling with an anti- $\beta_1$ -integrin antibody and internalization for 15 min in SNX17-eGFP-expressing cells. The fluorescence intensity was determined in living cells by spinning-disc confocal microscopy. A still of a movie is shown. **(h)** Co-immunoprecipitation of endogenous  $\beta_1$  integrin and SNX17 from  $\beta_1$ -wt- and  $\beta_1$ -TT/AA-expressing cells pre-treated with or without primaquine. Wcl, whole-cell lysate. Scale bars, 20  $\mu$ m. In **d-g**, lower panels show an enlargement of the area indicated by the white rectangle. Uncropped images of blots are shown in Supplementary Fig. S6.

together with  $\alpha_5$  4xKR rescued the instability and recycling rates induced by the TT/AA mutation (Fig. 5i,j). Expression of the  $\beta_1$  8xKR+TT/AA along with the  $\alpha_5$  wt was not sufficient to fully stabilize the TT/AA mutation, indicating that ubiquitylation of either the  $\alpha_5$  or the  $\beta_1$  subunit can mediate  $\alpha_5\beta_1$  degradation (Fig. 5i). Thus, SNX17 primarily functions to prevent  $\beta_1$ -integrin degradation and not  $\beta_1$ -integrin recycling.

### SNX17 is an important regulator of integrin-mediated cell functions

As Kindlin and SNX17 share the  $\beta_1$ -tail-binding site, mutations in this site affect Kindlin- and SNX17-mediated functions. To determine whether SNX17 influences integrin-mediated functions, we analysed cell spreading and migration in SNX17-depleted cells. Indeed,  $\beta_1$ -TT/AA- and  $\beta_1$ -Y795A-expressing cells and SNX17-depleted fibroblasts did not spread to the same extent as  $\beta_1$  wt cells (Fig. 6a and Supplementary Movie S1) and were less motile in single-cell migration

assays (Fig. 6b and Supplementary Movie S2). Scratch-wound assays confirmed the decreased cell velocity of  $\beta_1$ -TT/AA-expressing and SNX17-depleted cells and indicated a higher persistence when compared with  $\beta_1$  wt fibroblasts (Fig. 6c). Fibroblasts lacking  $\beta_1$  integrins barely migrated under these conditions (Fig. 6b,c). Expression of shRNA-resistant wt SNX17 in SNX17-depleted cells rescued the spreading and migration defects, whereas SNX17QW/AA did not (Fig. 6a,b). Despite these differences, focal adhesion size and F-actin distribution were not significantly altered in cells expressing  $\beta_1$  TT/AA integrins or lacking SNX17 (Supplementary Fig. S5). Interestingly, expression of  $\beta_1$  8xKR $\pm$ TT/AA +  $\alpha_5$ 4xKR restored cell spreading but not cell migration (Fig. 6d,e). Thus, SNX17 modulates several integrin-mediated functions in fibroblasts.

### DISCUSSION

The present study identified a spatiotemporally controlled series of  $\beta_1$ -integrin/protein interactions in which the TT788/789 and the

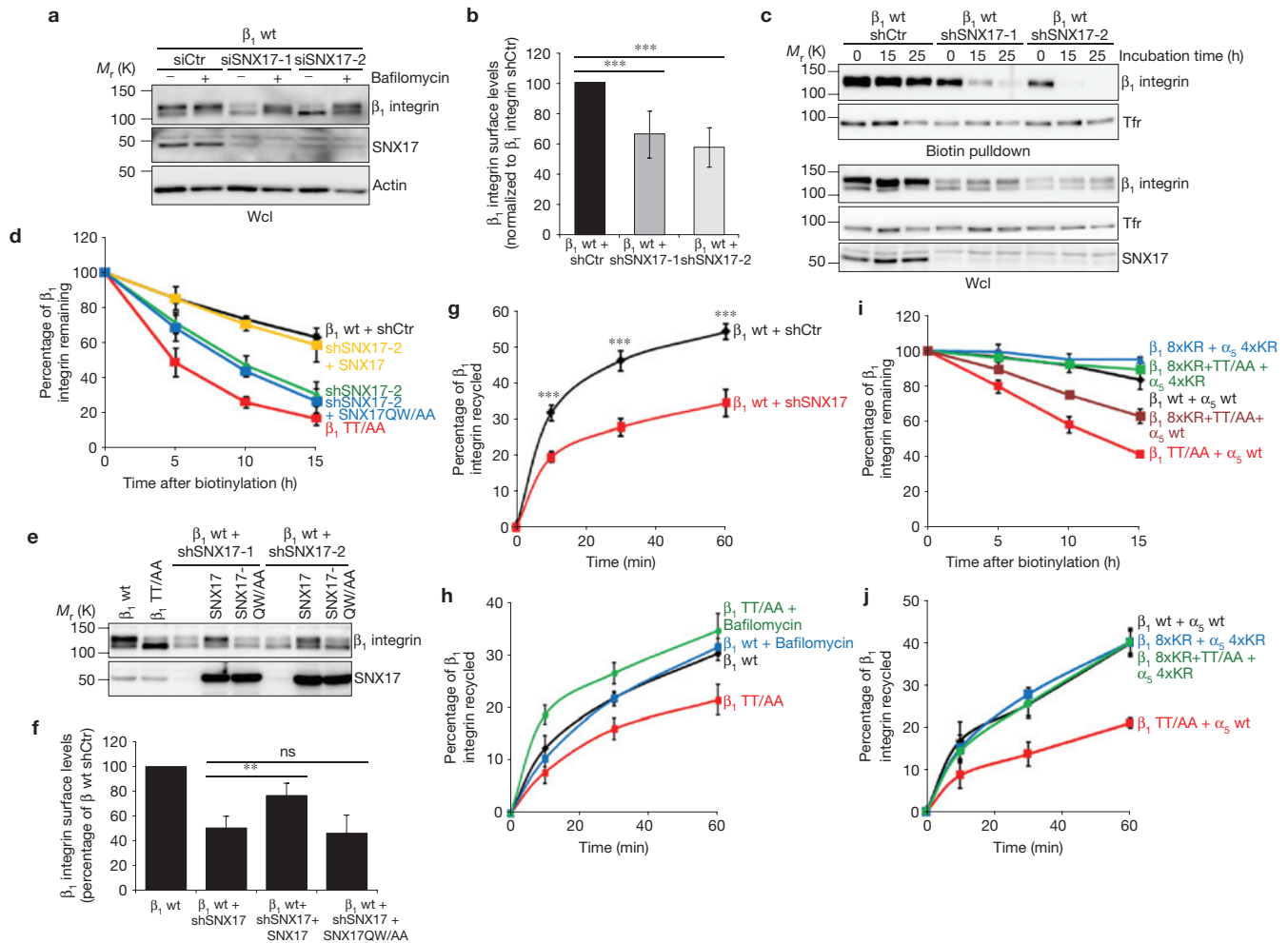


**Figure 5** Depletion of SNX17 reduces surface levels of  $\beta_1$  integrins. (a) Western blot analysis of control (siCtrl) or two siSNX17-transfected cells (siSNX17-1 and siSNX17-2) treated with or without bafilomycin for 20 h. Actin served as loading control. (b) Quantification of  $\beta_1$  surface levels in control and SNX17-depleted cells determined by FACS (mean  $\pm$  s.d.;  $n = 9$ ;  $***P < 0.0001$ ). (c,d) Degradation of cell-surface integrins was determined by biotin pulldown and western blot analysis (c) or capture-ELISA (d) (mean  $\pm$  s.d.;  $n = 5$ ). SNX17 levels in the shSNX17-2 knockdown cell line were restored by re-expressing either siRNA-insensitive wt SNX17 or SNX17QW/AA. (e) Western blot analysis of cell lysates derived from the indicated  $\beta_1$ -integrin-expressing and SNX17-depleted cells. SNX17 levels were restored in the SNX17-depleted cell lines by re-expressing either siRNA-insensitive wt SNX17 or SNX17QW/AA. (f)  $\beta_1$ -integrin surface levels in SNX17-depleted cells were restored by re-expressing siRNA-insensitive

wt SNX17 but not with SNX17QW/AA (mean  $\pm$  s.d.;  $n = 3$ ;  $**P = 0.0079$ ; ns, not significant). (g) Quantification of  $\beta_1$ -integrin recycling in SNX17-depleted cells by capture-ELISA (mean  $\pm$  s.e.m.;  $n = 7$ ;  $***P < 0.0008$ ). Note the strong reduction in the level of  $\beta_1$ -integrin recycling after SNX17 depletion. (h)  $\beta_1$ -integrin recycling is restored to wt levels in  $\beta_1$  TT/AA cells treated with bafilomycin. The quantity of biotinylated  $\beta_1$  integrin remaining within the cells was determined by capture-ELISA using  $\beta_1$ -integrin-specific antibodies (mean  $\pm$  s.e.m.;  $n = 3$ ). (i) Quantification of the stability of cell-surface  $\beta_1$  integrins by capture-ELISA. The indicated cell lines were surface biotinylated and incubated under starving conditions (mean  $\pm$  s.d.;  $n = 3$ ). (j) Quantification of  $\beta_1$ -integrin recycling determined by capture-ELISA. Cells express either  $\alpha_5$  wt and  $\beta_1$  wt or  $\alpha_5\beta_1$  with K > R-mutant tails (mean  $\pm$  s.e.m.;  $n = 4$ ). All  $P$  values, Student's  $t$ -test. Uncropped images of blots are shown in Supplementary Fig. S6.

membrane-distal NxxY motif of the  $\beta_1$ -integrin tail control the functions of  $\beta_1$  integrins at the plasma membrane and subsequently their sorting from early endosomes back to the plasma membrane. Kindlins bind these motifs with the F3-FERM subdomain and the plasma membrane with the PH domain and promote  $\beta_1$ -integrin activity and linkage to actin dynamics<sup>28,29</sup>. Following internalization,  $\beta_1$  integrins release Kindlins from their tails and are transferred into early endosomes where the free Kindlin-binding site recruits SNX17, which prevents  $\beta_1$ -integrin routing to lysosomes (Fig. 6f). Thus, the consecutive usage of the Kindlin-binding site first by Kindlins at the plasma membrane and then by SNX17 at early

endosomes could couple integrin function with integrin quality control. If so, one would predict that a major role of integrin internalization and recycling is to sort functional integrins for re-use and non-functional integrins (for example, damaged by actomyosin-mediated tension) for degradation.

SNX17 is a member of the SNX family of proteins, which contain a PX domain that serves as a phosphoinositide-binding motif to aid SNX recruitment to phosphoinositide-enriched endosomal membranes<sup>30</sup>. SNX17 harbours the characteristic PX domain at the amino terminus and a FERM domain at the carboxy terminus, which binds NPxY motifs with its phosphotyrosine (PTB)-related F3 subdomain<sup>20</sup>. The

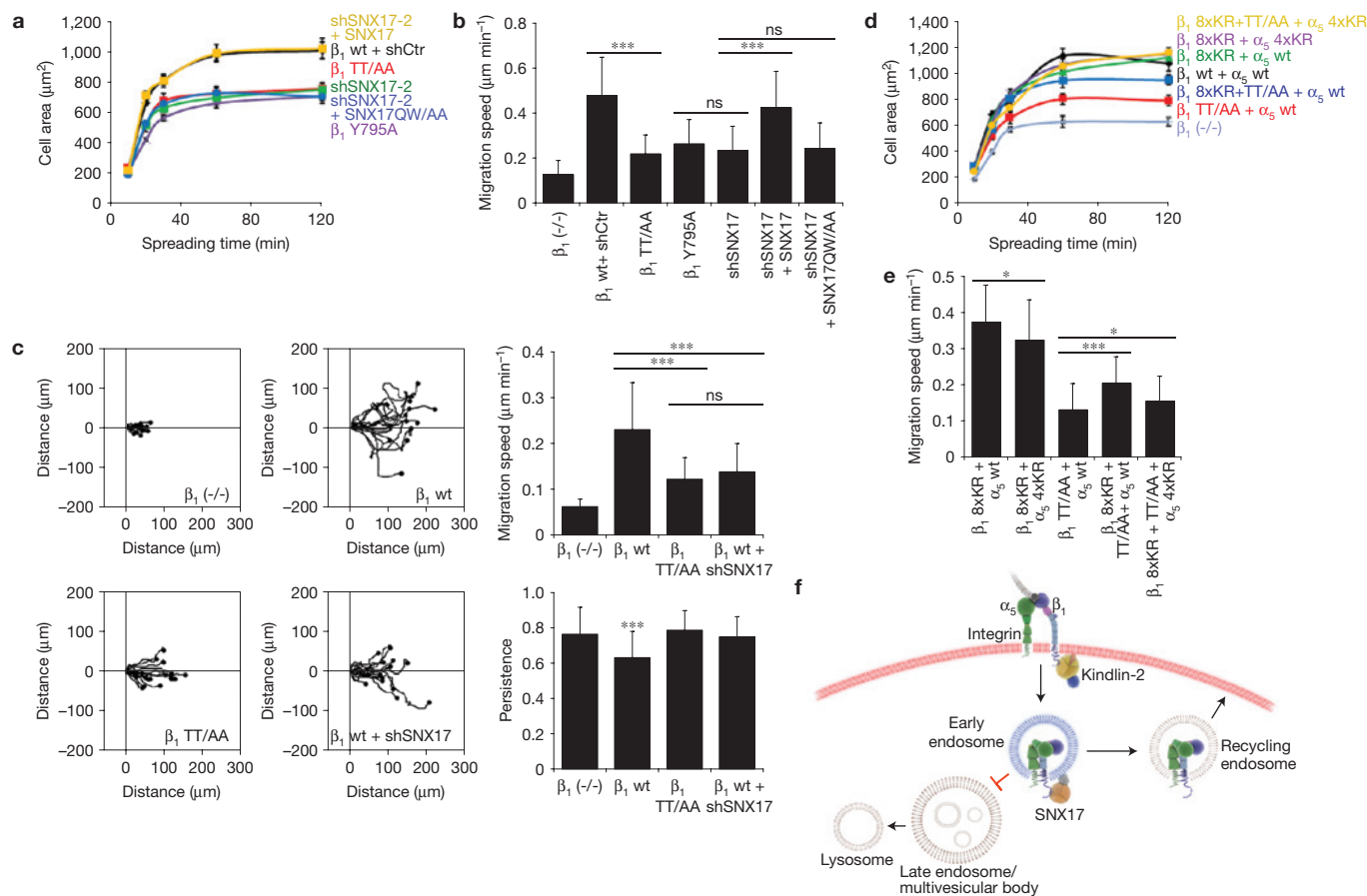


**Figure 6** SNX17 is required for  $\beta_1$ -integrin function. **(a)** Quantification of spreading area of the indicated cell lines (mean  $\pm$  s.e.m. of two independent experiments,  $n = 40$  cells). **(b)** Quantification of single-cell migration velocity of the indicated cell lines extracted from time-lapse microscopy recordings by single-cell tracking (mean  $\pm$  s.d. of three independent experiments,  $n = 82$  cells; \*\*\* $P < 0.0001$ ; ns, not significant). **(c)** Migration analysis of  $\beta_1$  wt,  $\beta_1$  (-/-),  $\beta_1$  TT/AA and SNX17-depleted cells in a scratch assay by time-lapse video microscopy. The movement of individual cells into the wound was followed using cell-tracking software and representative trajectories are shown (left panels). The speed (distance migrated per minute; upper right) and persistence of migration of cells (lower right) were quantified from the track plots (means  $\pm$  s.d. of 52 cells analysed in six individual wounds of two independent experiments; \*\*\* $P < 0.0001$ ; ns, not significant). **(d)** Quantification of spreading area of the indicated

cell lines (mean  $\pm$  s.e.m. of two independent experiments,  $n = 40$  cells). **(e)** Quantification of single-cell migration velocity of the indicated cell lines extracted from time-lapse microscopy recordings by single-cell tracking (mean  $\pm$  s.d. of three independent experiments,  $n = 60$  cells; \*\*\* $P < 0.0001$ ; \* $P < 0.0325$ ). All  $P$  values, Mann-Whitney  $U$ -test. **(f)** Model of serial Kindlin and SNX17 binding to the  $\beta_1$ -integrin cytoplasmic domain to regulate integrin affinity and trafficking. Kindlins bind the  $\beta_1$ -integrin tail with their FERM domain and to PIP2/PIP3 in the plasma membrane (red) with their PH domain to regulate the ligand affinity of integrins. Following integrin internalization, Kindlins are dislodged and SNX17 is recruited to the unoccupied Kindlin-binding site in the  $\beta_1$  tail in endosomes to prevent  $\beta_1$ -integrin degradation and to promote their recycling back to the cell surface. The  $\beta_1$ -tail/SNX17 interaction in endosomes is supported by the interaction of the SNX17 PX domain with PtdIns(3)P enriched in endosomal membranes (blue).

recruitment of SNX17 to NPxY motifs was shown to be required for turnover of several transmembrane proteins including the low-density lipoprotein receptor<sup>22,23</sup> (LDLR), LDLR-related protein 1 (LRP1; refs 24,31), P-selectin<sup>25,32</sup> and the amyloid precursor protein (APP; ref. 26). However, whether SNX17 promotes their trafficking to the plasma membrane or prevents their degradation is still unclear. We found that inhibition of lysosomal degradation restored  $\beta_1$  TT/AA recycling rates, indicating that the primary function of SNX17 binding to  $\beta_1$ -integrin tails is to prevent their degradation rather than to promote recycling (Fig. 6f). How SNX17 inhibits lysosomal degradation of  $\beta_1$  integrin is unclear and needs to be addressed in future. One possibility is that SNX17 prevents integrin sorting into inner vesicles of multi-vesicular bodies, a pre-requisite for degradation by the lysosome, for example by recruiting a

deubiquitinase that removes ubiquitin moieties from integrin tails required to interact with components of the ESCRT machinery<sup>33</sup>. Alternatively, it is possible that SNX17 prevents access of the ESCRT machinery to  $\beta_1$  integrins.

The lethality of the  $\beta_1$  TT/AA and distal Y795A mice results from a combination of functional impairments including defective integrin activation, abnormal actin dynamics and decreased integrin recycling. The reduced adhesion, spreading and migration of SNX17-depleted cells indicate that  $\beta_1$  functions are severely impaired when their degradation rate is not controlled by SNX17. The reduced  $\beta_1$ -TT/AA-integrin surface levels may also affect other functions including surface expression and signalling of growth factor receptors, co-internalization and re-secretion of fibronectin, and maybe other ECM proteins<sup>11,34</sup>. □

## METHODS

Methods and any associated references are available in the online version of the paper at [www.nature.com/naturecellbiology](http://www.nature.com/naturecellbiology)

Note: Supplementary Information is available on the Nature Cell Biology website

## ACKNOWLEDGEMENTS

We thank J. Norman and R. Ruppert for help with recycling assays and cell sorting, C. Boulegue for mass spectrometry analysis, M. Iglesias for artwork, C. Franke for His-Kindlin-2 purification and R. Zent, A. Pozzi and D. Teis for discussions and critically reading the manuscript. This work was supported by the Deutsche Forschungsgemeinschaft (SFB-914), the Tiroler Zukunftsstiftung and the Max Planck Society.

## AUTHOR CONTRIBUTIONS

R.T.B. and C.S. designed and carried out the experiments; A.M. and R.T.B. carried out the proteomics screen; H.M. generated the knock-in mice; M.W. generated Kindlin-null fibroblasts; H-Y.T. carried out the GST-pulldown experiments and contributed to the immunostainings; R.T.B., C.S. and R.F. wrote the manuscript; R.F. initiated and supervised the studies, and designed the experiments.

## COMPETING FINANCIAL INTERESTS

The authors declare no competing financial interests.

Published online at [www.nature.com/naturecellbiology](http://www.nature.com/naturecellbiology)

Reprints and permissions information is available online at [www.nature.com/reprints](http://www.nature.com/reprints)

- Hynes, R. O. Integrins: bidirectional, allosteric signaling machines. *Cell* **110**, 673–687 (2002).
- Moser, M., Legate, K. R., Zent, R. & Fässler, R. The tail of integrins, talin, and kindlins. *Science* **324**, 895–899 (2009).
- Shattil, S. J., Kim, C. & Ginsberg, M. H. The final steps of integrin activation: the end game. *Nat. Rev. Mol. Cell Biol.* **11**, 288–300 (2010).
- Calderwood, D. A. *et al.* The phosphotyrosine binding-like domain of talin activates integrins. *J. Biol. Chem.* **277**, 21749–21758 (2002).
- Calderwood, D. A. *et al.* The Talin head domain binds to integrin  $\beta$  subunit cytoplasmic tails and regulates integrin activation. *J. Biol. Chem.* **274**, 28071–28074 (1999).
- Ma, Y. Q., Qin, J., Wu, C. & Plow, E. F. Kindlin-2 (Mig-2): a co-activator of  $\beta_3$  integrins. *J. Cell Biol.* **181**, 439–446 (2008).
- Montanez, E. *et al.* Kindlin-2 controls bidirectional signaling of integrins. *Genes Dev.* **22**, 1325–1330 (2008).
- Moser, M. *et al.* Kindlin-3 is required for  $\beta_2$  integrin-mediated leukocyte adhesion to endothelial cells. *Nat. Med.* **15**, 300–305 (2009).
- Moser, M., Nieswandt, B., Ussar, S., Pozgajova, M. & Fässler, R. Kindlin-3 is essential for integrin activation and platelet aggregation. *Nat. Med.* **14**, 325–330 (2008).
- Caswell, P. T., Vadrevu, S. & Norman, J. C. Integrins: masters and slaves of endocytic transport. *Nat. Rev. Mol. Cell Biol.* **10**, 843–853 (2009).
- Sung, B. H., Zhu, X., Kaverina, I. & Weaver, A. M. Cortactin controls cell motility and lamellipodial dynamics by regulating ECM secretion. *Curr. Biol.* **21**, 1460–1469 (2011).
- Roberts, M. S., Woods, A. J., Dale, T. C., Van Der Sluijs, P. & Norman, J. C. Protein kinase B/Akt acts via glycogen synthase kinase 3 to regulate recycling of  $\alpha_v \beta_3$  and  $\alpha_5 \beta_1$  integrins. *Mol. Cell. Biol.* **24**, 1505–1515 (2004).
- Woods, A. J., White, D. P., Caswell, P. T. & Norman, J. C. PKD1/PKCmu promotes  $\alpha_v \beta_3$  integrin recycling and delivery to nascent focal adhesions. *EMBO J.* **23**, 2531–2543 (2004).
- Margadant, C., Monsuur, H. N., Norman, J. C. & Sonnenberg, A. Mechanisms of integrin activation and trafficking. *Curr. Opin. Cell Biol.* **23**, 607–614 (2011).
- Lobert, V. H. *et al.* Ubiquitination of  $\alpha_5 \beta_1$  integrin controls fibroblast migration through lysosomal degradation of fibronectin-integrin complexes. *Dev. Cell* **19**, 148–159 (2010).
- Ussar, S. *et al.* Loss of Kindlin-1 causes skin atrophy and lethal neonatal intestinal epithelial dysfunction. *PLoS Genet.* **4**, e1000289 (2008).
- Harburger, D. S., Bouaouina, M. & Calderwood, D. A. Kindlin-1 and -2 directly bind the C-terminal region of  $\beta$  integrin cytoplasmic tails and exert integrin-specific activation effects. *J. Biol. Chem.* **284**, 11485–11497 (2009).
- Ong, S. E. *et al.* Stable isotope labeling by amino acids in cell culture, SILAC, as a simple and accurate approach to expression proteomics. *Mol. Cell Proteomics* **1**, 376–386 (2002).
- Mann, M. Functional and quantitative proteomics using SILAC. *Nat. Rev. Mol. Cell Biol.* **7**, 952–958 (2006).
- Ghai, R. *et al.* Phox homology band 4.1/ezrin/radixin/moesin-like proteins function as molecular scaffolds that interact with cargo receptors and Ras GTPases. *Proc. Natl Acad. Sci. USA* **108**, 7763–7768 (2011).
- Tadokoro, S. *et al.* Talin binding to integrin  $\beta$  tails: a final common step in integrin activation. *Science* **302**, 103–106 (2003).
- Burden, J. J., Sun, X. M., Garcia, A. B. & Soutar, A. K. Sorting motifs in the intracellular domain of the low density lipoprotein receptor interact with a novel domain of sorting nexin-17. *J. Biol. Chem.* **279**, 16237–16245 (2004).
- Stockinger, W. *et al.* The PX-domain protein SNX17 interacts with members of the LDL receptor family and modulates endocytosis of the LDL receptor. *EMBO J.* **21**, 4259–4267 (2002).
- Van Kerkhof, P. *et al.* Sorting nexin 17 facilitates LRP recycling in the early endosome. *EMBO J.* **24**, 2851–2861 (2005).
- Knauth, P. *et al.* Functions of sorting nexin 17 domains and recognition motif for P-selectin trafficking. *J. Mol. Biol.* **347**, 813–825 (2005).
- Lee, J. *et al.* Adaptor protein sorting nexin 17 regulates amyloid precursor protein trafficking and processing in the early endosomes. *J. Biol. Chem.* **283**, 11501–11508 (2008).
- Van Weert, A. W., Geuze, H. J., Groothuis, B. & Stoorvogel, W. Primaquine interferes with membrane recycling from endosomes to the plasma membrane through a direct interaction with endosomes which does not involve neutralisation of endosomal pH nor osmotic swelling of endosomes. *Eur. J. Cell Biol.* **79**, 394–399 (2000).
- Meves, A., Stremmel, C., Gottschalk, K. & Fassler, R. The Kindlin protein family: new members to the club of focal adhesion proteins. *Trends Cell Biol.* **19**, 504–513 (2009).
- Liu, J. *et al.* Structural basis of phosphoinositide binding to kindlin-2 protein pleckstrin homology domain in regulating integrin activation. *J. Biol. Chem.* **286**, 43334–43342 (2011).
- Cullen, P. J. Endosomal sorting and signalling: an emerging role for sorting nexins. *Nat. Rev. Mol. Cell Biol.* **9**, 574–582 (2008).
- Donoso, M. *et al.* Polarized traffic of LRP1 involves AP1B and SNX17 operating on Y-dependent sorting motifs in different pathways. *Mol. Biol. Cell* **20**, 481–497 (2009).
- Williams, R. *et al.* Sorting nexin 17 accelerates internalization yet retards degradation of P-selectin. *Mol. Biol. Cell* **15**, 3095–3105 (2004).
- Raiborg, C. & Stenmark, H. The ESCRT machinery in endosomal sorting of ubiquitylated membrane proteins. *Nature* **458**, 445–452 (2009).
- Caswell, P. T. *et al.* Rab-coupling protein coordinates recycling of  $\alpha_5 \beta_1$  integrin and EGFR1 to promote cell migration in 3D microenvironments. *J. Cell Biol.* **183**, 143–155 (2008).

## METHODS

**Mouse strains.** The targeting constructs with the  $\beta_1$ -integrin threonine-to-alanine mutation in positions 788 and 789 ( $\beta_1$  TT/AA) and the tyrosine-to-alanine mutation in position 795 ( $\beta_1$  Y795A) were generated as previously described<sup>35</sup>. All animal studies were approved by the Regierung von Oberbayern.

**Antibodies.** The following antibodies were used for western blotting (WB) and immunofluorescence (IF): actin (A-2066, Sigma; 1:3,000 for WB),  $\beta_1$  integrin (MAB1997, MB1.2, Chemicon; 1:400 for IF),  $\beta_3$  integrin (04-1060, EP2417Y, Millipore; 1:1,000 for WB),  $\beta$ -catenin (C2206, Sigma; 1:800 for IF), E-cadherin (13-1900, ECCD-2, Zymed; 1:200 for IF), laminin111 (ab30320, Abcam; 1:400 for IF), EEA1 (610457, BD Transduction Laboratories; 1:100 for IF), GAPDH (CB1001, 6C5, Calbiochem; 1:5,000 for WB), Kindlin-2 (K3269, Sigma; 1:1,000 for WB), Lamp1 (provided by L. Huber, Medical University Innsbruck, Austria; 1:100 for staining), paxillin (610051, 349, BD Transduction Laboratories), SNX17 (10275-1-AP, Proteintech; 1:1,000 for WB), Talin-1 (T3287, 8d4, Sigma; 1:1,000 for WB), Tfr (13-6,800, H68.4, Invitrogen, 1:1,000 for WB) and ubiquitin (3936, P4D1, Cell Signaling; 1:1,000 for WB). Kindlin-1 (1:5,000 for WB), Kindlin-3 (1:5,000 for WB) and  $\beta_1$ -integrin (1:10,000 for WB) antibodies used for western blotting are home-made<sup>36,37</sup>. Phalloidin (A12379 and A22287, Molecular Probes; 1:400 for IF) was used to stain F-actin. DAPI (Sigma) was used to stain nuclei.

The following antibodies were used for flow cytometry:  $\beta_1$ -integrin PE (102207, HM $\beta_1$ -1, BioLegend; 1:400),  $\beta_1$ -integrin biotin (555004, Ha2/5, BD Pharmingen; 1:400),  $\beta_1$ -integrin 9EG7 (550531, 9EG7, BD Pharmingen; 1:100),  $\beta_3$ -integrin PE (12-0611, 2C9.G3, eBioscience; 1:400),  $\beta_4$ -integrin PE (MCA2369, 346-11A, Serotec; 1:400),  $\alpha_2$ -integrin FITC (554999, Ha1/29, BD Pharmingen; 1:400),  $\alpha_5$ -integrin PE (557447, 5H10-27, BD Pharmingen; 1:400),  $\alpha_5$ -integrin biotin (557446, 5H10-27, BD Pharmingen),  $\alpha_6$ -integrin PE (555736, GoH3, BD Pharmingen) and  $\alpha_v$ -integrin PE (551187, RMV-7, BD; 1:400).

**Plasmids and constructs.** Point mutations into the  $\beta_1$ -integrin (TT788/789AA, Y783A, Y795A, 8xKR (K752R, K765R, K768R, K770R, K774R, K784R, K794R, K798R), 8xKR+TT788/789AA),  $\alpha_5$ -integrin (4xKR (K1022R, K1027R, K1038R, K1042R)) and SNX17 (QW360/361AA) cDNA were introduced by site-directed mutagenesis. For stably expressing the  $\beta_1$ -integrin cDNAs (wt, TT788/789AA, Y783A, Y795A, 8xKR, 8xKR+TT/AA), the human  $\alpha_5$  integrin (wt, 4xKR,  $\alpha_5$ -eGFP) and the mouse SNX17 (wt, Flag-tagged, eGFP-tagged and mCherry-tagged), we used the retroviral expression vector pCLMFG or pLZRS. For recombinant expression of GST-tagged SNX17, wt SNX17 and SNX17QW360/361AA, cDNA was cloned into the pGEX-6P-1 vector (GE Healthcare). Lamp1-mRFP and Rab7-mRFP vectors were obtained from J. Norman (Beatson Institute, Glasgow, UK), and Rab5a-GFP was provided by L. Huber (Medical University Innsbruck, Austria) and transiently expressed by transfection with Lipofectamine 2000 (Invitrogen).

For stably depleting SNX17 expression, shRNA target sequences were introduced into the pSuper.Retro vector (OligoEngine) to produce retroviral particles: 5'-GTACATGCAAGCTGTTCGG-3' (shSNX17-1), 5'-GATTGTGCTCAGAAAGAGT-3' (shSNX17-2).

To obtain a GFP-tagged Kindlin-2, the Kindlin-2 cDNA (ref. 36) was ligated in frame with the GFP using sequence- and ligation-independent cloning<sup>38</sup>. The CAG promoter, GFP fusion and SV40 polyA were flanked by ITR elements; thus, co-transfection of this construct with a sleeping beauty SB100x expression vector<sup>39</sup> resulted in transposase-mediated genomic integration of this DNA sequence.

**Cell lines.** Heterozygous  $\beta_1$  TT/AA mice were intercrossed with homozygous  $\beta_1$ -floxed mice and mouse embryonic fibroblasts were isolated from E9.5 embryos, immortalized with the SV40 large T antigen and cloned before deletion of the floxed  $\beta_1$ -integrin allele by adenoviral Cre transduction. Disruption of the  $\beta_1$  allele and expression of the  $\beta_1$  TT/AA were checked by PCR. To generate  $\beta_1$ -null rescue cell lines,  $\beta_1$  wt or  $\beta_1$  mutant variants were virally re-expressed in  $\beta_1$ -null fibroblasts derived from floxed  $\beta_1$  parental cells.

Fibroblasts homozygous for floxed *kindlin-1* and *-2* genes were isolated from kidneys of 21-day-old double-floxed mice (whose generation will be described elsewhere), immortalized as described above and cloned. To obtain Kindlin-1 and *-2* double-null cells, the floxed *kindlin* alleles were removed by adenoviral Cre transduction.

**Transient and stable transfection/transduction.** Cells were transiently transfected with Lipofectamine 2000 (Invitrogen) according to the manufacturer's protocol. To generate stable cell lines, VSV-G pseudotyped retroviral vectors were produced by transient transfection of HEK293T (human embryonic kidney)

cells. Viral particles were concentrated from cell culture supernatant as described previously<sup>40</sup> and used for infection.

**Embryo isolation and histological analysis.** For whole-mount analysis, staged embryos (E6.5 to E9.5) were dissected in ice-cold PBS. For histological analysis, decidual swellings were isolated, fixed in 4% paraformaldehyde (PFA) and embedded in paraffin. Sections were stained with haematoxylin and eosin or antibodies as indicated.

**Whole-mount immunohistochemistry.** Embryos were dissected in cold PBS and fixed in 4% PFA for 2 h at 4 °C. Samples were incubated in 0.5% NP-40/PBS for 20 min and in PBSST (0.1% Triton X-100 and 5% BSA in PBS) for 2 h at 4 °C and then incubated with the primary and secondary antibody, both overnight at 4 °C. Nuclei were stained with DAPI solution for 30 min. Finally, embryos were dehydrated by increasing methanol concentrations, cleared in benzyl alcohol/benzyl benzoate (1:2) and imaged with a confocal microscope (DMIRE2; Leica) using Leica Confocal Software (version 2.5 Build 1227). After imaging, embryos were rehydrated for genotyping.

**ES cells and embryoid bodies.** ES cells were isolated and cultured as previously described<sup>41</sup>. Embryoid bodies were generated as described previously<sup>41</sup>.

**Metabolic labelling.** Cells were grown overnight to 80% confluency and incubated for 30 min at 37 °C in methionine/cysteine-free labelling media containing 10% dialysed FBS. For pulse labelling, the cells were incubated for 30 min at 37 °C in labelling medium containing [<sup>35</sup>S]methionine/cysteine (200  $\mu$ Ci/10 cm plate, EasyTag Express <sup>35</sup>S Protein Labeling Mix, PerkinElmer). After labelling, the cells were either immediately collected (time 0) or chased for 4 h, 8 h and 22 h in regular growth medium containing 10% FBS. Cells were lysed in immunoprecipitation buffer (50 mM Tris-HCl (pH 7.5), 150 mM NaCl, 1% Triton X-100, 0.1% sodium deoxycholate, 1 mM EDTA and protease inhibitors) and cleared by centrifugation. For  $\beta_1$  immunoprecipitation, lysates were first incubated with  $\beta_1$  antibodies for 1 h on ice followed by incubation with protein G Sepharose (Sigma) for 2 h at 4 °C with gentle agitation. After several washes with lysis buffer, proteins were eluted from the beads by boiling with Laemmli sample buffer and subjected to SDS-PAGE. The gels were fixed, dried and exposed to film.

**Turnover of surface integrins.** The half-life of surface proteins was determined by biotinylation. Briefly, fibroblasts were grown to 80% confluence, washed twice in cold PBS and surface biotinylated with 0.2 mg ml<sup>-1</sup> sulpho-NHS-LC-biotin (Thermo Scientific) in PBS for 45 min at 4 °C. Following washes with cold PBS, the cells were incubated in regular growth medium for 0, 5, 10 and 15 h at 37 °C. Cells were lysed in immunoprecipitation buffer and biotinylated proteins were pulled down with streptavidin-Sepharose (GE Healthcare). After three washes with lysis buffer, samples were analysed by SDS-PAGE and western blotting. For capture-ELISA, cells were lysed in a low volume of lysis buffer (75 mM Tris, 200 mM NaCl, 7.5 mM EDTA and 7.5 mM EGTA, 1.5% Triton X-100, 0.75% Igepal CA-630 and protease inhibitors).

**Integrin-trafficking assays.** Integrin-trafficking assays were performed as described previously<sup>42</sup>.

**Capture ELISA.** Maxisorb 96-well plates (Life Technologies) were coated overnight with anti- $\beta_1$ -integrin antibody (MAB1997, Chemicon; 1:250) in carbonate buffer at 4 °C. Unspecific binding was blocked by 5% BSA in PBS/0.1% Tween-20 (PBS-T) for 1–2 h at room temperature before adding 50  $\mu$ l cell lysate for incubation overnight at 4 °C to capture integrins. Following extensive washes with PBS-T, plates were incubated with streptavidin-HRP in 1% BSA in PBS-T for 1 h at 4 °C. Biotinylated  $\beta_1$  integrin was detected after several washing steps by chromogenic reaction with ABTS peroxidase substrate (Vector Laboratories).

**Selective immunoprecipitations.** Selective isolation of  $\beta_1$  integrins on the cell surface and in endocytic vesicles was achieved by cell-surface immunoprecipitation. Cell-surface  $\beta_1$  integrins of live cells were labelled with a rabbit anti- $\beta_1$ -integrin antibody (home-made; 1:1,500) for 1 h on ice. After two washes with ice-cold PBS to remove unbound antibody, cells were incubated for 20 min in medium with or without 0.5 mM primaquine to inhibit integrin recycling to the cell surface<sup>42</sup>. Cells were then washed twice with PBS, lysed in immunoprecipitation buffer and cleared by centrifugation.  $\beta_1$ -integrin immune complexes were pulled down by incubation with protein G Sepharose (Sigma) for 2 h at 4 °C with gentle agitation. After several washes with lysis buffer, proteins were subjected to SDS-PAGE and western blot analysis.

**SILAC-based peptide pulldowns.** Pulldowns were performed as described previously<sup>43</sup> with  $\beta_1$  wt cytoplasmic tail peptides (758–598: HDRREFAKFEKEKMNAKWDGTGENPIYKSAVTTVVNPKYEGK-OH),  $\beta_1$  TT/AA tail peptide (HDRREFAKFEKEKMNAKWDGTGENPIYKSAVAVVNPKYEGK-OH),  $\beta_1$  Y795A tail peptide (HDRREFAKFEKEKMNAKWDGTGENPIYKSAVTTVVNPKAEGK-OH), a scrambled peptide (EYEFEPDKVDGTGAKGTKMAKNEKKFRNYTVHNIWESRKVAP-OH) and  $\alpha_5$  peptide (KLGFFKRSLPYGTAMEKAQLKPPATSDA-OH). All peptides were desthiobiotinylated. Before use, peptides were immobilized on 75  $\mu$ l Dynabeads MyOne Streptavidine C1 (10 mg ml<sup>-1</sup>, Invitrogen).

After cell-lysate generation and incubation with tail peptides, proteins were eluted and precipitated as described previously<sup>43</sup>. The protein pellet was dissolved in SDS-PAGE sample buffer and separated on a 4–15% gradient SDS-PAGE gel. The gel was stained with Coomassie blue using the GelCode Blue Safe Protein Stain reagent (Thermo Scientific) and used for mass analysis.

**Expression and purification of recombinant proteins.** Plasmids encoding GST-SNX17 or GST-SNX17QW/AA were transformed into BL21(DE3) Arctic Express *Escherichia coli*, and protein expression was induced with 1 mM IPTG. Afterwards, cells were pelleted, lysed and centrifuged. Supernatants were incubated with glutathione Sepharose beads (GST-binding resin, Novagen) and GST-tagged proteins were eluted according to the manufacturer's instruction.

Plasmid coding for His-tagged Kindlin-2 was transformed into BL21 T1 pRARE bacteria. Supernatants were generated as described above, incubated with His-Select Ni Affinity gel (Sigma) and His-tagged Kindlin-2 was eluted and subjected to gel filtration for further purification.

For pulldowns, synthetic peptides were immobilized on 20  $\mu$ l Dynabeads MyOne Streptavidine C1 (10 mg ml<sup>-1</sup>, Invitrogen) for 3 h at 4 °C, incubated with 2% BSA in Mammalian Protein Extraction Reagent (Thermo Scientific) for 30 min to block unspecific binding before adding 50 ng recombinant GST-tagged SNX17 protein and further incubation on a rotator for 2 h at 4 °C. For competition experiments, 50 ng GST-SNX17 and 500 ng His-Kindlin-2 or 500 ng BSA were incubated with the tail peptides for 3 h at 4 °C. After three washes with RIPA buffer, proteins were eluted from the beads by boiling with 80  $\mu$ l SDS-PAGE sample buffer for 5 min, separated by SDS-PAGE gel and blotted with SNX17 antibody.

**Quantitative PCR.** RNA was isolated from cells using the RNeasy mini kit (Qiagen) and 1  $\mu$ g of total RNA was transcribed into cDNA using the iScriptDNA Synthesis kit (Bio-Rad). Quantitative PCR assays were performed with the iCyclerIQ (Bio-Rad) using SYBR green and the following primers:  $\beta_1$  integrin-forward (5'-atgcaaatcttgaggagaat-3'),  $\beta_1$  integrin-reverse (5'-tttgctgctgattgacatt-3'),  $\beta_3$  integrin-forward (5'-ccacacaggcgtgaatc-3'),  $\beta_3$  integrin-reverse (5'-cttcagggtacatcggtga-3'), GAPDH-forward (5'-tcgtgatctgactgcccctg-3'), GAPDH-reverse (5'-caccacctgtgctgtagcctat-3').

**Immunofluorescence microscopy.** For immunostaining, cells were cultured on glass coated with 10  $\mu$ g ml<sup>-1</sup> fibronectin (Calbiochem). For the detection of endosomes, cells were fixed with 4% PFA/PBS for 15 min on ice, washed with PBS and permeabilized with 0.01% saponin/PBS for 10 min on ice. Cells were blocked with 3% BSA/PBS for 1 h followed by incubation with the primary antibody in 3% BSA/0.01% saponin/PBS overnight at 4 °C and secondary antibodies for 1 h at room temperature in the dark. All other staining was performed as described previously<sup>44</sup>.

To determine the endocytic trafficking of  $\beta_1$  integrins from the cell surface by surface labelling, cells were washed with cold PBS and incubated with an anti- $\beta_1$ -integrin antibody (102202, HM $\beta$ 1-1, BioLegend; 1:400) for 30 min on ice. Surface-bound antibody was allowed to internalize for different times at 37 °C in regular growth medium. At each time point, the samples were washed with cold PBS and the remaining antibody at the cell surface was removed by two acid washes (0.2 M acetic acid/0.5 M NaCl/PBS) for 2 min on

ice. Subsequently, the cells were fixed, permeabilized and stained as described above.

Images were collected at room temperature by confocal microscopy (DMIRE2; Leica) with a  $\times 63/1.4$  objective using the Leica Confocal Software (version 2.5, build 1227) or collected with an AxioImager Z1 microscope (Zeiss) with a  $\times 63/1.4$  oil objective.

**Time-lapse video microscopy of cell spreading and migration.** Cell spreading and single-cell migration assays were done as described previously<sup>44</sup>. Cell spreading was also measured with cells seeded on fibronectin-coated glass slides, fixed with 4% PFA at 37 °C at indicated time points and stained with phalloidin-Alexa488 for F-actin. Images were taken with an AxioImager Z1 microscope (Zeiss, Germany) with a  $\times 20$  objective and the spreading area was calculated using MetaMorph 7 (Molecular Devices) imaging software.

For single-cell migration, the acquired images were analysed using the manual tracking plugin of ImageJ and the Chemotaxis and Migration Tool (v2.0) of the QWT project.

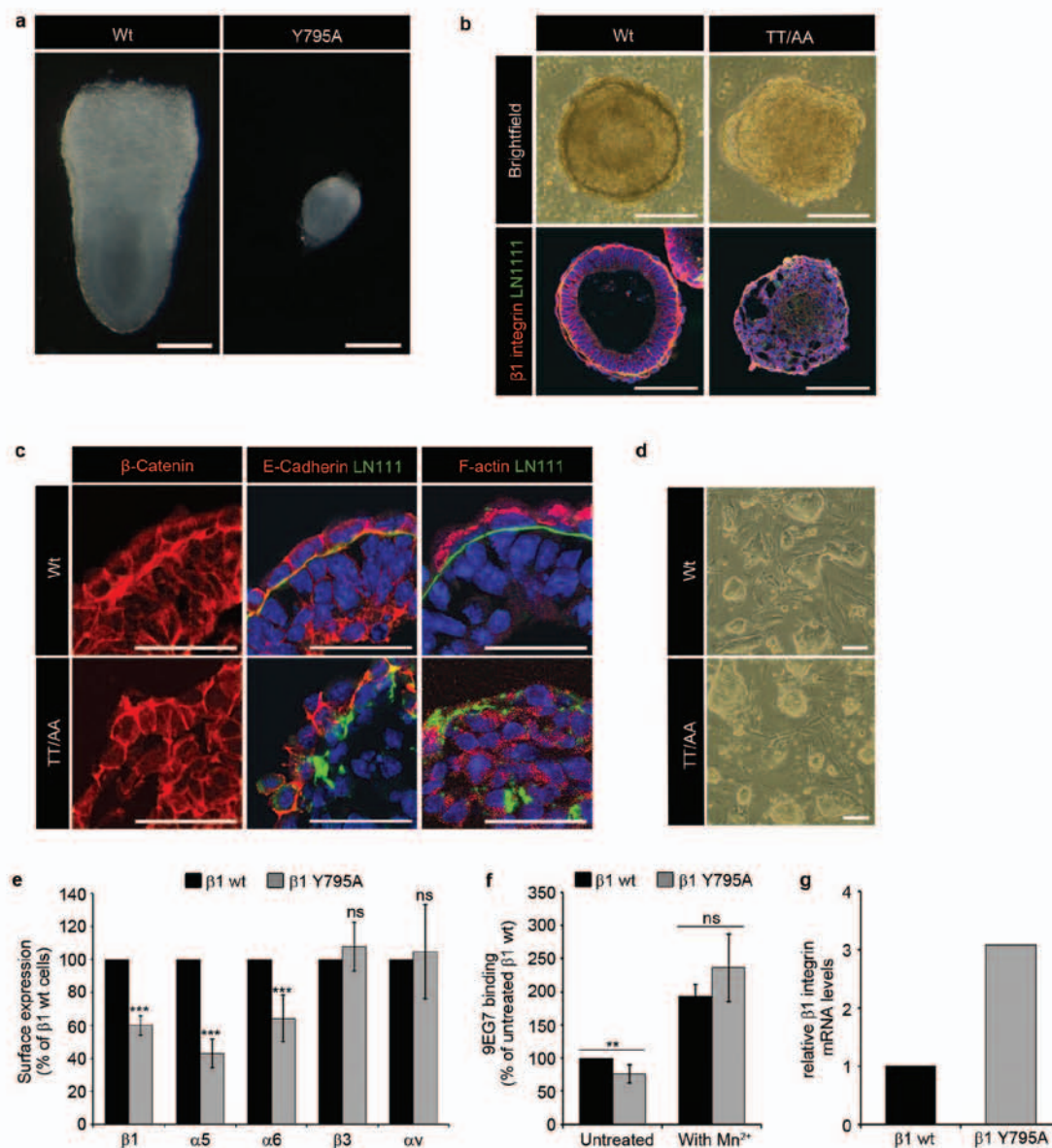
Cell-wounding assays were performed with confluent monolayers of cells cultured in fibronectin-coated 6-well dishes. Cells were serum-starved overnight before wounds were applied with a 200  $\mu$ l plastic micropipette followed by thorough washing with PBS. Wound closure was imaged in serum-free medium at 15 min intervals overnight. The acquired images were analysed using the manual tracking plugin of ImageJ and the Chemotaxis and Migration Tool (v2.0) of the QWT project.

Images of live cells were recorded at 37 °C and 5% CO<sub>2</sub> on a Zeiss Axiovert 200 M (Zeiss, Germany) equipped with  $\times 10/0.3$ ,  $\times 20/0.4$  and  $\times 40/0.6$  objectives, a motorized stage (Märzhäuser) and an environment chamber (EMBL Precision Engineering) with a cooled CCD (charge-coupled device) camera (Roper Scientific). Image acquisition and microscope control were carried out with MetaMorph software (Molecular Devices).

**Statistics.** Statistical analysis was performed using the GraphPad Prism software (version 5.00, GraphPad Software). Statistical significance was determined by the unpaired *t*-test or Mann-Whitney *U*-test as indicated. Results are expressed as the mean  $\pm$  s.d. unless indicated otherwise.

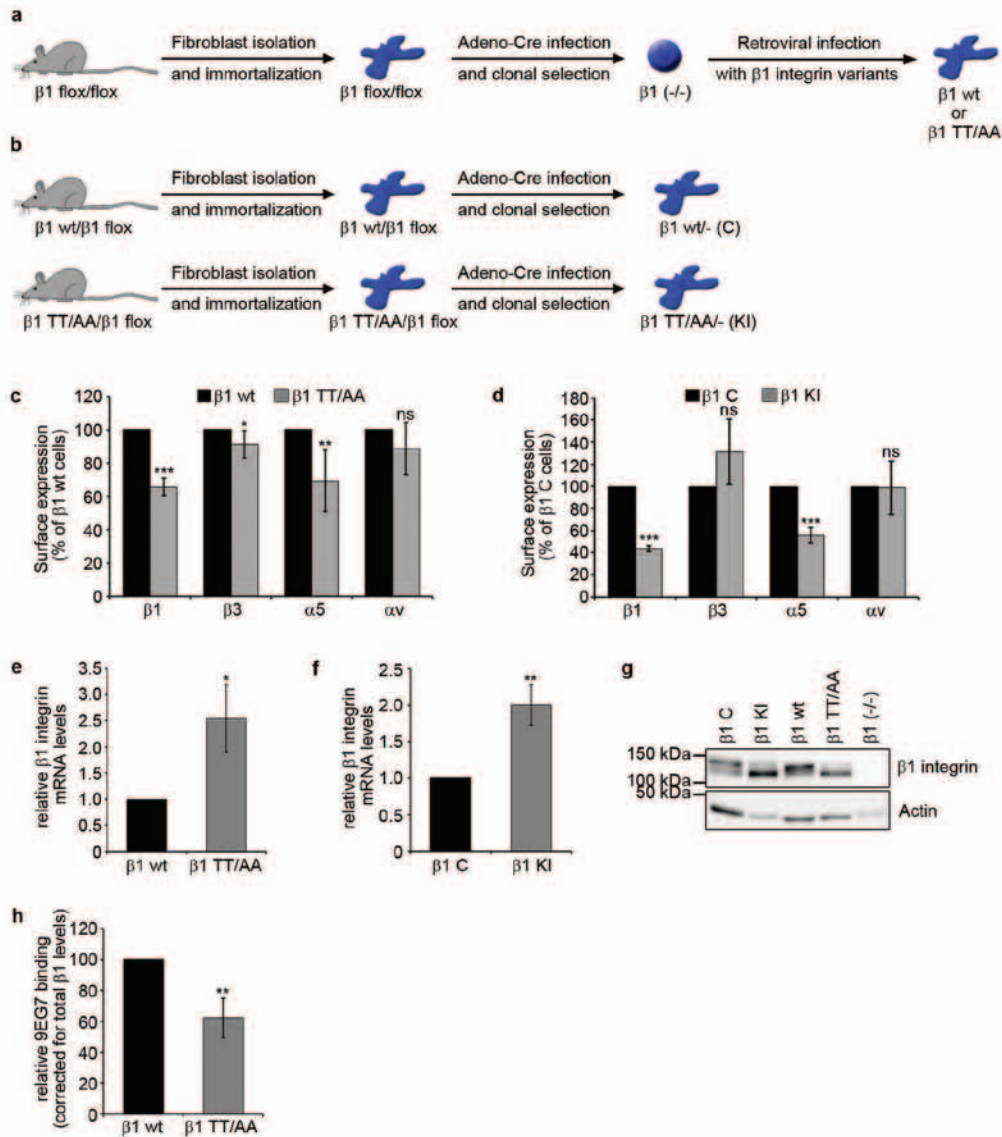
35. Czuchra, A., Meyer, H., Legate, K. R., Brakebusch, C. & Fässler, R. Genetic analysis of  $\beta_1$  integrin 'activation motifs' in mice. *J. Cell Biol.* **174**, 889–899 (2006).
36. Ussar, S., Wang, H. V., Linder, S., Fässler, R. & Moser, M. The Kindlins: subcellular localization and expression during murine development. *Exp. Cell Res.* **312**, 3142–3151 (2006).
37. Azimifar, S. B. *et al.* Induction of membrane circular dorsal ruffles requires co-signalling of integrin-ILK-complex and EGF receptor. *J. Cell Sci.* **125**, 435–448 (2012).
38. Li, M. Z. & Elledge, S. J. Harnessing homologous recombination in vitro to generate recombinant DNA via SLIC. *Nat. Methods* **4**, 251–256 (2007).
39. Mates, L. *et al.* Molecular evolution of a novel hyperactive Sleeping Beauty transposase enables robust stable gene transfer in vertebrates. *Nat. Genet.* **41**, 753–761 (2009).
40. Pfeifer, A., Kessler, T., Silletti, S., Cheresh, D. A. & Verma, I. M. Suppression of angiogenesis by lentiviral delivery of PEX, a noncatalytic fragment of matrix metalloproteinase 2. *Proc. Natl Acad. Sci. USA* **97**, 12227–12232 (2000).
41. Montanez, E. *et al.* Analysis of integrin functions in peri-implantation embryos, hematopoietic system, and skin. *Methods Enzymol.* **426**, 239–289 (2007).
42. Roberts, M., Barry, S., Woods, A., van der Sluijs, P & Norman, J. PDGF-regulated rab4-dependent recycling of  $\alpha_3\beta_3$  integrin from early endosomes is necessary for cell adhesion and spreading. *Current Biol.* **11**, 1392–1402 (2001).
43. Meves, A. *et al.*  $\beta_1$  integrin cytoplasmic tyrosines promote skin tumorigenesis independent of their phosphorylation. *Proc. Natl Acad. Sci. USA* **108**, 15213–15218 (2011).
44. Böttcher, R. T. *et al.* Profilin 1 is required for abscission during late cytokinesis of chondrocytes. *EMBO J.* **28**, 1157–1169 (2009).

DOI: 10.1038/ncb2501



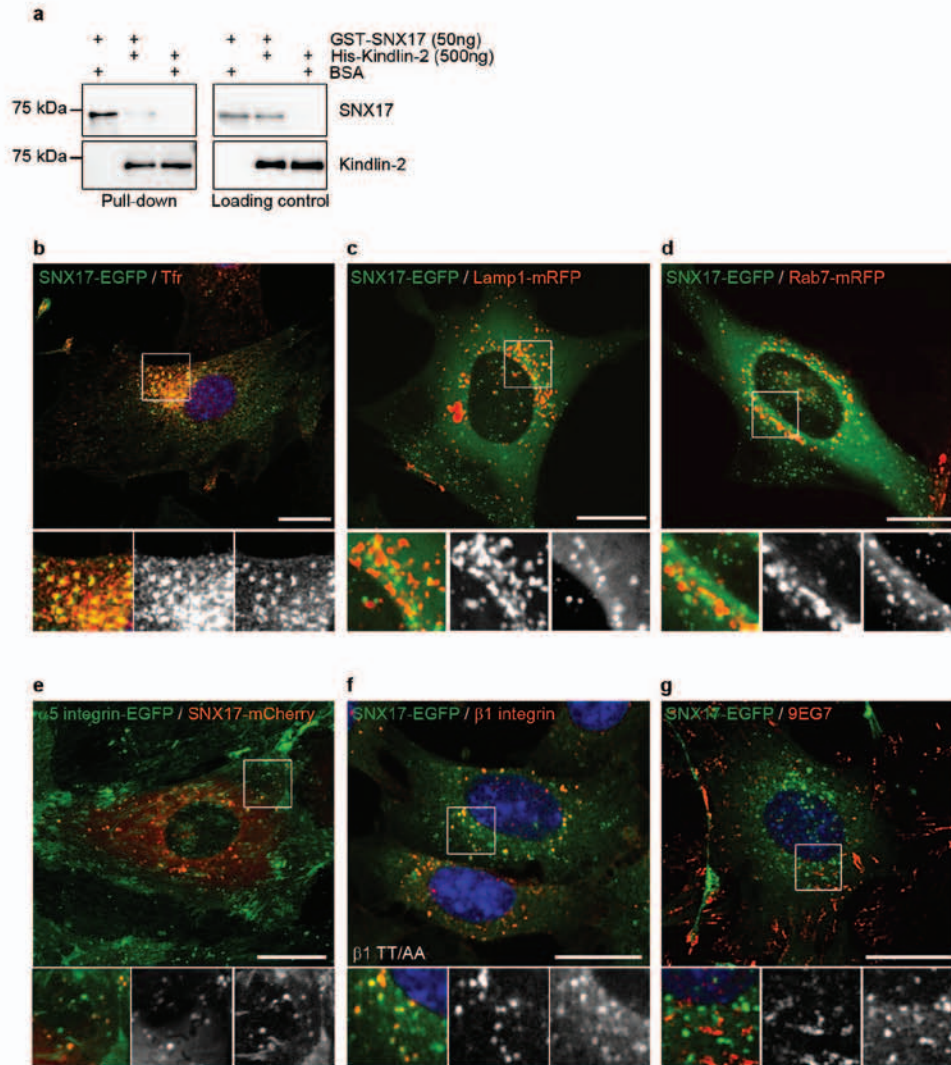
**Figure S1** Defects of  $\beta 1$  TT/AA and  $\beta 1$  Y795A ES cells. **(a)** Brightfield images of E7.5 embryos without implantation chamber. **(b)** Upper panels show brightfield images of EBs on the 5<sup>th</sup> day of suspension culture. Lower panels show cryo-sections of EBs on the 5<sup>th</sup> day of suspension culture stained for  $\beta 1$  integrin (red) and laminin111 (green). Nuclei were counterstained with DAPI (blue). **(c)** Cryo sections of EBs on the 5<sup>th</sup> day of suspension culture stained for  $\beta$ -catenin, E-cadherin, F-actin and laminin111. Nuclei were

counterstained with DAPI (blue). **(d)** ES cell colonies on feeder cells. **(e)** Expression of integrin subunits on ES cells determined by FACS (mean  $\pm$  SD;  $n=5$ ; \*\*\* $p$  (student's  $t$ -test) $\leq 0.0005$ ; ns=not significant). **(f)** Integrin activation on ES cells measured by 9EG7 binding and corrected for total  $\beta 1$  integrin expression (mean  $\pm$  SD;  $n=5$ ; \*\* $p$  (student's  $t$ -test)=0.0043; ns=not significant). **(g)** Expression of  $\beta 1$  integrin mRNA in ES cells measured by qRT-PCR ( $n=2$ ). Scale bar, 100  $\mu$ m (a, b, d), 50  $\mu$ m (c).



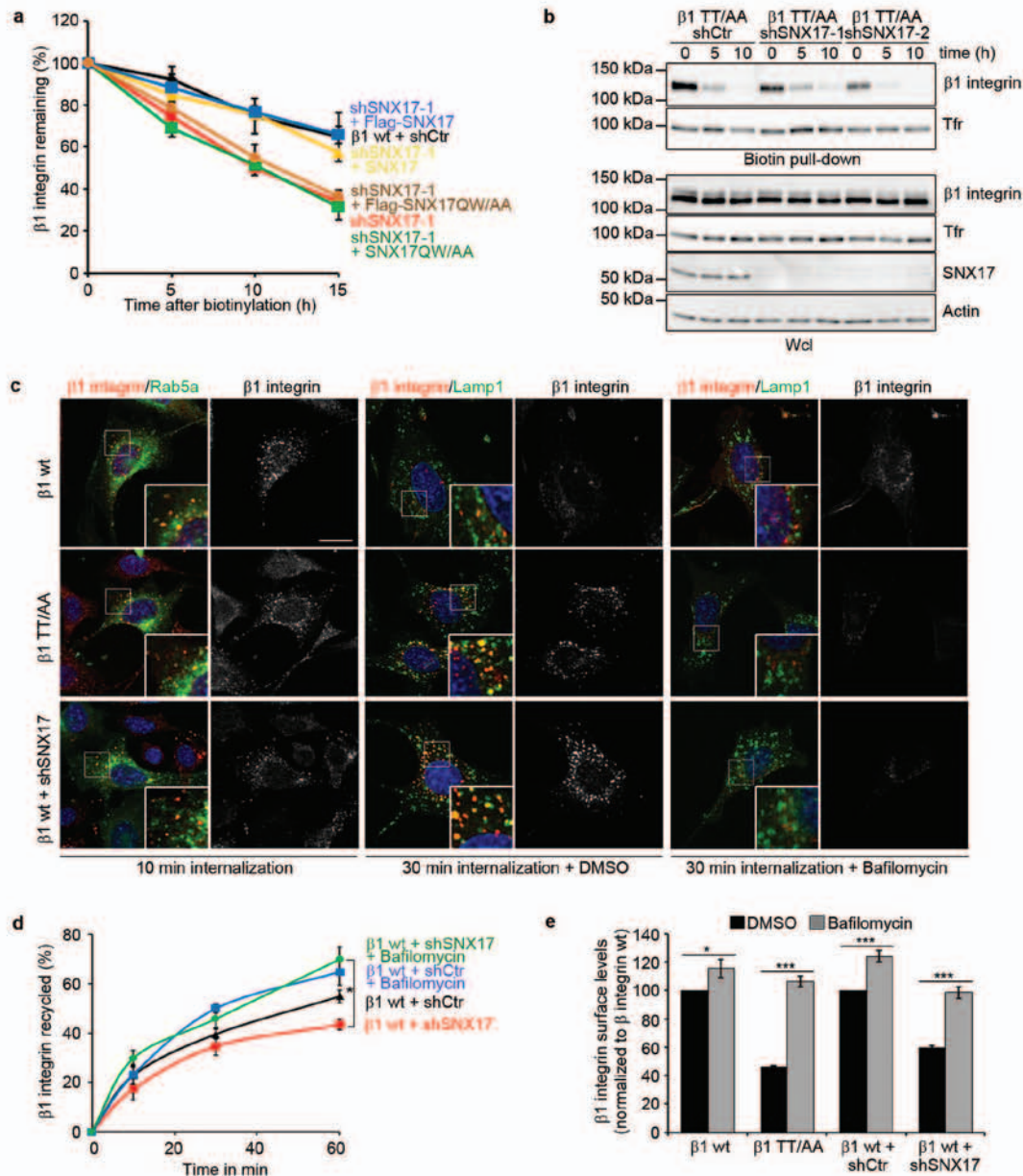
**Figure S2** Characterization of fibroblasts expressing  $\beta 1$  TT/AA integrin. **(a, b)** Scheme depicting the generation of  $\beta 1$  wt and  $\beta 1$  TT/AA fibroblasts.  $\beta 1$  wt and  $\beta 1$  TT/AA fibroblasts were either obtained by retroviral expression of  $\beta 1$  variants in  $\beta 1$  null cells (a) or by immortalization of fibroblasts from mouse embryos (b). **(c, d)** Surface expression of different  $\alpha$  and  $\beta$  integrin subunits on  $\beta 1$  wt and  $\beta 1$  TT/AA fibroblasts determined by FACS (mean  $\pm$  SD; n=6 (c); n=4 (d)); \*p (student's t-test)<0.05, \*\*p (student's

t-test)=0.0022, \*\*\*p (student's t-test)<0.0001; ns=not significant). **(e, f)**  $\beta 1$  integrin mRNA levels determined by qRT-PCR (mean  $\pm$  SD; n=3 with two independent cDNAs; \*p (student's t-test)=0.015, \*\*p (student's t-test)=0.0032). **(g)** Western blot analysis of fibroblast cell lines with antibodies against  $\beta 1$  integrin and actin. **(h)**  $\beta 1$  integrin activation measured by 9EG7 binding and corrected for  $\beta 1$  integrin expression (mean  $\pm$  SD; n=4; \*\*p (student's t-test)=0.0097).



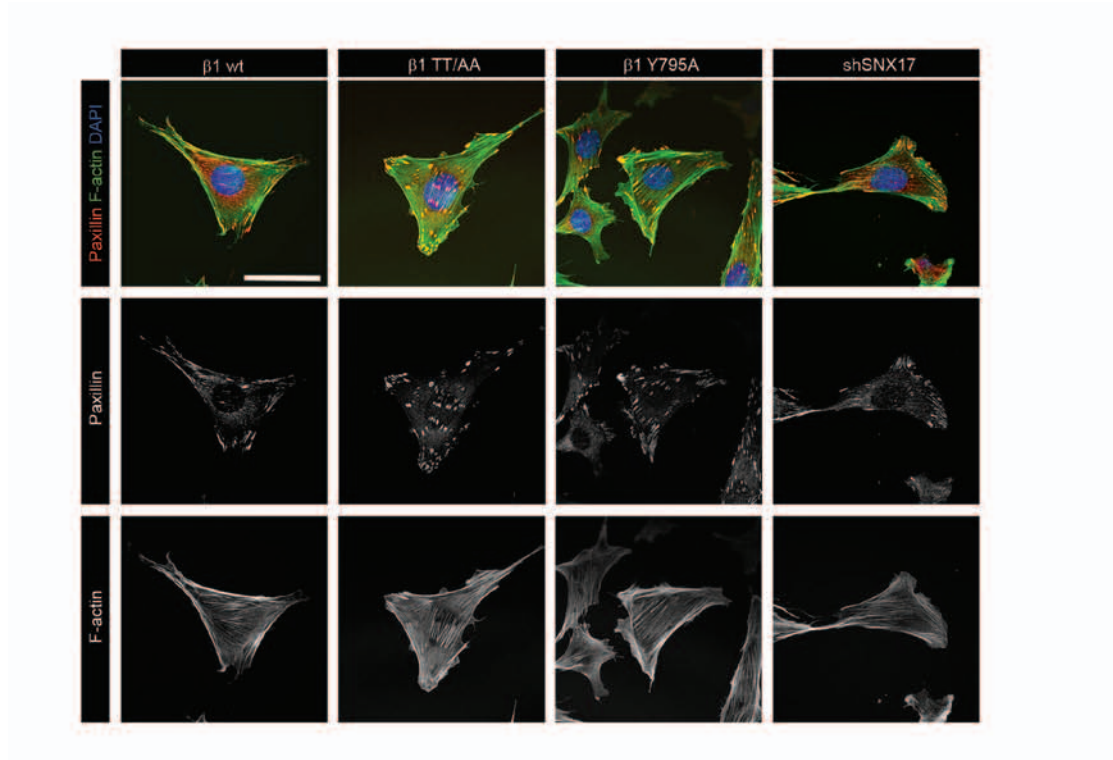
**Figure S3** SNX17 localization in fibroblasts. **(a)** Streptavidin-bead pull-down assay with a biotinylated wild-type  $\beta 1$  integrin cytoplasmic tail peptide and recombinant GST-tagged SNX17 and His-tagged Kindlin-2. **(b)** Immunostaining of SNX17-EGFP expressing cells for Tfr (red). Nuclei were counterstained with DAPI (blue) (correlation coefficient  $0.032 \pm 0.121$ ; mean  $\pm$  SD of 13 cells analyzed). **(c, d)** SNX17-EGFP expressing cells were transfected with Lamp1-mRFP (c) and Rab7-mRFP (d) and the fluorescence distribution was determined in living cells by spinning disk confocal microscopy. Stills of movies are shown (correlation coefficient

$-0.454 \pm 0.106$ ; mean  $\pm$  SD of 15 cells analyzed). **(e)** Distribution of SNX17-mCherry and  $\alpha 5$  integrin-EGFP in living cells determined by spinning disk confocal microscopy. A still of a movie is shown. **(f)** Distribution of  $\beta 1$  TT/AA integrins in SNX17-EGFP expressing cells after surface labeling with an anti- $\beta 1$  integrin antibody and internalization for 15 min. Cells were fixed, stained and the fluorescence was determined with confocal microscopy. **(g)** Localization of active  $\beta 1$  integrins after surface labeling with a 9EG7 antibody and internalization for 15 min in SNX17-EGFP expressing cells. The fluorescence was determined with confocal microscopy. Scale bars, 20  $\mu$ M.



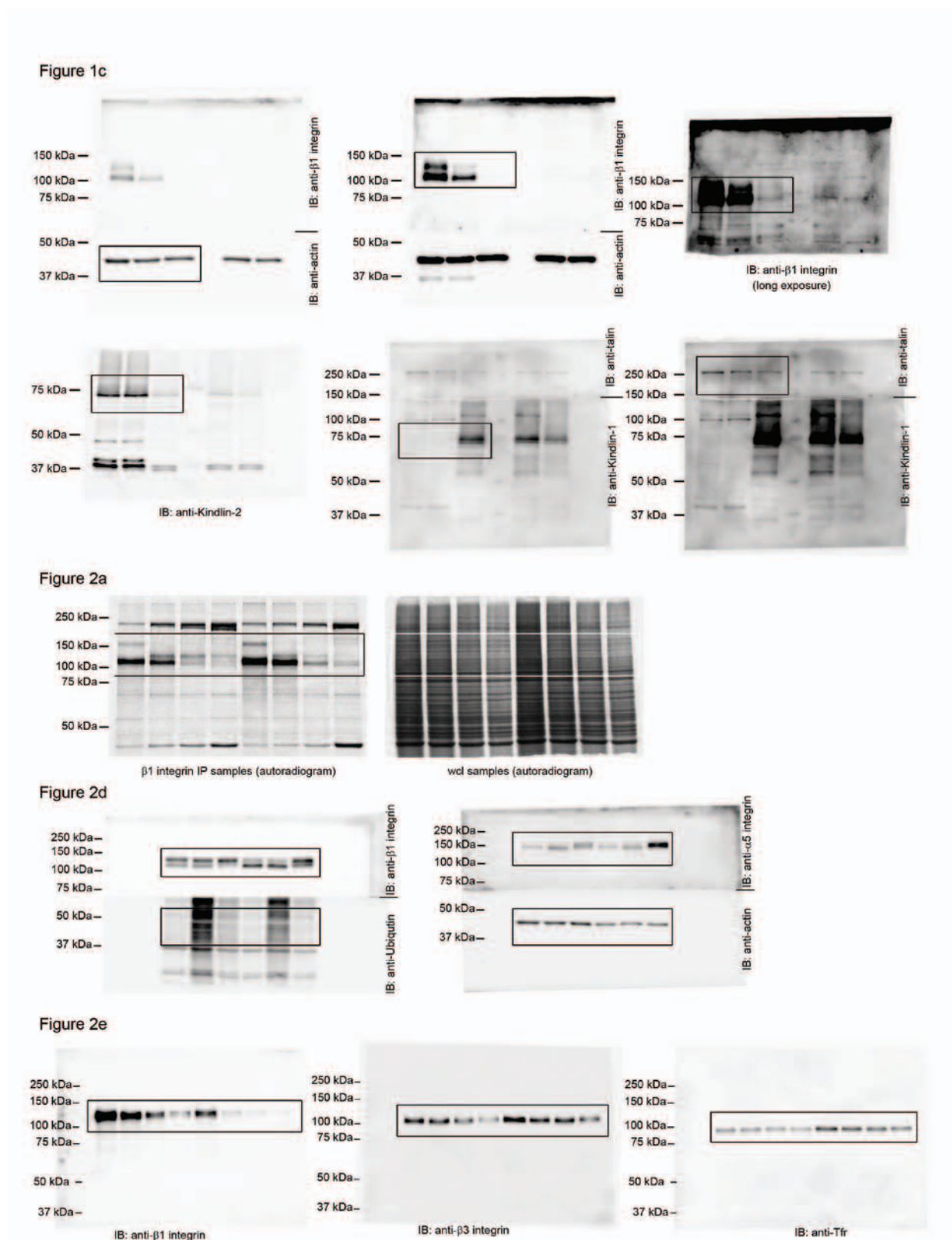
**Figure S4** SNX17 regulates  $\beta 1$  integrin surface levels. **(a)** Stability of surface  $\beta 1$  integrin in the indicated cell lines determined by surface biotinylation followed by capture-ELISA (mean  $\pm$  SD;  $n=3$ ). SNX17 levels were restored in SNX17-depleted cells by re-expressing either siRNA-insensitive wt SNX17 or SNX17QW/AA. **(b)** SNX17-depleted  $\beta 1$  TT/AA expressing cells were surface biotinylated and incubated for the indicated time points, before biotinylated proteins were pulled-down with streptavidin-sepharose and analyzed by western blotting. **(c)** Localization of endogenous  $\beta 1$  integrin after surface labeling with an anti- $\beta 1$  integrin antibody and internalization for 10 and 30 min in  $\beta 1$  wt,  $\beta 1$  TT/AA and

SNX17-depleted cells, respectively treated with or without bafilomycin. Cells either expressed Rab5a-GFP or were fixed and stained with antibodies against Lamp1. Nuclei were counterstained with DAPI (blue). Scale bar, 20  $\mu$ m. **(d)** Bafilomycin normalizes the recycling of  $\beta 1$  wt in SNX17-depleted cells. The quantity of biotinylated  $\beta 1$  integrin remaining within the cells was determined by capture-ELISA using  $\beta 1$  integrin specific antibodies (mean  $\pm$  s.e.m.;  $n=3$ ). **(e)** Quantification of  $\beta 1$  surface levels by FACS in indicated cell lines treated for 8 h with and without bafilomycin (mean  $\pm$  SD;  $n=3$ ; \* $p$  (student's t-test)=0.0133, \*\*\* $p$  (student's t-test)<0.0006; ns=not significant).



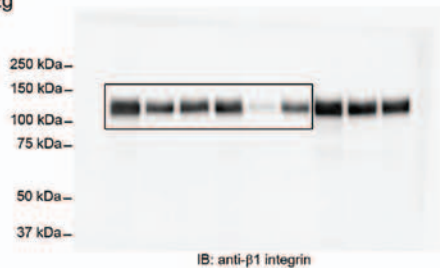
**Figure S5** Focal adhesions and the actin cytoskeleton are not affected in  $\beta 1$  TT/AA,  $\beta 1$  Y795A and SNX17-depleted cells.  $\beta 1$  wt,  $\beta 1$  TT/AA,  $\beta 1$  Y795A and SNX17-depleted  $\beta 1$  wt cells were stained with an antibody

against paxillin (red) and fluorescently labelled phalloidin to visualize F-actin (green). Nuclei were counterstained with DAPI (blue). Scale bar, 50  $\mu$ M.



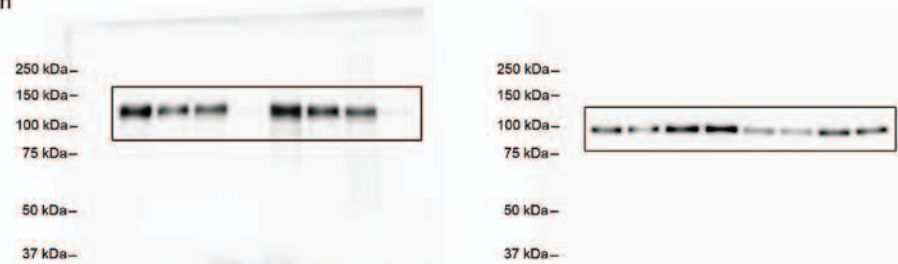
**Figure S6** Full scans of the key immunoblots. Boxes indicate cropped images used in the figures and numbers indicate the molecular weight.

Figure 2g



IB: anti- $\beta 1$  integrin

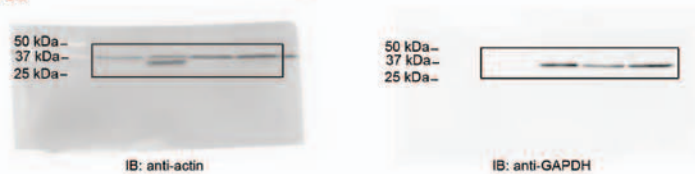
Figure 2h



IB: anti- $\beta 1$  integrin

IB: anti-Tfr

Figure 3c



IB: anti-actin

IB: anti-GAPDH

Figure 4a

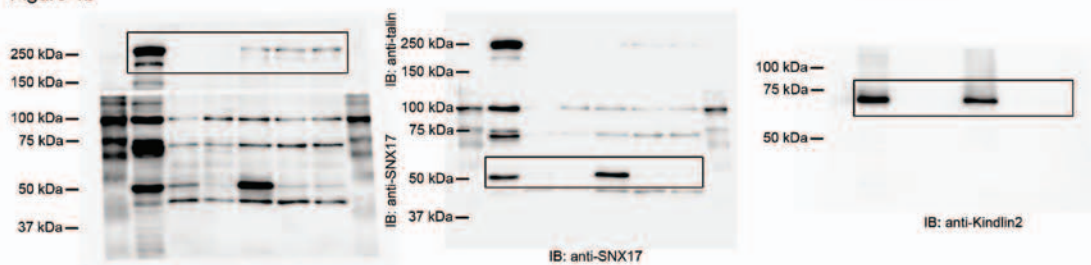


IB: anti-Kindlin-2

IB: anti-Kindlin-3

IB: anti-Kindlin-1

Figure 4b



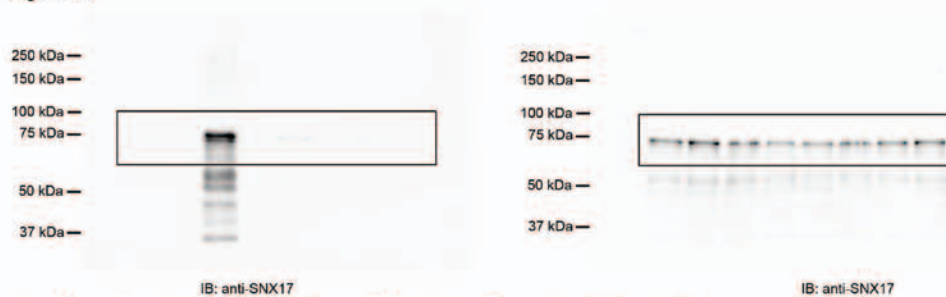
IB: anti-talin

IB: anti-SNX17

IB: anti-SNX17

IB: anti-Kindlin2

Figure 4c



IB: anti-SNX17

IB: anti-SNX17

Figure S6 continued

Figure 4h

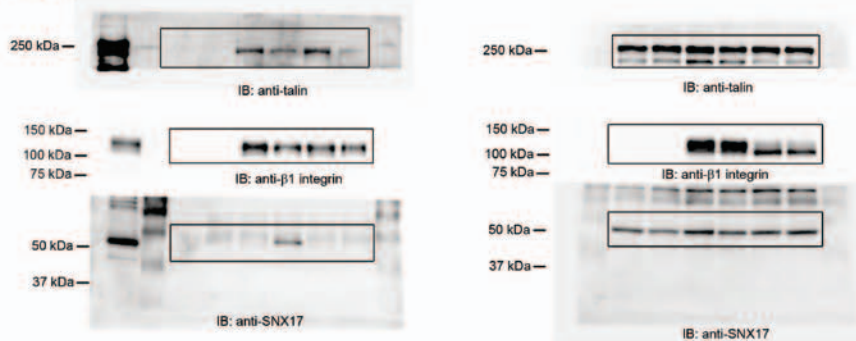


Figure 5a

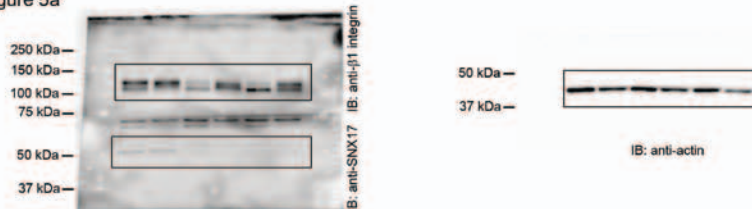


Figure 5c

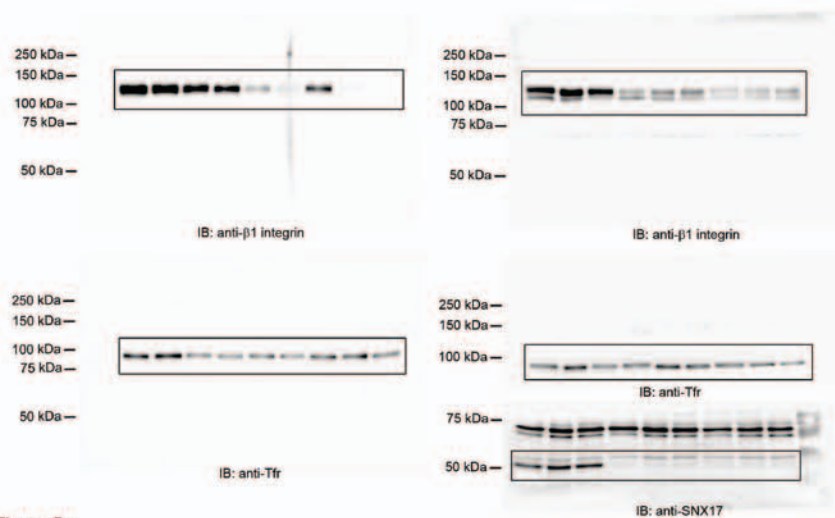


Figure 5e

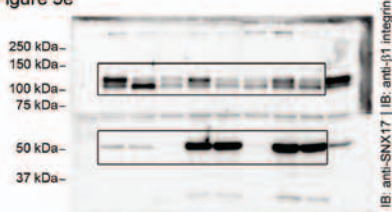


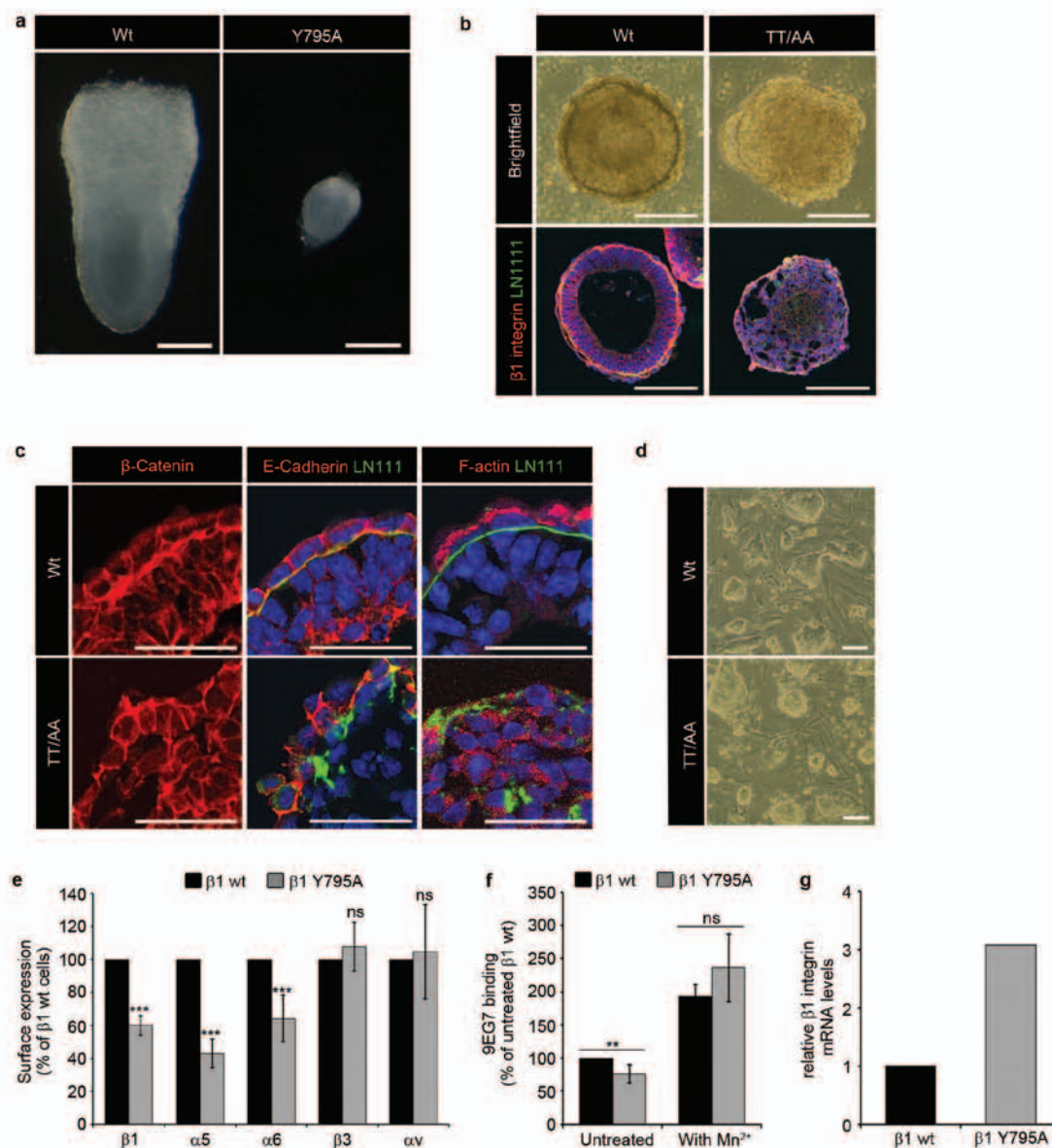
Figure S6 continued

**Supplementary Movie 1** Time-lapse video recording of spreading  $\beta 1$  (-/-),  $\beta 1$  wt  $\beta 1$  TT/AA, and SNX17-depleted cells on FN (pictures taken every 10 min, imaging period 4 hrs).

**Supplementary Movie 2** Time-lapse video recording of migrating  $\beta 1$  wt,  $\beta 1$  TT/AA, SNX17-depleted cells (shSNX17) and SNX17-depleted cells rescued with wild-type SNX17 (shSNX17 + SNX17) on FN (pictures taken every 10 min, imaging period 6 hrs).

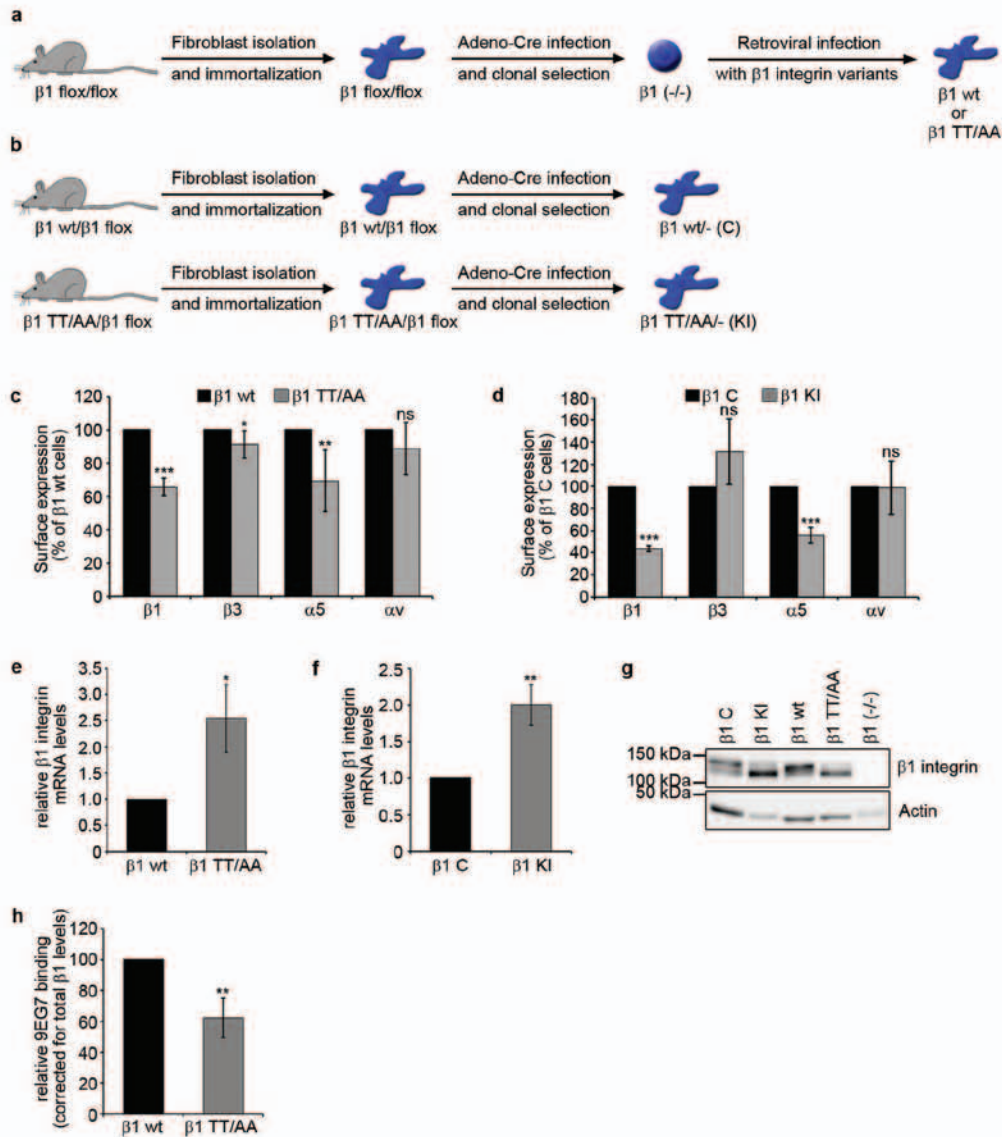
**Supplementary Table 1** List of  $\beta 1$  interactors from the SILAC-based  $\beta 1$  wt tail peptide versus scrambled peptide pull-down. List of the proteins that showed an increased binding (>2.0 fold) to the  $\beta 1$  wt tail peptide against the scrambled peptide. Protein names, gene names, SILAC-ratios and intensities are listed.

DOI: 10.1038/ncb2501



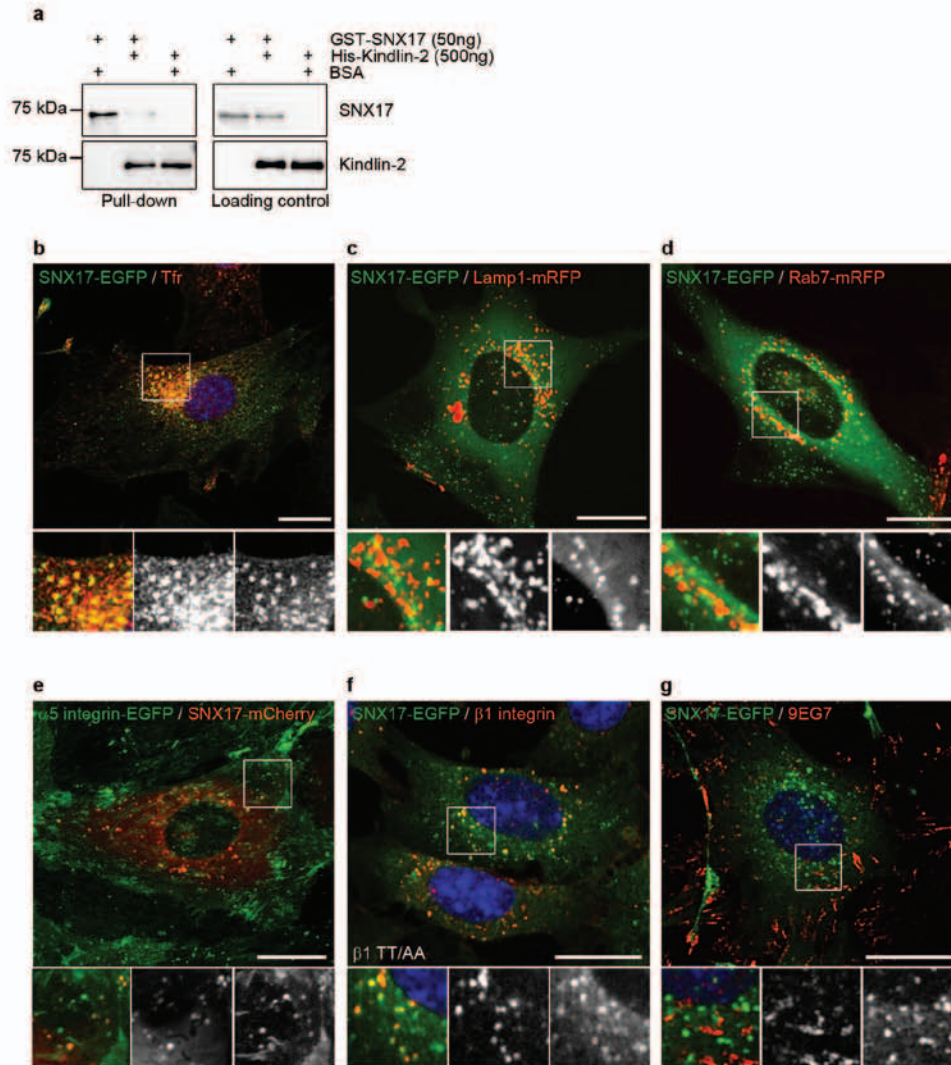
**Figure S1** Defects of  $\beta 1$  TT/AA and  $\beta 1$  Y795A ES cells. **(a)** Brightfield images of E7.5 embryos without implantation chamber. **(b)** Upper panels show brightfield images of EBs on the 5<sup>th</sup> day of suspension culture. Lower panels show cryo-sections of EBs on the 5<sup>th</sup> day of suspension culture stained for  $\beta 1$  integrin (red) and laminin111 (green). Nuclei were counterstained with DAPI (blue). **(c)** Cryo sections of EBs on the 5<sup>th</sup> day of suspension culture stained for  $\beta$ -catenin, E-cadherin, F-actin and laminin111. Nuclei were

counterstained with DAPI (blue). **(d)** ES cell colonies on feeder cells. **(e)** Expression of integrin subunits on ES cells determined by FACS (mean  $\pm$  SD;  $n=5$ ; \*\*\* $p$  (student's  $t$ -test) $\leq 0.0005$ ; ns=not significant). **(f)** Integrin activation on ES cells measured by 9EG7 binding and corrected for total  $\beta 1$  integrin expression (mean  $\pm$  SD;  $n=5$ ; \*\* $p$  (student's  $t$ -test)=0.0043; ns=not significant). **(g)** Expression of  $\beta 1$  integrin mRNA in ES cells measured by qRT-PCR ( $n=2$ ). Scale bar, 100  $\mu$ m (a, b, d), 50  $\mu$ m (c).



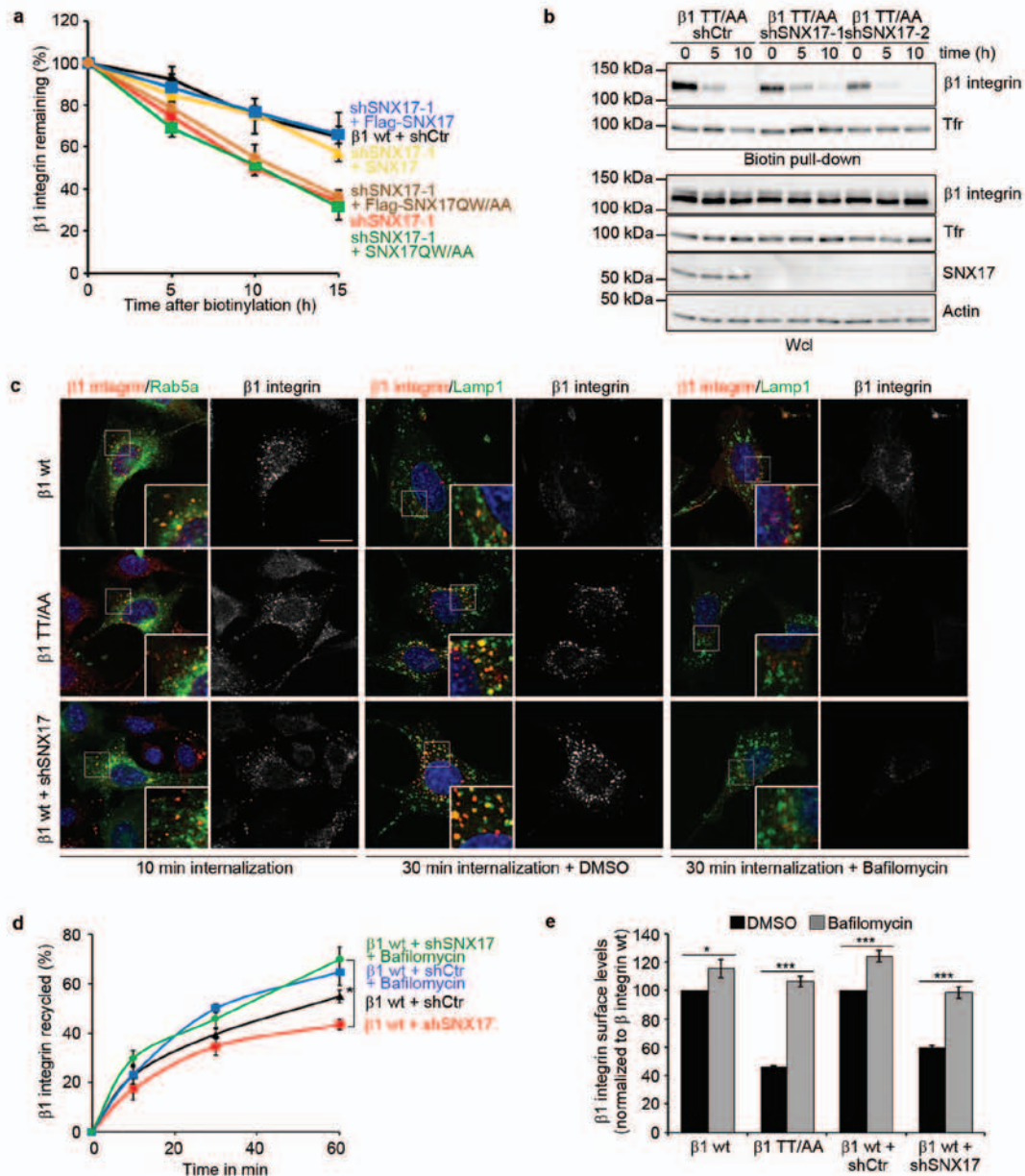
**Figure S2** Characterization of fibroblasts expressing  $\beta 1$  TT/AA integrin. **(a, b)** Scheme depicting the generation of  $\beta 1$  wt and  $\beta 1$  TT/AA fibroblasts.  $\beta 1$  wt and  $\beta 1$  TT/AA fibroblasts were either obtained by retroviral expression of  $\beta 1$  variants in  $\beta 1$  null cells (a) or by immortalization of fibroblasts from mouse embryos (b). **(c, d)** Surface expression of different  $\alpha$  and  $\beta$  integrin subunits on  $\beta 1$  wt and  $\beta 1$  TT/AA fibroblasts determined by FACS (mean  $\pm$  SD; n=6 (c); n=4 (d)); \*p (student's t-test)<0.05, \*\*p (student's

t-test)=0.0022, \*\*\*p (student's t-test)<0.0001; ns=not significant). **(e, f)**  $\beta 1$  integrin mRNA levels determined by qRT-PCR (mean  $\pm$  SD; n=3 with two independent cDNAs; \*p (student's t-test)=0.015, \*\*p (student's t-test)=0.0032). **(g)** Western blot analysis of fibroblast cell lines with antibodies against  $\beta 1$  integrin and actin. **(h)**  $\beta 1$  integrin activation measured by 9EG7 binding and corrected for  $\beta 1$  integrin expression (mean  $\pm$  SD; n=4; \*\*p (student's t-test)=0.0097).



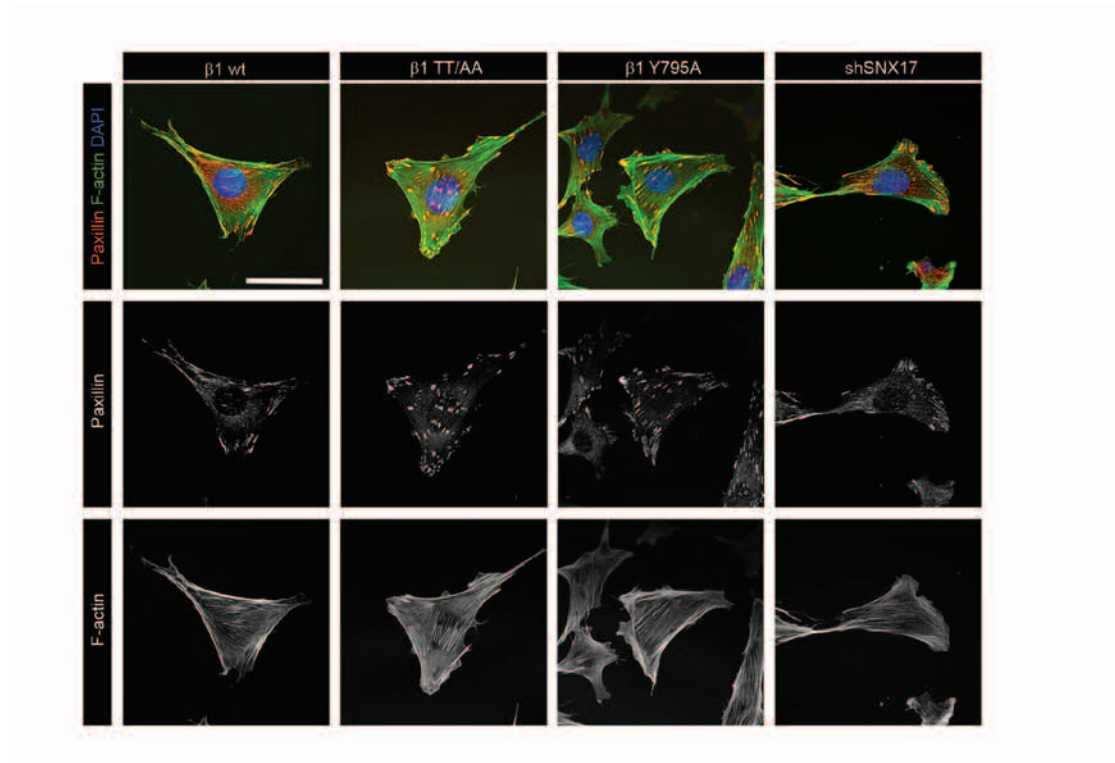
**Figure S3** SNX17 localization in fibroblasts. **(a)** Streptavidin-bead pull-down assay with a biotinylated wild-type  $\beta$ 1 integrin cytoplasmic tail peptide and recombinant GST-tagged SNX17 and His-tagged Kindlin-2. **(b)** Immunostaining of SNX17-EGFP expressing cells for Tfr (red). Nuclei were counterstained with DAPI (blue) (correlation coefficient  $0.032 \pm 0.121$ ; mean  $\pm$  SD of 13 cells analyzed). **(c, d)** SNX17-EGFP expressing cells were transfected with Lamp1-mRFP (c) and Rab7-mRFP (d) and the fluorescence distribution was determined in living cells by spinning disk confocal microscopy. Stills of movies are shown (correlation coefficient

$-0.454 \pm 0.106$ ; mean  $\pm$  SD of 15 cells analyzed). **(e)** Distribution of SNX17-mCherry and  $\alpha$ 5 integrin-EGFP in living cells determined by spinning disk confocal microscopy. A still of a movie is shown. **(f)** Distribution of  $\beta$ 1 TT/AA integrins in SNX17-EGFP expressing cells after surface labeling with an anti- $\beta$ 1 integrin antibody and internalization for 15 min. Cells were fixed, stained and the fluorescence was determined with confocal microscopy. **(g)** Localization of active  $\beta$ 1 integrins after surface labeling with a 9EG7 antibody and internalization for 15 min in SNX17-EGFP expressing cells. The fluorescence was determined with confocal microscopy. Scale bars, 20  $\mu$ M.



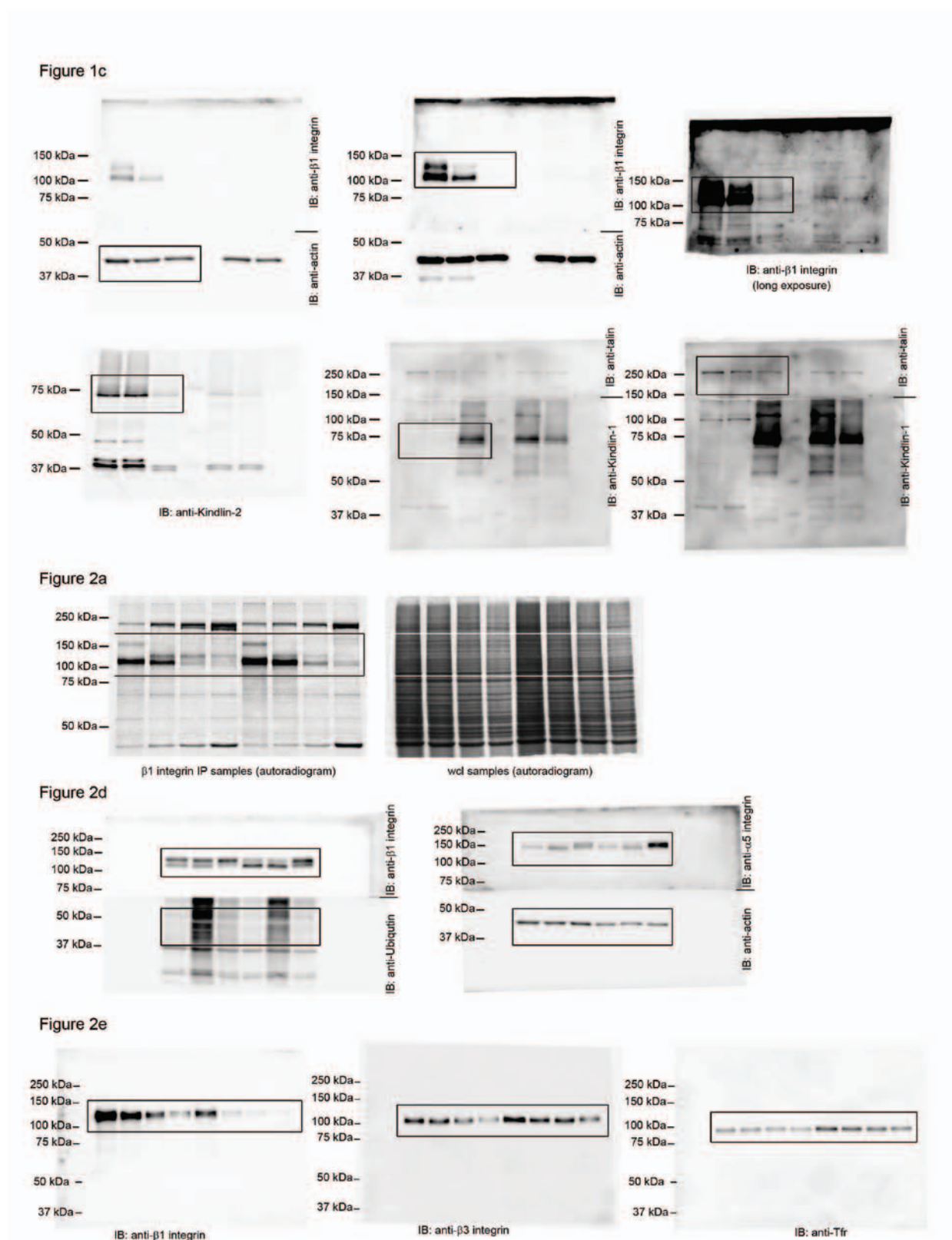
**Figure S4** SNX17 regulates  $\beta 1$  integrin surface levels. **(a)** Stability of surface  $\beta 1$  integrin in the indicated cell lines determined by surface biotinylation followed by capture-ELISA (mean  $\pm$  SD;  $n=3$ ). SNX17 levels were restored in SNX17-depleted cells by re-expressing either siRNA-insensitive wt SNX17 or SNX17QW/AA. **(b)** SNX17-depleted  $\beta 1$  TT/AA expressing cells were surface biotinylation and incubated for the indicated time points, before biotinylated proteins were pulled-down with streptavidin-sepharose and analyzed by western blotting. **(c)** Localization of endogenous  $\beta 1$  integrin after surface labeling with an anti- $\beta 1$  integrin antibody and internalization for 10 and 30 min in  $\beta 1$  wt,  $\beta 1$  TT/AA and

SNX17-depleted cells, respectively treated with or without bafilomycin. Cells either expressed Rab5a-GFP or were fixed and stained with antibodies against Lamp1. Nuclei were counterstained with DAPI (blue). Scale bar, 20  $\mu$ m. **(d)** Bafilomycin normalizes the recycling of  $\beta 1$  wt in SNX17-depleted cells. The quantity of biotinylated  $\beta 1$  integrin remaining within the cells was determined by capture-ELISA using  $\beta 1$  integrin specific antibodies (mean  $\pm$  s.e.m.;  $n=3$ ). **(e)** Quantification of  $\beta 1$  surface levels by FACS in indicated cell lines treated for 8 h with and without bafilomycin (mean  $\pm$  SD;  $n=3$ ; \* $p$  (student's t-test)=0.0133, \*\*\* $p$  (student's t-test)<0.0006; ns=not significant).



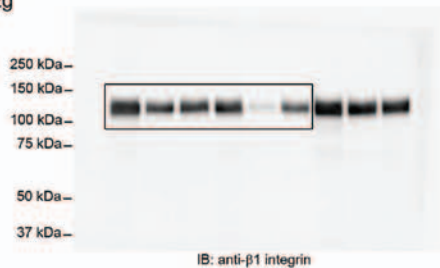
**Figure S5** Focal adhesions and the actin cytoskeleton are not affected in  $\beta 1$  TT/AA,  $\beta 1$  Y795A and SNX17-depleted cells.  $\beta 1$  wt,  $\beta 1$  TT/AA,  $\beta 1$  Y795A and SNX17-depleted  $\beta 1$  wt cells were stained with an antibody

against paxillin (red) and fluorescently labelled phalloidin to visualize F-actin (green). Nuclei were counterstained with DAPI (blue). Scale bar, 50  $\mu$ M.



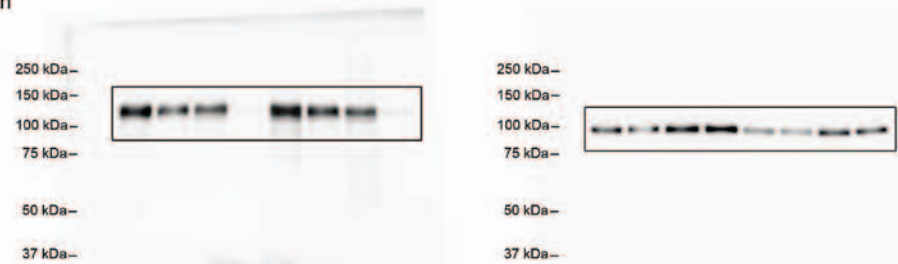
**Figure S6** Full scans of the key immunoblots. Boxes indicate cropped images used in the figures and numbers indicate the molecular weight.

Figure 2g



IB: anti- $\beta 1$  integrin

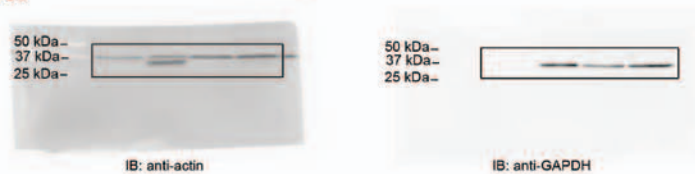
Figure 2h



IB: anti- $\beta 1$  integrin

IB: anti-Tfr

Figure 3c



IB: anti-actin

IB: anti-GAPDH

Figure 4a

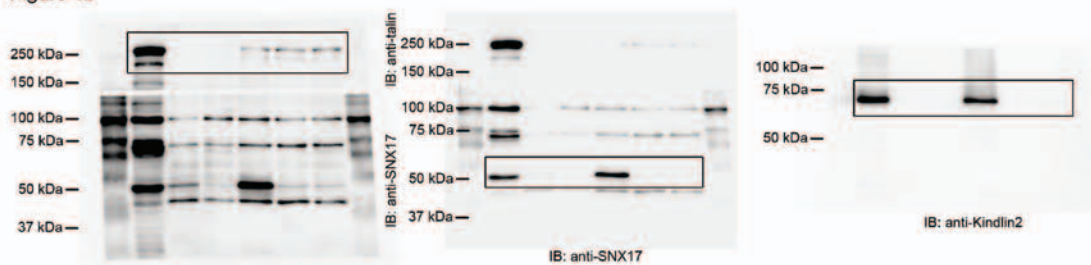


IB: anti-Kindlin-2

IB: anti-Kindlin-3

IB: anti-Kindlin-1

Figure 4b



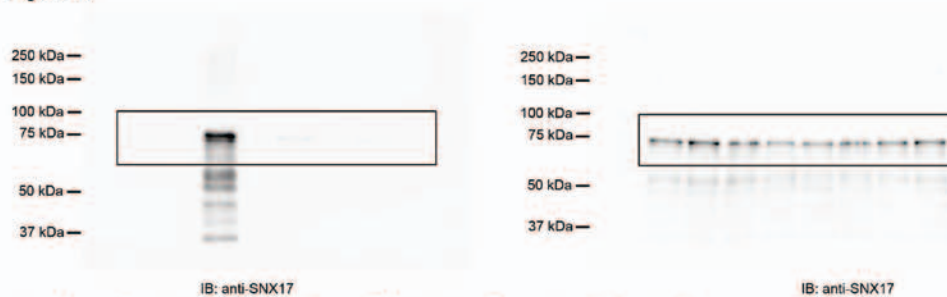
IB: anti-talin

IB: anti-SNX17

IB: anti-SNX17

IB: anti-Kindlin2

Figure 4c



IB: anti-SNX17

IB: anti-SNX17

Figure S6 continued

Figure 4h

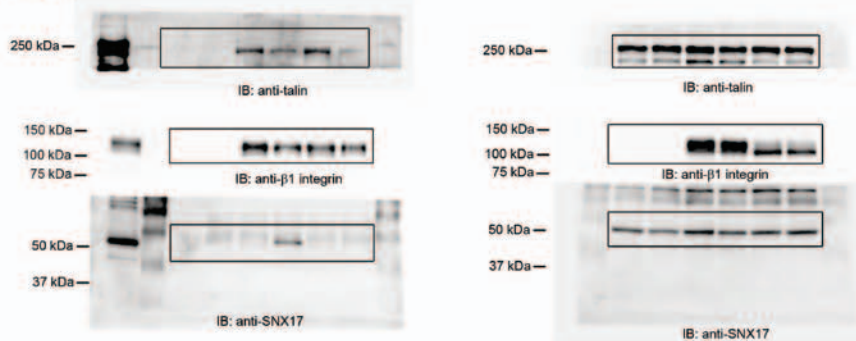


Figure 5a

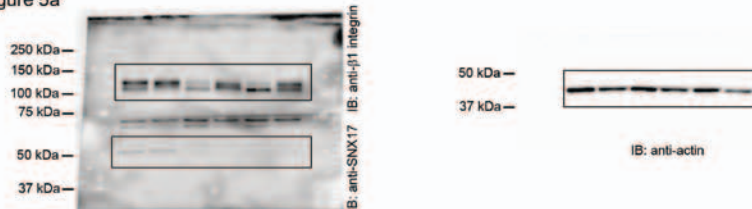


Figure 5c

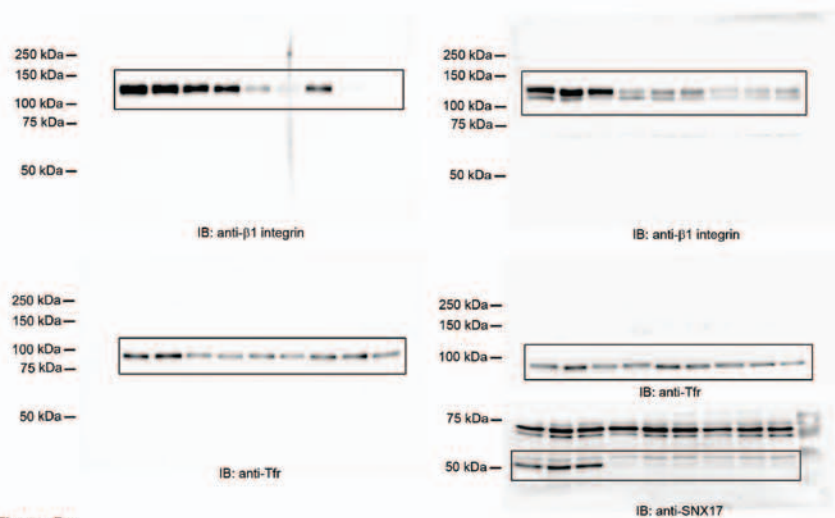


Figure 5e

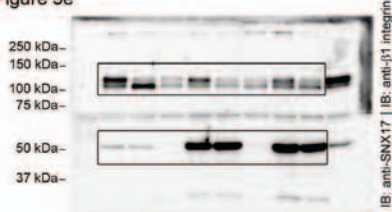


Figure S6 continued

**Supplementary Movie 1** Time-lapse video recording of spreading  $\beta 1$  (-/-),  $\beta 1$  wt  $\beta 1$  TT/AA, and SNX17-depleted cells on FN (pictures taken every 10 min, imaging period 4 hrs).

**Supplementary Movie 2** Time-lapse video recording of migrating  $\beta 1$  wt,  $\beta 1$  TT/AA, SNX17-depleted cells (shSNX17) and SNX17-depleted cells rescued with wild-type SNX17 (shSNX17 + SNX17) on FN (pictures taken every 10 min, imaging period 6 hrs).

**Supplementary Table 1** List of  $\beta 1$  interactors from the SILAC-based  $\beta 1$  wt tail peptide versus scrambled peptide pull-down. List of the proteins that showed an increased binding (>2.0 fold) to the  $\beta 1$  wt tail peptide against the scrambled peptide. Protein names, gene names, SILAC-ratios and intensities are listed.